Optical Photorefractive Phase-Conjugate Mirrors and Resonant Systems

Thesis by

Chi Ching CHANG

Submitted to University of London
for
the Degree of Doctor of Philosophy

Department of Electronic and and Electrical Engineering
UNIUNIVERSITY COLLEGE LONDON
Torrington Place, London WC1E 7JE
UNITED KINGDOM

December 1995

ProQuest Number: 10017440

All rights reserved

INFORMATION TO ALL USERS
The quality of this reproduction is dependent upon the quality of the copy submitted.

In the unlikely event that the author did not send a complete manuscript
and there are missing pages, these will be noted. Also, if material had to be removed,
a note will indicate the deletion.

ProQuest 10017440

Published by ProQuest LLC(2016). Copyright of the Dissertation is held by the Author.

All rights reserved.
This work is protected against unauthorized copying under Title 17, United States Code.
Microform Edition © ProQuest LLC.

ProQuest LLC
789 East Eisenhower Parkway
P.O. Box 1346
Ann Arbor, MI 48106-1346

ACKNOWLEDGEMENTS

I would like to thank my supervisor Dr. David R. Selviah for his most helpful advise, guidance, thoughts and discussion. Especial thanks must go to my advisor the Head of department, Prof. John Midwinter, who has offered other useful insights to my project.

I gratefully acknowledge the National Science Council, Taiwan, ROC and Chung Cheng Institute Technology, Taiwan, ROC for making this work possible by funding the project over the past three years.

I would like to express my appreciation to Prof. H. F. Yau (Inst. of Optical sciences, National Central University, Taiwan, ROC) encouraged me to embark on this research and provided much valuable criticism and advice. I also have received very generous help from many people in the progress of this research, and I wish to thank all of them for their kindness. Dr. S. Tao gave a number help for arranging the experiments and for taking time to engage in many useful discussions. Subsequently, I should particularly like to thank Dr. Peter Poon for his constructive discussions on the programming of SLM.

Many thanks for the support and friendship of my colleagues Dr. Annine Marinopoulou, Lawrence Commander, Dr. Sally Day. Thanks are also due to Photox Optical Systems, UK for supplying the iron-doped lithium niobate crystal and one of the barium titanate crystals and Sanders Associates, USA for supplying the barium titanate crystals. Thanks also to Laser lines, UK for allowing us to borrow the ADLAS frequency doubled 400 mW Nd:YAG diode pumped laser to perform some of the experiments reported.

My last, and by far my greatest, debt is to my wife Nina, who has assisted me at every stage in so many ways. Her contribution to this work has quite simply been incalculable.

To my father

ABSTRACT

This thesis describes and assesses experimentally novel configurations for various types of phase conjugation in the barium titanate crystals and novel designs for optical resonant systems with photorefractive phase-conjugate mirrors (PCMs) and holographic memory for use in optical associative memories (OAM). The thesis describes 3 novel self-pumped phase-conjugate mirror (SPPCM) configurations and 4 novel mutually pumped phase-conjugate mirror (MPPCM) configurations and 1 novel optically switchable phase-conjugate mirror with several beams conjugated over a wide range of angles.

A novel compact 2-f coherent correlator design for use in optical neural networks (ONNs) is described. The thesis describes how to record improved efficiency volume holograms in a novel setup using 2 $BaTiO_3$ phase-conjugating mirrors (PCMs). The thesis also describes our discoveries which is the extending the earlier research began by Dr. Tao of UCL on the improvement of holographic diffraction efficiency (DE) possible arising from Bragg shifts occurring during recording. The thesis presents experimental work on the dependence of DE on the incident beam intensities and the beam ratio. The thesis describes a novel optical resonator in which optical eigenmodes are established between SPPCMs. This is the first time to our knowledge any resonator has been demonstrated and reported between 2 PCMs. In addition 21 angularly multiplexed volume holograms were inserted into the resonator to give 21clearly defined eigenmodes or memories.

The optimum results were obtained for our "-c curve configuration" in which a SPPCM efficiency of 30% was obtained and phase conjugation was maintained over a range of 4mm in lateral translations of the beam and over a range of 40 degrees in the incident angle of the beam. We have proposed a simple model with Four Interaction Regions (FIR) to further account for our discoveries. The "Arch", "Fish-Head", "Fish" and "Manta Ray" configurations are our four new configurations that we have discovered for MPPCM of two incoherent beams which are all remarkably insensitive to angular and lateral positional changes in either of the two input beams or in the crystal itself. The four configurations are also notable in that they have high reflectivity efficiencies and fast response times. These three configurations are part of a family of MPPCMs all of which have similar internal beam paths within the crystal having three internal reflections. The phase conjugate behaviour of the Fish-Head is established relatively fast (~1sec) and has a high reflectivity efficiency (30%) and no crosstalk is observable between the two beams.

TABLE OF CONTENTS

Chapter Five

SELF-PUMPED PHASE-CONJUGATE MIRRORS WITH NOVEL CONFIGURATIONS

Chapter Six

MUTUALLY PUMPED PHASE-CONJUGATE MIRRORS WITH NOVEL CONFIGURATIONS

Chapter Seven

ABBREVIATIONS AND SYMBOLS

-C^3: -c curve configuration

CCD: charge coupled device

DFWM: degenerate four-wave mixing

DMPPCM: double mutually pumped phase-conjugate mirror

DPC: double phase conjugation

FIR: four-interaction regions

FWM: four-wave mixing

HOFNET: high order feedback neural network

IMIBC: induced mutually incoherent beam coupling

ISPPCM: induced self-pumped phase-conjugate mirror

MIBC: mutually incoherent beam coupling

MIPCM: mutl-beam induced phase-conjugate mirror

MPPCM: mutually pumped phase-conjugate mirror

NMIPC: non-degenerate mutl-beam induced phase conjugation

OAM: optical associative memory

ONN: optical neural network

OPC: optical phase conjugation

PCM: phase-conjugate mirror

PCR: phase-conjugate resonator

PD: photodetector

SAM: spatio-angular multiplexing

SBS: stimulated Brillouin scattering

SLM: spatial light modulator

SPB: stimulated photorefractive backscattering

SPBFWM: stimulated photorefractive backscattering four-wave mixing

SPFWM: self-pumped four-wave mixing

SPPCM: self-pumped phase-conjugate mirror

TBC: two beam coupling

TIR: total internal reflection

TIR: two-interaction regions

TWM: twe-wave mixing

Chapter One

INTRODUCTION

The main aim of the research described in this thesis is to develop and investigate the phase conjugate techniques necessary to realise optical feedback for use in an optical neural network resonator for pattern recognition applications. A subsidiary aim is to make related advances to realise such a resonator, such as in the memory storage efficiency and thresholding phase conjugation.

1.1 Historical Background and Motivation

The ability of optics to process large amounts of data in parallel has generated a lot of interest in the implementation of neural network architectures by optical means. Optics and neural networks appear to be an ideal match of requirements and capabilities. The resurgence of interest in neural networks was followed by numerous proposals and experimental demonstrations of optoelectronic implementations [Abu87, And86 & 87, Cas89 & 90, Cau89, Dun91, Far85, Mao91, Fis87, Psa88, Kan90, Lee89, Owe87a, 87b, 91, & 93, Pet90, Sha89, Xu90, Wag87]. The use of photorefractive materials such BaTiO3 and $LiNbO_3$ had a significant beneficial impact on the architecture and implementation of neural networks [Lee89, Wag87, Psa87 & 88 & 90, Sof86, Owe87, Yar86, Owe93, Due93].

These materials have several properties:

1. ***phase conjugation*** These materials can act as real-time phase-conjugate mirrors (PCMs) [Hal85]. A PCM generates a reflection that is the spatial conjugate of the input beam, i.e. each point on the reflected wave propagates back along the same path taken by the corresponding point on the input wave. The important point about phase-conjugate reflection is that any phase changes incurred by the incoming light during the course of its journey will be reversed as the conjugate wave travels back along the path. This means that any phase distortions introduced by the optical

system will be corrected and an undistorted image produced at the input to the system.

2. ***beam coupling and thresholding*** In these material there are optically induced temporary changes in the refractive index, which allow them to be used as real-time holographic processing materials. The interference of two or more beams within a photorefractive crystal of $BaTiO_3$, for instance, generates a holographic phase grating that persists for as long as the beams remain. This allows one beam to couple power into another. The ability to amplify optical signals makes photorefractive materials especially useful in iterative optical schemes. In addition, the physical process giving rise to these effects can be made to exhibit thresholding properties [Cro86], allowing them to be used as continuous fields of neurons within a single crystal being capable of forming arrays of hundreds or thousands of neurons.

3. ***amplifications*** When two counterpropagating light fields interact within a photorefractive material along with a third, weaker beam, they can form a PCM by means of the four-wave mixing (FWM) mechanism. These counterpropagating light fields can either arise spontaneously from scattering within the non-linear material or result from the interaction of two external pump beams. In the latter case, power can be coupled from the pump beams into the reflected field, amplifying the conjugate beam intensity by several orders of magnitude. These make photorefractive materials and PCMs in particular, powerful tools in the implementation of iterative optical networks. Amplified phase conjugation naturally forms reflex iterative processing schemes and produces systems which are self-aligning and tolerant to aberrations and system error.

Neural network computers are aimed at simulating the performance of the brain [Bea90]. They consist of elementary processing units or neurons linked by weighted interconnections. The system may learn through suitable modification of the interconnection weights in accordance with a given learning strategy. The massive parallelism of a neural network architecture is very well adapted to optics, as long as the processing speed of each element is not a critical parameter. A suitable model for neural networks is provided by associative memories, where a given stored image has to be retrieved in response to a partial or noisy input. They have been the subject of active research and several optical implementations have already been reported [Owe89]. One such realisation is illustrated schematically in Fig. 1.1 [Sof86].

Fig. 1.1 *Principal type of optical associative memory using photorefractive non-linear device. Complete image was reconstructed by reading a multiplexed hologram with an incomplete input image. A phase-conjugate mirror (PCM) placed after the lens [Sof86].*

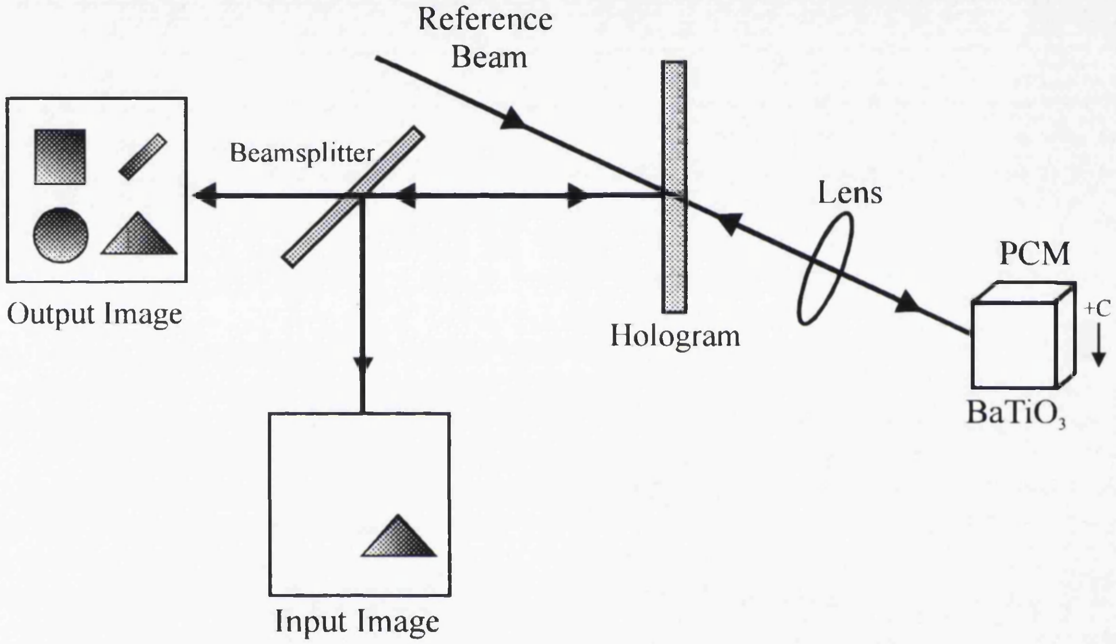

A single hologram is simultaneously illuminated by a partial object beam and the approximate reference beam it produces after being phase-conjugated. The associated information is unlocked by this phase-conjugate reference since it retrieves the full image. The key element is a photorefractive $BaTiO_3$ phase conjugator that, at the same time, provides retroreflected phase conjugation, gain and thresholding. Due to the combined effect of gain and thresholding, only those signals strongly correlated with the partial object beam are emphasised. The principal has been demonstrated to work with different objects superimposed in the hologram memory by angular coding of the reference beam directions [Yar86], so that only the image of the partially excited hologram is retrieved from the multiplexed hologram. The system is particularly relevant in pattern recognition, robotics vision, and in image processing operations. On the other hand, by using a photorefractive crystal to store the volume hologram, real-time modification of the memory is also possible, making, in principal, the adaptive or learning behaviour of the system accessible.

The advantages of this system are clear. Not only are the signals amplified, but any aberrations introduced by the optical system are corrected and the system self-aligns as a result of the phase conjugation operation. However, practial implementations of the above scheme have so far only been able to demonstrate single pass systems without the resonator (feedback) because insufficient gain was available to overcome the losses. The losses result from (1) the weak reflectivity and gain in the phase-conjugate signal from existing PCMs, and (2) the low diffraction efficiency of the holographic memory. So, the aim of our research in this thesis is to find new techniques to overcome these problems.

1.2 Research Objectives

Numerous optical pattern recognition systems have been proposed and demonstrated, however, in this thesis we will be concentrating on one type in which multiplexed holograms recorded in photorefractive crystals are used as the memory and phase conjugate mirrors are used to access the memories in parallel. Such a system can perform correlations of an unknown input pattern with every stored memory in parallel. The phase-conjugate mirrors (PCMs) act as an optical feedback system to send signals back though the system itself rather than around the outside back to the input. In this way the systems realised can be made more compact and are easily aligned, indeed parts are often self aligning so that they can self-adapt to a vibrating or slowly distorting environment, e.g. sag in the mechanics or expansion due to temperature and can compensate for phase aberrations caused by convection from warm components within the system. The speed of processing pixels can be fast since images are processed as a whole. The speed of PCMs depends to a large extent on the incident power and so there is a speed/power trade off. Typically total powers of 5 mW result in response times of a few seconds in a 5 mm cube crystal of barium titanate when used as a "cat" self-pumped phase conjugate mirror (this configuration is described in detail later). Higher speeds can also be achieved using semiconductor phase conjugation but this usually requires infra-red beams whereas the memory store usually requires higher energy photons such as green or blue. Essentially the systems consist of a resonant cavity in which the stored patterns are the eigenmodes of the system. Insertion or injection of an unknown pattern suppresses the strength of some eigenmodes. The resonator often has a gain medium or mechanism to offset the round trip losses. The result is that after multiple reflections back and forth in the resonator the eigenmode patterns which are dissimilar to the input are suppressed and those most similar to the input are enhanced and are output. The introduction of non-linear elements to the resonator allows the system to suppress all eigenmodal patterns except for the one most similar to the unknown input pattern resulting in pattern recognition. Several advances in recording techniques, materials and theoretical analysis during the last few years have brought the possibility of realising a useful system closer. Consider, for example, the memory capacity of the holographic store. This can either be formed in spectral hole burning media for which 2000 holograms have been reported (with a density of 0.20 GBits/cm2) [Koh93, Man93, and Wil93], or in photorefractive crystals [Mok91, Tao93, Mok93, Burr94, Jen93, Tao94, and Sel94]. Although some spectral hole burning materials have been demonstrated at room temperature (with persistence times of minutes to hours) the large memory capacities were obtained at low temperatures [Man93] (below 3oC persistence times are about a month) so in this research we will concentrate on photorefractive crystals for room temperature operation.

Current compact digital disc ROMs have a storage capacity of 1.3 Gbyte on a 5.25 inch disc with an area of 140 cm^2 giving a storage density of 9.3 $MBytes/cm^2$. The memory capacity in photorefractive crystals has been raised in the last few years from 500 through 750, 5,000 to 10,000 images [Tao93, Tao95, Mok 91 & 93, and Bur94] in iron doped lithium niobate crystals of 1 cm3 to 3 cm3; the storage density has also been increased from 12.3 $MBit/cm^3$ through 35.2 $MBit/cm^3$ to 0.23 $gbit/cm^3$ (these figures assume that binary images were stored so one pixel corresponds to one bit); the efficiency has been improved for large numbers of memories from 0.01% to 0.5% using a novel multiplexing technique [Tao93] combining both angular and spatial multiplexing "Spatio-Angular Multiplexing (SAM)" which has been extended, in principle, to include wavelength multiplexing as well [Jen93]; accurate experiments [Tao94] have reported 230% improvements in diffraction efficiency for Fourier Transform holograms due to tiny corrections in the angle of the readout beams (0.006°); theoretical modeling of these Bragg-shift effects have been in good agreement with experiment for plane gratings [Tao94]. Our aim is to implement optical high order neural networks by using a phase-conjugate resonator. Although this radical idea has already been proposed by many researchers [Lee89, Wag87, Psa87 & 88 & 90, Sof86, Owe87, Yar86, Owe93, Due93], the problems arising from how to increase the gain, and satisfy the conditions for efficient phase conjugation must be investigated. We use a novel 2-f correlator in place of the standard 4-f correlator used in the high order feedback neural network (HOFNET) [Sel90 & 91]. This system should have the following advantages: (1) more compact, (2) lower losses, (3) high storage capacity, and (4) high processing speed. This resonator will have two phase-conjugate mirrors [PCMs], one a four-wave mixing PCM and the other a multi-beam induced PCM (both of which will be explained in detail later). In order to make advances to achieve this we have developed novel phase conjugation techniques to satisfy the requirements of this system.

1.3 Layout of Thesis

The contents of this thesis are divided into three parts. The first part contains review of both optical phase conjugation and phase-conjugate mirrors which are relevant to an appreciation of our research and are necessary to understand the physical mechanism of our new discoveries. The second part contains our new research work and the last part is concerned with suggested future research work. The following is a brief synopsis of the major issues addressed in each chapter. In chapter 2, a typical method for generating phase conjugate outputs is discussed first, followed by theoretical consideration of the photorefractive effect and of two-wave mixing (TWM), four-wave mixing (FWM) and beam fanning in photorefractive materials. Then an overview of some of the most important geometries to date for photorefractive self-pumped and mutually pumped phase-conjugate mirrors is presented. Thereafter, a novel scheme (induced self-pumped phase conjugation: ISPPC) is descrbed which both increases the efficiency of self-pumped phase conjugate reflection and shortens the response time. In chapter 2 we also describe several applications for optical phase conjugation which are also relevant work to our research.

The new research work starts from chapter three and continues until chapter six inclusive and is the bulk of this thesis. Chapter 3 provides a thorough description and analysis of compact associative memories based on our novel 2-f correlation setup. We show how a system using spectral corelation, such as the HOFNET, can be efficiently made more compact. Additionally, in this chapter, we describe our novel holographic recording scheme which is unusual in its use of 2 phase-conjugate mirrors during recording. Bragg-shift (the angular shift between the optimum readout angle and the recording angle) diffraction which was observed during the holographic storage process is shown to depend on the total expsoure.

Chapter 4 describes our novel multi-beam induced PCM (MIPCM). The use of this MICPM for performing optical feedback is shown by construction and sucessful demonstration of a novel multi-mode self-pumped phase-conjugate resonator with 21 modes. Chapter 5 reports several novel configurations for self-pumped phase conjugators and asseses their performance advantages. Chapter 6 describes four novel configurations for mutually pumped phase-conjugate mirrors, named "Arch", "Fish-Head" "Fish", and "Ray" MPPCM , respectively. Following presentation of the experimental results we discuss the possible physical mechanisms to explain our observations. At the end of Chapter 6 we describe a novel double Fish-Head MPPCM in which 3 beams are phase conjugated simultaneoiusly in two pairs and which also demonstrates thresholding behaviour and we discuss possible applicaions. Finally, Chapter 7 draws togather the conclusions of our main achievements and lists a collection of ideas for future work.

Chapter Two

PHASE-CONJUGATE MIRRORS AND THEIR APPLICATIONS

The objective of this chapter is to describe the principles of the generation of phase-conjugate waves by means of four-wave mixing (FWM) in electro-optic materials (especially in photorefractive crystals) and the applications of phase conjugation which are related to our research and are of help to understand the mechanism of our new discoveries. We start by historical reviews and generally depict the principle of optical phase conjugation in Section 2.1. This review enables us to place our work in the frame work and context of other research to show the benefits of our approach. Once a diffraction grating has been formed in the photorefractive media such as $LiNbO_3$, $BaTiO_3$, and SBN by illumination, a phase-conjugate wave may be created through a diffraction process similar to holography [Sol81]. The physical phenomenon that leads to the formation of this diffraction grating is the photorefractive effect. Section 2.2 is devoted to the physics of the photorefractive effect which mainly occurrs in electro-optic materials. Our discussion is then directed to the microscopic mechanism: the band-transport model, which is generally accepted as a good model for the generation of phase-conjugate light waves in photorefractive media. During holographic recording in a photorefractive crystal, the two interfering light waves are diffracted by the generated refractive index grating and give rise to a very interesting energy coupling phenomenon, known as two-wave mixing (TWM). Section 2.3 analyses two-wave mixing in photorefractive materials using the coupled wave theory [Kuk79]. Significant beam amplification which also can occur during the beam coupling is discussed in detail as well. Section 2.4 describes how to generate the phase-conjugate light wave by four-wave mixing (FWM) [Whi80]. Here we concentrate on the case when the frequencies of all of the interacting light waves are the same, and will refer to this, as usual, as degenerate four-wave mixing (DFWM). The discussion is then guided to the derivation of the coupled wave equations describing the spatial evolution of the interacting light waves. Also, we introduce briefly the concept of holography and analyse the similarities between FWM and holography to understand the mechanism of phase-conjugation generation in several phase-conjugate mirrors (PCMs). Photorefractive fanning effects result from the physical behaviour of scattering and TWM and this can initiate phase conjugation in certain types of PCM. The physics of the fanning effect, which is very important to the understanding of our discoveries during the research, is discussed in Section 2.5. Section 2.6 is a review of all types of PCM and all phase-conjugate resonators (PCRs) to date. In these devices the pump beams for FWM phase conjugation are provided either by external pump beams or from the signal beam itself (either directly or by the generation of a photorefractive oscillation within the crystal pumped by the signal beam). Applications of PCMs are discussed in Section 2.7. We summary in Section 2.8 by pointing out several outstanding problems that deserve future studies. This provides the motivation for the research reported in this thesis which attempts to address these problems.

2.1 Optical phase Conjugation (OPC)

Optical phase conjugation is a technique that incorporates non-linear optical effects to precisely reverse both the direction of propagation and the overall phase factor for each plane wave in an arbitrary beam of light [Fis83]. The idea underlying optical phase conjugation can be traced back to 1948, when Gabor [Gab48] discussed the principle behind wavefront reconstruction. It was not until 1965, however, five years after the laser made its first appearance, that Kogelnik [Kog65] subsequently realized that holography could be used to compensate for static inhomogeneities in a medium. The concept of real-time holography, in which a grating can be recorded in a medium, and read out in real time, provided the next important step in phase conjugation research [Ger67 & Ste71]. Independently of this, dynamic holographic research work by Zel`dovich et. al. [Zel72] showed that phase distortion could also be corrected through the process of stimulated Brillouin scattering (SBS). No pump beams are required for phase conjugation by SBS, but the intensity of the incident light wave must exceed a threshold value (~1Mw/cm^2) for the process to occur. It was not until several years later, however, that these parallel but formally unrelated research directions were established on a more rigorous basis by the application of the formalism of nonlinear optics to phase-conjugate wavefront generation. Almost the entire catalogue of nonlinear optical processes has been used to produce phase-conjugate light waves in real time. The mechanisms involved are many and various, and span a very wide range of wavelengths, response times, and efficiencies (or reflectivities), etc. Non-linear optical phase conjugation was first observed in the backward scattered light wave produced by SBS [Zel85] in a solid-state laser application [Roc88]. Another technique that can be used for producing phase -conjugate light waves in the use of the non-linear photon echo effect [Fis83] in an atomic medium; however, atomic motion has a serious adverse effect on phase conjugation. Yariv first demonstrated three-wave mixing [Yar76 & 77] in asymmetric crystals to create reversed wavefront replicas, but the phase matching condition restricts the angular range of illumination of the input light wave to very small values. Hellwarth et. al. [Hel77] proposed the phenomenon of four-wave mixing [FWM] [Yar77 & Blo77]. This uses the optically induced polarization of a nonlinear medium that has cubic symmetry in the electric field strength which occurs in all isotropic materials such as most, gases, liquids, and glasses, as well as in appropriate crystals, to eliminate the restrictions of three-wave mixing in generating phase-conjugate light waves. Notable here is the work of Yariv [Yar76] and Hellwarth [Hel77], and the use of the coupled-wave analysis for FWM proposed by Yariv et. al. [Yar77] and Bloom et. al. [Blo77]. In our work we will restrict our attention to the generation of phase-conjugate waves by means of self-pumped four-wave mixing (FWM) [Yariv78] mechanism in photorefractive $BaTiO_3$ crystals that will be studied in detail in this chapter.

Photorefractive phased-conjugate optical system have gained a particularly large following and feature often in the current literature on optical phase-conjugation. A variety of arrangements for photorefractive optical phase conjugation, by means of FWM [Yar78], have been proposed and demonstrated in several phase conjugators such as the self-pumped phase conjugator (SPPC) [Fei82], several kinds of mutually pumped phase conjugator (MPPC) [Wei87, Smo87, Ewb88 & 90, Wan90, and Sha90], and the induced self-pumped phase conjugator (ISPPC) [Yau92 & Riu93]. Phase-conjugate mirrors [PCMs] have found application in optical signal & image processing [Gün88], optical pattern recognition [Ande86 & Owe87], laser phase locking [Cro86 & Fei86], Phase-conjugate resonators [AuY79, Bel79 & 85, Fis89, and Pep94], interferometers [Ewb85, Chi86, and Kwo86], gyros copes[Yeh85 & 86, and McM86 & 87], and many other devices. In this thesis we are concerned and mainly with identifying novel phase-conjugate mirrors (PCMs) with optimal performance and with constructing phase-conjugate resonators (PCRs) using these phase-conjugate devices to implement optical associative photorefractive holographic memories using an optical neural network (ONN) architecture [Owe87, And87, Sel91, and Due93]. For the purpose of understanding these inventions the radical concept and theory of optical phase conjugation must be described in detail in advance in the next section.

2.1.1 Definition of a phase-conjugate light wave

Optical phase conjugation is an nonlinear optical interaction that generates what is known as, a phase-conjugate wavefront. A device that produces such a wavefront is called a PCM. The concept of phase conjugation is illustrated in Fig. 2.1. Here, the incident wave

$$E_{in}(r,t) = \mathrm{Re}\left[A_{in}(r)e^{-j\omega t}\right] \tag{2.1}$$

falls onto a PCM, and the wave

$$E_{pc}(r,t) = \mathrm{Re}\left[r_c A_{in}^{*}(r)e^{-j\omega t}\right] \tag{2.2}$$

which is known as the phase-conjugate wave, is generated by means of a non-linear optical process. Where $A_{in}(r)$ is the complex amplitude of $E_{in}(r, t)$ and $A_{in}^{*}(r)$ is the complex conjugate of $A_{in}(r)$. The constant r_c appearing in Eq. (2.1) is known as the phase-conjugate amplitude reflectivity. Furthermore,

$$E_{in}(r,t) = E_{pc}(r,-t)\,. \tag{2.3}$$

Fig. 2.1 *Phase conjugation of a wavefront by a phase-conjugate mirror (PCM).*

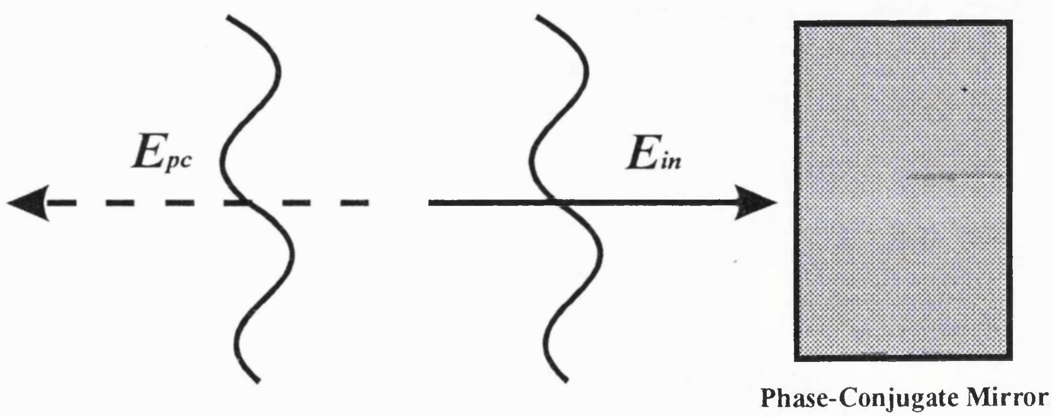

This indicates that the shape of the wavefront here remains the same and that there is inversion only with respect to the time axis. The phase-conjugate wave here can be treated as a time-reversed wave. In the process of reflection from a PCM, the most advanced portion of the incident wavefront generates the most retarded portion of the phase-conjugate wavefront. This property is opposite of that which occurs in reflection from an ordinary mirror as described in following subsection.

2.1.2 Properties of phase-conjugate light wave

One of the principle applications of phase conjugation is the removal of phase aberrations from optical systems. Fig. 2.2 compares the aberration wavefront correction abilities of conventional and phase-conjugate mirrors. The aberration correction process only occurs in the phase-conjugate mirror, which is illustrated schematically in Fig. 2.2b.

Fig. 2.2 *Phase correction by optical phase conjugation illustrated for the case of a plane wave by: (a) reflection from a conventional mirror, (b) reflection from a PCM. 1: wavefront before incidence on glass, 2: wavefront after passing through glass, 3: wavefront after reflection by mirror, 4: wavefront after passing through glass a second time.*

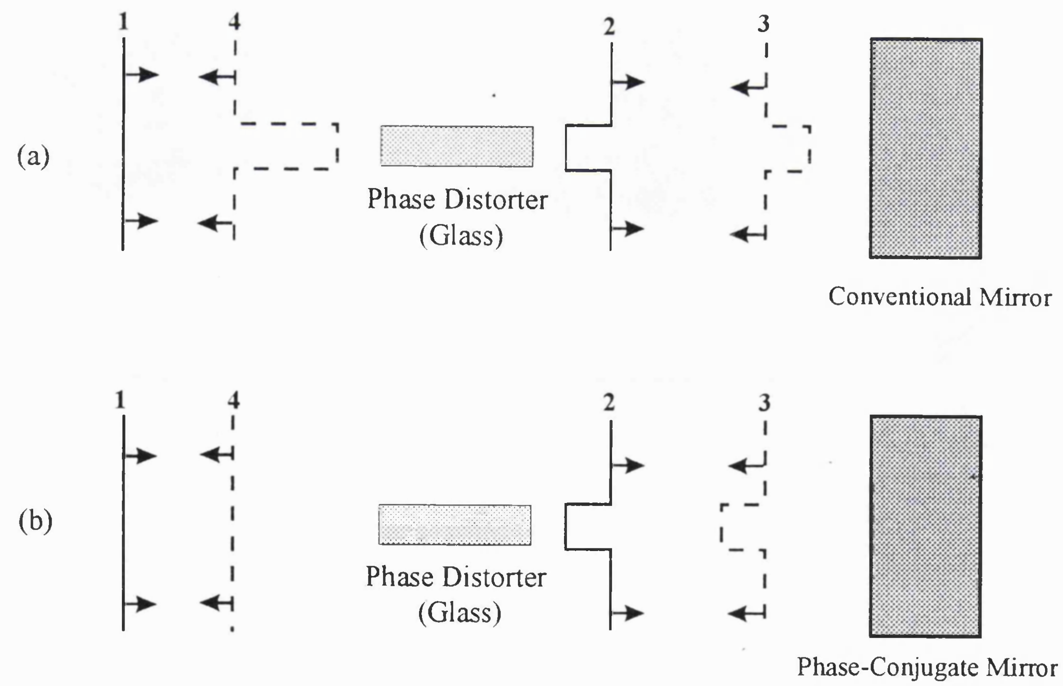

Initially plane wavefront 1 passes through glass (distorting medium) having a higher refractive index than air. As a result of a phase delay caused by the glass the wavefront is converted to wavefront 2. If this wave was incident on a conventional mirror, the reflected wavefront 3 would become reversed from 2 since the direction of propagation is reversed at the surface of the mirror as a result of the folding back of the wave. If the wave passes through the glass a second time, the wavefront 4 is produced with a double phase delay at the part of the wavefront, which is passed through the glass, changes from 3. One the other hand, if wavefront 2 is incident on a phase-conjugate mirror, the reflected wave 3 has the same shape as the incident and only the direction of propagation reversed, as was seen in Eq. 2.3. If this wave again passes through the same glass, there is a phase delay at the portion of wavefront, which passed through the glass only, and the phase delays coming and going through the glass offset each other. Because of this, spatial phase correction is a feature of phase-conjugate light.

Fig. 2.3 *Phase conjugation of an image. A beam bearing the image of a resolution chart (top left) passes through a distorter (diffuser) and its phas-conjugate image passed back through the distorter again (bottom left) after phase conjugation by a phase-conjugate mirror (induced self-pumped phase-conjugate mirror [Yau92], illustrated).*

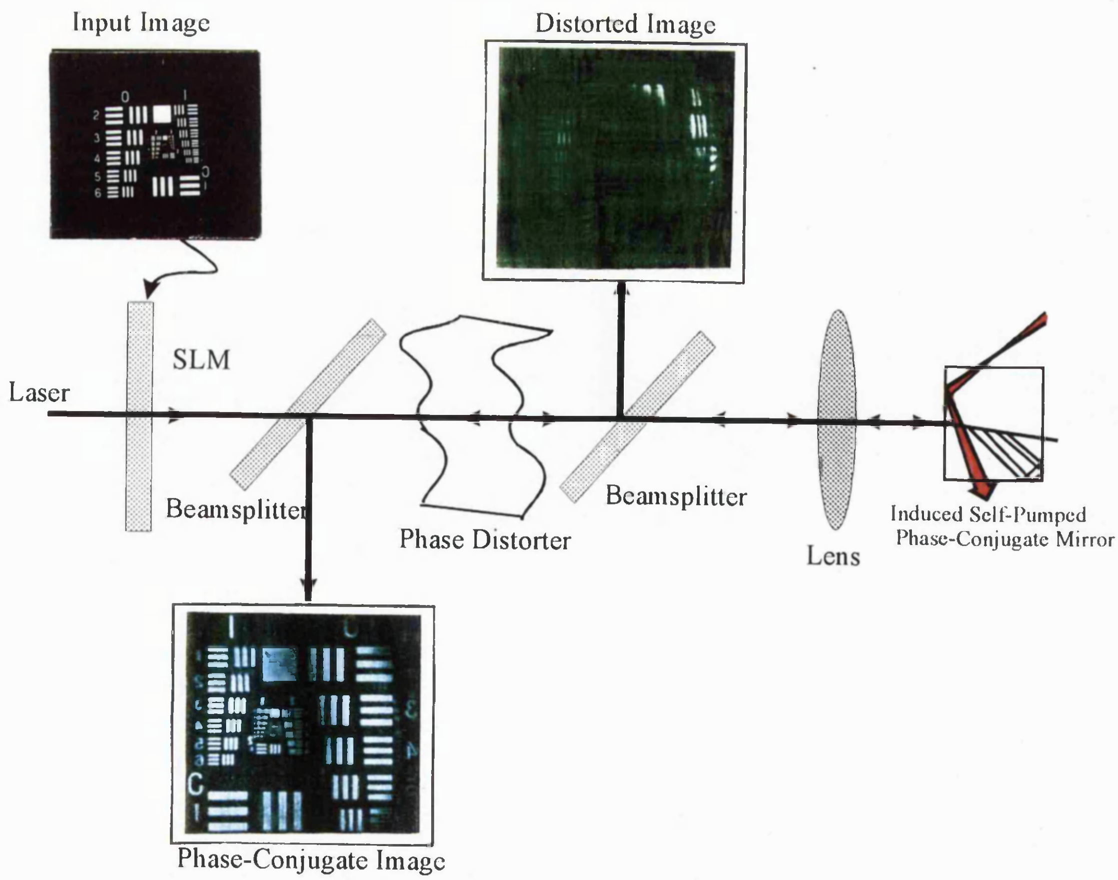

Here, we give an example carried out by us to prove experimentally the idea described above. An incident wavefront containing information in the form of an image (US Airforce resolution chart), which we show as a plane wave, passes through an aberrating medium (such as phase distorter or diffuser) and becomes distorted. After reflection from one kind of PCM, e.g. induced self-pumped phase-conjugate mirror (ISPPCM) (which will be discussed in detail in Section 2.6.4), the sense of the distortion is reversed, and after passing a second time through the aberrating medium, the wavefront distortion is removed (shown in Fig. 2.3). In the example of Fig. 2.3 a special geometry uses total internal reflections at the crystal corner and self-generated pumped waves giving the freedom to choose the orientation that optimises the phase-conjugate signal providing an excellent quality of reproduction. Conjugator reflectivities as high as 56% have been reported [Yau92] in spite of Fresnel reflection losses.

2.2 The Photorefractive Effect

The photorefractive effect was first observed in non-linear optical experiments as a reversible form of optical damage [Ash66]. At room temperature, the photorefractive damage has a persistence ranging from microseconds or less for semiconductor to months or more for $LiNbO_3$. However, the effect is reversible in the sense that can be erased by intense uniform illumination. This form of optical damage occurred at relatively low intensity thresholds and, therefore, proved to be detrimental in many non-linear experiments. This effect was quickly put to use, by Chen et al. [Che68] to record and store phase (index) gratings in doped $LiNbO_3$ using low intensity laser beams without the need for chemical development as with photographic film. This stimulated not only investigations concerned with the physical understanding of the effect itself, but also a large number of applications ranging from optical mass memory storage in volume media to non-linear wave-mixing, all resulting from the ability to form gratings in real time and to store them for long periods of time (e.g. few day to months kept in dark room for doped $LiNbO_3$ crystals).

The photorefractive effect is defined as spatial modulation of the index of refraction due to charge redistribution in an optical non-linear material. The effect arises when charge carriers, photogenerated by a spatially modulated light intensity, separate by drift and diffusion processes and become trapped to produce a non-uniform space-charge distribution. The resulting internal space-charge electric filed modulates the refractive index to create a phase grating which can diffract a light beam. This photorefractive response can be considered as a third-order non-linear effect relating the index change to the excitation light intensity. However, at variance with other third-order phenomena, the photorefractive index gratings are non-local effects due to charge redistribution within the crystal, and involve the photoionisation, transport, and retrapping of charge carriers. The photorefractive effect is most often explained mathematically by means of a set of equations introduced by Kukhtarev et al. [Kuk79]. Here, we present two models that explain the nature of the photorefractive effect.

2.2.1 The physics of the photorefractive effect: band-transport and hopping models

To understand these models and to investigate the response of the material we consider the effect of a sinsoidal interference pattern, as would be produced by interfere of two mutually coherent plane waves, a pump beam and a signal beam, generated from a laser at an angle, θ, to one another (Fig. 2.4(a)) in a photorefractive material.

Fig. 2.4 *The generation of a sinusoidal interference pattern in a photorefractive material: (a) experimental arrangement and (b) wavevector diagram.*

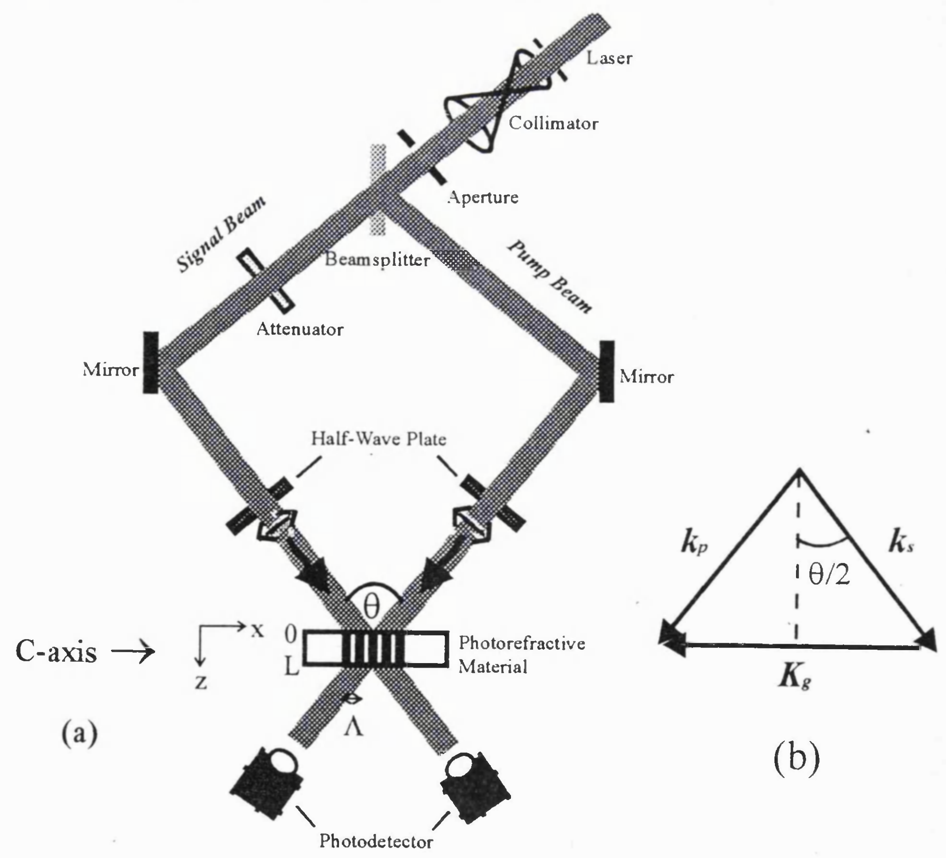

The two coherent beams with wavevectors $\boldsymbol{k}_p$ and $\boldsymbol{k}_s$ are made to interfere inside the crystal and induce a light intensity grating with period $\Lambda=2\pi/K_g$, $\boldsymbol{K}_g=\boldsymbol{k}_p-\boldsymbol{k}_s$ being the grating wavevector) Fig. 2.4(b)). Then, the photorefractive effect gives rise to an associated refractive index pattern with the same period, and allows charge separation to take place, which may be electron migration in a conduction band, hole migration in a valence band, or both.

Fig. 2.5 *Model of the photorefractive effect in a photorefractive medium (the carriers are electrons). (a) Band-transport model. (b) Hopping model.*

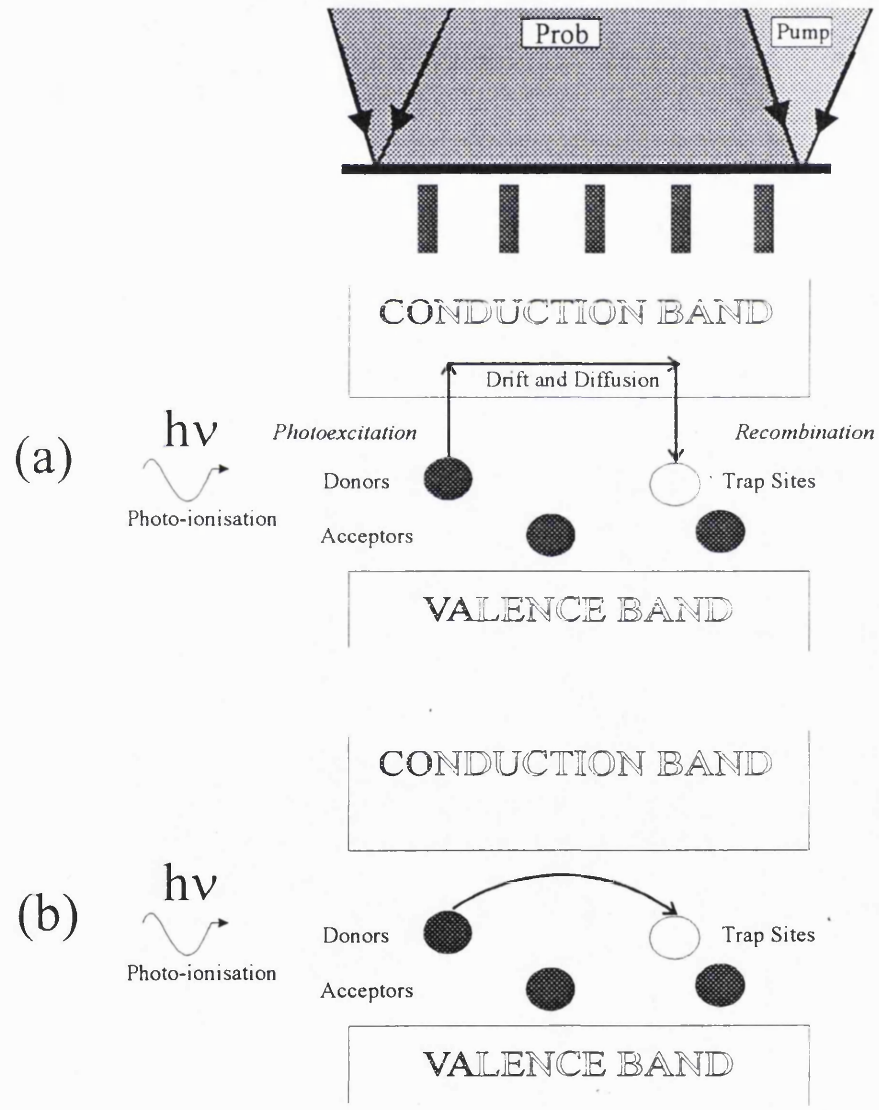

Fig. 2.5 shows the band-transport [Kuk79] and hopping models [Fei80]. In the first, a majority carrier (electron) is photoexcited into the conduction band, then drifts and diffuses through the band, and finally is trapped by a donor site left vacant by

recombination. A charge distribution corresponding to the intensity distribution is thought to migrate by drift or diffusion as a unit [Kuk79]. On the other hand, in the hopping model an electron on absorbing a quantum of energy has a constant probability of hopping to adjacent donor sites. A carrier distribution matching the intensity distribution is thought to be formed in the medium [Fei80].

The two models are in agreement when the modulation of the charge distribution is low [Mul85 & Duc86]. If the electric field distribution is described in terms of the charge distribution, both models can be treated similarity. Simple models of the photorefractive effect consider only one charge species and, although in reality this depends upon the material, the main properties of the photorefractive effect can be established by considering electrons only. Basically, the generation of phase-conjugate light can be explained by means of a band-transport model.

Now, if the intensity $I(\boldsymbol{r})$ of the light within the crystal (shown in Fig. 2.6(a)) is non-uniform, the charge density $\rho(\boldsymbol{r})$ (Fig. 2.6(b)) within the material will become nonuniform, because electrons will tend to migrate from regions of high intensity to regions of low intensity. This non-uniform charge distribution will produce a non-uniform static electric field $\boldsymbol{E}_{st}$ in accordance with Poisson's equation

$$\varepsilon_0 \nabla \cdot \left(\varepsilon \cdot \boldsymbol{E}_{st}(\boldsymbol{r})\right) = \rho(\boldsymbol{r}). \tag{2.4}$$

In the scalar approximation [Kuk79], the change in refractive index is given by

$$\Delta n(\boldsymbol{r}) = -\frac{1}{2} n^3 r_{eff} \boldsymbol{E}_{st}(\boldsymbol{r}) \tag{2.5}$$

where n is the mean refractive index and r_{eff} is the appropriate combination of components of the electro-optic tensor. For simplicity, for example, we assume two beams of light interfere within the crystal to produce an intensity distribution of the form $I(\boldsymbol{r})=I_0+I_1\cos qx$. Under most circumstances, the spatial distribution of charge density within the crystal will then be of the form $\rho(\boldsymbol{r})= \rho_1\cos qx$, where the amplitude of the charge density variation depends on the material properties of the optical medium. From Eq. 2.4, the spatial variation of the static electric field will be of the form $E_{st}(\boldsymbol{r}) = E_{st}^0 + E_{st}^1 \sin qx$ and, according to Eq. 2.5, and the change in refractive index will be of the form $\Delta n(\boldsymbol{r})=n_1\sin qx$.

Fig. 2.6 *Photorefractive index gratings produced by a pair of interfering (Fig. 2.4) The periodic variation of the intensity in the crystal creates a space-charge separation which mimics the intensity pattern. The space-charge field induces an index grating in the medium via Pockel's effect. This static electric field will change the optical properties of the material by means of the linear electro-optic effect. Λ is the index grating spacing and φ is the phase difference between I(r) and Δn(r).*

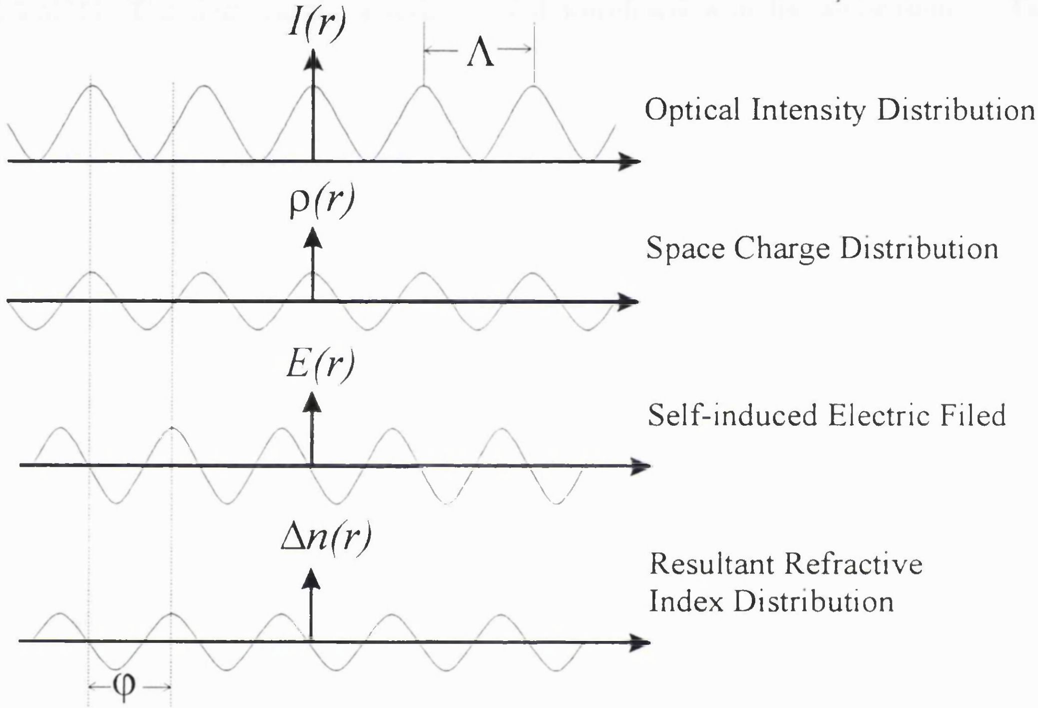

Note that $\Delta n(r)$ (as shown in Fig. 2.6(d)) is shifted in phase φ with respect to the intensity distribution $I(r)$. This phase shift can lead to the transfer of energy between tow beams interacting in a photorefractive crystal called asymmetric two-beam coupling. This non-local property of the photorefractive effect arises from the physical motion of charges in the material, usually over a distance of the order of micrometres. A asymmetric two-beam coupling plays an important role in the operation of a PCM that operates by means of the photorefractive effect. If the coupling is sufficiently strong, the two-beam coupling gain may exceed the absorption and reflection losses of the example, and optical amplification can occur.

The photorefractive effect has been examined theoretically and experimentally in the family of photorefractive materials including the ferroelectric crystals of barium titanate ($BaTiO_3$) and strontium barium niobate (SBN), the sillenite crystals of bismuth silicon oxide (BSO), bismuth germanium oxide (BGO) and bismuth titanium oxide (BTO), along with semiconductor materials such as gallium arsenide (GaAs), indium phosphide (InP) and cadmium telluride (CdTe), and very recently organic compounds such as DMNPAA:PVK:ECZ:TNF. Some more thorough reviews and monographs on the effect have been published [Gün82, 87, 88, & 89, Hal85, Smi77, Fei88, Pep90, Pet91, Moe94, and Vol95]. The electrical characteristics of photorefractive media can be found in Table 2.1.

Table. 2.1 *Physical properties of materials existing the photorefractive effect.*

Parameter	$LiNbO_3$	$KNbO_3$	$BaTiO_3$	$Bi_{12}SiO_{20}$	SBN
Crystal symmetry Group	3m	4mm	4mm	$\bar{4}$3mm	4mm
Wavelength λ (μm)	0.515			0.515	0.515
Refractive Index n	2.3	2.23	2.4	2.6	2.35
Static Dielectric Constant ε	98 (ε_{11})	55	4300 (ε_{11}) 168 (ε_{33})	56	3400(ε_3)
Electro-optic Coefficient r_{ij} (pm/V)	31 (r_{33})	64 (r_{33})	1640 (r_{42}) 80 (r_{33})	5 (r_{41})	37 (r_{13}) 1340(r_{33})
Donor Density N_D (m^{-3})	10^{23}	-	-	10^{25}	-
Trap density N_A (m^{-3})	10^{22}	-	$2x10^{22}$	10^{22}	-
Ionic cross-section Area s (m^2)	-	-	-	$1.6x10^{-23}$	-
Coeff. of Recombination γ_R (m^3/s)	10^{-15}	-	$5x10^{-14}$	$2x10^{-17}$	-
Transition μ (m^2/Vs)	10^{-5}	-	$5x10^{-5}$	$3x10^{-6}$	-
Absorption Coeff. α (cm^{-1})	-	-	-	0.3	-
References	Car86	Gün88	Val83	Val83	Emb87

Table. 2.1 *Physical properties of materials existing the photorefractive effect (continued).*

Parameter	GaAs	InP	CdTe
Crystal symmetry Group	$\bar{4}3mm$	$\bar{4}3mm$	$\bar{4}3mm$
Wavelength λ (μm)	1.06	1.06	1.06
Refractive Index n	3.6	3.3	2.8
Static Dielectric Constant ε	12.9	12.7	9.4
Electro-optic Coefficient r_{ij} (pm/V)	1.4(r_{41})	1.45 (r_{41})	5.5(r_{41})
Donor Density N_D (m^{-3})	-	-	-
Trap density N_A (m^{-3})	1.5×10^{21}	2×10^{20}	$\sim 10^{21}$
Ionic cross-section Area s (m^2)	-	-	-
Coeff. of Recombination γ_R (m^3/s)	-	-	-
Transition μ (m^2/Vs)	-	-	-
Absorption Coeff. α (cm^{-1})	1.5	1.4	-
References	Val83	Fab88	Byl87

As shown above, various types of bulk material can show photorefractive effects in non-uniform illumination. In particular, the very different electrooptic responses are observed. We have summaried their advantages and disadvantages as follows:

(i) advantages:

(a) the ferroelectric photorefractive materials, such as $BaTiO_3$ and SBN, show the largest intrinsic photorefractive effects because of their large electrooptic properties. This gives rise to the larger nonlinear effects of fanning and self-pumped phase conjugation.

(b) the sillenite photorefractive crystals, such as BSO, BGO, and BTO, have response times in the region of milliseconds at CW laser power.

(c) the semiconductor photorefractive materials, such as GaAs, InP, and CdTe, have fast response times on the microsecond time scale, and can be used in the infrared with lower absorption making them compatible with current telecomunication technologies.

(ii) disadvantages:

(a) the ferroelectric photorefractive materials exhibit poor charge mobility that limits their speed of response to the order of seconds with CW laser powers.

(b) the sillenite photorefractive crystals exhibit small electrooptic effects

(c) the semiconductor photorefractive materials have small electrooptic coefficients which gives rise to small nonlinear effects.

For convenience, the photorefractive effects for semiconductors are also included. We see that the electro-optic coefficient of $BaTiO_3$ (r_{42}=r_{51}) is extremely large. High reflectance in the production of phase-conjugate light is obtained by this effect. That motivated us to use this kind of photorefractive material in this project.

2.3 Two-Wave Mixing (TWM)

The process of forming a refractive index variation pattern inside a nonlinear medium using two-beam interference (as shown in previous section) is identical to that for hologram formation. Such a refractive index variation is often periodic and is called a volume phase grating. Unlike the holographic process known traditionally, beam coupling occurs in real time. This is a unique property of photorefractive materials. In what follows, we briefly review the coupling and energy transfer of two beams inside a photorefractive material.

Consider the interaction of two beams inside a photorefractive medium (Fig. 2.7). If the two beams are of the same frequency, a stationary interference pattern is formed. Let the electric field of the two waves be written.

$$E_i(r,t) = A_i e^{j(\omega t - k_i \cdot r)}, \qquad i=1,2 \qquad (2.6)$$

where A_1, A_2 are the wave amplitudes, ω is the angular frequency, and k_1, k_2 are the wave vectors. For simplicity, we assume that both beams ate polarized perpendicular to the plane of incidence (i.e., s-polarised containing the 2 writing beams).

Within a scaling factor, the intensity can be written

$$I = |\boldsymbol{E}|^2 = |\boldsymbol{E}_1 + \boldsymbol{E}_2|^2 . \tag{2.7}$$

Fig. 2.7 *Schematic diagram illustrating the basic geometry for photorefractive two-wave mixing (TWM).*

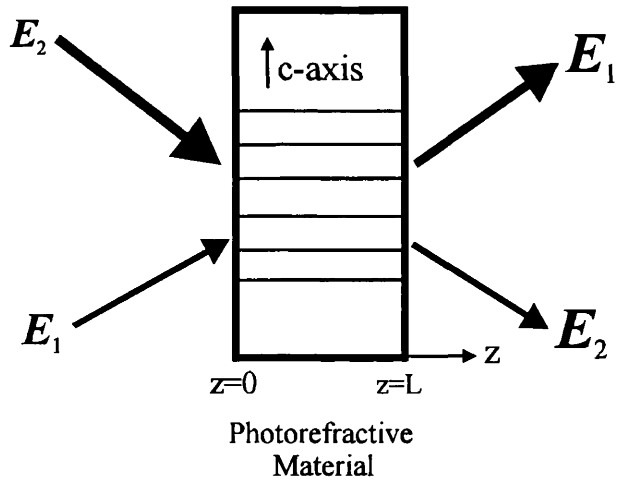

Using Eq. (2.6) for the electric field, the intensity of flight in the medium can be written

$$I = |A_l|^2 + |A_2|^2 + A_1^* A_2 e^{-j\boldsymbol{K}\cdot\boldsymbol{r}} + A_1 A_2^* e^{j\boldsymbol{K}\cdot\boldsymbol{r}} \tag{2.8}$$

where

$$\boldsymbol{K}=\boldsymbol{k}_2-\boldsymbol{k}_1 \tag{2.9}$$

and $|\boldsymbol{K}| = 2\pi/\Lambda$, where Λ is the period of the fringe pattern. The intensity [Eq. (2.8)] has a spatial variation inside the photorefractive material. According to Kukhtarev's model [Kuk79], such an intensity pattern will generate and redistribute photocarriers, creating a space-charge field in the material. This field induces a volume refractive index grating due to the Pockels effect. In general, the index grating will have spatial phase shift relative to the interference pattern [Vin79] as described in the previous section. The refractive index, including the fundamental component of the intensity-induced gratings, can be written

$$n = n_0 + \left[\frac{1}{2} n_1 e^{j\varphi} \frac{A_1^* A_2 e^{-j\boldsymbol{K}\cdot\boldsymbol{r}}}{I_0} + c.c.\right] \tag{2.10}$$

where

$$I = I_1 + I_2 = |A_l|^2 + |A_2|^2 \tag{2.11}$$

n_0 is the refractive index when no light is present, φ is real, and n_1 is a real and positive number. For the sake of simplicity, we assume a scalar grating. The phase φ indicates the degree to which the index grating is shifted spatially relative to the intensity pattern. In a photorefractive material that operates by diffusion only (i.e., no external static field), for example, $BaTiO_3$, the magnitude of φ is π/2 with its sign depend on the direction of the c-axis. $\boldsymbol{K}$ is the grating wave vector given by Eq. (2.9). The parameter, n_1, depending on the grating spacing and direction and on the material properties of the crystal, e.g., the electro-optic coefficient. Expressions for $n_1 e^{j\varphi}$ can be found in Ref. [Kuk74] and in [Fei80 & 81, Duc84].

The spatial phase shift between the interference pattern and the induced volume index grating [Ash66 & Vin79] allows for non-reciprocal steady-state transfer of energy between the laser beams [Kuk73, Mar79, & Mar81]. To investigate the coupling, we substitute Eq. (2.10) for the refractive index and $\boldsymbol{E}=\boldsymbol{E}_1+\boldsymbol{E}_2$ for the electric field into the wave equation. This leads to a set of coupled wave equations

$$\begin{aligned} \frac{dA_1}{dz} &= \gamma \frac{A_1 A_2^* A_2}{I_1 + I_2} - \frac{\alpha A_1}{2} \\ \frac{dA_2}{dz} &= -\gamma^* \frac{A_2 A_1^* A1}{I_1 + I_2} - \frac{\alpha A_2}{2} \end{aligned} \tag{2.12}$$

where A_j are the slowly varying amplitudes of the optical electric fields; $I_j = |A_j|^2$ are the respective intensities; α is the incident intensity absorption per unit length, and γ is the coupling strength per unit length.

The solution for the incident intensities $I_1(z)$ and $I_2(z)$ are [Feinberg80]

$$I_1(z) = I_1(0)\frac{1+1/q}{1+(1/q)e^{-\gamma z}}e^{-\alpha z}, \tag{2.13}$$

$$I_2(z) = I_2(0)\frac{1+q}{1+qe^{-\gamma z}}e^{-\alpha z} \tag{2.14}$$

where z is normal to the crystal surface and q is the input intensity ratio

$$q = \frac{I_1(0)}{I_2(0)}. \tag{2.15}$$

In the absence of absorption (i.e., $\alpha=0$), $I_2(z)$ is an increasing function of z and $I_1(z)$ is a decreasing function of z, provided γ is positive. The sign of γ depends on the direction of the c-axis. As a result of the coupling for $\gamma>0$ beam 2, $\boldsymbol{E}_2$, gains energy from beam 1, $\boldsymbol{E}_1$. If this two-wave mixing gain is large enough to overcome the absorption loss, then beam 2, ($\boldsymbol{E}_2$) is amplified. This amplification enhances fanning which will be described in detail in the next section, stimulated scattering and can cause oscillation of a laser beam in a photorefractive crystal [Fei82, McM87].

If we refer to $\boldsymbol{E}_2$ as the signal beam, then a useful parameter is the gain

$$G=\frac{I_2(z)}{I_2(0)}=\frac{1+q}{1+qe^{-\gamma z}}e^{-\alpha z} \tag{2.16}$$

where we recall that q is the intensity ratio at input face (z=0). For the particular case where $I_2<<I_1$, Eqs 2.13 & 2.14 lead to $I_1(z)\approx I_1(0)\approx I_0$ and $I_2(z)\approx I_2(0)e^{\gamma z}$ indicating that the weak beam experiences an exponential growth (beam amplification), whereas the strong, pump, beam becomes only slightly depleted. The logarithmic gain per unit length is γz, i.e. it occurs when there is no phase shift $\varphi\neq 0$ between the incident light distribution and the refractive index grating. The gain coefficients γ are large ($\geq$10 cm^{-1}) for $LiNbO_3$, $BaTiO_3$, and $KNbO_3$, and small ($\leq$1 cm^{-1}) for BSO and GaAs. A value γ=16.3 cm^{-1} has been reported for semiconductor gallium arsenide when recording is performed with a wavelength near the band edge [Par89]. The gain in a material such as BSO can be significantly enhanced by applying alternating electric fields [Ste85] or by oscillating the light interference fringes during recording when a DC filed is applied [Hui81, Ste82, Reg85, & Buc95]. Gains as high as 20 or more have been reported for BSO. The increase in γ can be understood as a resonance effect enhancing the $\pi/2$-shifted component of the complex amplitude of the field. Now, we consider the amplification of a weak signal beam with intensity $I_2(0)=1.0\text{x}10^{-6}$ W/cm^2 by using a photorefractive $BaTiO_3$ crystal. Let the pump beam intensity be $I_1(0)=1.0\text{x}10^{-3}$ W/cm^2 and the coupling strength be $\gamma L=10$. The intensity gain, according to Eq. (2.16), is $G=958$ assuming $\alpha=0$. If the signal beam intensity is $I_2(0)=1.0\text{x}10^{-8}$ W/cm^2, the gain becomes $G=9.6\text{x}10^4$.

The process [i.e., energy gain (loss) in the signal (pump) beam] can be explained by the self-diffraction of the pump (signal) beam by the dynamic volume hologram written by the two beams in conjunction with the constructive (destructive) interference of the diffracted component of one beam with the transmitted component of the other. The photorefractive coherent amplifier, in which a signal beam is amplified by a coherent pump beam, has been incorporated into many applications such as into a two-wave mixing beam steering system [Rak84] and into a beam deflector [Mat93]. It has also been used in a ring resonator/oscillator which will be discussed later in Section 2.6.6 of this chapter.

2.4 *Four-Wave Mixing (FWM)*

When two counterpropagating (pump) waves and a third input (probe) wave interact inside a nonlinear medium, a phase conjugate replica of the signal (probe) wave is generated (Fig. 2.8). This process is known as four-wave mixing [FWM] [Yar78, Spe86]. FWM generally denotes the interaction of four light waves with different frequencies $\omega_1 ... \omega_4$ and propagation directions $k_1 ... k_4$. The interaction is due to a third-order nonlinear polarization of the material leading to a number of different effects, such as third-harmonic generation and Raman-type frequency mixing. These effects have been investigated extensively [Blo79] since the pioneering work of some researchers [Yab74, Lev74, Mak75] in this area.

Fig. 2.8 *Grating interpretation of FWM, (a) schematic diagram, (b) grating due to E_4-E_1 interference, and (c) grating due to E_4-E_2 interference.*

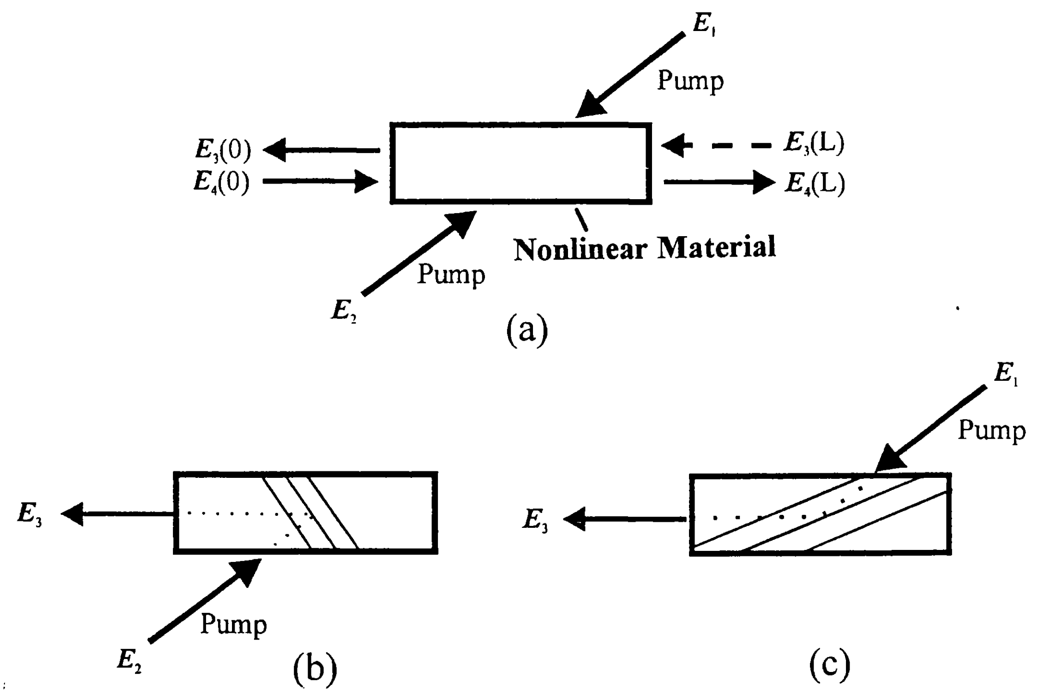

In degenerate four-wave mixing (DFWM), the frequencies of the incident light waves are equal ($\omega_1=\omega_2=\omega_3=\omega_4=\omega$) and the wave vectors are mutually antiparallel in pairs $k_1=-k_2$, $k_3=-k_4$ in the k-matching condition ($\Sigma k=0$). This is only one possible form of degeneracy, so that the term DFWM is not fully specific. In the simplest but experimentally most important form of FWM especially for understanding our new discoveries (described in Chapter 4, 5, and 6), only two pump waves with $\omega_1=\omega_2=\omega$ and $k_1=-k_2$,, and a signal wave with $\omega_4=\omega$ and k_4 arbitrary are incident on the nonlinear material (Fig. 2.8(a)). Due to the third-order polarization, a reflected wave with $\omega_3=\omega$ is created which has the opposite direction $k_3=-k_4$ to the probe wave. If a fourth wave, E_3, with $k_3=-k_4$ is incident, this wave can be amplified [Cro84].

The FWM process can be viewed as the writing of a real-time volume grating by two interacting waves and the simultaneous readout of the grating by the third wave. The recording implies the formation of four refractive index caused by the interference of all pairs of waves:

(a) a transmission grating formed by E_1-E_4 and E_2-E_3,

(b) a reflection grating formed by E_1-E_3 and E_2-E_4,

(c) $2k$ grating formed by E_1-E_2 and E_3-E_4.

In particular, the conjugate of the signal wave arises from the diffraction of wave E_2 by the transmission grating. Consider the transmission case, the incident waves E_4 and E_1 interfere (Fig. 2.8(b)) and induce a grating with a vector $K_g=k_4-k_1$. Bragg diffraction of E_2 leads to the wave E_3 with $k_3=k_2-K_g=k_2-k_4+k_1=k_4$. A second contribution to the wave E_3 comes from the grating that is produced by the interference of E_4 and E_2 and diffracts the wave E_1 (Fig.2.8(c)). In the case of an instantaneous, non-local and linear response of the material, the two contribution to the reflected wave are equal and in phase and it is sufficient to consider only the grating which is produced by interference of E_4 and E_1.

In order to understand the essential interaction amongst the four waves in a photorefractive material we use the kogelnik coupled-wave approach [kog69]. Consider now that such a photorefractive medium interacts with three incident electromagnetic waves of the same frequency and polarization:

$$E_i(r,t)=A_i e^{j(\omega t-k_i\cdot r)}, \qquad i=1,4 \qquad (2.17)$$

causing a refractive index pattern made up of the four gratings, transmission, reflection, and two $2k$ gratings. The general expression for the complex refractive index, n, is

$$n = n_0 + \left[\frac{1}{2} n_1 e^{j\varphi} \frac{A_1^* A_4 + A_2 A_3^*}{I_0} e^{-jK \cdot r} + c.c. \right] \tag{2.18}$$

where only the transmission grating has been considered, $I_0 = \sum |A_i|^2$ and n_0 is the average refractive index of the materials.

In order to obtain the stead-state solution, we substitute the index distribution equation (2.18) into the Helmholtz scalar equation to yield four coupled differential equations for the z-dependence of the complex wave amplitudes. The general solution of these coupled equations is given in reference [Cro84]. A very simplified situation, while reatining the main features of the effect, occurs under the following assumptions:
(i) lossless medium; (ii) predominant transmission grating; (iii) undepleted pump approximation, i.e. I_1, $I_2 >> I_3$, I_4, where $I_i = |A_i|^2$, so that I_1 and I_2 remain constant.

According to assumption (ii) one can infer that the z-dependence of wave E_4 arises from diffraction of wave E_2 by the transmission grating. For the transmission grating geometry of Fig. 2.9, the coupled equations can be obtained from those derived by Kogelnik [kog69], and can be written as

Fig. 2.9 *Optical phase conjugation by FWM. The PCM consists of a non-linear medium interacting with two counterprogating pump beams E_1 and E_2.*

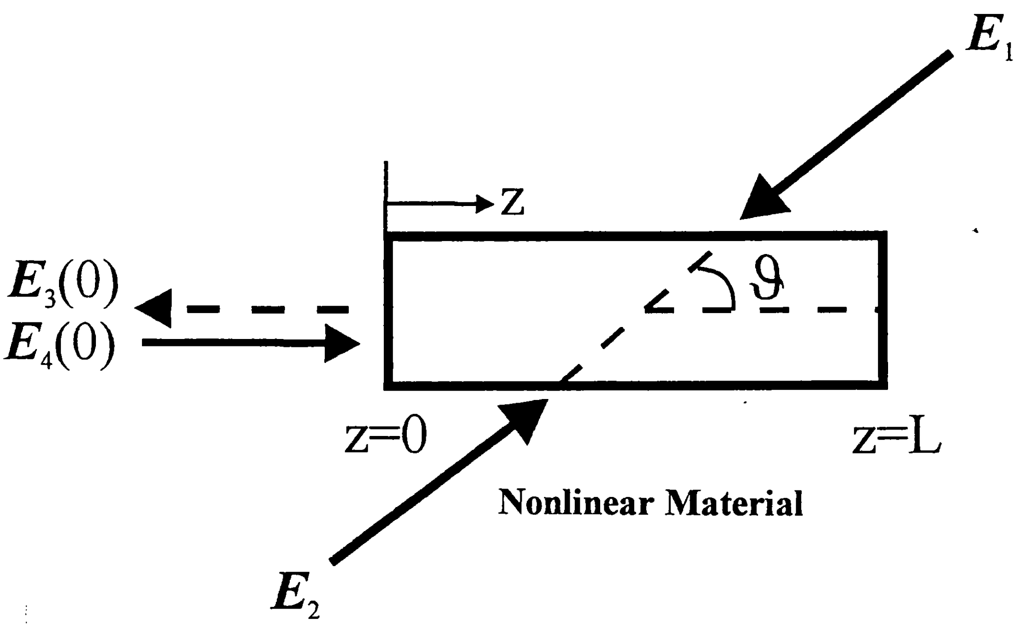

$$
\begin{aligned}
&\frac{dA_1(z)}{dz} = 0 \\
&\frac{dA_2(z)}{dz} = 0 \\
&\frac{dA_3^*(z)}{dz} = j\kappa \frac{A_1^* A_4 A_2^* + A_1 A_1^* A_3^*}{I_0^2} \\
&\frac{dA_4(z)}{dz} = j\kappa \frac{A_1 A_2 A_3^* + A_2 A_2^* A_4}{I_0^2}
\end{aligned}
\tag{2.19}
$$

where $\kappa = \left(\omega n_1 e^{j\varphi}\right)/2c\cos\vartheta$ is the appropriate coupling constant applicable to diffraction by transmission grating. And, the boundary condition are $A_3(0) = A_4(0)$ and $A_4(L) = 0$.

The solution is as follows [Cro84],

$$
\begin{aligned}
&A_1(z) = A_1(0) \\
&A_2(z) = A_2(L) \\
&A_4(z) = -\frac{A_2(L)A_3^*(0)}{A_1^*(0)} \frac{e^{-j\kappa L} - e^{-j\kappa z}}{m_p + e^{-j\kappa L}} \\
&A_3^*(z) = -A_3^*(0)e^{-j\kappa z} \frac{m_p + e^{-j\kappa L(z-L)}}{m_p + e^{-j\kappa L}}
\end{aligned}
\tag{2.20}
$$

where $m_p = |A_2(0)|^2/|A_1(L)|^2$ is the pump ratio. The phase-conjugate reflectivity, r_c, is obtained from the value of $A_3(z)$ in the plane z=0,

$$
\begin{aligned}
r_c &= \frac{A_4(z)}{A_3^*(0)} = -\frac{A_2(L)}{A_1^*(0)} \frac{1 - e^{-j\kappa L}}{m_p + e^{-j\kappa L}} \\
&= -\left(\frac{A_1 A_2}{A_1^* A_2^*}\right)^{\frac{1}{2}} \frac{\sinh(j\kappa L/2)}{\cosh(j\kappa L/2) + \frac{1}{2}\ln m_p}.
\end{aligned}
\tag{2.21}
$$

2.4.1 FWM Amplification (Gain)

FWM in photorefractive media provides phase conjugation and energy coupling between beams of coherent radiation. Significant signal beam amplification can be achieved under the appropriate conditions. If such amplification is introduced into a resonator, oscillation can be easily achieved. In this section, we discuss the amplification by FWM under the appropriate conditions required for it to occur. In practice, with two equal intensity pumps, the phase-conjugate reflectivity, r_c, can be simplified

$$r_c = \tanh\left(\frac{j\kappa L}{2}\right) \tag{2.22}$$

and intensity reflectivity $R_c = |r_c|^2$ is

$$R_c = \frac{I_4(0)}{I_3(0)} = \tanh^2\left(\frac{j\kappa L}{2}\right) \tag{2.23}$$

This formula, obtained independently by Yariv and Pepper [Yar77] and Bloom and Bjorklund [Blo77], shows that, for $\kappa L>\pi/2$, the reflectivity is larger than 100%. Under theses conditions the phase-conjugate mirror has gain. Reflectivity much higher than 100% have been experimentally observed by several groups, and values of R_c of the order of 10^2 (10^4 %) are not uncommon. In fact, optimum reflectivity result for pump beams having unequal intensities. More details about the dependence of r_c and R_c on κL are given in reference [Cro84]. The possibility of oscillation (parametric oscillator) can be easily achieved by using a FWM phase-conjugate mirror with reflectivity, R_c, larger than 100%.

2.5 Beam Fanning Effect

Photorefractive beam fanning [Ash66, Cro82] is a common phenomenon in which a primary incident beam is scattered into a broad asymmetric fan as it propagates through a photorefractive crystal. In photorefractive crystals with a large two-beam coupling (TBC) coefficient, for example, $BaTiO_3$ and SBN crystals [Fei82a], beam fanning is strong. It is a decisive factor in enabling self-pumped phase-conjugation to occur [Fei80 & 82a, Cro84]. However, in some cases beam fanning is undesirable; for example, it may prevent high-gain signal amplification in TWM in thick photorefractive crystals [Fai86, For89, Vas91]. As a result, various methods to suppress beam fanning have been proposed [Rab91, Jos90, & Raj89]. The existence of beam fanning can, thus, greatly influence the optical nonlinear coupling in photorefractive materials. Various studies of the mechanism of beam fanning have been reported [Vor80, Rup86, Val87, & Fei82a]. In this section we will introduce the basic concept of beam fanning in photorefractive crystals that is very relevant to the research reported in this thesis.

When a laser beam passes through a photorefractive medium, it may encounter some scattering centers in the medium. The scattered light appears to be asymmetrical with respect to the beam except for propagation along the c-axis. Although the fraction of energy scattered may be extremely small, the energy transfer process described in Section 2.3 can take place between the scattered beams and the main beam, resulting in the amplification of the scattered components. Consequently, the output intensity exhibits a very non-uniform spatial distribution [Fei82a], which is shaped like a fan when observed on a plane normal to the direction of the beam propagation; hence, the name "beam fanning".

The beam fanning originates from the energy coupling between the incident beam and the scattered beams. Scattering due to surface roughness, refractive index inhomogeneity, impurities in solids, etc., occurs when a beam of light passes through a photorefractive crystal. If the incident beam has a finite transverse cross section, the scattered beam has a large number of angular components, the overlap leads to the formation of photo-induced gratings. Depending on the orientation of the crystal, some of the angular components may be amplified by the incident beam via the energy transfer of TBC. The amplified scattering can be quite strong as many of the phptorefractive media exhibit strong coupling strengths (i.e.,γL), even though the initial scattering is quite small. Photorefractive beam fanning plays an important role in the initiation of many phase conjugators and resonators, even though the fanning itself can be a source of noise in many experimental measurements.

2.6 Phase-Conjugate Mirrors (PCMs)

Photorefractive phase-conjugate mirrors (PCMs) with several different configurations have been constructed that exploit the properties of the photorefractive effect. In this section, we discuss all of the designs which are shown in Figures 2.10-2.15. These are self-pumped phase-conjugate mirrors (SPPCMs) (Section 2.6.1 - 2.6.3), mutually pumped phase-conjugate mirrors (MPPCMs) (Section 2.6.5), and a type of PCM (Section 2.6.4) called an induced self-pumped phase-conjugate mirror (ISPPCM) which I developed before starting my PhD thesis research. The designs are described briefly in the sections following in turn.

2.6.1 Self-pumped phase-conjugate mirror (SPPCM)

A series of photorefractive "self-pumped" phase conjugators were developed [Fis81, Whi82, Cro82a, 82b, 83 & 84, and Fei82] which did not require external pump beams. The various devices are shown in Fig. 2.10. They include a unidirectional ring oscillator based on TWM [Whi82], and others based on FWM. All of these devices share the ability to self-generate, as an output beam, the phase conjugate of image-bearing input beams and also these oscillators are known as self-pumped phase-conjugate mirrors (SPPCMs).

Fig. 2.10 *Self-pumped phase conjugators: (a) using FWM in a photorefractive crystal with a "linear" cavity, (b) using FWM in a photorefractive crystal with a "semi-linear" cavity, (c)operating through FWM in a photorefractive crystal using total internal reflection from acorner of the crystal, and (d) operation through TWM in a photorefractive crystal with a "ring" cavity.*

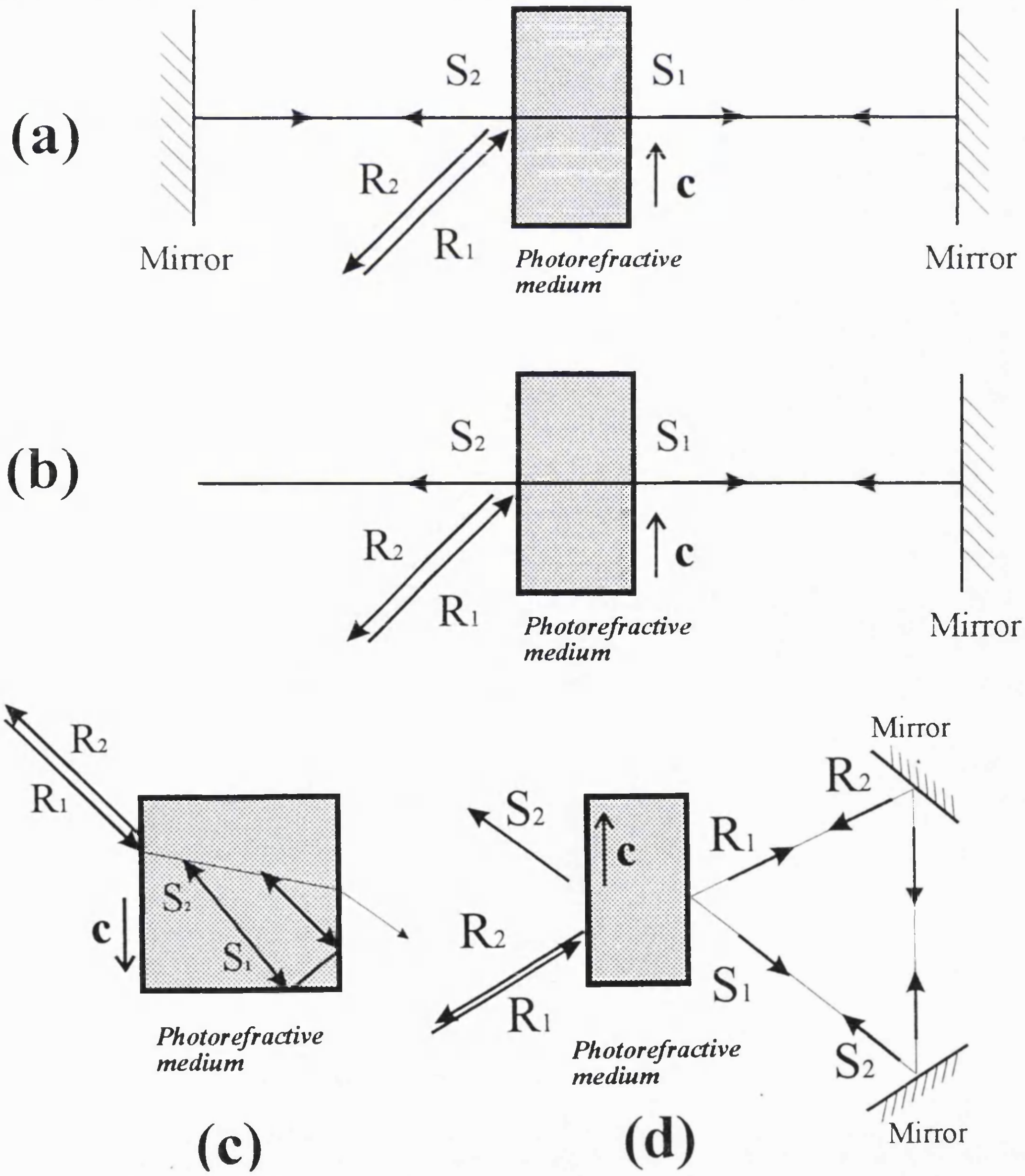

The first SPPCM was the linear configuration demonstrated by White [Whi82]. It consists of a photorefractive crystal placed between two mirrors that have been carefully aligned to form a resonator cavity (Fig. 2.10(a)). The input beam causes a pair of counterpropagating beams to form between the two mirrors. These self-generated beams serve as "pump" beams to generate the phase-conjugate signal by FWM. Once the device is working, one of the resonator mirrors can be removed (Fig. 2.10(b)), although the device needs both mirrors in order to start [Cro82].

Subsequently, the total-internal reflection SPPCM (Fig. 2.10(c)) was developed. This is also known as theTIR, or the two-interaction region or the "cat" SPPCM) [Fei82]. This phase conjugator also generates its own pump beams, but the self-generated pump beams are contained completely inside the crystal by internal reflection at the crystal faces (Fig. 2.10(c)). In addition, the pump beams automatically self-align to maximise the phase-conjugate gain. In 1983, Cronin-Golomb et. al. [Cro83] demonstrated a self-pumped phase conjugator that uses mirrors to deflect the incident beam into a ring that loops back k into the photorefractive crystal (Fig. 2.10(d)). All of these oscillators included some type of optical feedback to the interaction region, either through an external ring or through linear paths, or through an internal reflecting loop within the crystal. Since no external pump is needed, it is possible to use the SPPCM as a mirror of a laser resonator, with the ability to oscillate and correct in real time for intracavity phase distortions [Cro82, McF83].

2.6.2 Cat-total internal reflection SPPCM

In order for comparing with our novel phase conjugators, which will be demonstrated in detail in Chapters 4 and 5, this section we describe “cat” phase conjugator in more detail.

Figure 2.11 shows a schematic of a SPPCM using two crystal faces as internal reflectors. Abeam entering the crystal from the left with extraordinary polarization (Fig. 2.11(a)) suffers asymmetric self-defocusing or fanning in the plane formed by the incident beam and the +c axis of the crystal, creating a fan of light that illuminates the sidefaces of the crystal (Fig. 2.11(b)) [Mac83, Fei82b]. The edge act as a two-dimensional corner reflector and, by means of two total internal reflections, it directs the fan of light back towards the incident beams.

Fig. 2.11 *"Cat" SPPCM formed by beam bending through the photorefractive effect and reflection from a crystal corner. (a): incident beam passing through the $BaTiO_3$ crystal before the photorefractive grating is built up; (b): beam bending and fanning; (c): beam bending and reflection from crystal corner after photorefractive gratings have built up; (d): schematic of FWM giving phase conjugation.*

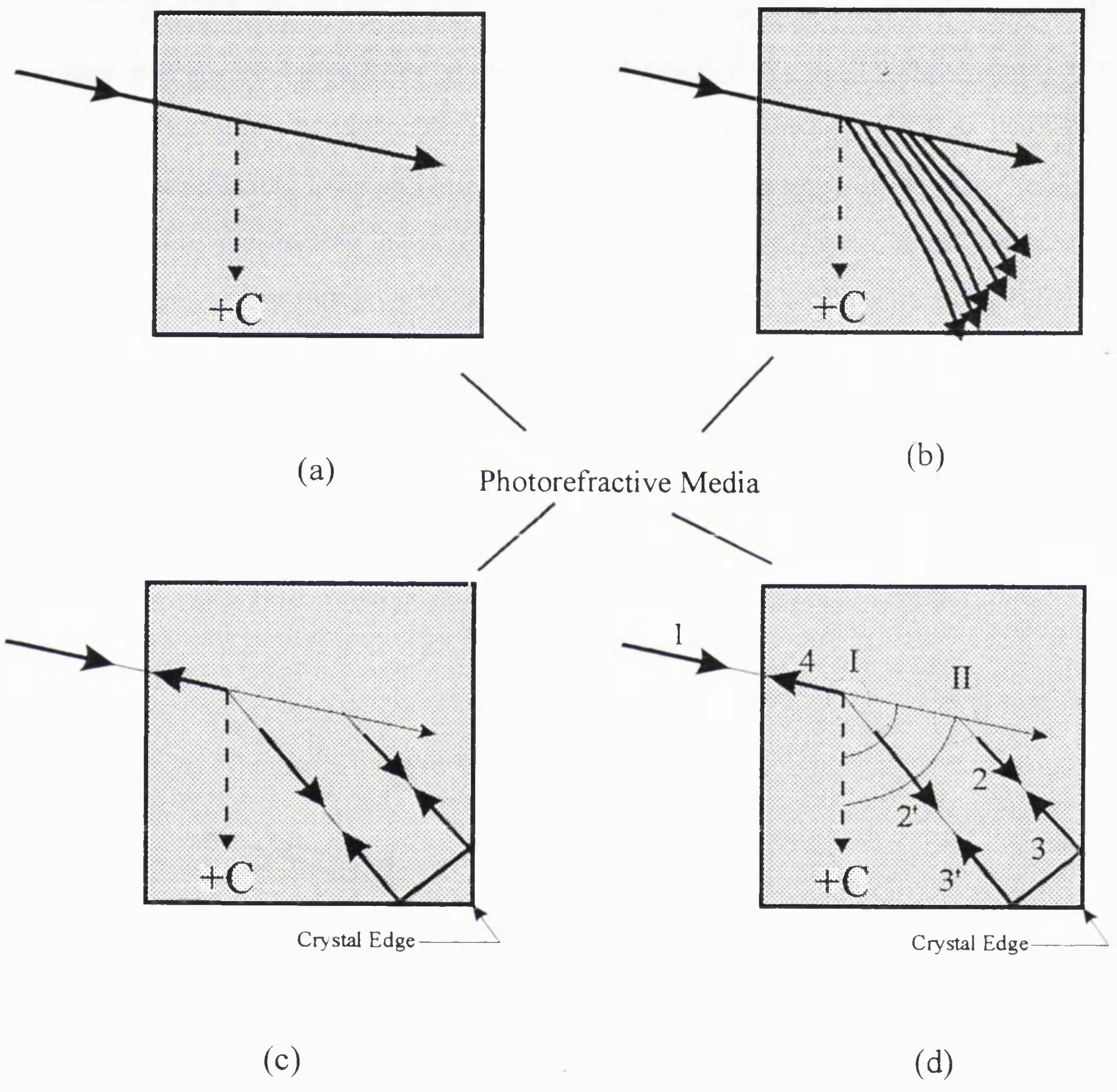

Fig. 2.11(c) shows that the fan actually collapses into at least two narrow beams (scattered light beams). The scattered light beam, 2' (2), created in interaction region I (II) is reflected twice by adjoint faces in the high-gain $BaTiO_3$ crystal to become beam 3 (3'). It is speculated [by Feinberg et. al. [Fei82b] that each beam is composed of a pair of counter propagating beams, so there are two counter propagating loops of light in the crystal, see Fig. 2.11(d). Each pair of counter propagating beams interacts in each

interaction region, through photorefractive gratings, with the incident beam (1) to create the phase-conjugate signal beam (4). The phase-conjugate beam leaves the crystal exactly back along the direction of the incident beam. Phase-conjugate reflectevities typically of up to 30% have been measured in this configuration [Fei82b].

2.6.3 Other internal reflection SPPCMs

Another configuration for a SPPCM that is completely self-contained is shown in Fig. 2.12 [Gün85]. The object beam incident through face A fans towards the face B which is covered by a reflecting layer and reflects the diffracted wave towards the face C which is also covered by a reflecting layer. Each pair of counter propagating beams between the mirrors B and C act as pump beams and mix with the incident beam by the photorefractive effect to create a phase-conjugate beam. Depending on the orientation of the crystal with respect to the incident beam direction , the phase-conjugate beam can have a stable reflectivity, but it may also self-pulsate or oscillate in a chaotic manner [Gün85].

Fig. 2.12 *SPPCM formed by beam fanning through the photorefractive effect with internal reflections from a pair of parallel mirrors coated crystal faces.*

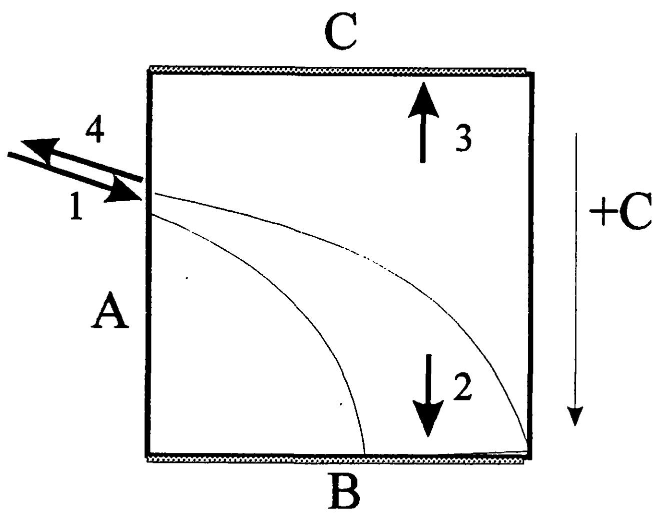

These self-pumped phase-conjugate mirror configurations that need no external mirrors and which are both self-starting were demonstrated in $BaTiO_3$ crystals (Figs. 2.11 and 2.12) [Fei82a, Gün85]. The pump beams are self-generated from the incident wave and are internally reflected at the crystal faces. Since the pump beams do not leave the crystal, the device is compact, relatively insensitive to vibration, and completely self-aligning. The quality of phase conjugation by the above device was demonstrated by focusing complicated images into the crystals and observing the faithfulness of reproduction even though the image-bearing input and output beams passed through a severe phase aberrator.

It is worth mentioned that the above two SPPCMs [Fei82, Mac83, Gün85] depend on beam fanning inside the photorefractive crystal for their initiation, the magnitude of which relies on the number of scattering centres (or imperfections) encountered by the input beam and the interaction length of the two beam coupling occuring between the input beam and the scattered light. However, if we want to optimise the reflectivity and response time of SPPCMs, the angle, position, and intensity of the incident beam must satisfy some critical conditions. The use of a spherical lens to focus the signal beam tightly decreases the fanning response time by increasing the intensity (power density) but reduces the magnitude of the beam fanning by decreasing both the number of scattering centres accessed and the two-beam coupling interaction length. Use of a cylindrical lens to produce a line focus parallel to the extraordinary polarization direction increases both the number of scattering centres accessed in the high-gain direction and the interaction length and results in an order-of-magnitude decrease in the self-pumped phase-conjugate response time [Sal91].

2.6.4. Induced self-pumped phase-conjugate mirrors (ISPPCM)

If we introduce an additional suitable "inducing" beam into the crystal, the SPPCM can be established more easily and achieve high reflectivity and shorter response times in photorefractive media. The details are discussed below:

Fig. 2.13 shows the configuration for the induced self-pumped phase-conjugate mirror (ISPPCM). The beam to be conjugated was first adjusted so that alone it caused no conjugate wave occur. Depending on the impinging position and incident angle, it fanned to surface D and reflected to surface C (see Fig. 2.13(a)). The inducing beam was then allowed to impinge on the crystal. Only after, the inducing beam had been switched on and had deflected to the lower right corner of the crystal the self-pumped phase-conjugate output was observed.

Fig. 2.13 *Induced SPPCM (a) The geometry of divergent beam to be phase conjugated inside the crystal before the inducing beam impinges on the crystal. (b) The inducing be is turned on so two beams enter the crystal. (c) The schematic diagram of the proposed 4-interaction-region model.*

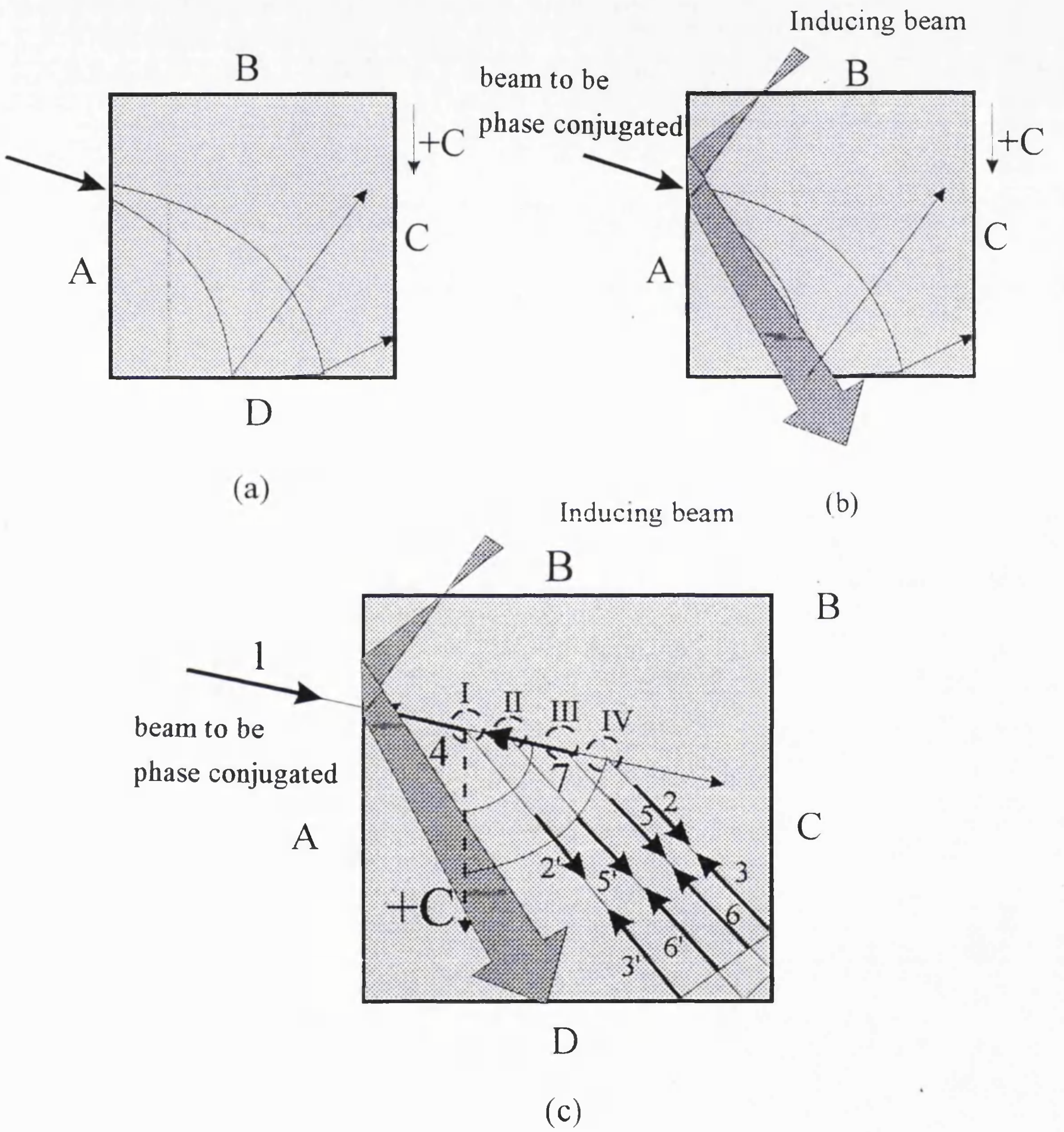

One model was proposed to explain this phenomenon by Prof. Yau and myself [Yau92] in Taiwan before I began the research for this thesis. We speculated that the various portions of the scattered light of the inducing beam interfere with one another and establish a complicated grating system since they themselves are coherent. When the incident beam to be phase conjugated falls on this grating system, some parts of it will deflect to the lower right corner and will satisfy the conditions for self-pumped four-wave mixing (as shown in Fig. 2.13(b)). An induced self-pumped phase-conjugate wave, thus, is generated. According to this model, the more intense is the inducing beam, the more prominent is the grating system; thus, the incident beam to be phase conjugated has a better chance of meeting the self-pumping conditions and this may result in a shorter tine before phase conjugation. We speculated further [Yau92] that when the inducing beam establishes its self-pumped phase conjugating loop in the crystal, it chooses the optimum one. Since the phase-conjugate wave reflectivity depends on the loop configuration, it is, thus, independent of the intensity of the induced beam. In last three years, throughout this reaserch we have obtained several experimental evidences, such as muti-beam induced phase-conjugate nirror and self-pumped phase-conjugate resonator which will be described in detail in Chapters 3 and 4, to support thses ideas.

Furthermore, we found that once the inducing beam is removed, the main beam shows itself to be composed of four rays (see Fig. 2.13(c)) and phase conjugation continues and the loops remain after the inducing beam is turned off [Yau92]. We observed that this group of four rays constitutes two geometrically separate loops, each of which produces its own phase conjugate waves; thus, more conjugate waves are generated. Accordingly, the reflectivity of this SPPCM should be higher than that of the Cat SPPCM which only has one loop. This is only true if the phase-conjugate beams formed by each loop are phase locked otherwise we might see instability in the output. Experimental results [Yau92] have confirmed that a higher and actually more rather than less stable output as a function of time is produced. The reflectivity obtained in this experiment was found to be 56%, which is higher than that found in the Cat SPPCM with 30% reflectivity [Fei82b]. Since the configuration consists of two geometrically separate loops, we speculated that, in a very simple model instead of 2 interacting regions as in the Cat SPPCM, there are at least four regions: region II and region III constitute one loop, and region I and IV constitute another one (see Fig. 2.13(c)). Actually it is more likely that in reality discrete interaction regions do not exist and that gratings are distributed along the path of the rays giving distributed reflections but the simple model may be helpful for intuitive thinking.

From the above analysis, we conclude that a photorefractive crystal of $BaTiO_3$, illuminated with an Ar+ laser beam in such a way that it does not generate any phase conjugate wave may yield conjugate waves with high reflectivity and shorter response time due to the influence of another inducing beam. This inspired us to investigate the phase conjugation of multiple beams induced simultaneously in a $BaTiO_3$ by crystal using one inducing beam. More details about this will be discussed in Chapter 4.

2.6.5 Mutually pumped phase-conjugate mirrors (MPPCMs)

The mutually pumped (or double) phase-conjugate mirrors (MPPCMs), illustrated in Fig. 2.14, is pumped by two input waves, S_1, and, S_2. These input waves need not be, and preferably are not, mutually phase-coherent. The waves $\mathbf{R}_1$ and $\mathbf{R}_2$ are both generated by the non-linear interaction. $\mathbf{R}_1$ is created by the scattering of S_2 off the grating $\mathbf{R}_2 S_1^*$, $\mathbf{R}_1$ will be the phase-conjugate of S_1 but will be phase-coherent with S_2. Likewise, $\mathbf{R}_2$ is the phase-conjugate of S_2 but is phase-coherent with S_1.

Fig. 2.14 *Schematic of the mutually pumped phase-conjugate mirror geometry.*

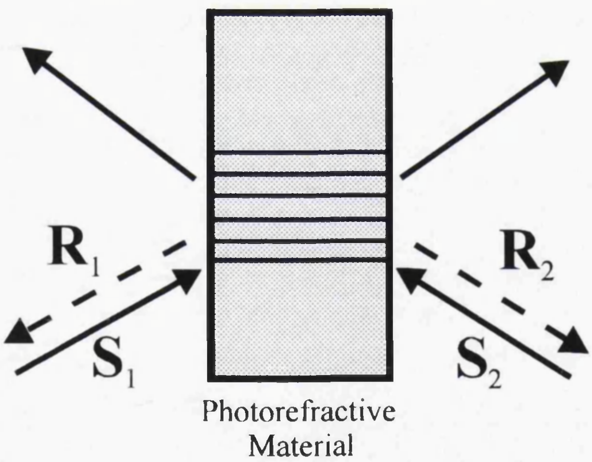

Fig.2.14 shows a diagram of a generic MPPCM. Two input waves (which may be from different lasers) are directed into the photorefracitve crystal. Under appropriate conditions, a phase-conjugate replica of each beam appears. Both waves are required for either conjugate to exist and the energy for the conjugate of one wave is supplied by the othe beam. For example,if S1 is blocked the conjugate of S_2 (or $\mathbf{R}_2$) disappears instantly while the conjugate of S_1 (or $\mathbf{R}_1$) disappears slowly with the characteristic erasure time of crystal. A similar behaviour is observed if S_2 is blocked.

The MPPCM is potentially very useful because it can form an amplified phase-conjugate reflection of a signal beam (or probe beam) even though the beam supplying the energy (the pump beam) is incoherent with respect to signal beam. In addition, several other applications are found in optical processing [Cau87, Wei87,and And93], for coupling two incoherent laser beams [Seg87, Shi93, and Wri94], and in optical neural networks [Dun91] for pattern recognition. The MPPCM was predicted theoretically by Cronin-Golomb et al.[Cro87], and was demonstrated experimentally by Weiss et al.[Weiss87]. This behaviour is displayed by each of the MPPCMs previously reported[Eas87, Smo87,Ewb88, and sha90]as well as in the geometry reported for our new MPPCMs in Chapter 6. Six configurations have already been discovered which demonstrate mutually pumped phase conjugation. The various configurations reported to date can be categorised by the number of internal reflecitons that the beams experience: no reflections in the double phase conjugate [Wei87], bridge [Sha90], and modified bridge [Wan90] configurations; one reflection in the bird-wing [Ewb88] configuration; two in the mutually incoherent beam coupling [Smo87] configuration; and three in the frog-legs [Ewb90] configuration. These conjugators (diagrams for the demonstrated MPPCM's are shown in Fig.2.15)differ in their geometry rather than in their physical mechanism and have the following characteristics:

(i) conjugation of two waves occurs at the same time,
(ii) the two conjugating waves may be mutually incoherent,
(iii) no cross talk is observed between conjugating waves,
(iv) digital temporal information can be immediately transferred between two waves,
(v) images can be conjugated with excellent fidelity, and subtraction and addition of images can be performed.

Even though the basic physical mechanisms(FWM & beam fanning)are the same foreach of the MPPCs, there are significant bendfits to be derived from specific geometric arrangements. For example. both the response time and magnitude of the magnitude of the phase-conjugat signal will vary significantly depending on which geometry is employed for a particular crystal. Having described the concept and merit of the MPPCMs, the behaviour of our new configurations for MPPCM will be examined in greater detail in Chapter 6.

Fig. 2.15 *Geometry of some of the MPPCMs. In MPPCMs, two mutually incoherent laser beams,* $\mathbf{S}_1$, *and* $\mathbf{S}_2$, *pump each other to generate a pair of phase-conjugate reflections,* $\mathbf{R}_1$ $(\mathbf{S}_1^*)$ *and* $\mathbf{R}_2$ $(\mathbf{S}_2^*)$ *by cross readout of photorefractive gratings (formed inside the crystal). Here,* $\mathbf{S}_1$, $\mathbf{S}_2$, $\mathbf{R}_1$, *and* $\mathbf{R}_2$ *are short notations for* $\mathcal{E}_1(\mathrm{r})e^{-j(\omega_1 t-\mathbf{k}_1\cdot\mathbf{r})}$, $\mathcal{E}_2(\mathrm{r})e^{-j(\omega_2 t-\mathbf{k}_2\cdot\mathbf{r})}$, $\mathcal{E}_1^*(\mathrm{r})e^{-j(\omega_1 t+\mathbf{k}_1\cdot\mathbf{r})}$, *and* $\mathcal{E}_2^*(\mathrm{r})e^{-j(\omega_2 t+\mathbf{k}_2\cdot\mathbf{r})}$, *respectively. The MPPCMs demonstrated are (a) the double phase-conjugate mirror [Weiss87], (b) the mutually incoherent beam coupling [Smo87], (c) the bird-wing phase conjugator [Ewb88], (d) the bridge phase conjugator [Sha90], and (e) the modified phase conjugator [Wan89], (f) the frog-legs phase conjugator [Ewb90].*

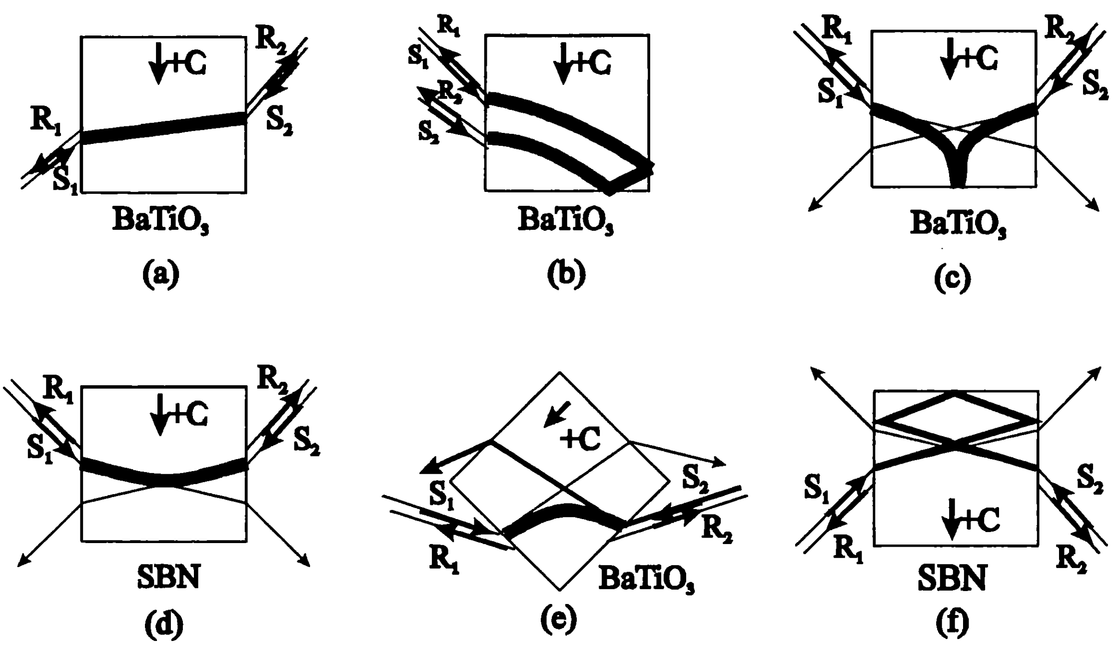

2.6.6 Optical ring resonators

Resonators can be constructed in which some or all of the gain is provided by a conventional laser gain medium. Such resonators exhibit properties associated with phase conjugation and photorefractive holography. In this section we describe three basic optical ring resonators which can be categorised into three types (Fig. 2.16) as:

(i) unidirectional ring resonator in which the photorefractive crystal and one pump beam provide gain for the resonator beam by TWM,

(ii) bidirectional ring resonator in which the two counterpropagating waves in a ring laser interact by TWM in the photorefractive medium,

(iii) FWM ring resonator which uses FWM in a photorefractive medium to sustain the resonator beam.

Fig. 2.16 *Various optical ring resonators using a photorefractive crystal. (a) unidirectional ring resonator. A single pump wave in a photorefractive crystal creates gain by TWM for a beam that travels around the ring resonator in one direction. (b) the bidirectional ring resonator: A conventional laser medium provides gain for beams traveling in either direction around the ring resonator. These two beams interact with each other via TWM in a photorefractive. (c) FWM resonator. Two pump waves in a photorefractive crystal create a phase-conjugate pair of resonator beams.*

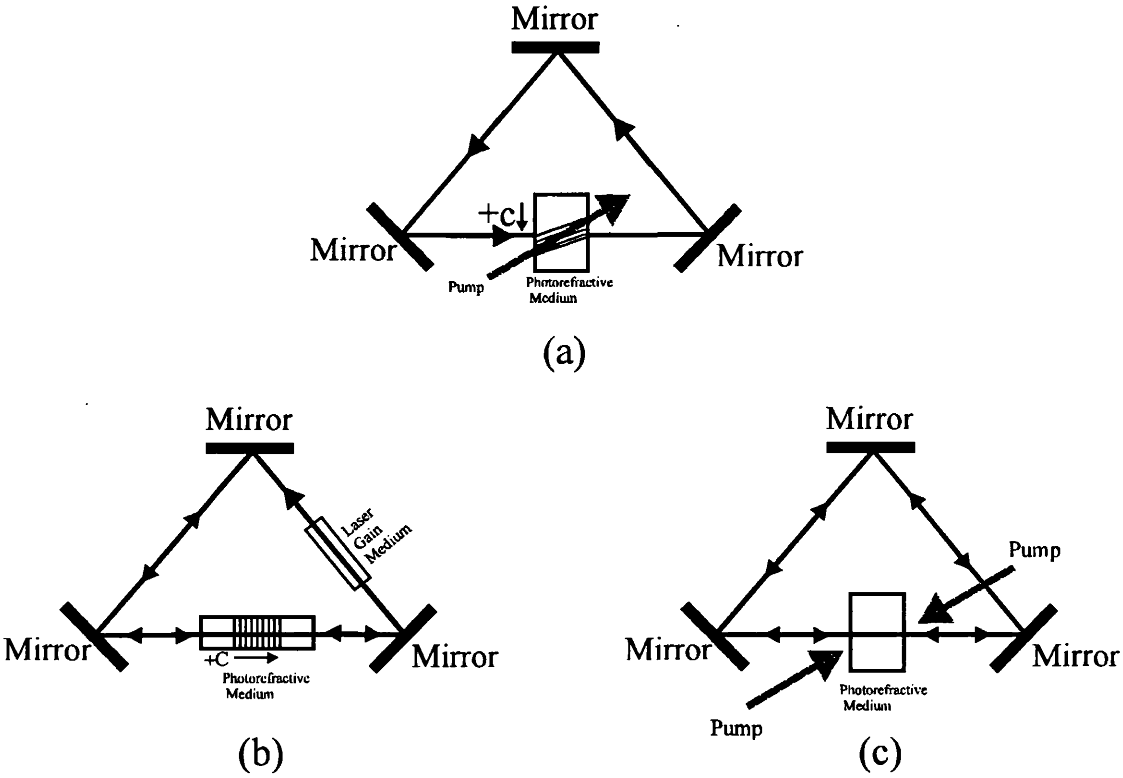

(i) Unidirectional ring resonator

The unidirectional ring resonator consists of a photorefractive crystal inserted in a ring cavity and pumped by one external beam [Whi82]. To make sure that light circulating in the cavity in one direction experiences TWM gain the orientation of the crystal in the cavity and the angle of incidence and polarisation of the pump beam are chosen. When this gain is large enough to support oscillation, the resonating beam builds up from the amplification of stray light. The unidirectional ring resonator exhibits two attractive properties: (i) there has a slightly frequency shift (on the order of a few Hz) between the oscillating beam and the pump beam [Fei85].; (ii) oscillation occurs almost no matter what the optical path length of the cavity. An associative memory based on a photorefractive unidirectional ring oscillator will described in Section 2.7.5.

(ii) Bidirectional ring resonator

The properties of a ring laser which contains, in addition to the usual gain medium, a photorefractive crystal in which the counterpropagating beams interact with each other by TWM (Fig. 2.16(b)). It was found that. Theoretically analysed results [Yeh84] show (1) there is a frequency shift between the counterpropagating oscillator beams; (2) the only situation for which oscillation of both beams might occur is when the cavity is not detuned and the beams have the same frequency. However, the likely experimental result shows that the loss for one oscillation direction larger than the other so oscillation will occur only when the cavity is in resonance and then in only one direction.

(iii) FWM ring resonator

White et al. [Whi82] first demonstrated a FWM ring resonator, which is of interest because the two oscillation beams are a phase-conjugate pair. In this ring resonator a ring cavity contains a photorefractive crystal, which is pumped by two counterpropagating beams (Fig. 2.16(c)). The counterpropagating oscillating waves are generated if the coupling strength is large enough and have frequency shifts relative to the pump beams depending on the cavity length, the intensity ratio of the pump beams, and on the cavity losses.

2.7 Applications for Optical Phase Conjugation

The reported experiments on photorefractive materials show that theycan act as efficient CW phase conjugators with weak light beams in the milliwatt range give the most promise applications, In addition they can exhibit a remarkable optical amplification effect and can demonstrate associated processes such as oscillation and thresholding and others are available. These facts have triggered an explosion of exciting applications for optical phase-conjugate mirrors, and some of the most relevant will be described in this section. Applications rely on the phase of the conjugated wave or on the image content of the generated wave, and as with other phase-conjugation applications, the major drawback of present phase-conjugate mirrors comes from material limitations: slow response times, low light sensitivities, limited lateral and angular acceptances, expensive materials or crystal growing difficulties. In spite of the lack of commercial success due to these limitations, many of the demonstrated applications are very promising. Although the potential applications of optical phase conjugation are wide ranging, pratical uses of PCMs already implemented are still in their infancy. Many possibilities and discussed here.

2.7.1 Lensless and speckle-free imaging

Optical phase-conjugate mirrors have been successfully applied to lensless imaging , an important example being mask-copying in photolithography [Lev81]. In Fig. 2.17, the signal beam coming from the illuminated mask with features of the order of 10^{-6} m is relected at a high quality beamsplitter and addresses to a $LiNbO_3$ phase-conjugate mirror. The retroreflected conjugate wave then forms an image on the substrate surface, coated with a light-sensitive material. As shown in Section 2.2, most of the optical aberrations are corrected in the projection process because of the phase conjugation. Higher spatial resolutions over image fields larger than with conventional lens lithography have been obtained [Lev81]. Further improvments of this experiment for eliminating pumping and having a faster response time have been achieved with a $BaTiO_3$ SPPCM [Gow84].

Fig. 2.17 *Schematic of a lensless photolithographic setup using a FWM phase conjugation [Lev81].*

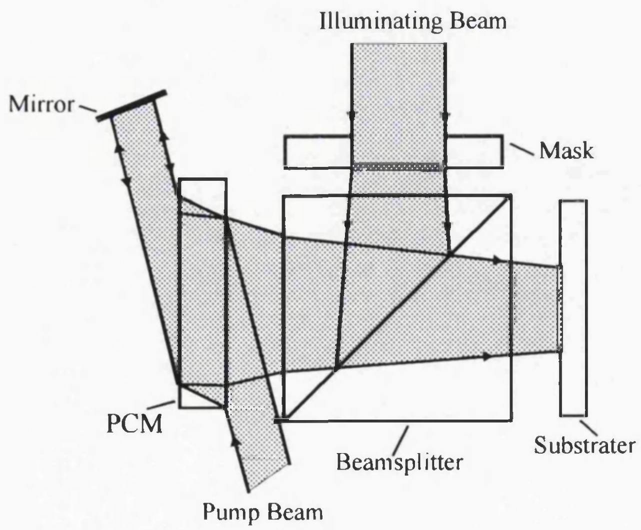

2.7.2 Phase distortion correction in laser cavities

The PCMs have been proved useful as elements of laser resonator cavities in order to correct aberrations from the laser medium, mirrors or other intracavity components. The first experimental demonstration of such a device was achieved by Cronin-Golomb et al. [Cro82]. Fig. 2.18 is the schematic showing the experimental setup.

In Fig. 2.18, the distorter consists of a piece of etched glass. With the aid of a conventional mirror, lasing with the PCM can be initiated, since the coherence of the fluorescence is insufficient to allow the formation of the required photorefractive grating in the crystal. The auxiliary mirror can be removed once the grating has been established in the crystal. In the normal laser cavity the distorter drastically lowered the spatial mode quality and the output power decreased from 2 W down to 1 mW. On the contrary, with the PCM the mode shape was restored and the power output boosted back to 500 mW. Later on, several other configurations apart from SPPCMs were used.

Fig. 2.18 *Correction of the phase disturbance introduced by a distorter inside a laser cavity using (a) a conventional mirror (CM) and (b) a $BaTiO_3$ SPPCM .*

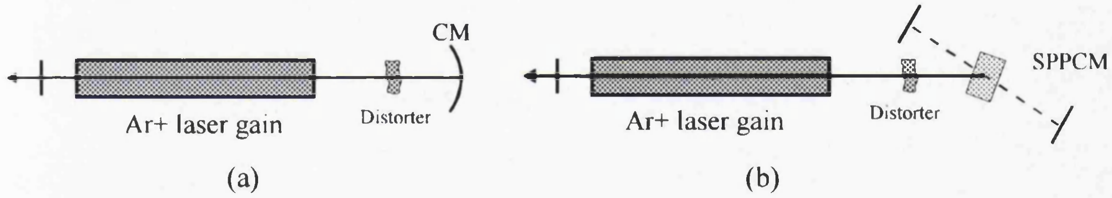

2.7.3 Phase-locking of independent lasers

There are many applications that require that two or more independent lasers to be locked together. In this application, we discuss how the output beams of individual lasers can be coherently combined into a single intense beam and phase locked together with PCMs. For example, the signal transmitted and received by an optical fibre can be coherently processed if a local laser is phase-locked to the frequency of the incoming laser beam. The first experimental demonstration of phase-locking two separate lasers using PCMs was proposed by Feinberg et al. [Fei86]. The schematic of Feinberg's configuration is sketched in Fig. 2.19.

In Fig. 2.19, the beam from the "master" argon-ion laser incident on a photorefractive $BaTiO_3$ crystal excites a self-pumped phase-conjugate beam in a "Cat" PCM. A slave laser, without output mirror, is pointing at the $BaTiO_3$ crystal. In the slave laser cavity, lasing takes place between PCM and the remaining mirror, as shown in Fig. 2.19(a). The frequencies of the two lasers stayed locked within less than 1 Hz for $BaTiO_3$. Fig. 2.19(c) schematically demonstrates the setup for phase-locking several independent lasers. Cronin-Golomb et al. [Cro86] demonstrated this process with semiconductor lasers showing that strong coupling could be obtained between beams in the near infrared (a $BaTiO_3$ PCM working at λ=850 nm was used). This suggests the applicability of the method to phase-locked arrays of diode lasers.

Fig. 2.19 *Scheme for phase-locking (a) two independent lasers, (b) three independent lasers and (c) many independent laser using PCMs. The pump beams of FWM phase conjugation were provided by the master laser. The optical feedback was provided by the slave laser. The frequency of the slave laser is locked to the frequency o the master laser [Feinberg86].*

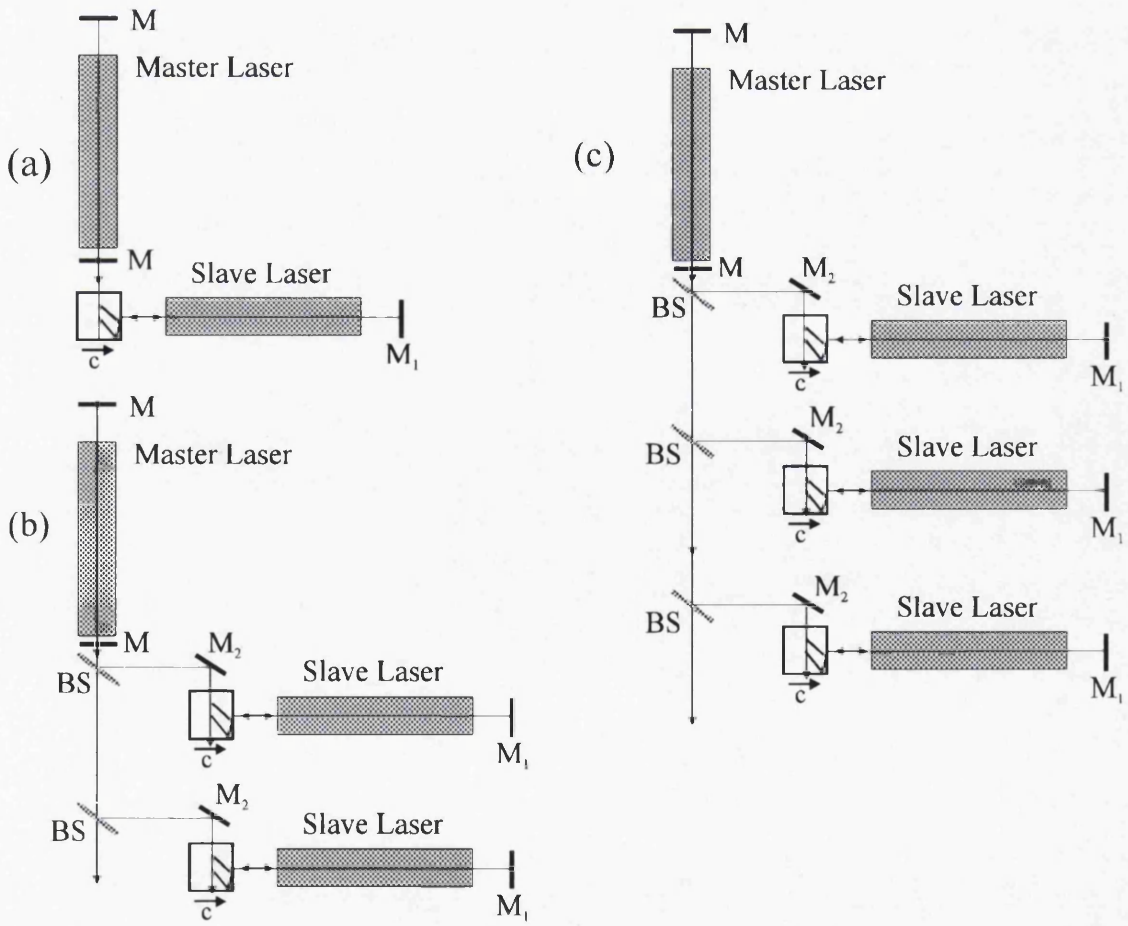

2.7.4 Phase-conjugate interferometers

PCMs are very useful tools in interferometry. They eliminate the need for a perfect wavefront. A Twyman-Green interferometer as shown in Fig. 2.20, using a PCM, has been proposed by Feinberg [Fei83] and Howes [How86 & 87]. The property of this SPPCM is that the wavefront incident on the mirror is reflected back along the same ray directions as the incident wavefront. Thus, the wavefront deformations change sign as shown in Fig. 2.20. Since the returning rays have the same directions as the incident rays, the quality of the focusing lens is not important. However, the quality of the light source collimator is important. Any wavefront distortions produced by this collimator will appear in the final interferogram, but duplicated. In other words the wavefront is not tested against a flat reference but against another wavefront, with deformations opposite in sign. Then the lens under test is the collimator, and the sensitivity is the same as that in the common Twyman-Green interferometer, but with only a single pass through the lens. The main advantage is that no perfect lenses are necessary.

Fig. 2.20 *Twyman-Green interferometer with a SPPCM. The spatial filter (SF) and the lens (L_1) provide an approximately collimated laser beam to the beamsplitter (BS), which divides the beam into two directions and couples the two beams (one is returning from the SPPCM the other is reflecting from a conventional mirror (CM)) into screen (S). The $BaTiO_3$ crystal acts as Cat SPPCM: it corrects for any distortion between the crystal and the BS, yet preserves information about the distance between them.*

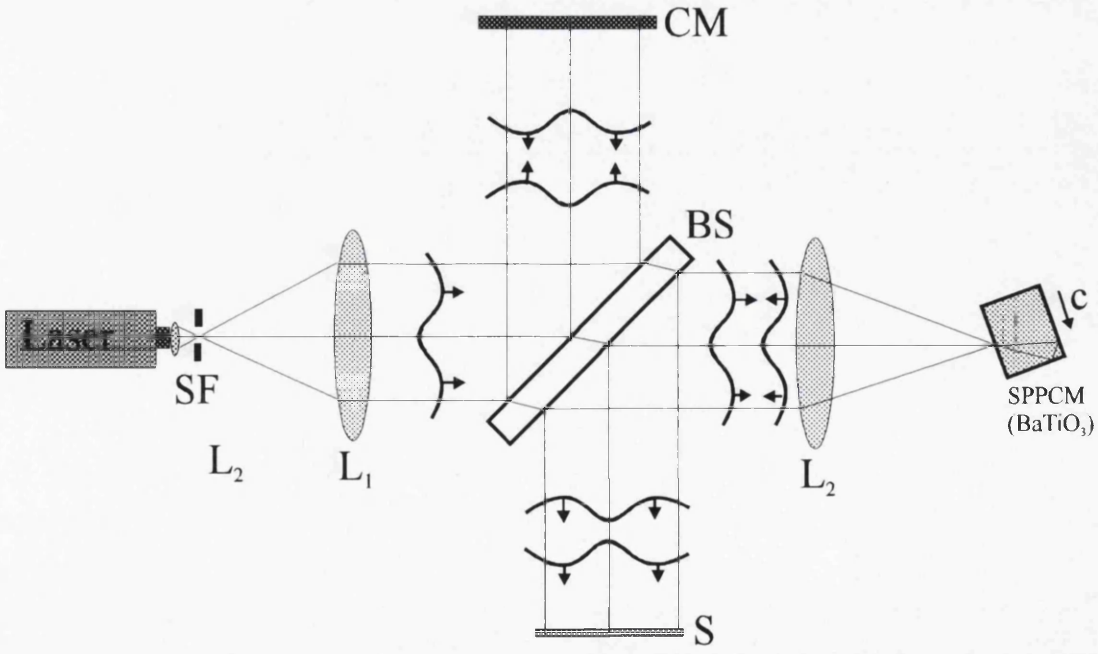

2.7.5 Optical information processing

Optical image processing A highlight experiment in the field of real-time optical image processing with photorefractive materials was performed with the basic layout shown in Fig. 2.21. Image correlation was performed with a FWM arrangement in a photorefractive medium [Pep78 & Whi80], where one of the pump beams, 2, carries the object information represented by the complex amplitude f_2, and the other one, 3, is a plane wave with uniform amplitude f_3. The signal beam, 1, carries the reference pattern f_1. Beams, 1 & 2, are focused on the crystal by lenses that yield the Fourier transforms $\Im\{f_1\}$ and $\Im\{f_2\}$ of f_1 and f_2. The three beams 1, 2, and 3 interact inside the photorefractive crystal and generate the conjugated beam, 4, whose amplitude $\Im\{f_4\}$ is

$$\Im\{f_4\} \propto \Im^*\{f_1\}\Im\{f_2\}\Im\{f_3\}. \qquad (2.24)$$

Fig. 2.21 *Real-time optical correlator using nonlinear FWM on a photorefractive crystal. M:mirror; BS:beamsplitter; L:lens; S:screen; SF:spatial filter.*

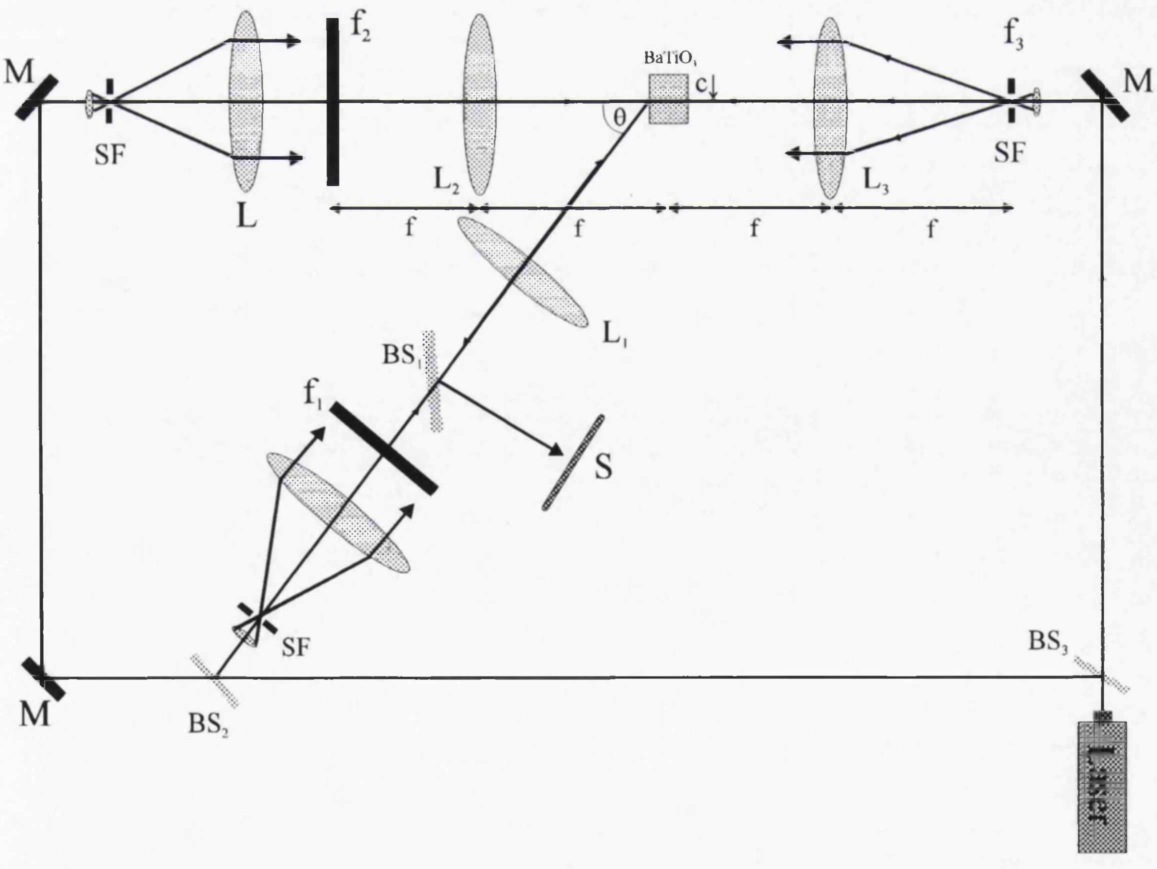

After Fourier transform $\Im\{f_4\}$ through another lens, one obtains a final beam, whose amplitude f_4, i.e. the correlation product of the object and the reference patterns, is

$$f_4 \propto (f_2 \otimes f_1^*) * f_3, \tag{2.25}$$

where ⊗ denotes the correlation operation and stands for convolution operation. Since f_3 is practically a delta function, the final output becomes

$$f_4 \propto (f_2 \otimes f_1^*) \tag{2.26}$$

Another related scheme had also been proposed by myself [Cha92a & 92b] to implement shift- and rotational- invariant pattern recognition successively. In our scheme the input, f_2, is the first order circular harmonic component of the reference instead.

Optical associative memory A suitable application for optical neural networks is provided by associative memories, which can combine holography and optical resonators. One can retrieve a complete optical image from a partial or noisy version of the image. During the last decade many researchers have made great efforts in the field of optical associative memory, such in numerical algrorithms [Hop82, Far85, & Psa85], geometries [Koh84], and holographic models [Coh86, Sof86, Sel91, & Mao92] for an optical associative memory.

Here we describe Anderson's approach using a ring resonator with a holographic mirror [And86 & 87], as shown in Fig. 2.22. The information is stored by injecting an image into the resonator, and exposing the hologram to the injected image (as the object beam) and its round-trip version (as the reference beam). This is repeated for each of the images to be stored. The hologram is then fixed, so that it is not erased by light. The injected light is removed and the gain of the cavity is increased until it self-oscillates. The spatial modes of this cavity correspond to the images previously stored in the hologram, and the beam in the cavity hops from mode to mode. Injecting a partial version of one of the stored images increases that image's gain over the others, and only that image resonators. Because the hologram contains the entire image, the entire image is displayed from only a partial input. The best results are obtained when the different modes compete for the cavity gain, which is provided by TWM in a separate $BaTiO_3$ crystal.

Fig. 2.22 *Optical associative memory with a generalised transformation (T) in a ring resonator cavity. (a) Recrding the hologram. (b) Recalling the entire image by injecting a partial image. Optical gain is provided TWM with an external pump beam in a photorefractive crystal [And86].*

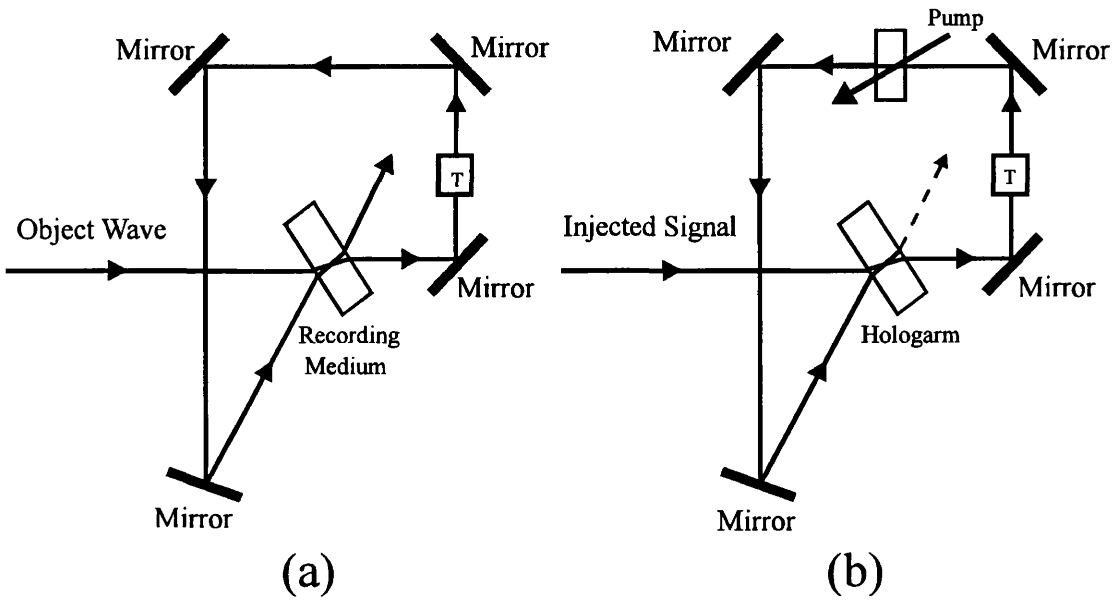

2.8 Conclusions

Beam fanning (Section 2.5) enhanced by two-wave mixing (Section 2.4) is a key effect to initiate phase conjugation and we will show later that can even more detailed understanding of it is essential for explaining our discoveries reported in this thesis.

A comparison of the photorefractive properties of a range of materials showed that Barium Titanate is an optimum choice for experiments on phase conjugation due to its large electrooptic coefficient (r_{42}=r_{51}=1640) which can result in high diffraction efficiencies in certain geometries for blue (488 nm) and green (514.5 nm) light. This is convenient as an argon laser has available to us for our current investigations.

The self-pumped phase-conjugate mirror configurations that need no external mirrors and which are both self-starting in photorefractive $BaTiO_3$ crystals. The pump beams are self-generated from the incident wave and are internally reflected at the crystal faces. Since the pump beams do not leave the crystal, the device is compact, relatively insensitive to vibration, and completely self-aligning. This gives the most promising of applicable in practice systems.

Moreover, any discoveries made in the use of Barium Titanate for phase conjugation are likely to be also applicable to Rhodium doped Barium Titanate operating in the infrared (between 720 nm to 1004 nm) where compact efficient semiconductor laser are readily available giving the prospect of more compact systems in the future.

Chapter Three

DESIGN OF OPTICAL ASSOCIATIVE MEMORY USING PHOTOREFRACTIVE HOLOGRAPHIC TECHNIQUES

3.1 Introduction

In this chapter we describe a novel, compact associative memory system, and advances relating to photorefractive crystals in conjunction with phase-conjugate mirrors (PCMs) in various configurations, which bring the possibility of realising a useful compact and practical optical associative memory system several steps closer. An optical neural networks (ONNs) is proposed, which is essentially a structural variant of the conventional 4-f correlation system [Van64] with the additional new features of a high efficiency holographic memory and a phase-conjugate feedback system with 2 PCMs in a 2-f correlation system. The proposed compact associative memory model has a simple conceptual structure which facilitates its implementation as a high order feedback neural networks (HOFNET) [Sel91 & Mao92].

Sections 3.2 to 3.3.2 are essentially reviews of earlier work while Sections 3.3.3 to 3.4 describe our new research. Section 3.4.1 is a review too. We begin by reviewing in Section 3.2, the developments in optical parallel processing systems and associative memories employing photorefractive memories, which are stored in a volume medium by holographic multiplexing, and two photoreractive phase-conjugate mirrors. We then go on to describe several advances: Section 3.3 proposes the novel development to make the present system, which is used to implement associative memory for ONNs, more compact. In addition, we discuss briefly two fundamental correlation systems based on the 4-f correlation system and holographic technique for associative memory, then we theoretically analyses our compact associative memory system, which is based on 2-f correlation in detail; Section 3.4 describes the use of two PCMs during recording of the holographic memories to reduce recording times and to achieve higher diffraction efficiencies; Section 3.5 experimentally demonstrates the exposure dependence of Bragg shift occurring in the photorefractive volume medium during the holographic storage. By using the Bragg-angle-shifted reading beams to readout the holograms, which are recorded by using non-unity beam ratios between the reference and object beams, we can obtain significantly higher diffraction efficiencies. Finally we conclude in Section 3.6.

3.2 Reviews of Optical Associative Memory

This review encompasses research on optical pattern recognition systems employing four-wave mixing (FWM) and self-pumped phase conjugation during last decade; earlier work can be found in the reference lists in the early papers. In 1984 King's College London and GEC Hirst Research Centre London, UK reported [Con84] on the beam power and recording geometry necessary for accurate real time correlation using degenerate four-wave mixing (DFWM). Pattern recognition can be achieved by correlation, or comparison, of two patterns. The photorefractive crystal was BSO and the best results were obtained using a paraxial geometry in which the two beams were incident at a small angle of 18° to each other so that the interference volume of the beams extended outside the crystal. They demonstrated recognition of one simple pattern out of four memorised patterns. This work did not include storage of images for longer than a few seconds since BSO is a very sensitive material and earlier holograms are strongly erased by subsequent recordings. The maximum number of gratings stored in a BSO crystal to date is four [Tao93].

The phase-conjugate resonator including a holographic store was first introduced for use as an associative memory by Dana Anderson in 1985 [And86] and this was followed by simultaneous reports from Hughes Research Laboratories [Sof86] and by California Institute of Technology [Yar86]. These letters were followed up by more detailed discussions by the two groups [Yar86 & 91, Sof86, and Owe87 & 93].

In Dana Anderson's initial paper [And86] he proposed but did not demonstrate a configuration in which a holographic store is placed in a "linear" PCR consisting of a FWM, externally pumped PCM with gain and a plane mirror. He also proposed and demonstrated a "ring" PCR containing the holograms and an externally pumped two-wave mixing (TWM) configuration to introduce gain to offset the loop loss. The gain medium was a crystal of barium titanate operating at 514.5 nm from a single frequency argon ion laser. This system was designed to have two eigenmodes and would usefully resonate with equal strength in each mode. The modes were designed to be due to two orthogonal patterns which were stored in a bleached silver halide emulsion. He demonstrated that "injection" of part of one of the patterns caused the system to injection lock so that resonance of the other eigenmode was suppressed. It was also hoped that each image could be stored using a slightly different frequency but experimental work was not successful due to insufficient thermal stability of cavity length. In Dana Anderson's later system a PCM based on a bistable ring resonator was used and was supplemented by spatial filtering using optical fibres.

In the optical resonator configuration, introduced by Owechko [Owe87], feedback takes place back through the system itself. This is achieved by placing PCMs at each end of the system to send the beams backwards and forwards exactly along the same path. This approach is particularly attractive as aberrations in optical components, misalignment and vibration can all be automatically compensated and the design could potentially lead to a more compact system. In the original system design an angularly multiplexed hologram was to be placed in the resonant cavity to perform the correlations. Hughes [Owe87] demonstrated several key features of an optical associative memory. Angularly multiplexed Fourier transform holograms were used with a single PCM. The images were gray scale and were illuminated via a diffuser to improve fidelity. Shift invariance of the object to be recognised was demonstrated due to the translation invariance property of Fourier transform holograms. The holograms were formed on thermoplastic film with the object and reference beams at $+10^\circ$ and -15° to the normal to optimise the diffraction efficiency. The PCM was produced by DFWM in barium titanate using 514.5 nm single-longitudinal mode argon-ion laser illumination. The presence of a non-linear element in the ONNs allowed them to converge to a stable state and increased the storage capacity. However, the non-linearity in the PCMs [Owe89] was not usually used for this. The PCMs were used in their approximately linear range and other elements were used to introduce the nonlinearities. The Hughes group proposed resonator system consisting of two PCMs into which cavity was to be placed an angularly multiplexed hologram. A full resonator was not implemented because of the relatively low diffraction efficiency of the thermoplastic hologram. However, we are not aware that any such system has been demonstrated and reported until now. The maximum number of angularly multiplexed holograms reported in reference [Owe87] was two although we understand [Owe93] that up to 7 were stored in practice and that this was limited by the high loss through the hologram and other optical components used and due to the low gain obtained elsewhere.

More recently a group from Kyoto University, Japan [Tan90 and Che92] has investigated the use of 0.09% and 0.1% mol Fe:$LiNbO_3$ as a FWM medium and have demonstrated a gain of 3 independent of the total incident optical intensity in an optical associative memory configuration using Fe:$LiNbO_3$ crystals for both the memory and for the phase-conjugate medium. Similar work has also been carried out in China at Nankai University [Zha93] using two $LiNbO_3$ crystals for both storage and phase conjugation. In China [Gon93], Ningbo University demonstrated an interesting configuration in which a Ce:KNSBN crystal was used as both memory material and as the PCM. These experiments using the same type of crystal throughout may lead the way to more compact systems using spatially separated parts of the same crystal with compact planar reflecting and focusing optics [Tak93].

The Hughes Research group has, more recently [Sof90a & 90b, Owe90, Dun90, Owe91, Wan91, and Yar91], directed their attention to a system in which a single barium titanate crystal is used to perform both as the storage medium for several holograms and as a self-pumped phase conjugate mirror, which they refer to as a "Self-Pumped Optical Neural Network (SPONN)". When both functions are combined in the same crystal cross interactions take place which mean that it is difficult to optimise both the storage capacity and the PCM reflectivity. It does, however, have the advantage that crosstalk is reduced between images due to spatial (in the depth dimension of the crystal) and angular multiplexing. Effectively each image or set of weights is shared between several gratings and beams must diffract from all of the gratings in succession to reconstruct the image. In reference [Owe91] the experiments were preformed using a self pumped barium titanate crystal (supplied by Sandoz Associates) with a single frequency argon ion laser at 514.5 nm. Associative recall was demonstrated when only 1/1000 of the image stored was entered. The group also showed [Sof90a & 90b] that a single pixel or neuron could be deactivated by storing another image identical except that the phase of that individual pixel was shifted, presumably by π radians. This shifts all of the gratings so that they cancel when the exposure is the same. However, more than one hologram could not be stored in the crystal as cross connections were formed between the hologram being stored and earlier holograms. This may be because both images were shared between the same large continuum set of angularly and spatially multiplexed gratings. The same group has also investigated combining storage of holograms and a mutually pumped phase conjugate mirror [Dun90] in the same crystal of barium titanate. In this configuration two beams enter the crystal, one writes gratings which are read by the other beam.

More recently a new approach [Owe91] investigated by the Hughes research group removes the requirement for the barium titanate crystal to perform as a PCM and only uses it to store holograms. This involves the formation of a set of gratings between a fanned beam and an un-fanned beam. Beams at certain angles entering the crystal are fanned out by scattering and two-wave mixing and a spatial phase aberrator was used to increase fanning and connectivity. Multiple holograms have been stored without crosstalk and without suffering from Bragg degeneracy. In this case the crystal stored several images. Two sets of weights representing positive and negative weights were used and the outputs resulting were subtracted electronically in a computer. 14 random patterns with 2048 neurons were arbitrarily divided into two sets. 5 exposures of the complete set were required for training the net so that it could correctly distinguish which set contained an entered pattern. It has been suggested that the holograms could be fixed by switching the ferroelectric domains which is permanent at room temperature. However, the memory is likely to be limited by the sensitivity of the crystal to erasure by subsequently recorded images. Further related research is described in the following references [Ath86, Whi88, Hen89, Gün89, Wag91, Bas92].

3.3 Compact Associative Memory for ONNs

This section describes the design of a compact associative memory architecture for optical neural networks (ONNs). Most of the conventional neural networks are very complicated, and need a lot of components. The use of a 4-f correlation system to implement inner-product or outer-product, results in a long system (in the high order feedback neural network (HOFNET) [Sel91 & Mao92]) that made losses in the round trip. So reducing these losses will be the main aim for establishing the resonant ONNs.

We have designed a compact optical photorefractive resonator neural networks shown in Fig. 3.1. It is a modification of the resonating loop reported by Owechko et al., which is shown in Fig. 1.1. Our system is more compact than that Owechko et al. proposed. In addition, two key differences between the systems are the nonlinear storage crystal of Fig. 3.1 in place of the hologram of Fig. 1.1 (Owechko proposed this idea but did not demonstrated it) and the address system which consists of a microlens array and a 2-D SLM. In our resonator neural network implementation the crystal is photorefractive lithium niobate ($LiNbO_3$), which is capable of recording multiple holograms with highest diffraction efficiency using Spatio-Angular Multiplexing [Tao93 & 95] and phase-conjugate holographic storage (will be described in Section 3.4). Contrast this use of a crystal with Fig. 2.22, in which a fixed hologram is used.

Fig. 3.1 *Schematic diagram illustrating the High Order Resonant Neural Network (HORNET) using (1) the compact configuration (2f correlation system), (2) optical feedback by two PCMs, (3) SAM hologram, and (4) the new addressing system of the SAM memory: MA, microlens array; SLM, spatial light modulator; BS, beamsplitter; FTL, Fourier transform lens; PCM, phase-conjugate mirror.*

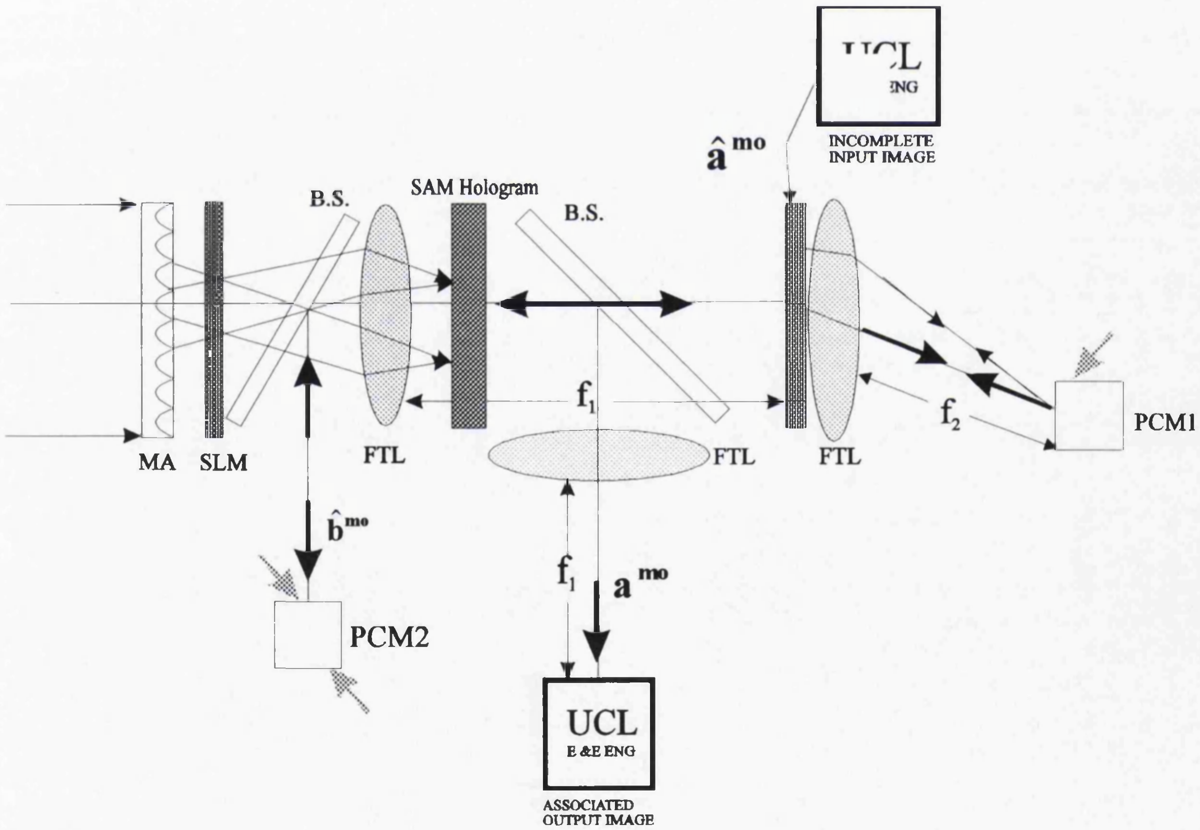

3.3.1 Associative memory by means of holographic techniques

The implementation of associative recall of two-dimensional images by vector-matrix multiplication techniques [Goo78] is very complicated. However, holographic correlation methods are more appropriate in such situations. Also, optical holography can process analog phase and amplitude objects. A schematic diagram showing the recording of the holographic memory is shown in Fig. 3.2. In Fig. 3.2 a set of Fourier transform holograms of the objects to be memorised are recorded sequentially using a plane wave reference beam with a different angular offset for each object. The plane wave illuminating the object (centered on axis) propagates parallel to the optic axis, and, therefore, the Fourier spectra of different objects, modulated with different carrier frequencies, are all centered on the axis. The diffraction process for these holograms stored in a volume has a very strong wavelength and angular selectivity. This is relevant to evaluate the capacity of a photorefractive volume medium to record different holograms by using holographic multiplexing schemes, which will be discussed in the following section. Various recording arrangements are possible [Sta75, Mok91, Tao93, & Psa94 &95]; for example, Tao et al. [Tao93] arrange all the memories to overlap partially in the front focal plane of the Fourier transform lens, use distinct tilted reference beams and record the holograms into a photorefractive volume medium ($LiNbO_3$:Fe).

Fig. 3.2 *A schematic shows the arrangement for recording multiple holograms of different images $f_m(x,y)$. A series of angular offset reference beams were used to record these images. The image and the recording material are situated in the front and back focal planes of lens L_1.*

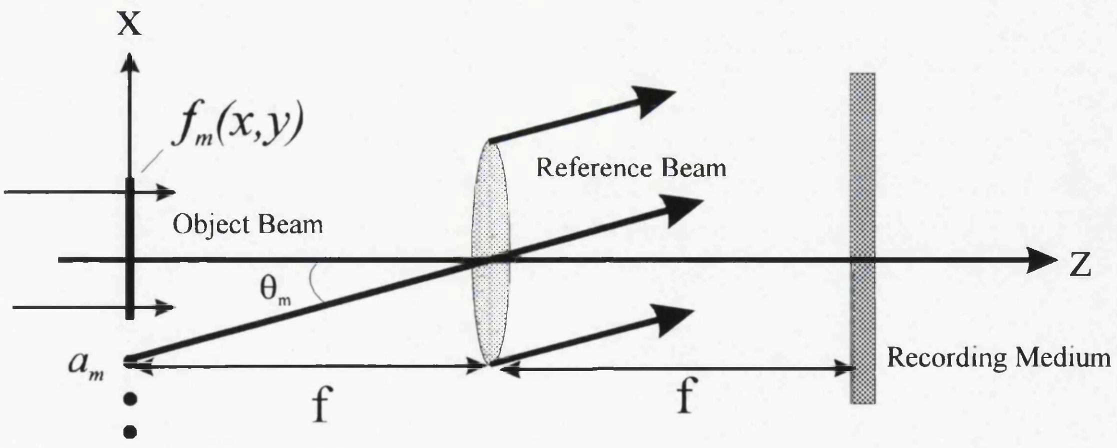

We now analyse the recording and the retrieval of one of the objects. The amplitude transmittance of the object is $f_m(x,y)$, and the associated reference source is located at

$x = -d_m$. The amplitude transmittance t of the hologram, assumed to be proportional to the incident intensity, is given by

$$t \propto \left| F_m(x_1, y_1) + \exp\left(j \frac{2\pi}{\lambda} \sin\theta_m x_1 \right) \right|^2, \tag{3.1}$$

where θ_m is the angular offset of the reference beam, and $F_m(x_1, y_1)$ is the Fourier transform of $f_m(x, y)$ evaluated at the frequency pair $(x_1/\lambda f, y_1/\lambda f)$. Here, we assume that the total exposure associated with all the stored objects lies in the linear dynamic range of the recording material [Col71]. In general, the correlation operation of 4-f correlation system can be categorised into two methods. One is the spatial correlation and the other is the spectral correlation which can be described as follows:

Spatial correlation architecture We read this hologram located in the back focal lens of lens L_1 (or the front focal plane of lens L_2) with an object $g_m(x, y)$, which is placed in the front focal plane of lens L_1 and centered on axis, and can be a distorted or incomplete version of $f_m(x, y)$ (Fig. 3.3(a)). The amplitude in the x_1, y_1 plane just after the hologram (retaining only the term of interest) is

$$G_m(x_1, y_1) F_m^*(x_1, y_1) \exp\left(j \frac{2\pi}{\lambda} \sin\theta_m x_1 \right), \tag{3.2}$$

Where the symbol * denotes a complex conjugate. In the plane x_2, y_2 we obtain the Fourier transform of $G_m(x_1, y_1) F_m^*(x_1, y_1)$ centered at the point $x_2 = d_m$. This Fourier transform is the correlation of f and g. If $g_m(x, y)$ is identical to $f_m(x, y)$, the autocorrelation is a sharp peak centered at $x_2 = d_m$.

Spectral correlation architecture We read this hologram located at the x, y plane with an reference plane wave offset with an angle θ_m (Fig. 3.3(b)). The object $g_m(x, y)$, distorted or incomplete version of $f_m(x, y)$, is placed in the front focal plane of lens L_2 (located at x_1, y_1 plane) and centered on axis. The amplitude in the x_1, y_1 plane just after the hologram (retaining only the term of interest) is

$$F_m^*(x_1, y_1) \exp\left(j \frac{2\pi}{\lambda} \sin\theta_m x_1 \right). \tag{3.3}$$

At the back focal plane of lens L_1 we obtain the $f_m^*(x,y)$, which is the same as $f_m(x,y)$ for a real object and superimposed with object $g_m(x,y)$. At the back focal plane of lens L_2 in the x_2, y_2 plane, the correlation of the Fourier transform of $f_m(x,y)$ and $g_m(x,y)$ centered at the point is

$$F_m(x_1,y_1)\otimes G_m(x_1,y_1)=\Im\{f_m(x,y)g_m(x,y)\}. \tag{3.4}$$

Where $\otimes$ denotes correlation and $\Im$ is the Fourier transform. As described in spatial correlation this Fourier transform is the correlation of *f* and *g*. If $g_m(x,y)$ is identical to $f_m(x,y)$, the autocorrelation is a sharp peak at the centre of the correlation plane.

Fig. 3.3 *Schematics showing the correlation systems: (a) spatial correlation recording a multiple hologram of different images $f_m(x,y)$; (b) spectrum correlation*

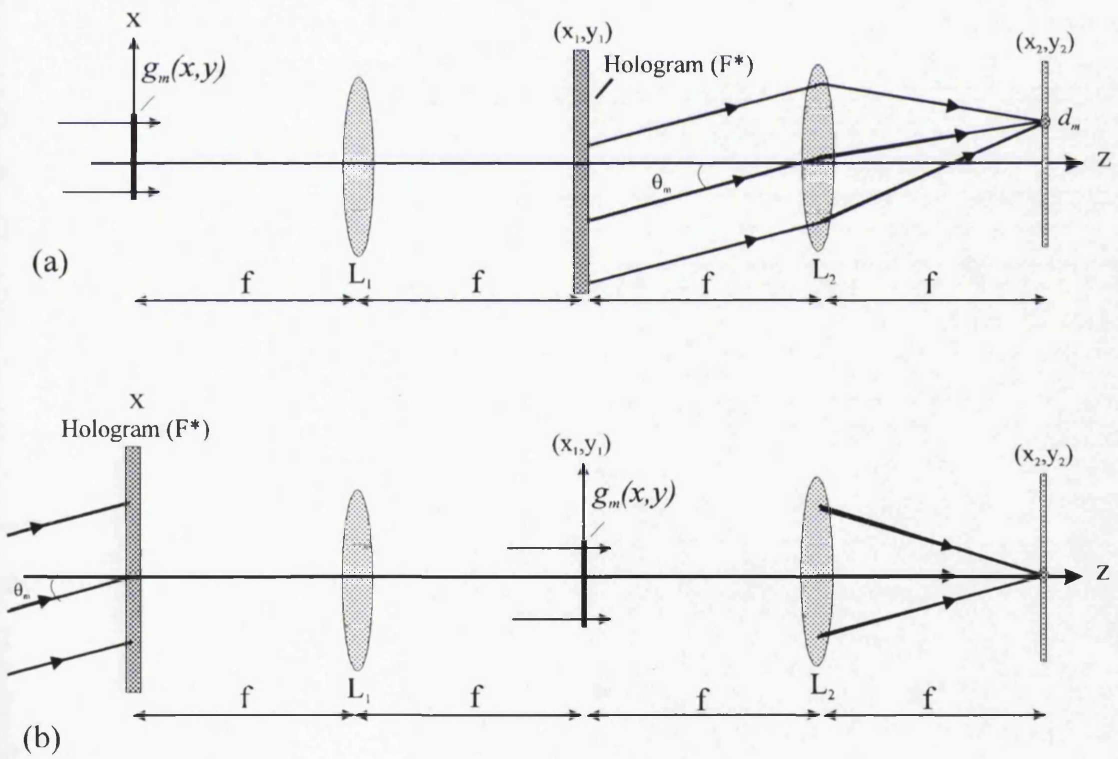

In both cases, if $g_m(x,y)$ is a partial or somewhat distorted version of $f_m(x,y)$, the correlation peak will be less intense and rather diffused. We can isolate the peak and eliminate the unwanted light in its vicinity using a small hole positioned at $x_2 = d_m$ in the spatial correlation plane or at the centre of the spectral correlation plane. Alternatively, by means of a nonlinear thresholding mechanism, the diffused light can be suppressed, and the peak retained and even enhanced. If a mirror is placed in x_2, y_2 plane, the sharp peak acts as a point source and gives rise to a plane wave which addresses the hologram in the reverse direction. Since the hologram contains all the information about $f_m(x,y)$, the complete object $f_m(x,y)$ is reconstructed on axis in the x, y plane, and is retrieved using a beamsplitter in the spatial correlation case. There is a problem is the spectrum correlation case due to inversion of image.

The hologram contains the Fourier spectra of all the object memorised, and when it is address by $g_m(x,y)$ in the input plane, a large number of spatially separated cross-correlation peaks are obtained in the x_2, y_2 plane. The angular separation between the reference beams used during the recording process is sufficiently large that those correlation peaks do not overlap each other. These peaks will be present even if the hologram is recorded in a thick medium. Since $f_m(x,y)$ is the most similar to $g_m(x,y)$ say, the peak at $x_2 = d_m$ will be the brightest and sharpest of all. A nonlinear thresholding operation quenches all the peaks except the brightest. If the hologram is thin, the back-propagating plane wave will reconstruct all the memorised images, but they will be spatially separated in the output plane. The desired object $f_m(x,y)$ will, of course, be on-axis. With a thick hologram, only $f_m(x,y)$ is reconstructed, but the shift invariance, a characteristic of a Fourier transform hologram, is lost.

The associative characteristics of holography, and the possibility of complete image retrieval from a partial input, were appreciated at its very inception [Van64, Col66 & 71, and Gab69]. By incorporating thresholding feedback, gain, and iteration, the recent developments have led to improved selectivity and signal-to-noise ratio. Owechko et al. [Owe87] have used a phase-conjugate mirror (PCM) after lens L_2 to achieve thresholding, amplification, and feedback (Fig. 3.4(a)). This PCM ideally selectively feeds back the strongest correlation peak while quenching all others. The gain of the PCM is generally not sufficient, but it is possible to form a resonator with two PCMs that will permit iteration (Fig. 3.4(b)). The PCM was implemented by degenerate four-wave mixing (DFWM) in a photorefractive $BaTiO_3$ crystal. The pump-probe angle, and the angle between the grating wavevector and the crystal c-axis, were optimised to achieve maximum phase-conjugate reflectivity. Two objects were stored, and either complete image was reconstructed from its associated partial input. The system with two PCMs did not resonate because the gain did not exceed the losses. Since the diffraction efficiency of the hologram was 10% it alone accounts for a loss of 90 % in the round trip. If more reflectivity could be obtained that would ease the difficulty of realising such a system.

Fig. 3.4 *Schematics showing the Owechko's associative memory system based on correlation systems with (a) one PCM for achieving thresholding, amplification, and feedback and (b) two PCMs for iteration.*

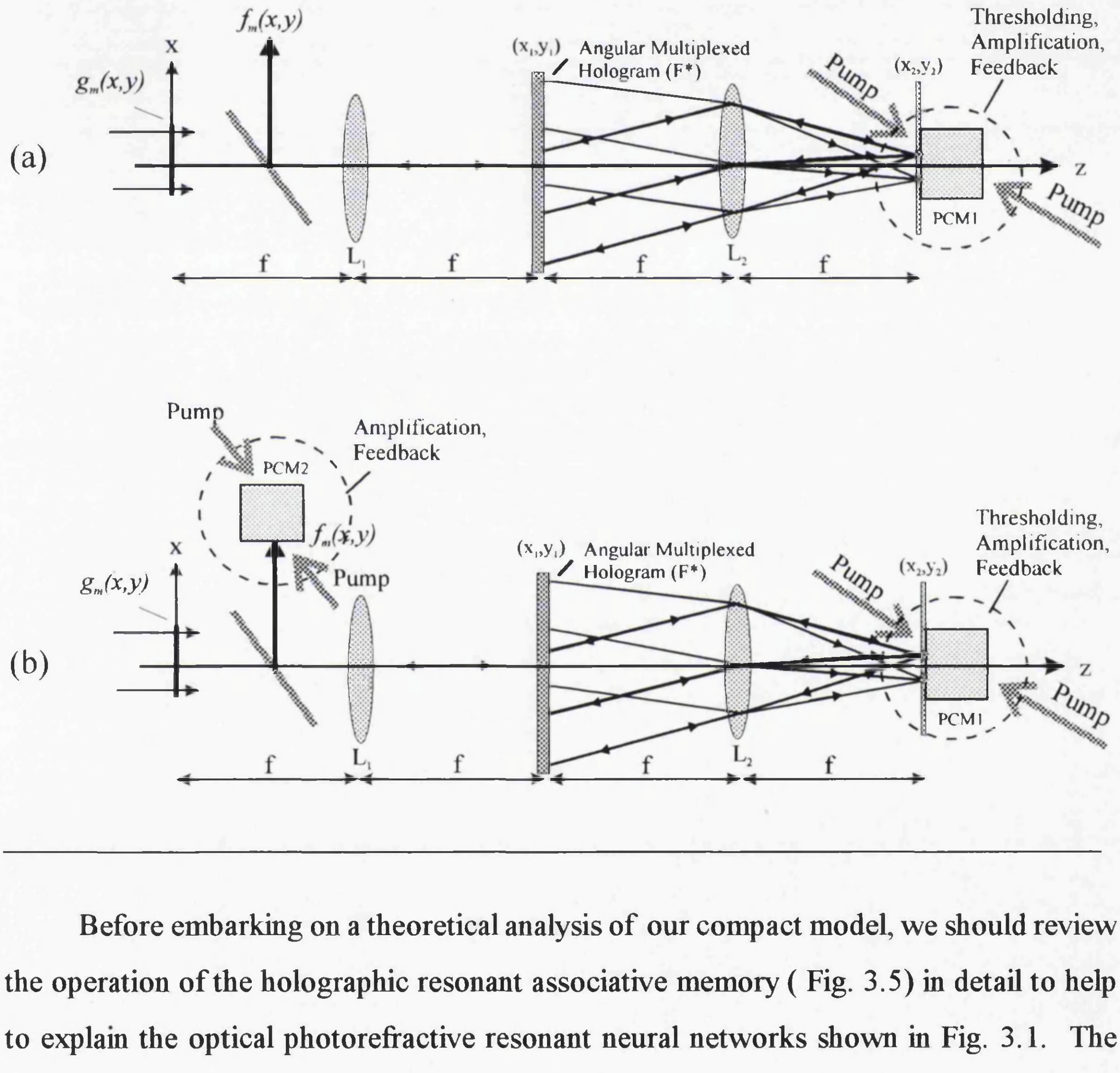

Before embarking on a theoretical analysis of our compact model, we should review the operation of the holographic resonant associative memory (Fig. 3.5) in detail to help to explain the optical photorefractive resonant neural networks shown in Fig. 3.1. The holographic resonant associative memory is primed with a partial or distorted input pattern $\hat{\mathbf{a}}^{mo}$. This is reflected off the second beamsplitter in Fig. 3.5 toward the fixed, previously recorded hologram (which consists of the Fourier transforms of object $\mathbf{a}^m$ recorded using different angularly shifted plane wave references $\mathbf{b}^m$, as illustrated in Fig. 3.6) to address it. A set of partially reconstructed reference beams $\hat{\mathbf{b}}^{mo}$ is excited. Each reconstructed reference beam is weighted by the correlation of the input object with the stored object associated with that particular reference beam. The reference beams are phase conjugated by a thresholding PCM_1 (which is positioned in the object and reference legs of the hologram, as shown in Fig. 3.5) and retroreflected back toward the hologram, which reconstructs the complete stored objects and sets up a resonant loop between the PCM_1 and PCM_2. The loop is biased by the presence of the hologram and by the injected signal $\hat{a}^{mo}$, and it suppresses all stored patterns (and their reference beams) except for the one most closely matching $\hat{a}^{mo}$. The stored image with the strongest correlation with the input survives at the expense of the weakly correlated ones. This causes a readout of the stored image a^m, an undistorted version, closet to the input $\hat{a}^{mo}$.

Fig. 3.5 *Readout of data in the resonator associative memory.*

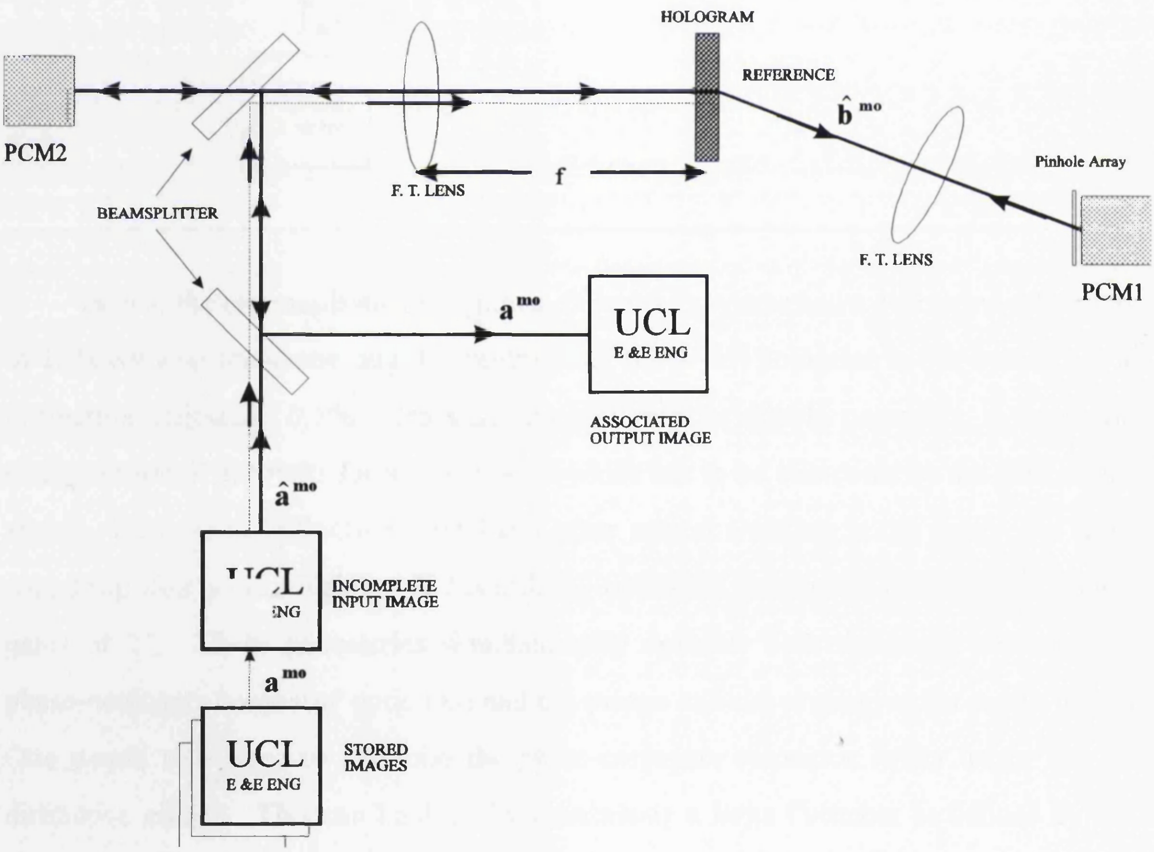

In the resonator configuration of Fig. 3.5, the reference beams and the reconstructed objects are phase conjugated by PCM_1 with thresholding and PCM_2 with gain, respectively, and the process is iterated until a self-consistent solution of the system is found. These self-consistent solutions or eigenfunctions of the system are simply the stored objects in the hologram.

Fig. 3.6 *Recording of data in the reference-based associative memory.*

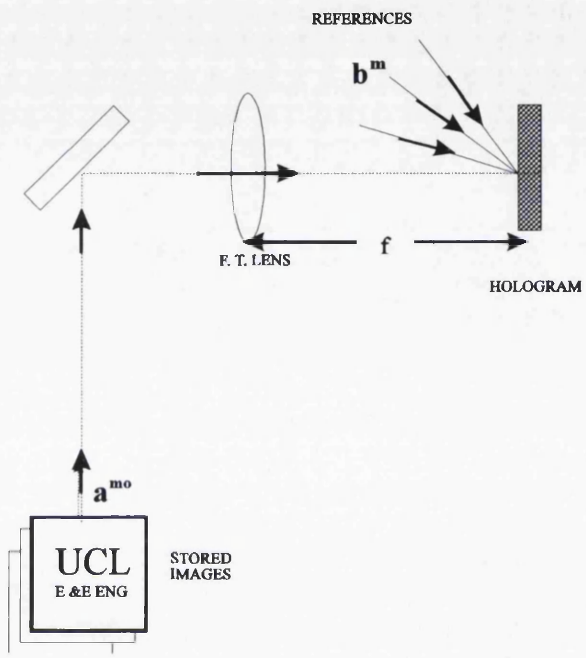

In fact, the thermoplastic hologram in Owechko's system had a diffraction efficiency of 10% whereas the spatio-angular multiplexing (or SAM) hologram in our system has a diffraction efficiency 0.5%. Because the hologram is double passed in a resonator configuration, it accounts for a loss of 99% which has to be overcome by the gain of the system. Because of diffractive spread and other optical elements in the cavity, the total round trip loss is even higher. PCMs utilising optimised geometries typically can obtain gains of 25. These geometries simultaneously optimise both the angle between the phase-conjugate resonator optic axis and the pumps and the grating vector c-axis angle. One would also want to minimise the phase-conjugate resonator cavity losses due to diffractive effects. This can be done by maintaining a large f number as defined by the cavity length and diameter of the output coupler. Two such PCMs in the object and reference leg of the system should, therefore, have sufficient combined gain to overcome the losses in the system.

Unfortunately, the configurations used for the associative memory cannot realise the optimum value for the gain. This is because different parts of the 2-D input image enter the crystal at different angles. Most of the angles differ from the optimum value, and, therefore, the gain is reduced from that of the simple phase-conjugate resonator. The associative memory also has unavoidable losses produced by the various beamsplitters in the system. Because of the reduced gain and inherent losses of the system, Owechko's system did not oscillate. For oscillation to occur, the hologram diffraction efficiency or the system gain must be increased. This can easily be achieved in the SAM hologram by overlapping adjacent holograms less but this is at the expense of using a larger crystal. Similarly more TWM crystals (described in section 2.4) can be added to amplify the gain at intermediate points in the system. A hybrid optoelectronic version of a similar system where the nonlinearities are implemented electronically was constructed by Owechko et al. [Owe88]. The system consisted of a hologram in an optoelectronic cavity, and gain, feedback and nonlinear processing of the reference beams were provided by vidicom detectors, an image processor, and liquid crystal light valves. The system also contains a number of components such video cameras and liquid crystal light valves, and is therefore quite bulky, like most complex optical systems. It is difficult to say at this point to what extent it can be scaled down.

3.3.2 The compact correlation system design

The high order resonant neural network (HOFNET) was inspired by the system proposed by Owechko et al. and HOFNET by Selviah et al., and it uses a $LiNbO_3$ crystal to have high memory capacity. There are two main key points which were changed in designing the system to implement the neural network. One is making the HOFNET system more compact and the other is designing an all optical resonator with FWM PCM for gain and a new multi-beam induced phase-conjugate mirror (or MIPCM) for feedback (will be described in following chapter). The spectrum correlation for optical neural networks was proposed by Selviah et al. [Sel91] (called high order feedback neural networks or HOFNET in short) and is more convenient than the VanderLugt spatial correlation. In this section, we try designing one novel system to make the HOFNET [Sel91] more compact by using 2-f correlation [Hor89] instead of conventional 4-f spectrum correlation. The theoretical derivation is considered in what follows.

Assume that an input pattern generated on a spatial light modulator (SLM) with its amplitude transmittance $t(x,y) = |t(x,y)|e^{j\varphi(x,y)}$, in the x_1, y_1 plane shown in Fig. 3.6(a), is illuminated by a uniform plane wave of unit amplitude and that the wave immediately past the SLM, then propagates through the lens L_1 of focal length f_1 to x_3, y_3 plane.

Fig. 3.6 *Optical Fourier transform module: (a) general system and (b) variable-scale system.*

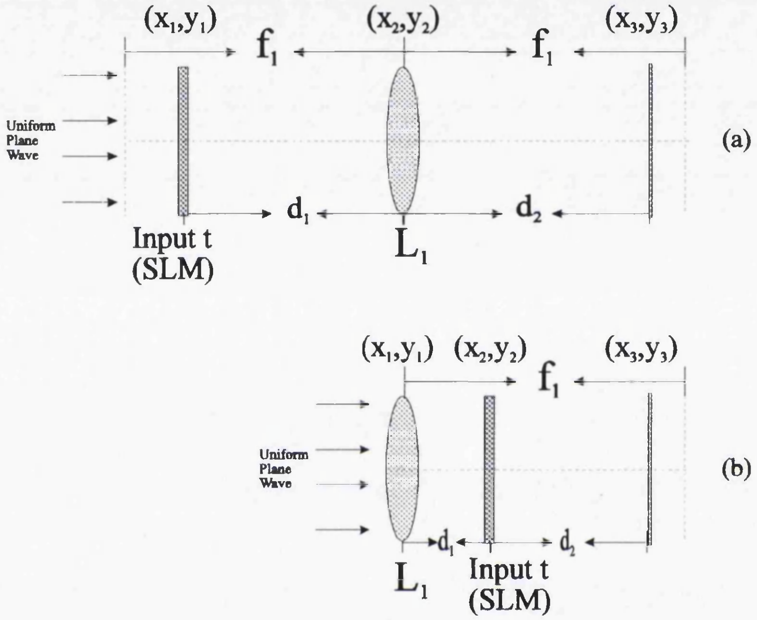

By use of the diffraction formula and the Fourier transform property of a lens [Goo68], we find the distribution in the x_3, y_3 plane is

$$\psi_3(x_3,y_3) = \frac{1}{j^2\lambda^2 d_1 d_2} h(x_3,y_3;d_2)\iint t(x_1,y_1)h(x_1,y_1;d_1)\iint h(x_2,y_2;\tfrac{1}{d_1}+\tfrac{1}{d_2}-\tfrac{1}{f_1})$$

$$\exp\left\{-j2\pi\left[x_2\left(\tfrac{x_1}{\lambda d_1}+\tfrac{x_3}{\lambda d_2}\right)+y_2\left(\tfrac{y_1}{\lambda d_1}+\tfrac{y_3}{\lambda d_2}\right)\right]\right\}dx_2 dy_2 dx_1 dy_1, \qquad (3.5)$$

where

$$h(x,y;d) \equiv \exp\left[\frac{jk(x^2+y^2)}{2d}\right]$$

If the input pattern appears behind the lens L_1 as shown Fig. 3.6(b), the transform appears in the back focal plane if the lens is illuminated with a uniform plane wave of unity amplitude. We find that the distribution in the x_3, y_3 plane [Goo68] becomes

$$\psi_3(x_3,y_3)=\frac{f_1}{j\lambda d_2^2}e^{jkf_1}h(x_3,y_3;d_2)T(\frac{x_3}{\lambda d_2},\frac{y_3}{\lambda d_2}), \tag{3.6}$$

where T is the Fourier transform of t. Notice the scale factor d_2 instead of f as in Eq. 3.6. This indicates that, when the input pattern is behind the lens, the scale of the Fourier transform is a function of d_2 and that the transform does not appear in the back focal plane of the lens. That means a quadratic phase factor $\exp\left[\frac{-jk(x_3^2+y_3^2)}{2d_2}\right]$ has been introduced at the back focal plane. The phase factor is proportional to the distance from the input pattern to filter d_2.

A typical 4-f correlator as shown Fig. 3.7(a) consists of a Fourier-transform operation, a matched filter (can be SAM hologram) that introduces $G^*(\frac{x_3}{\lambda d_2},\frac{y_3}{\lambda d_2})$, and a second Fourier-transform operation. Such a system, with a scale searching capability, is shown in Fig. 3.7(b). The wave distribution emerging from the x_3, y_3 plane is $\psi_3(x_3,y_3)G^*(\frac{x_3}{\lambda d_2},\frac{y_3}{\lambda d_2})$. A second lens, with focal length f_2, takes the Fourier transform of this product and images the filtered signal at the output image plane x_4, y_4 plane. Before doing that, one phase compensation lens can be used to remove the quadratic phase term as in Eq. 3.6 at the filter plane. L_3 is placed close to the filter at x_3, y_3 plane (see Fig. 3.7(c)) and should have a focal length f_3 equal to d_2 because it introduces a phase factor $\exp\left[\frac{-jk(x_2^2+y_2^2)}{2f_3}\right]$ or $\exp\left[\frac{-jk(x_2^2+y_2^2)}{2d_2}\right]$ at that plane. The wave distribution at the x_4, y_4 plane can be represented as

$$\psi_4(x_4,y_4)=\frac{e^{jkd_3}}{j\lambda f_2}h(x_4,y_4;d_3)\iint P_3(x_3,y_3)\psi(x_3,y_3)G^*(\tfrac{x_3}{\lambda d_2},\tfrac{y_3}{\lambda d_2})h(x_3,y_3;-f_2)$$
$$h(x_3,y_3;d_3)\exp[-jk\tfrac{x_3x_4+y_4y_4}{d_3}]dx_3dy_3, \tag{3.7}$$

where P_3 is the pupil function of L_3 (L_3=1 when lens is large enough in our case) and the matched filter G* can be a SAM hologram [Tao93].

Now, if we move one Fourier transform lens L_2 in the 4-f correlation system to contact the lens L_3, we introduce a phase factor, $\exp[\frac{-jk(x_3^2+y_3^2)}{2f_2}]$, at the correlation plane. Then, we use the thin lens combination formula,

$$\frac{1}{f_2}+\frac{1}{f_3}=\frac{1}{f_c} \tag{3.8}$$

Fig. 3.7 *Evolution of the optical correlator from a 4f to a 2f system: (a) VanderLugt 4f system; (b) & (c) 3f system; (d) & (e) 2f system.*

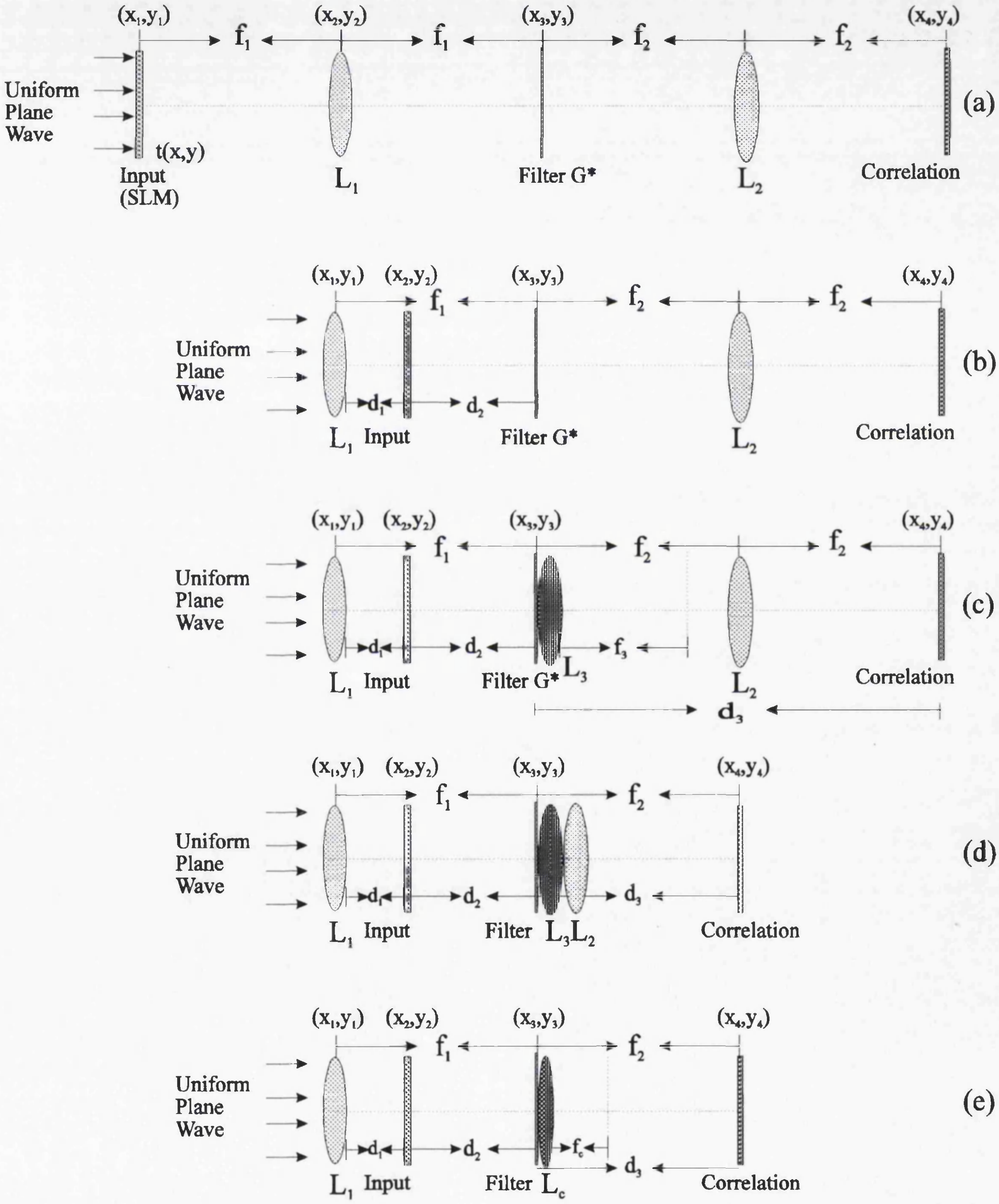

to combine lenses L_2 and L_3 as shown in Fig. 3.7(d) into one lens L_c in Fig. 3.7(e) to make the 2f system. Thus, $\psi_4(x_4, y_4)$ can be rewritten as

$$\psi_4(x_4,y_4) = \frac{e^{jkd_3}}{j\lambda f_c} h(x_4,y_4;d_3) \iint P_c(x_3,y_3)\psi(x_3,y_3) G^*(\tfrac{x_3}{\lambda d_2},\tfrac{y_3}{\lambda d_2}) h(x_3,y_3;-f_c)$$
$$h(x_3,y_3;d_3)\exp[-jk\tfrac{x_3x_4+y_4y_4}{d_3}]dx_3dy_3, \qquad (3.9)$$

where $P_c(x_3, y_3)$ is the pupil function of L_c (L_c=1 when lens L_c is large enough in our case).

By substituting Eq. 3.6 into Eq. 3.9, we can make the arrangement as following:

$$\psi_4(x_4,y_4) = -j(\tfrac{f_1}{f_c})e^{jk(f_1+d_3)} h(x_4,y_4;d_3)\iint T(\tfrac{x_3}{\lambda d_2},\tfrac{y_3}{\lambda d_2}) G^*(\tfrac{x_3}{\lambda d_2},\tfrac{y_3}{\lambda d_2})$$
$$\exp[jk(\tfrac{x_3^2+y_3^2}{2})(\tfrac{1}{d_2}+\tfrac{1}{d_3}-\tfrac{1}{f_c})]\exp[-jk\tfrac{x_3x_4+y_4y_4}{d_3}]d(\tfrac{x_3}{\lambda d_2})d(\tfrac{y_3}{\lambda d_2}). \qquad (3.10)$$

The function $\psi_4(x_4,y_4)$ is the Fourier transform of the signal if d_2=d_3, $\frac{1}{d_2}+\frac{1}{d_3}-\frac{1}{f_c}=0$ and the change in scale is not taken into account. And, we know that in the correlation plane we physically observe light intensity and not the amplitude. Therefore, any arbitrary phase factor appearing with the correlation signal is not observable (that means the phase factor term in Eq. 3.10 can be dropped). The final output at the correlation (x_4, y_4) plane is

$$\psi_4(x_4,y_4) = \iint T(u,v) G^*(u,v) e^{j2\pi(ux_4+vy_4)} du dv, \qquad (3.11)$$

where $u=\frac{x_3}{\lambda d_2}$ and $v=\frac{y_3}{\lambda d_2}$. The output signal is equal to the convolution of the functions t and g (inverse Fourier transform of G*). This result can be applied to the spectral correlation system by exchanging the input t and matched filter G* in order [Sel91].

From the above analysis, a 2-f correlator has been designed. This system is typically half of the physical length of the 4-f VanderLugt correlation system. By using this configuration the HOFNET [Sel91] can be made more compact.

3.4 Improving Holographic Diffraction Efficiency

The resurgence of interest in the use of holography has been, in part, encouraged by many new developments and demonstrations in multiplexing holography and associated techniques. The successful storage of 500 high-resolution angularly multiplexed holograms in $LiNbO_3$ by Mok et al. [Mok91] and 756 high diffraction efficiency spatio-angular multiplexed hologram $LiNbO_3$:Fe by Tao et al. [Tao93] sparked renewed interest in holographic data storage followed by more recent results that have demonstrated the storage and recall of up to 10,000 complex image-bearing holograms superposed in relatively small volumes (e.g., on the order of 1 cm^3) [Mok93, Bur94, & Tao93 & 95].

Although the concept of using multiplex holography for data storage in implementing associative memory has been considered for several years, recent advances in several critical device technologies along with developments in storage material and architectures have greatly enhanced the likelihood of successful implementations. A number of design options for the overall mass memory for neural networks systems are available, each offering a unique set of trade-offs involving bit error rate, capacity, diffraction efficiency, data transfer rate, and ruggedisation/packaging issues. The details of the multiplexing techniques along with the demonstrations of the leading candidate schemes are the subject of this section. We also describe some aspects of current effort in this project to develop a holographic memory device with high diffraction efficiency using phase conjugation feedback.

3.4.1 Reviews of volume holographic memory

The understanding of the various multiplexing operations has been upgraded by numerous analyses and experiments. In this subsection, we mainly discuss the four most prominent holographic multiplexing schemes that allow the storage and retrieval of independent pages of data in a common recording volume: spatial [Mok94], angular [Sta72 & Mok93], wavelength [Rak92 & Yin93], and phase code [Den91 & For90]. All four multiplexing options are based on the Bragg-selective readout of thick (volume) holograms. It is worthwhile to mention that newer promising multiplexing techniques have been proposed and successfully demonstrated [Tao93 & 95]. Also, some combinations of angular, wavelength, and/or phase code multiplexing can be considered although the significant increase in cost and complexity of the resulting device and system may not be justified by the benefits.

The concept of storing information in the form of multiplexed holograms in volume media as memories originated from the 1960s [Lei66, Van63, & Ram72]. These holographic memories are promising for large capacity neural-network-based computer storage system, such as arithmetic databases or for computer needs in providing both archival and backup data storage as well as the emerging applications involving network data and multimedia services. They also offer the potential of providing parallel associative search capability to the database and perhaps can include data processing within the memory itself. The fundamental idea underlying a variety of holographic storage strategies is the recording of a large number of complex holograms in a common volume of holographic material (static or dynamic) and subsequently spatially multiplexing such common volume storage units to build up the required storage capacity [d'Au74]. Each object beam that is spatially modulated with data (page) is recorded with a reference beam. Bragg selectivity provided by the volume interaction allows independent retrieval of each stored page on the basis of optical parameters such as the wavelength, the angle of arrival of the reference beam or the spatial phase distribution of the reference beam.

A generically multiplexed storage architecture for volume holographic memory systems is shown in Fig. 3.8 in which the necessary object and reference beam were supplied from a tunable laser at wavelength, λ, for both the recording (data storage) and reconstruction (data retrieval) processes. Two spatial light modulators (SLMs) were used; one spatially encodes the object beam with a page of data to be recorded, and the other spatially phase modulates the reference beam, which is first passed through a scanning device (mirror on rotational stage or acoustic-optic deflector) then passes telecentrically onto the holographic medium, to serve as the proper page address. To date, there exist several multiplexed schemes fulfilled by controlling optical parameters for holographic storage, which can be categorised as follows:

Spatial Multiplexing In the spatially multiplexed scheme, the modulation frequencies for all the images are the same, while the positions on the recording plane are different. In such a scheme each information page (image) can be stored into a volume hologram written with the object and reference beam at a particular interbeam angle, θ, and area, A_i, located at x_i, y_i. To diminish the cross-talk occurring during the readout process, these images can be stored in well-separated locations on the recording medium by multiplexing the Fourier transform holograms. However, the capacity of storage was limited by the resolution of the image and the *f*-number of the lens used to Fourier transform the image into the Fouirer transform plane (hologram plane).

Fig. 3.8 *A generic schematic shows the setup of recording different types of multiple hologram by controlling optical parameters of storage from exposure to exposure as*

(a) spatial multiplexing: vary the location, (x_i, y_i), by shifting the crystal along xy plane;
(b) angular multiplexing: vary θ and/or δ by scanning the reference beam or rotating the recording medium along z-axis ;
(c) wavelength multiplexing: vary wavelength λ by tuning the laser;
(d) phase-encoded multiplexing: vary φ (x,y) by ;
(e) spatio-angular multiplexing: change (x_i, y_i) and vary θ and/or δ ;
(f) wavelength and angular multiplexing: vary λ and θ and/or δ;
(g) phase-encoded and angular multiplexing: vary φ (x,y) and θ and/or δ.

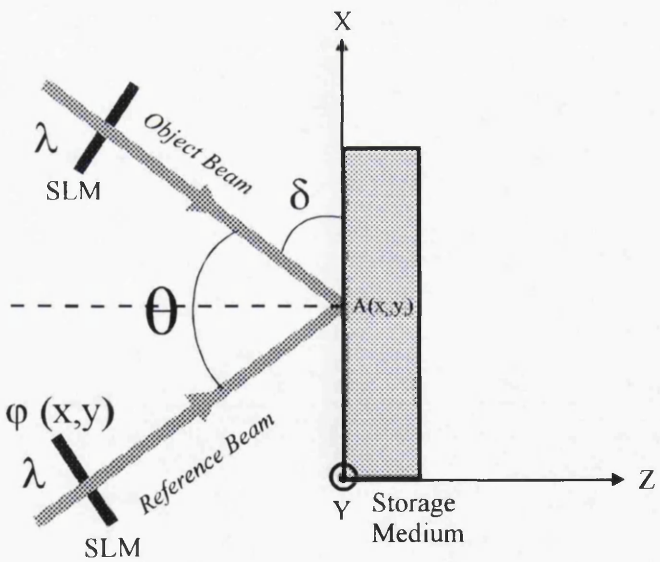

Angular Multiplexing Angular multiplexing is based on the observation that a volume hologram written with the object and reference beams with a particular interbeam angle, θ, and superimposed on the same area, A_i, located at x_i, y_i of the recording medium will reconstruct with an efficiency that is strongly dependent on the difference in angle of arrival between the recording and reading reference beams. The advantage of such recording is that is fully uses the volume of the crystal, and the resolvable angular spacing of reference beams to distinguish the pages which are multiplexed in the same area, so that very high storage density can be achieved. The disadvantage is that the exposures made later in a superposition can erase holograms recorded earlier. Therefore, the problem of exposure scheduling, in which photorefractive holographic recording times must be adjusted for each recorded holograms, is unable to eliminated. Cross-talk or interference between the holograms, which are superimposed together onto the same area, are inevitable when spatial data bearing object beams are used since multiple plane wave components contribute to the blurring of the angular selectivity.

Wavelength Multiplexing In the case of the wavelength multiplexed scheme, the reference and object beam angles are kept constant but the laser wavelength is varied from exposure to exposure. The addressing mechanism is provided by wavelength selection, which must be provided by a tunable laser. For data retrieval, a properly addressed reference beam (wavelength) illuminates the holographic storage medium yielding an optical reconstruction of the associated page of data.

Phase code Multiplexing In the phase-encoded multiplexed scheme, each reference beam consists of a set of plane waves with unique phase distribution across its component waves. Each reference beam is coded with a phase distribution from an orthogonal set of such codes. During readout, a particular object pattern (or a page of data) can be retrieved by illuminating the hologram with the corresponding phase code reference beam. By introducing the angular selectivity of volume hologram this significantly reduces the level of cross-talk, thus enabling the data storage application that requires a high level of multiplexing capability. Because each reference consists of a large set of plane waves, the phase code technique results in more uniform output behaviour during replay since effects that arises from individual plane wave components are averaged. However, inaccuracies introduced by the phase coding element, the reference beam phase spatial light modulator (SLM), are the possible drawbacks of the phase code approach. For data retrieval, a properly addressed phase code reference beam illuminates the holographic storage medium yielding an optical reconstruction of the associated page of data.

Spatio-Angular Multiplexing (SAM) In the case of spatio-angular multiplexed (SAM) scheme, each hologram, which is written with the object and reference beam with a particular interbeam angle, θ_i, and superimposed on the recording medium, is partially overlapped with its neighbors. Each information page stored can be retrieved by reading holograms with the appropriate reference beam, which was used for recording, without cross-talk. By using partially overlapping holograms, several advantages provided by SAM are: (i) the storage capacity can be increased since more holograms can be accommodated into a crystal, as compared to spatial multiplexing; (ii) the erasure effect can be minimised during the sequential recording, as compared to angular multiplexing; (iii) the diffraction efficiency can also be increased, as compared to existing multiplexing schemes, to date. The disadvantage is that the device made for replaying holograms becomes complicated.

In ONNs the density of memories can be increased using hybrid multiplexed scheme by incorporating several holographic multiplexings as described in previous section. However, the exposures made later in a superposition can erase holograms recorded earlier. Therefore the problem of exposure scheduling, in which photorefractive holographic recording time must be adjusted for each recorded holograms, is unable to eliminated. Because of the erasure that occurs when multiple holograms are recorded in photorefractive crystals, the diffraction efficiencies for multiple holograms fall off asymptotically as the inverse of the square of the number of hologram. Therefore, when 5000 holograms are stored, the diffraction efficiency for each hologram is only of the order of 10^{-6}. Obviously, it is very difficult to optical implement associative memory in ONNs by the use of these holograms.

3.4.2 Photorefractive phase-conjugate holographic storage

In this section in order for increasing the diffraction efficienies of holograms stored in volume photorefractive medium we propose on novel photorefractive holographic storage in the use of 2 self-pumped phase conjugate mirrors (SPPCMs) and demonstrate experimental results.

It is always important to store the original "template" images in memory and to be able to replay them with good fidelity, high efficiency and good signal-to-noise ratio. Two beams are usually used to record the holographic image one being the reference beam which is usually a plane collimated beam while the other is the object beam which usually passes though a spatial light modulator on which has been displayed the template image to be stored. A convenient optical configuration for this (Fig 3.9(a)) consists of the reference beam and the object beam equally inclined either side of the normal to the crystal face.

Fig. 3.9 *Holographic grating recording in a photorefractive crystal, (a) using the conventional configuration, (b) using a pair of mirrors, and (c) using a pair of phase conjugate mirrors*

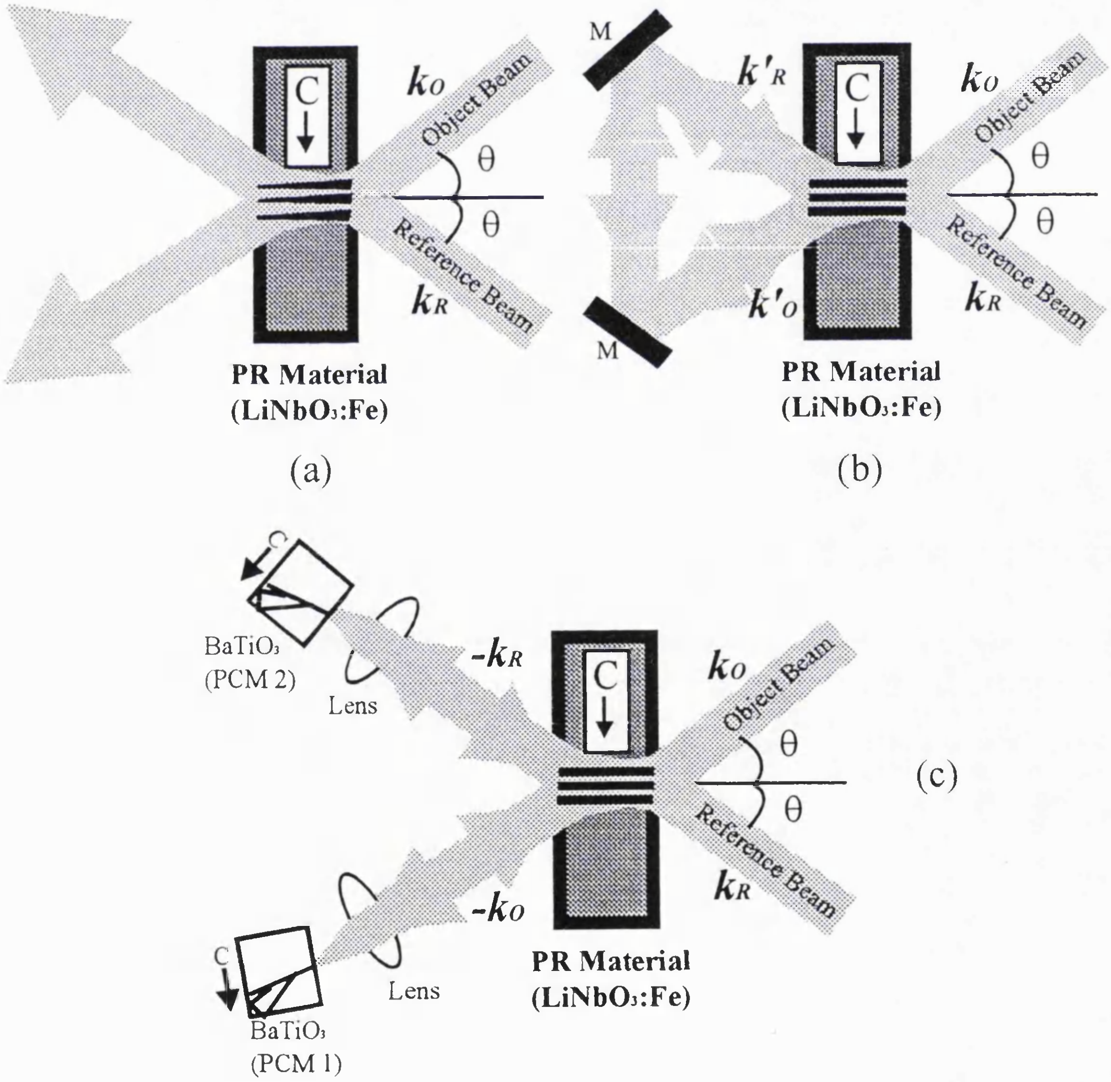

The two beams are arranged to overlap and interfere within the recording crystal to give a periodic interference pattern with the fringes oriented normal to the surface. The recording medium is often lithium niobate doped with a 0.05% weight of iron which is a brown crystal and so absorbs the light significantly - a typical 7 mm thick crystal had a transmittance of 34.0±0.2%. This means that the light intensity in the writing beams and, hence, in the interference fringes drops through the crystal and so the exposure effectively drops with penetration depth. This becomes more serious for thicker and darker crystals. Moreover, in order to record the hologram in a short time sufficiently powerful initial beams are required. It would certainly be more convenient if a lower power and generally more compact laser could be used.

If the reference and object writing beams are both plane and collimated we can set up the experiment shown in Fig 3.9(b). Here two mirrors are arranged to reflect the transmitted object beam back along the incident reference beam and at the same time the mirrors reflect the transmitted reference beam back along the incident object beam. Moreover, the incident reference beam diffracts from the grating as it is formed and is diffracted into the direction of the transmitted object beam and the incident object beam is diffracted into the direction of the transmitted reference beam. The two beams travelling from the mirrors into the crystal write a holographic grating which decays in strength with the depth penetrated. The grating formed by the reflected beams can be made to coincide with the grating written by the original beams to add constructively if the angles between the reflected beams are identical to those between the incident beams and the crystal and if a truly symmetric arrangement is used to ensure that the phase difference between the reflected beams is the same as that between the initial beams. The reverse decay of grating amplitude through the crystal due to the reflected beams offsets, to some extent, the decay in the opposite direction of the initial beams although the sum of two offset exponential decays of opposite sense and of differing magnitude can never give a constant exposure. The increased light intensity in the interference pattern in the crystal means that shorter exposures are required. This system requires critical alignment and will not work if the object beam is other than plane and collimated.

This leads to the second more promising configuration (Fig 3.9(c)) in which the two ordinary mirrors in (Fig 3.9(b)) have been replaced by two phase conjugate mirrors [Yar91] operating in a self-pumped phase conjugating mode without externally applied pump beams or other power source. In this case both the reference beam and the object beams (no matter how complex) are returned to retrace their original paths but in the opposite direction with the same phase as they had on their incoming journeys. The amplitudes of the beams decay exponentially in both directions through the photorefractive crystal again offsetting, to some extent, the non-uniform depth profile.

In our experimental system (Fig 3.10) the laser was a Spectra-Physics argon ion laser with intracavity etalon (λ=514.5 nm) which was power stabilised to within 0.5%. The total exposure intensity was 28 mW/cm^2 and both beams had an equal intensity and diameter. The size of the region illuminated was a circle of diameter 2 mm. Each beam was angled at θ =45° to the normal and was extraordinarily polarised (in the plane of the figure). The photorefractive crystal was Y-cut lithium niobate with 0.05% weight of iron doping resulting in a 34.0±0.2% transmissivity for our 7mm thick crystal and was mounted on a Micro-Controle motor-driven rotary stage, having angular resolution of 0.001°. The diffraction efficiency was monitored using a Newport picowatt digital power meter. Both the rotary stage and the power meter were controlled by an IBM compatible personal computer.

The lenses shown in Fig 3.10 are simply to focus the wide beams into the small barium titanate crystals (5 mm cubes) used for the phase-conjugate mirrors. This has the added advantage that the power density is increased which should improve the response times. The optimised reflectivity of the self-pumped crystals in the "Cat" configuration was 30% for the Chinese grown one and 35% for the American grown one. One of the phase-conjugate crystals was induced by illumination using a He-Ne red laser beam. This is a recent technique developed by us during this research and reported in reference [Sel93] in which a red beam is directed into the crystal at a completely different angle and improves the response time, the phase conjugate reflectivity and, most importantly here, the angular range over which the self-pumped phase conjugation is possible. It was not required to induce both phase-conjugate mirrors because only one was subjected to incident beams over a wide range of angles. The diffraction efficiency of the holograms (defined to be the ratio of the diffracted power to the transmitted power through the unrecorded crystal) was measured during the recording by using a red probe beam from a helium-neon laser (λ=632.8 nm) as shown in Fig 3.10. The red beam had to be incident at a larger angle from the normal than for the green beam to obtain the highest diffraction efficiency due to the longer wavelength. The power was recorded using a Newport picowatt digital power meter. The room temperature was measured to be 26.0±0.1°C.

Fig. 3.10 *(a) Schematical layout and (b) experimental arrangement for recording high diffraction efficiency holographic gratings. M:mirror; BS:beamsplitter; VBS:variable beamsplitter; HWP:half-wave plate; L:lens; FTL:Fourier transform lens; ES:electronic shutter; MCM:motor-controlled mirror; CR:x-t chart recorder; S:screen; PD:photodetecter; IB:inducing beam; OB:object beam; RB:reference beam.*

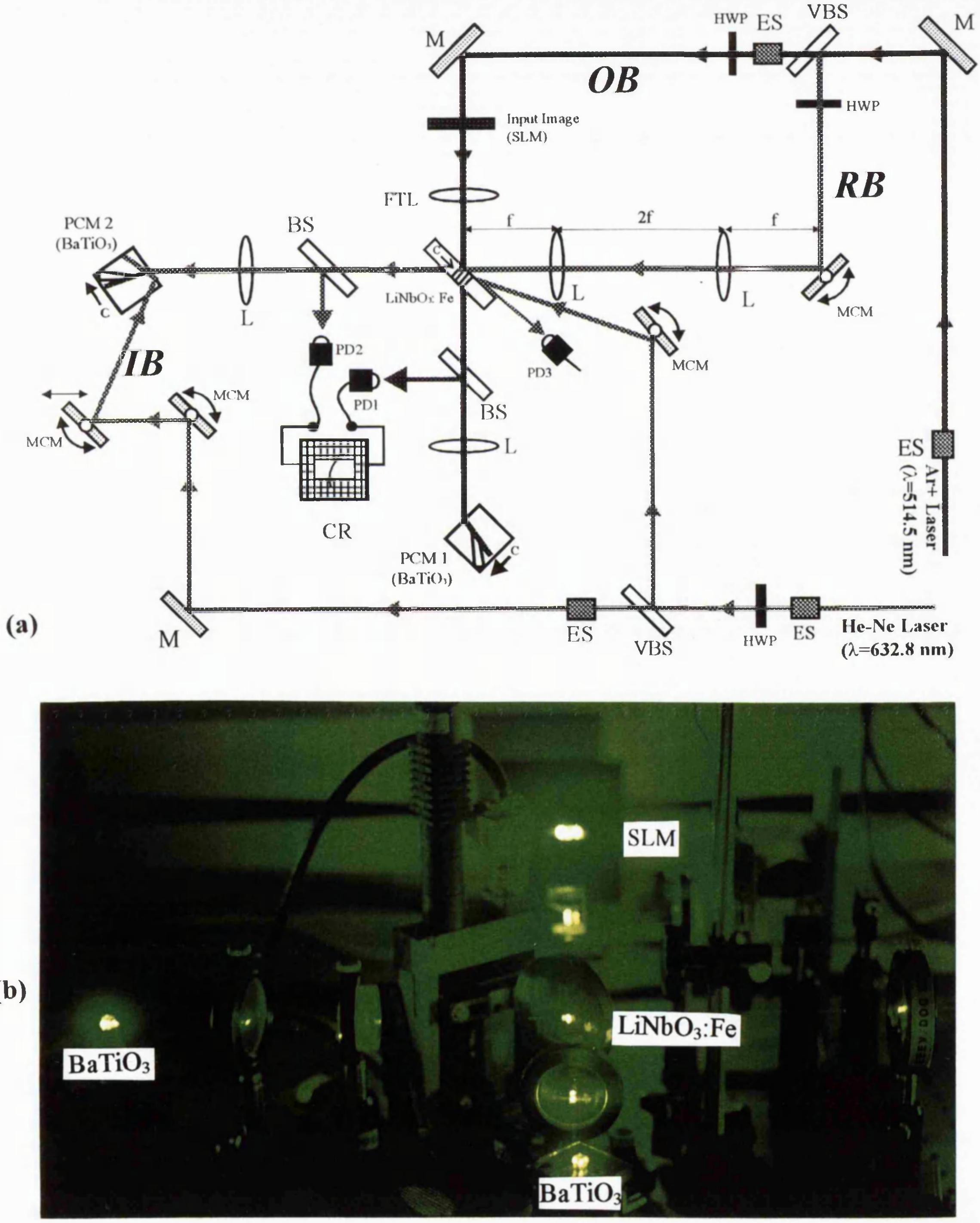

Figure 3.11 shows a plot of the diffraction efficiency as a function of time. The curve dotted was obtained experimentally without using phase conjugate mirrors with the recording set up shown in Fig 3.9(a) while the solid curve was obtained when phase conjugate mirrors were used in the configuration shown in figure 3. 9(c). Both curves have similar forms showing initial growth and relaxation back to a lower more stable value with time. The curves grow at the same rate for the first 15s and, thereafter, the curve using PCMs, grows at a much faster rate than that without PCMs and attains a higher maximum efficiency of 22.1% after 220s than without PCMs which has a maximum of 17.9% after 179s. This represents an improvement in diffraction efficiency of 4.2%. Both curves tend to a diffraction efficiency of about 16.5±1% at longer exposure times of 9 mins so the exposure must be stopped at the optimum time for maximum diffraction efficiency.

Fig. 3.11 *Plots showing the growth of the holographic grating diffraction efficiency with time; dotted curve uses the conventional configuration while solid curve uses the novel phase conjugate mirror recording configuration.*

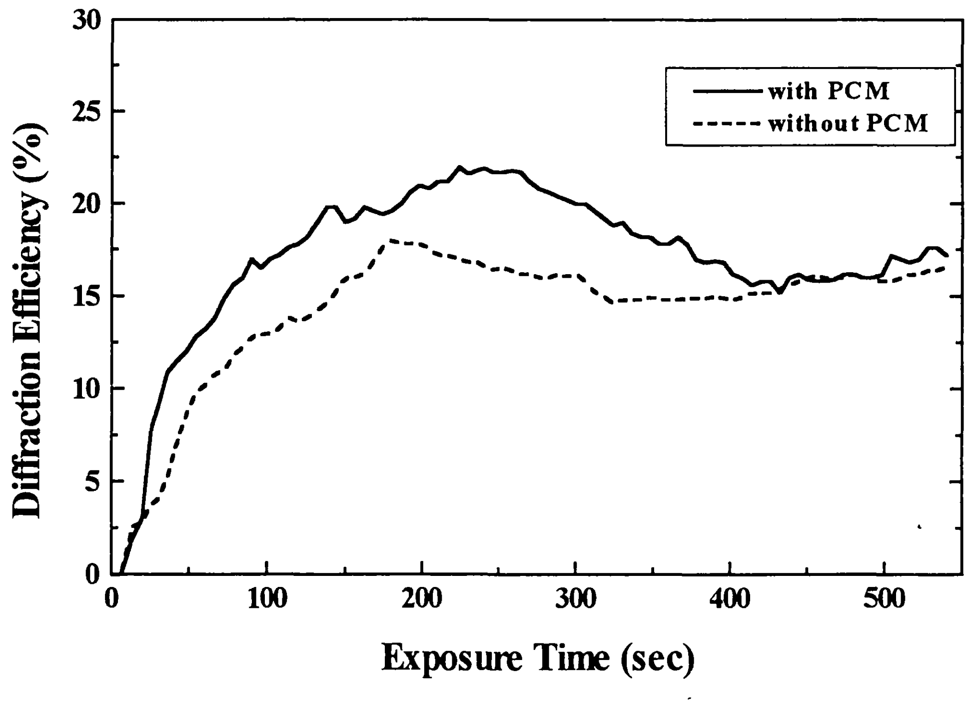

The curves do not appear to fit well to a model based on the usual inverse exponential saturation, but simply for the sake of comparison, we have calculated the writing time constants assuming the maximum refractive index modulation is achieved in each case at the maximum diffraction efficiency using the same method as that used in ref [Tao94] assuming that η_{sat} is a function of the total writing power. This gives a writing time constant of 30.4s for the curve using PCMs and 42.2s for the curve without. The experiment was repeated several times using different spatially separate parts of the same crystal and similar results were obtained. It is possible that this arrangement can be theoretically modelled by coupled wave theory although this has not yet been carried out.

We conclude that the method using two PCMs results in reproducible higher rates of growth of diffraction efficiency i.e. shorter writing time constants, resulting in a higher maximum diffraction efficiency. This supports our proposition that increased light intensity is achieved resulting in faster growth of diffraction efficiency. The higher maximum value may be linked to a better diffraction efficiency uniformity with depth. This recording method was also used to record up to 24 angularly multiplexed holographic gratings which were used in the system described in the next chapter.

3.4.3 Bragg-off diffraction in a $LiNbO_3$:Fe crystals

In volume holography, the angular selectivity is essential for both the storage and retrieval of multiplexed holograms. The selective angle determines the optimum angular separation during recording to achieve a storage capacity as high as possible with minimum cross-talk. The optimum access configuration must be used during readout that results in the highest diffraction efficiency and signal-to-noise ratio. Both the effects of polarisation and intensity coupling on the angular sensitivity have been demonstrated by S. Tao et al. [Tao93 & 94]. In their efforts they, for the first time, experimentally verified the theories proposed by Heaton et al [Hea84], who concluded that the maximum diffraction efficiencies of photorefractive gratings should happen at reading angles very slightly different from the writing angles. Tao et al. [Tao94] referred to this phenomenon as the "Bragg-shift". According to Heaton's and Tao's results, a slanted grating will be recorded by two writing beams with unequal beam intensity (beam ratio, q, is not equal to 1) in a photorefractive crystal using a symmetrical geometry. As a result, the maximum diffraction efficiency of grating occurs at a readout angle different from the recording angle. However, there is still a shift in the Bragg angle when the exposure of the recording process exceeds some level even when the grating is formed by two writing beams with equal beam intensities, i.e. $q=1$. In this section we experimentally investigate these peculiarities of the angular sensitivity and the diffraction efficiency of single transmission gratings recorded in a photorefractive $LiNbO_3$:Fe crystal.

We use an experimental arrangement similar to that used for investigating the phase-conjugate storage with two PCMs as shown in Fig. 3.10. The writing wavelength was 514.5 nm and the reading either 632.8 nm or 514.5 nm operating at a lower power level, which eliminated erasing during readout. We monitor the grating formation process by using a red probe beam from a helium-neon laser (λ=632.8nm). The diffraction efficiency of the grating was measured by blocking one of the writing beams.

We first performed a series of measurements of the optimum angular deviation for our sample and the results are shown in Table 3.1. and Fig. 3.12. In Table 3.1 we have found that The maximum diffraction occurs when the readout angles are 0.006° (q=1), and 0.008° (q=5), and 0.016° (q=10), respectively. There are slightly greater than those achieved when read out at the writing angle for q=1 and 5.

Table 3.1 *Experimental measurements of the grating formation with respect to different exposures for beam ratio, $q=I_R/I_O$, equal to 1, 5 and 10. A symmetric recording was used with a writing angle of 25° between the object beam and reference beam.*

	Exposure (J/cm²)	6.2	12.5	25.2	37.8	63.0	88.2	113.0	151.0
$q=I_R/I_O$ $=3.3mW/3.3mW=10$	Bragg-shifted angle (°)	0.000	0.004	0.006	0.008	0.014	0.018	0.022	0.022
I_{total}=6.6mW	η_{Bragg} (%)	5.1	10.1	12.2	11.4	7.9	5.9	4.2	3.6
I_{read}=13.5 μW	$\eta_{Bragg\text{-}shifted}$ (%)	5.1	12.0	14.2	16.8	13.4	15.0	10.3	8.3
$q=I_R/I_O$ $=5.5mW/1.1mW=5$	Bragg-shifted angle (°)	0.004	0.01	0.012	0.014	0.018	0.020	0.022	0.020
I_{total}=6.6mW	η_{Bragg} (%)	0.5	1.0	2.2	1.7	1.5	1.1	0.7	1.1
I_{read}=4.5 μW	$\eta_{Bragg\text{-}shifted}$ (%)	0.7	2.8	11.9	12.2	7.4	4.6	3.0	2.0
$q=I_R/I_O$ $=6.0mW/0.6mW=1$	Bragg-shifted angle (°)	0.006	0.010	0.012	0.016	0.020	0.020	0.024	0.020
I_{total}=6.6mW	η_{Bragg} (%)	1.6	2.8	1.3	3.4	4.4	5.0	4.1	6.3
I_{read}=3.2 μW	$\eta_{Bragg\text{-}shifted}$ (%)	2.5	6.6	4.4	32.0	31.3	28.1	14.1	10.9

Fig. 3.12 *3-D Plots showing the experimental results for angular shift and diffraction efficiency of the resultant grating with respect to exposure for beam ratio, $q(I_R/I_O)$, equal to 10. A symmetric recording was used with a writing angle of 25°.*

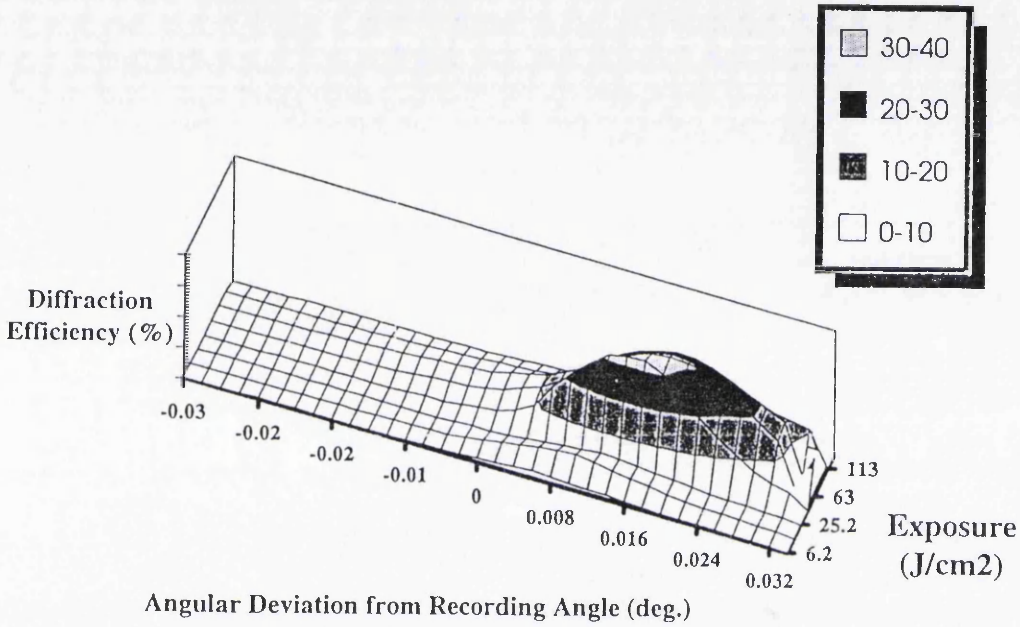

Fig. 3.13 shows the 3-dimensional plot of the diffraction efficiency with respect to angular deviation from recording angle and exposure of recording for q=10 case. we have found that the read out angle for the maximum efficiency (32%) is Bragg shifted with 0.008° when total exposure is 37.8 J/cm^2.

Compare our results with those obtained from Tao et. al. [Tao 93 & 94] and Heaton [Hea84], it can clearly be seen from our experimental measurements of selective angle for $LiNbO_3$ that is usually shifted into a typical angle depending on not only *intensity ratio* between two writing beams but the *total exposure* during the recording. These results suggest that to obtain the optimum readout performance from gratings written by two beams in $LiNbO_3$ crystal, readout beams must be angularly shifted with a desirable angle.

3.5 Conclusions

In conclusion, we have proposed a compact optical photorefractive holographic correlator employing a 2-f correlation system. This compact scheme is suitable for incorporation into an optical photorefractive resonator with the spatio-angular multiplexing (SAM) [Tao93] scheme for recording holograms to implement a high order feedback neural network (HOFNET) [Sel90 & 91] system. Based on the merits of the HOFNET the 2f systems physical length can be shortened to half as much as in the conventional 4f correlation system and losses can be avoided.

We have increased the diffraction efficiency of volume holograms stored in a photorefractive crystal by making use of two self-pumped phase conjugate mirrors (SPPCMs) as part of the recording technique. One of the SPPCMs was induced to widen the angular range over which phase conjugation of beams could take place which again has not been done before. We recorded 21 angularly multiplexed holograms. When a single grating was stored the highest efficiency of 32% was obtained using a diode pumped frequency doubled YAG. To our knowledge this is the highest efficiency reported to date for volume holograms in this material.

We discovered that the Bragg-shift depends on the total exposure during the recording and not just on the beam ratio. The Bragg-shift effect was discovered several years earlier at UCL by Tao et al. [Tao93] when she found that higher efficiency replay of volume gratings formed in photorefractive crystals was possible by altering the replay angle very slightly from that used for recording in the case when the two recording beams had had different intensities. In some case we found that an increase in efficiency from 3.4% to 32.8% was possible by choosing the correct angle.

Chapter Four

MULTI-BEAM INDUCED PHASE-CONJUGATE MIRROR (MIPCM) AND APPLICATIONS IN OPTICAL RESONANT SYSTEMS

4.1 Introduction and Motivations

In recent years, multiple beam optical phase conjugation has been displayed in two kinds of experimental arrangement: double colour pumped phase-conjugate geometries [Sol93 & 94] and multigrating phase conjugation by four-wave mixing (FWM) in a crystal. The exact result of multigrating phase conjugation by means of degenerate four-wave mixing in photorefractive media was first obtained by Krolikowski et. al [Kro87]. Thereafter, multiwave mixing in photorefractive BSO crystals was proposed, phase conjugation of four beams was performed [Vai87], and optical logic operations using phase conjugation interferometry was also demonstrated [Ogu90]. But no successful experimental demonstration of multiple beams in a self or mutual phase-conjugate arrangement in a photorefractive crystal has been reported so far. In both self and mutual phase conjugation, no external pumps are needed so that these devices are compact and feasibly applicable for optical feedback in optical associative memory [Owe87]. In this chapter a new technique, for the first time, has been developed to *induce* (not external pump) the phase conjugation for several input beams simultaneously in a 0°-cut undoped photorefractive $BaTiO_3$ crystal.

The phenomenon of "induced" phase conjugation was first reported by Yau et.al [Yau92] including myself before coming to UCL. In this phenomenon a single beam, to be phase conjugated, is positioned and angled correctly on one face (*a* face) of a 5 mm barium titanate crystal cube so that no self-pumped phase conjugate beam is generated. Then when a second "inducing" beam is positioned and angled on an adjoining face (-*c* face) of the crystal the first beam begins to be phase conjugated. The conjugate beam grows in strength to a maximum value with little oscillation. When the inducing beam is removed the first beam is no longer phase conjugated in the case when the two beams, operating at 514.5 nm with coherence length ~3m, are single-longitudinal mode and coherent. It is thought that one strong grating or a lot of gratings is formed which is erased by the signal beam when the inducing beam is removed. However, when the two beams, operating at 514.5 nm with coherence length ~5cm, are multi-longitudinal mode and incoherent the phase conjugation behaviour continues to exist after the inducing beam is removed. It is thought that of the many phase conjugate loops set up, some have a longer lifetime. It was found that higher efficiency phase conjugation was obtained using the incoherent inducing beam. Effectively these represent an optically switchable and latchable phase conjugation mechanism. We named these "induced self-pumped phase conjugation (ISPPC)". Qiu et al [Qiu93] also demonstrated the same effect using a differently angled inducing beam in a slightly larger volume crystal of $(BaSr)TiO_3$. In both experiments both of the beams were kept in the same polarisation, extraordinarily (horizontally) polarised and incident onto two adjoining faces of the crystal with the inducing beam always incident on the *-c* face. Despite the promise of ISPPC for high reflectivity and a fast response time for phase conjugation, the mechanism responsible for the phase conjugation in this phase conjugator has not been conclusively identified, and this lack of understanding hindered the control and optimisation of its optical phase conjugation property.

In this chapter we extend our previous investigation [Yau92] of ISPPC to deepen our understanding and to optimise the performance by demonstrating the simultaneous phase conjugation of several input beams incident on the *a* face (Fig. 4.1(a)). This was performed as follows: The input beam power, angle and position was set as in earlier work so that no phase conjugation occurs unless a switchable inducing beam is present on the *-c* face of the crystal. If now several (1 to 4) angled beams are directed onto the *a* face, only when the inducing beam is present multi-beam phase conjugation (Fig. 4.1(b)) occurs. The input beams are derived from the same laser with the same wavelength and are incoherently related whilst the inducing beam is incoherent and can be of a different wavelength. We refer to this phenomenon as "multi-beam induced phase conjugation (MIPC)". Unlike the setup of traditional phase-conjugate mirrors, which require a more precise arrangements, the optical setup of our multi-beam induced phase conjugation is relatively relaxed.

Fig. 4.1 *Schematic diagrams of multi-beam induced phase conjugation (MIPC), (A) before inducing beam is applied, and (B) after inducing beam is applied.*

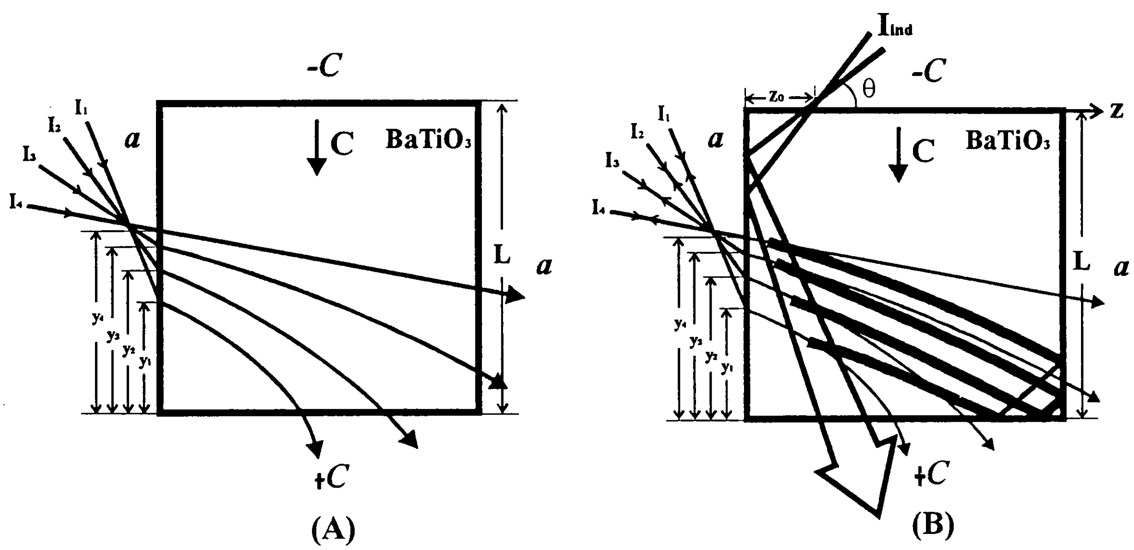

The chapter is organised in the following fashion. Section 4.2 gives the theoretical understanding of multiple beam phase conjugation in the form which is most appropriate for interpretation of the experiments with photorefractive crystals. In Section 4.3 we describe our novel configuration for phase conjugation with multiple beams in a photorefractive $BaTiO_3$ crystal, in detail, together with the details of the experimental apparatus used in our experiments. In Section 4.4 we demonstrate our investigation of the single beam induced self-pumped phase-conjugation process and more detailed analysis is given including more diagnostic experiments, such as intensity and polarisation dependence measurements. Section 4.5 mainly deals with four beams, the largest number to date, for the first time, to our knowledge, phase conjugating simultaneously and gives more details of the induced mutual incoherent beam coupling process with two beams, and two types of phase conjugation, one is induced self-pumped and the other is induced mutually pumped phase conjugation, occurring while three beams were guided into a crystal. However, externally pumped four-wave mixing multiple phase conjugation with 4 beams has already been shown [Nai87]. In Section 4.6 the discussion will be directed to the possible explanation for our results. Applications such as self-pumped phase-conjugate resonator and multi-mode phase conjugate resonator will be illustrated in Section 4.7. Finally, we give our conclusion in Section 4.8.

4.2 Theoretical Background

The popular self-pumped phase-conjugate mirror (SPPCM) [Fei82] and mutually incoherent beam coupler (MIBC) [Smo87 & Eas87] have been observed in some photorefractive crystals, respectively, and some theories [Mac83, Smo87 & Eas87] have been proposed to explain these devices, respectively. In these two phase-conjugate devices, two usually self-generated phenomena exist when a laser light beam illuminates a photorefractive crystal. One is the self-generated fanning, and the other is the self-pumped four-wave mixing (SPFWM) that corresponds to the SPPCM for single beam incident or MIBC for dual beams incident. In photorefractive crystals, the self-generated fanning often takes most energy from the incident beam by TWM. It should be noted that the self-generated fanning affects the formation of SPPCM [Bog93 & Zoz93] and MIBC [Smo87 & Eas87]. When the gains of the two effects are comparable, strong competition between the self-generated fanning effect and SPPCM or MIBC formation take place. We think that the competition of the two sets of gratings (transmission gratings) is an unstable process that leads to the dynamic instability of the SPPCM or MIBC. More often the fanning effect wins the competition and takes all the energy from the incident beam, in the other words, the phase conjugation has been destroyed.

Here, we describe how the SPPCM and MIBC are formed and the self-generated fanning disappears in a photorefractive crystal using the special technique- induced phase conjugation. For simplicity, we just consider (i) a single beam and (ii) two mutually incoherent beams incident on a photorefractive crystal. As described in Section 2.5, the self-generated fanning is always produced by TWM between the scattered light and the incident light. Fig. 4.2 shows the self-generating fanning of a single incident beam and two mutually incoherent incident beams, respectively. In fact, the self-generated fanning depends on the intensity of the input beam in some limited angular range of incidence with respect to the c-axis of the crystal.

Fig. 4.2 *Photos of the self-generated fanning of (a) a single beam incident and (b) two beams incident initially on a $BaTiO_3$ crystal, where the c-axis of the crystal is pointed from the top to the bottom on each photo.*

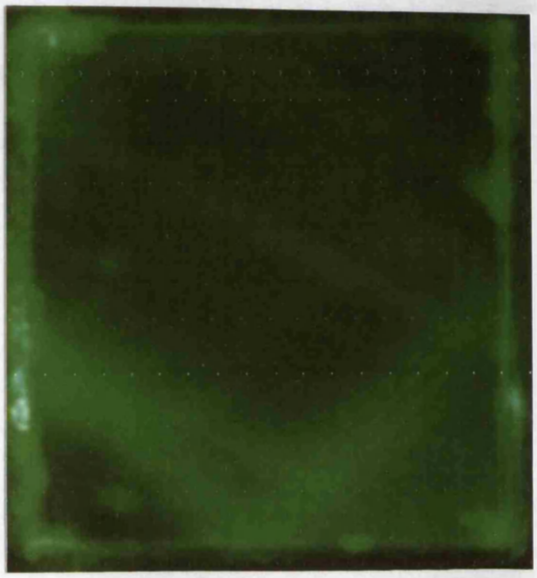

(a)

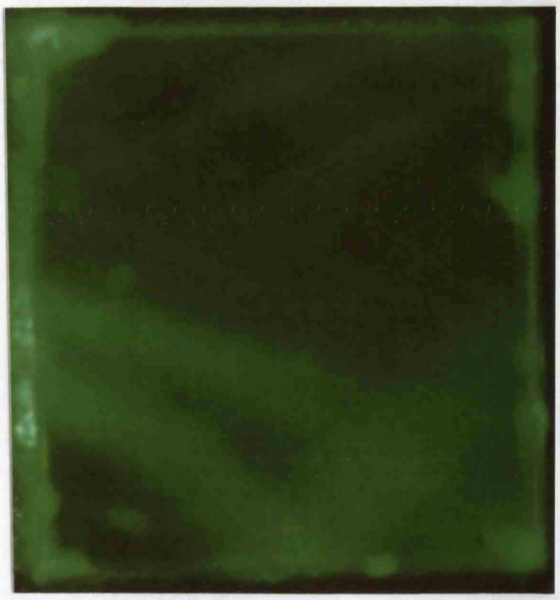

(b)

Ideally, the self-generated fanning is to be a seed for initiating phase conjugation under some critical conditions. Once the SPPCM or MIBC are formed, the self-generated fanning will disappear. Particularly, in certain arrangements, such as when multiple beams (to be phase conjugated) generated from replaying angularly multiplexed holograms are incident on a photorefractive crystal with a wide angular range, which do not chance upon the conditions for spontaneous self-pumped phase conjugation or mutually incoherent beam coupling or both.

Now we consider there are four waves in each interaction region [Mac83, He88] (Fig. 4.3), such as regions A and B in Figs. 4.4(a)-(b), the coupled wave equations of

(a) TWM for self-generated fanning are

$$\begin{aligned}
\frac{dA_1}{dz} &= -(1/2)\gamma_{21}(A_1A_2^*)A_2/I_0, \\
\frac{dA_2}{dz} &= (1/2)\gamma_{21}(A_1^*A_2)A_1/I_0, \\
\frac{dA_3}{dz} &= -(1/2)\gamma_{43}(A_3A_4^*)A_4/I_0, \\
\frac{dA_4}{dz} &= (1/2)\gamma_{43}(A_3^*A_4)A_3/I_0,
\end{aligned} \tag{4.1}$$

and

(b) FWM for self-pumped phase conjugation are

$$\begin{aligned}
\frac{dA_1}{dz} &= -(1/2)\gamma_{21}GA_2/I_0, \\
\frac{dA_2}{dz} &= (1/2)\gamma_{21}G^*A_1/I_0, \\
\frac{dA_3}{dz} &= -(1/2)\gamma_{43}GA_4/I_0, \\
\frac{dA_4}{dz} &= (1/2)\gamma_{43}G^*A_3/I_0,
\end{aligned} \tag{4.2}$$

where γ_{21} and γ_{43} and are the coupling constants which are related to the angles of the incident beams with respect to the c-axis of the crystal. I_0 is the total intensity of the four waves, that is, $I_0 = |A_1|^2 + |A_2|^2 + |A_3|^2 + |A_4|^2$ [Yeh94]. A_i (i=1,4) are the complex amplitudes of the four waves. A_i^* (i=1,4) are the complex conjugates of A_i (i=1,4). G, $(1/2)\gamma(A_1A_2^* + A_3A_4^*)/I_0$, is the amplitude of transmission grating. G^* is the complex conjugate of G.

Fig. 4.3 *Schematics of four-wave mixing (FWM) in photorefractive medium.*

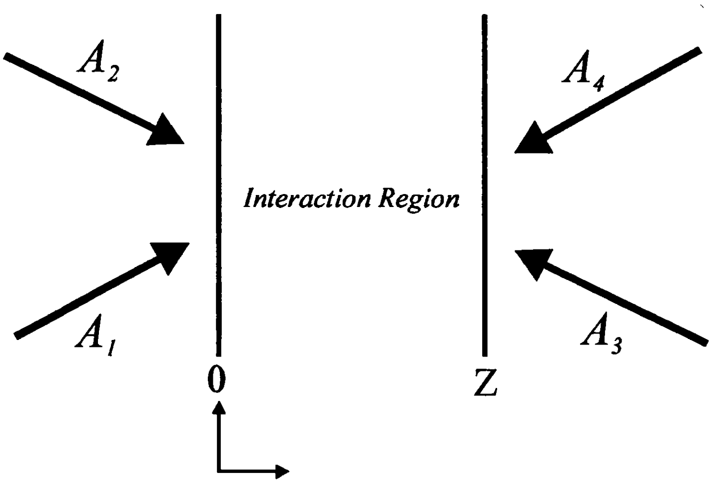

Fig. 4.4 *Schematic diagrams of (A) "Cat" self-pumped phase conjugate mirror with two interaction regions [Fei82 & Mac83], and (B) mutually incoherent beam coupler [Smo87 & Eas87] with two interaction regions A and B in a photorefractive crystal, respectively.*

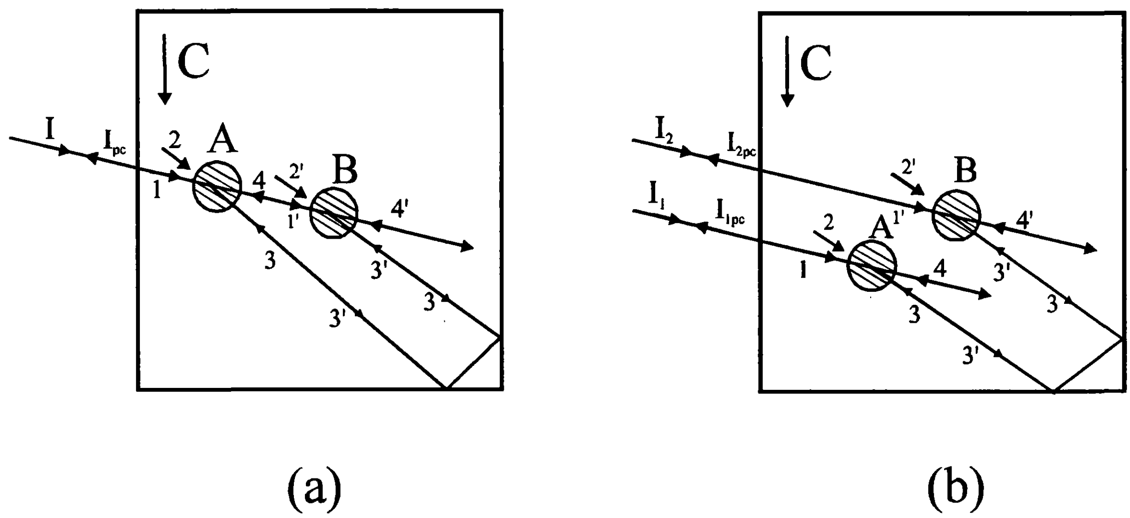

When the self-generated fanning forms, A_1 is the input beam and A_3 is the internal reflection beam in the photorefractive crystal, and A_2 and A_4 are the scattering light beams of A_1 and A_3, respectively. Here, the first two equations of Eq. 4.1 show the self-pumped fanning of the incident light beam, A_1, and scattering light beam, A_2, and the last two equations of Eq. 4.1 present the self-generated fanning of the internally reflected light beam, A_3, and the scattered light beam, A_4. When the SPPCM or MIBC forms, the corner total internal reflections create a pair of light beams A_3 and A_4, with $A_3=\sigma A_1$ and $A_4=\sigma A_2$, where σ is the loss of light in the SPPCM and the MIPC. Thus, the grating amplitude terms in Eq. 4.2, for the self-pumped FWM are

$$G=(1/2)(1+\sigma^2)\gamma(A_1A_2^*)/I_0 \tag{4.3}$$

and

$$G^*=(1/2)(1+1/\sigma^2)\gamma(A_3^*A_4)/I_0\,, \tag{4.4}$$

where $\gamma_{21}=\gamma_{43}=\gamma$. Under suitable conditions [Fei82 & Smo87] (precise incident angle and position of each input beam) for the SPPCM and the MIBC formations, G and G^* of the SPPCM and MIPC in each interaction region are greater than $(1/2)\gamma(A_1A_2^*)/I_0$ and $(1/2)\gamma(A_3^*A_4)/I_0$ for the self-generated fan formation. So the gains of the SPPCM and MIBC are $(1/2)(\sigma^2)\gamma(A_1A_2^*)/I_0$ and $(1/2)(1/\sigma^2)\gamma(A_3^*A_4)/I_0$ greater than those for self-generated fanning, respectively. In other words, the SPPCM and MIBC can win the competition between the phase conjugation formation processing and the self-generated fanning effect. Thus, the SPPCM and MIBC can be well established and the self-generated fanning grating is suppressed. It should be noted that a pair of light beams, A_3 and A_4, is generated by the internal reflection of the cubic crystal in each interaction of the SPPCM and MIBC.

According to above the analysis, in the SPPCM and MIBC, it is necessary that the internal reflection light beam be generated by the corner reflection at the correct angle and with a reasonable energy. In the crystal, the self-generated fanning of each input beam in multiple beams incident a $BaTiO_3$ crystal, as shown in Fig. 4.2, initially propagates in a wide angle range. Some scattered light propagates toward the corner direction and is internally reflected by the corner. The reflected light beams 3 and $3'$ meet the incident light beam in regions A and B, as shown in Fig. 4.4. In suitable incident conditions for SPPCM and MIBC, the gain of the FWM is greater than that of fanning, as described above. Thus, the self-pumped FWM takes place and wins the competition between the self-generated fanning and SPPCM (or MIBC) formation. In the interaction regions A and B of SPPCM (or MIBC), the FWM take place, as described by Eq. 4.2, thus the phase-conjugate light beam, I_{pc} (or I_{1pc} and I_{2pc}), of the incident beam, I (I_1 and I_2), is generated.

So far we have analysed the cases, i.e. either SPPCM for a single input beam or MIBC for two input beams, which were established in a cubic crystal, separately. Until now, there is no evidence that shows that the SPPCM and MIBC can coexist in a photorefractive crystal for multiple input beams. The larger the number of input beams incident (to be phase conjugated), the more self-generated fanning light there is to compete. In this case the phase conjugation conditions will be destroyed by this strong self-generated fanning. Based on these ideas of how induced phase conjugation occurs and on our theoretical analysis in previous paragraph, we think that by introducing one *inducing* beam, which can provide a wide angular range of gratings in the crystal, we can diffract more incident light into the internal reflection, overcome the energy losses from fanning, and to meet the phase conjugation conditions of either SPPCM or MIBC or both.

In conclusion, we have proposed a mechanism for the establishmentof SPPCM or MIBC which involves competition between fanning and FWM. We have used this theory to make a prediction of what will happen with an inducing beam. And we have previously shown and will again show in Section 4.3 that the predictions are in good agreement with experiments.

4.3 Experimental Design and Apparatus for MIPCM

To verify the above conclusion and theory in this section we experimentally induce both self-pumped phase conjugation and mutually incoherent coupling in a photorefractive crystal at the same time for the first to our knowledge. We arrange the experimental setup as follows. A Spectra Physics 165 Argon-ion laser with intra-cavity étalon was tuned the 514.5 nm wavelength in the green with a laser radiation coherence length of ~48 cm and was power stabilised to within 0.5%. The beam was a single longitudinal mode and was extraordinarily polarised, i.e., horizontal to the Newport 8x12 feet optical table. The laser was not decoupled from the setup, since a Faraday isolator was not available although ideally one should be used. The beam was subdivided by a series of beamsplitters and mirrors as shown in Fig. 4.5. The phase-conjugate outputs were coupled out by beamsplitters (BS_4 and BS_5) and monitored by photodetectors (PD_j ; j = 1,4) simultaneously. The electronic shutters (ES_j ; j= 1,5) all were controlled by a IBM computer through an IEEE interface (or general purpose interface, GPIB) to control (switch on and off) the input (which will be conjugated) and inducing beams. . The crystal used in our experiments was grown in the Institute of Crystal Material, Shandong University, China and was supplied to us by Photox Optical Systems, Oxford, UK.

Fig. 4.5 *Experimental arrangement for multi-beam induced phase conjugation.*

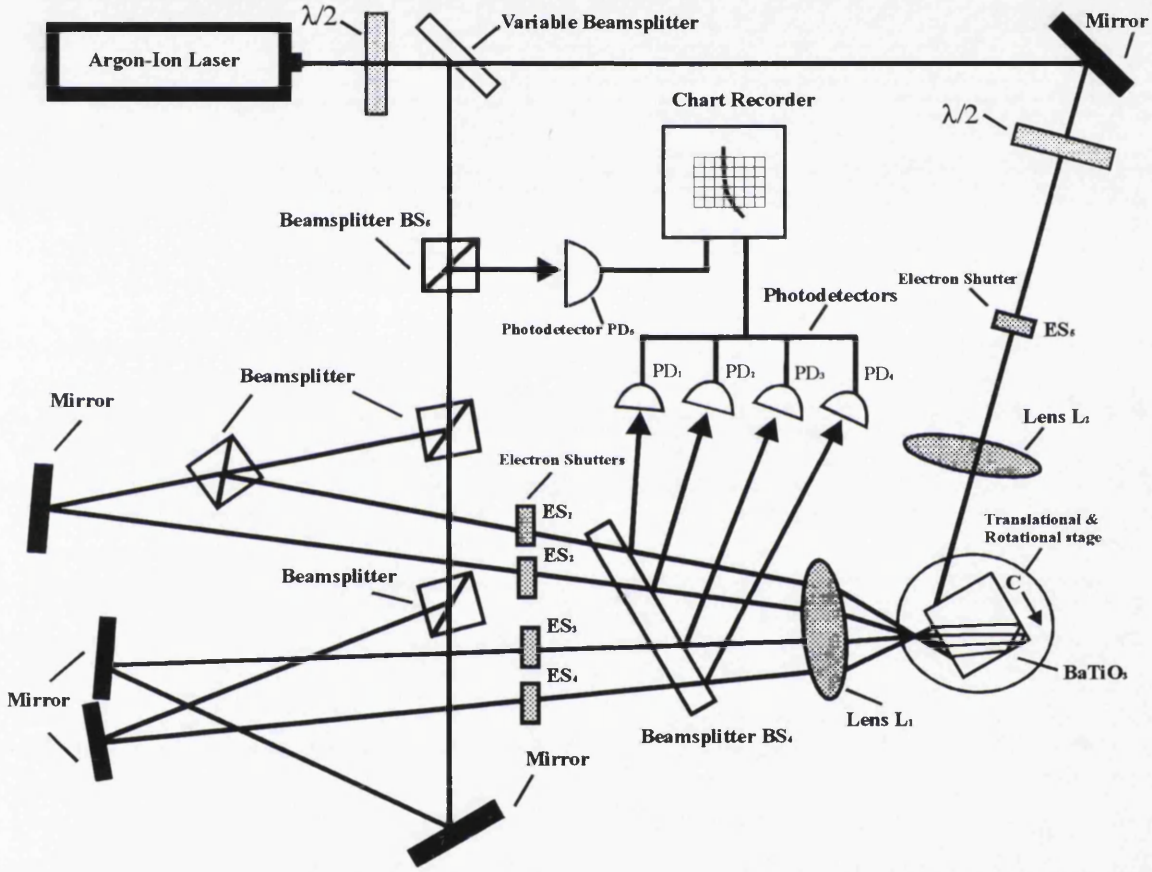

In our experiment, the system was arranged to generate four incident beams (I_j ; j = 1,4) each of diameter 0.5 mm and to orient them so that they all converged and were loosely focused by lens L (f = 125 mm) to one point making equal angles (approx. 15 degrees) to each other in the form of a fan. The beams were allowed to fan out from this point so that they, once again, no longer overlapped each other and then they were allowed to fall onto one polished face, *a*, (5.16 mm x 4.74 mm) of a single domain 0^o-cut undoped $BaTiO_3$ crystal of dimensions 5.16 mm x 5.00 mm x 4.74 mm at the same time whilst none of the 4 beams stimulated self-pumped or mutually-pumped phase conjugation. Fig. 4.6 schematically shows the phase conjugation formation of the four beams, $I_1 \sim I_4$, shining on a crystal at the same time with angles, $\theta_1 \sim \theta_4$, at positions, $y_1 \sim y_4$, without the inducing beam (Fig. 4.6(a)) and with the inducing beam, I_{ind}, with angle (Fig. 4.6(b)), respectively.

Fig. 4.6 *Schematic diagrams of multi-beam induced phase conjugation (MIPC), (A) before inducing beam is applied, and (B) after inducing beam is applied.*

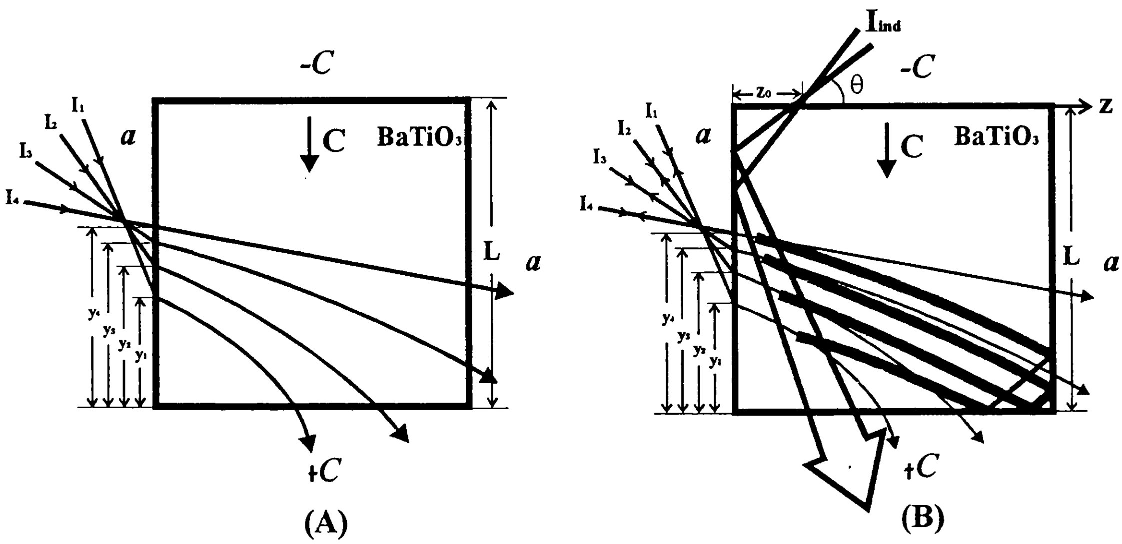

It is worth noting that each input beam itself diverged by a small angle into the crystal. The beams were angled in this way to simulate angled reference beams emerging from an angularly multiplexed hologram (as shown in Fig. 4.7) although in that case each beam is formed to closely adjacent spots rather than the same spot in general. When the beams entered the crystal their behaviour depended to some extent on their angle of incident (Fig. 4.6(a)). Beams almost normal to the surface travelled in a straight line through the crystal with the usual fanning of the beam towards the +C direction of the $BaTiO_3$ crystal. Beams entering the crystal at more inclined angles bent more while continuing to fan out until for the steepest angle the bent beam become incident on the adjacent +c face of the crystal where they reflected internally.

Fig. 4.7 *Schematic diagram of system for replaying the angularly multiplexed holograms stored in a photoreflective $LiNbO_3$:Fe crystal..*

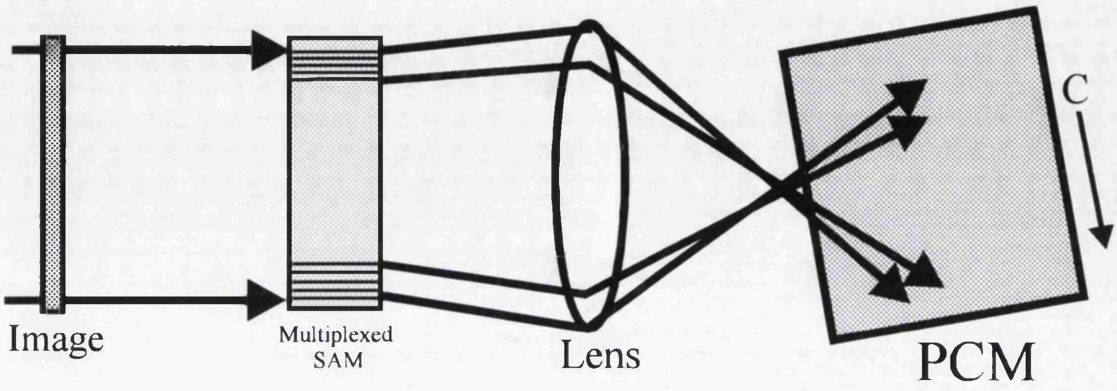

The optical setup is arranged as follows:

(a) the input beam intensities were chosen arbitrarily as I_1=4.0 mW, I_2=5.0 mW, I_3=4.7 mW, and I_4=5.4 mW, respectively from top to bottom (Fig. 4.6). Again this simulates the different strengths of the correlations in Fig. 4.7;

(b) the incident angles of the input beams with respect to the normal of the incident plane are $\theta_1=70^o$, $\theta_2=55^o$, $\theta_3=40^o$, ,and $\theta_4=25^o$, which were positioned at y_1=0.24L, y_2=0.31L, y_3=0.42L, and y_4=0.51L, respectively, where L=5.16 mm is the width dimension of the $BaTiO_3$ crystal as indicated in Fig. 4.6(B);

(c) the inducing beam, I_{ind}, with 4 mW enters the crystal from the -*c* surface at angle 60° (inducing angle) with respect to the normal to the surface so $\theta=30^o$ in Fig. 4.6(B).

The inducing beam also was focused just outside the crystal prior to entering in the form of a slightly (30 deg) divergent beam. This was done to ensure that a wide angular range of fanning grating were formed within the crystal. For the sake of simplicity, we designate the phase conjugate of an incident beam I_j as I_{jSP}. and I_{jMP} where the subscript SP or MP specifies the nature of output as self-pumped or mutually pumped, respectively. The strength of the light, travelling in the opposite directions and being detected using a series of beamsplitters and detectors was checked to be zero initially to confirm that no phase conjugation occurs at the start. Now, we concentrate on showing the experimental results in detail in following sections.

4.4 Single Beam Induced Self-Pumped Phase Conjugation

In our arrangement, the optimum coupling loop at the bottom-right hand corner of figure 4.8(a) is very difficult to form for each beam by itself because their coupling strengths per unit length, γ, are too far away from the optimum conditions for self-pumped phase conjugation, so γl_{eff} is less than 2.34 [Fei82] for each beam, where l_{eff} is the effective interaction length, i.e., the self-pumped FWM can not win the competition against the self-generated fanning and so SPPCM formation is not usually observed. For example, one incident beam (beam 1 only, i.e., switched off beams 2~4) (shown in Fig. 4.8(a)) entering the crystal from the left surface *a* at a lateral position y_1=0.24L with quite a large glancing angle of, θ_1=75°, will travel along the +C direction and immediately fans toward the +*c* surface then reflects twice by internal reflection from the +*c* and *a* surfaces.

Fig. 4.8 *Schematic of a single beam ISPPCM (a) before the inducing beam, I_{ind}, is applied and (b) after the inducing beam is applied.*

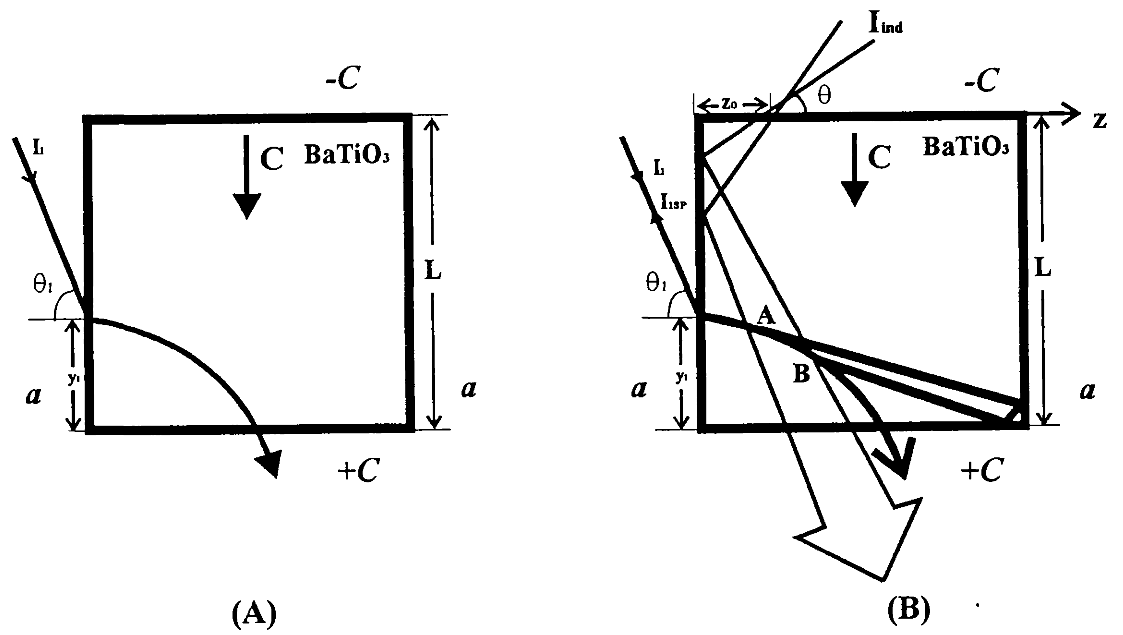

In this case the reflected light does meet the incident face at the correct angle and may return meet the incident beam so no phase-conjugate loop is formed. In the maximum coupling constant, γ, direction, the gain of TWM is large enough to couple most of the incident light in this direction of propagation. For this original direction of the incident beam, the light propagates mainly in a single pass and the loop of the SPPCM does not form. It takes a long time for the light power to move from the maximum coupling constant direction to the corner direction. The same argument can be used for the other three beams. When one inducing beam enters (Fig. 4.8(b)) into the crystal with an incident angle $\theta=30°$ on the -c surface at $z_0=1$ mm away from the upper left corner of the crystal then reflects from the left hand surface, *a*, with a large fan the incident beam, e.g. beam 1 will meet the fanning gratings formed by the inducing light. Since the incident light will be diffracted by the large angular range of fanning gratings it will have good chance to meet the conditions required for forming the phase conjugation loop of the SPPCM.

Fig. 4.9 shows the experimental results for the induced phase conjugation process in three different cases at $\theta_1=70°$; $y_1=0.24L$, $\theta_2=40°$; $y_2=0.42L$, and $\theta_4=25°$; $y_4=0.51L$, respectively, where L=5.16 mm. In each case described above the phase conjugation beam, I_{SP}, approached 60% (~ twice as good as for the Cat-SPPCM) efficiency for the ISPPCM with a response time of 1 second. These results are in very good agreement with those of the experimental results obtained by Yau et. al. [Yau92] in the ISPPC device. It shows that the ISPPCM has large angular and positional acceptance ranges for phase conjugation with uniform phase-conjugate reflectivites by virtue of the induced phase conjugation scheme.

These experimental results suggest that, for progressively weaker incident powers under the non SPPCM incident-angle condition, the amplitude of the photorefractive gratings reduce. Self-pumped phase conjugation appears to form provided the grating have an amplitude greater than threshold. Once the amplitude of the photorefractive grating decreases below the threshold due to the bending beam-fanning decay and overlap with other scattered light, the bending beam-fanning collapses and does not form again by self-generation, and the phase-conjugate light is not generated. However, by introducing one beam to induce the phase conjugation occur, the devices not only give higher reflectivity (~60%) but also have faster response (~1 sec). The input beam was continuously diffracted by reading the fanning gratings formed by the inducing beam so that increases the effective interaction length, l_{eff}, via the multiple interaction regions [Yau92]. So the gain-length product, γl_{eff}, will be increased to a large value. This is the reason the ISPPCM giving a much higher reflectivity.

Our interest next is to establish the intensity- and polarisation- dependence between the inducing and input beams (to be phase conjugated) in the ISPPCM for optimisation. Also we wish to find how fast the induced phase conjugation can be established?

Fig. 4.9 *Experimental results for single beam induced phase conjugation in three cases; (a)-(c) before the inducing beams applied, and (d)-(f) after the inducing beam has been applied, where the power of each of the input beams is kept in 20 mW while the inducing beam is 10 mW at* $\theta_1=70^o$; $y_1=0.24L_0$, $\theta_2=40^o$; $y_2=0.42L_0$, *and* $\theta_4=25^o$; $y_4=0.51L_0$

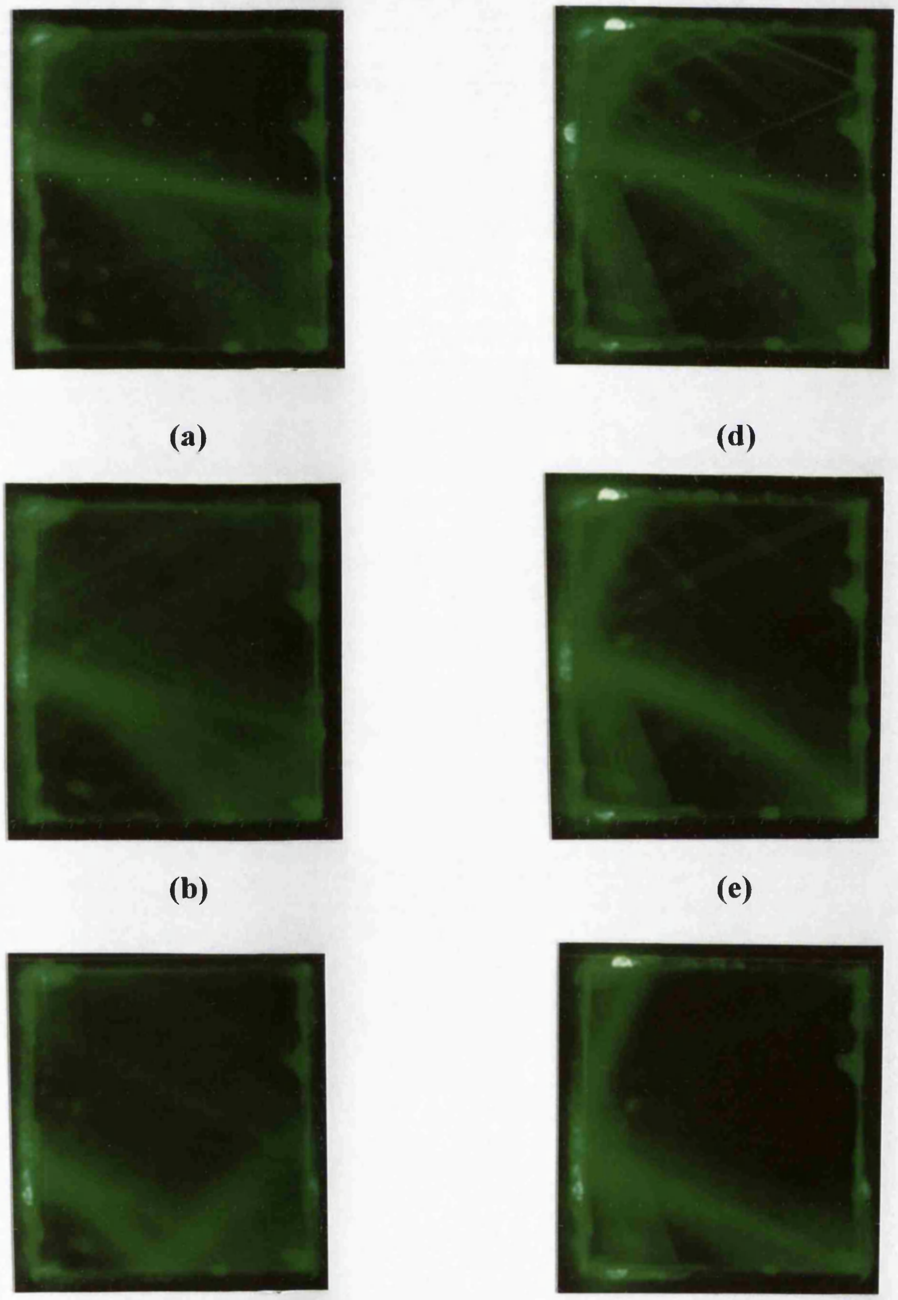

(a) (d)

(b) (e)

(c) (f)

4.4.1 Intensity dependence of ISPPCM

Figs. 4.10(a)-(c) show the power dependence of the phase-conjugate reflectivity, *R*, in the ISPPCM. Here we measured the dependence of the ISPPC reflectivity, *R*, and the response time, τ, on different experimental conditions. It is evident that *R* is nearly independent of the incident intensity in both (shown as Fig. 4.10(a)-(c)). We can also see that the higher intensity speed up the response time by noting the increased initial slope. It can be explained that the more intense inducing beam causes a stronger inhomogenity and a wider angular fan in a shorter time so the input beam can be guided by the fanning gratings to meet the phase conjugation conditions faster. However, although time taken to set up the phase conjugation can speeded up by the use of higher inducing powers it is not always helpful to keep the inducing beam turned on and it may even be detrimental.

Fig. 4.10 *The plots of phase-conjugate reflectivity, R, against the inducing time t_{ind} in three different inducing powers; (a) 20 mW, (b) 30 mW, and (c) 60 mW.*

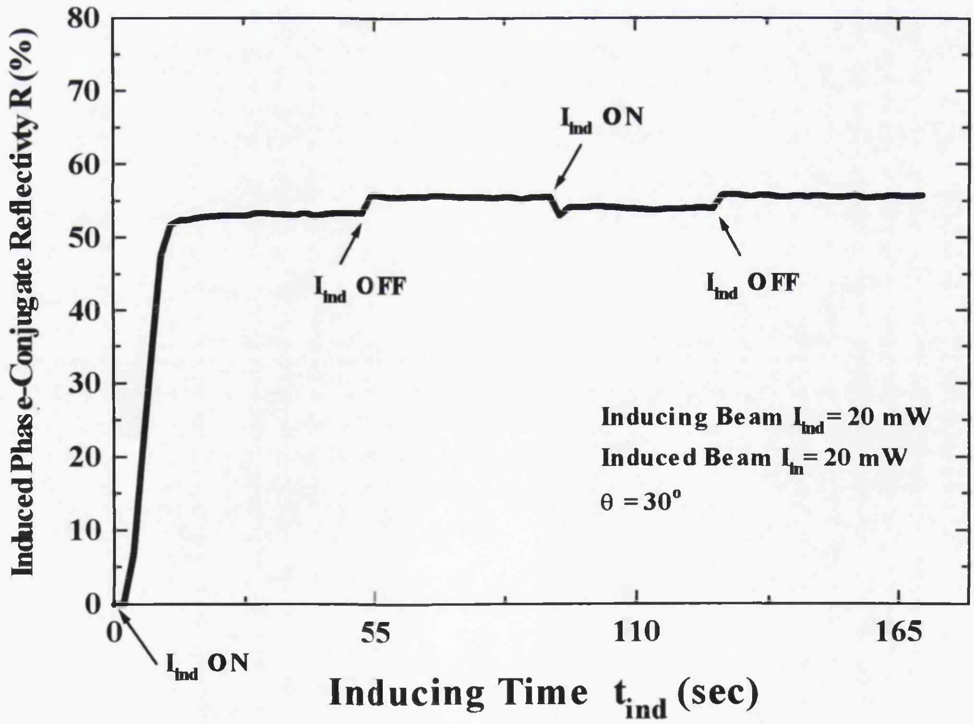

(a)

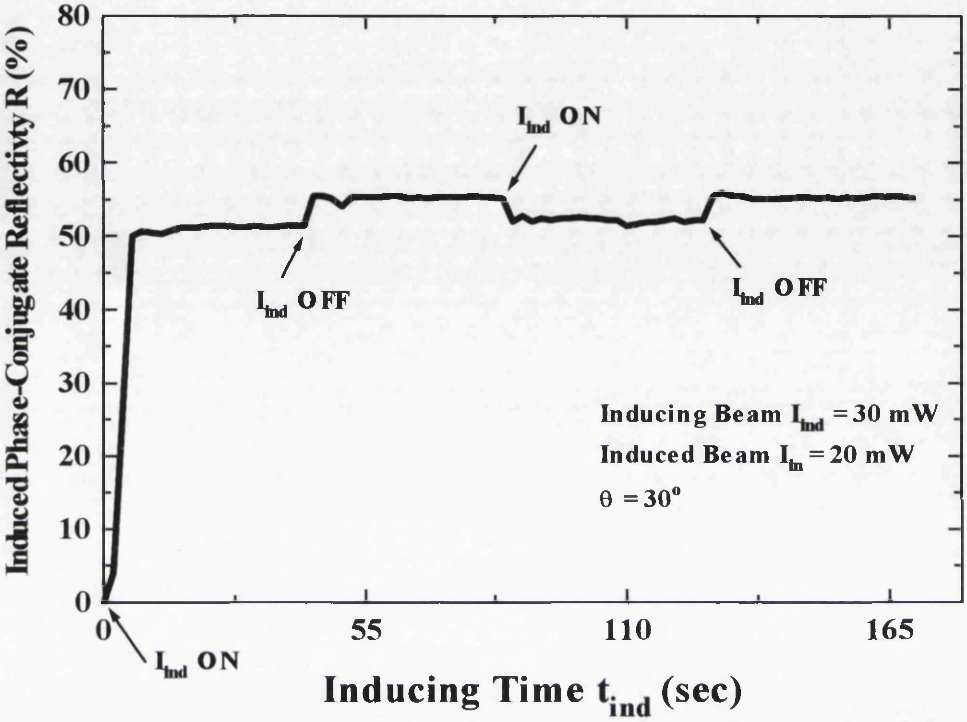

80
70
60
50
40
30
20
10
0
Induced Phase-Conjugate Reflectivty R (%)
I_ind ON
I_ind OFF
I_ind OFF
Inducing Beam I_ind = 30 mW
Induced Beam I_in = 20 mW
θ = 30°
0
55
110
165
I_ind ON
Inducing Time t_ind (sec)

(b)

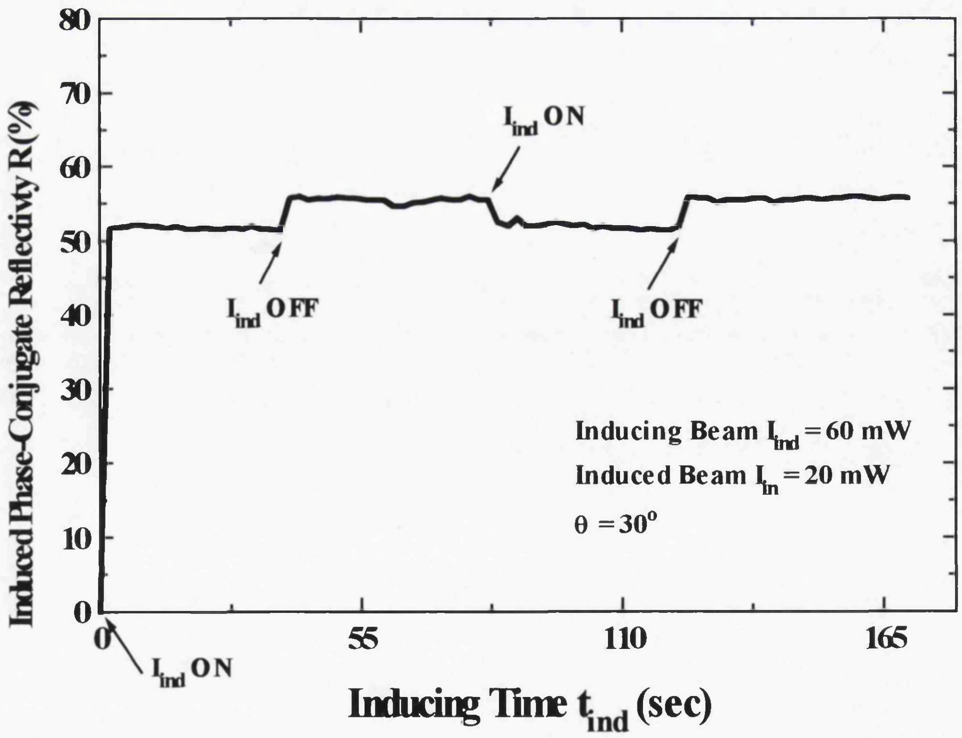

80
70
60
50
40
30
20
10
0
Induced Phase-Conjugate Reflectivty R (%)
I_ind ON
I_ind OFF
I_ind OFF
Inducing Beam I_ind = 60 mW
Induced Beam I_in = 20 mW
θ = 30°
0
55
110
165
I_ind ON
Inducing Time t_ind (sec)

(c)

As seen in Figs. 4.10(a)-(c) the reflectivities were increased in each case as soon as the inducing beam was blocked. These results are perhaps due to the fanning-assisted two-beam coupling effect which gives the inducing beam itself an effectively greater gain than the incident beam then more competition occurs between the input beam and inducing beam. It suggest that we were able to obtain higher phase-conjugate reflectivity after the inducing beam was turned off.

The following experimental investigation of the single beam self-pumped phase conjugation was carried out for two polarisation states of the inducing beam.

4.4.2 Polarisation dependence of ISPPCM

To further verify the above conclusion at the end of previous section and to induce the self-pumped phase conjugation, we carried out experiments exploring the means to restrain the self-generating effect (to eliminate the dynamic instability) and to induce the self-pumped phase conjugation to increase the phase conjugation efficiency, giving higher reflectivity and faster response times by using the o-polarised wave instead of the e-polarised wave to investigate the influence of the polarisation of inducing beam. In this experiment, the ISPPC process using an e-polarised inducing beam in $BaTiO_3$ was formed to have a faster response time than that induced by an o-polarised wave. This is related to the difference of the gratings formed by the inducing beam, which diffract the beam to be conjugated to the correct position for self-pumped phase conjugation. This means that the self-generated fanning effect can be effectively weakened when ordinary-polarised inducing light replaces the extraordinary-polarised inducing light. Using the experimental arrangement of Fig. 4.5 under the same incident conditions as those of Fig. 4.8 except for the polarisation of the inducing beam, we observed the time for initiating the self-pumped phase conjugation changes when the polarisation direction of the inducing light was changed with the results shown in Fig. 4.11.

In our experiment, even though the incident inducing light is ordinarily polarised, the observed reflectivity of the induced self-pumped phase-conjugate light has not changed, only the response time is extended by ~20 seconds which much slower that for the extraordinary polarised inducing beam. We note that the rate of build up of phase conjugation, i.e. the initial slope is the same in both cases but the onset of this build up is delayed in the case of an o-polarised inducing beam. This delay is because ordinary-polarised light does not satisfy the Bragg-diffraction conditions for the grating that is required to form the SPPCM. We found that the more stable phase-conjugate reflectivity (dashed line in Fig. 4.11) was obtained in ordinary induced self-pumped phase conjugation. It could be explained that the ordinary-polarised component is transmitted through the interaction region of the SPPCM and plays only the role of erasing the competing fanning gratings.

Fig. 4.11 *Plot of the phase-conjugate reflectivities against the inducing time t_{ind} by the use of extraordinarily polarised (solid line) and ordinarily polarised (dashed line) inducing beam.*

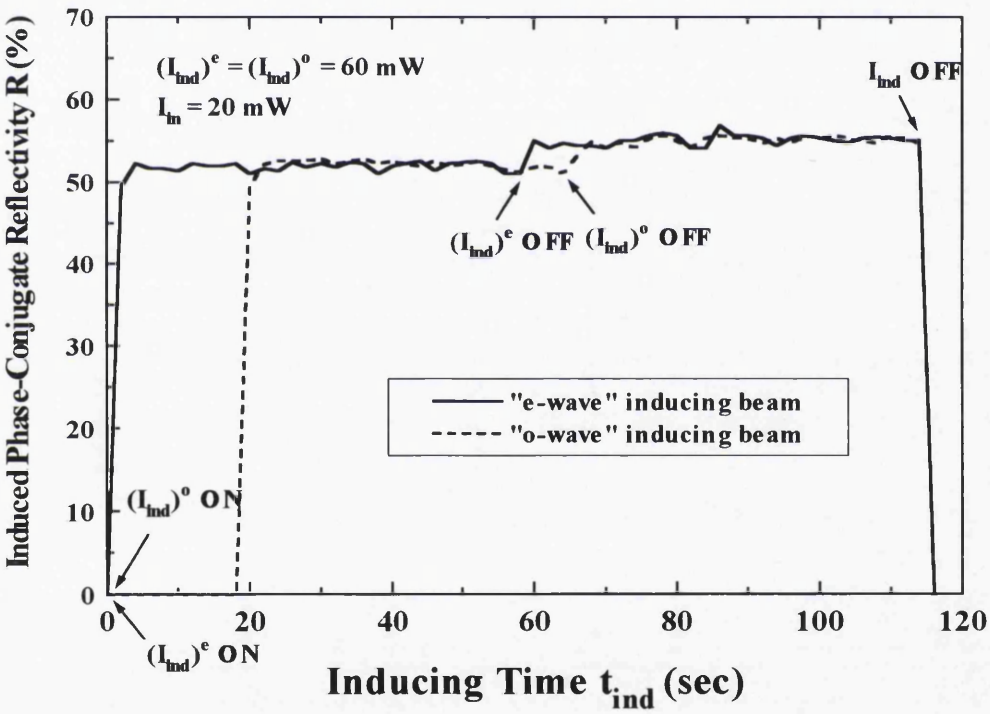

Also, the phase-conjugate reflectivity R_e, which is obtained using an extraordinarily polarised beam, is the same as (Fig. 4.11) the phase-conjugate reflectivity R_o, which is obtained by the use of an ordinarily polarised inducing beam. Reason is once onset the self-generated fanning effect is restrained, and previous self-generated fanning light is coupling into the self-pumped phase-conjugate loop. The results described above are universal for any incident condition. We can use partially extraordinary polarised light to induce the SPPCM to verify when their two polarisation states existing in inducing beam.

It must be mentioned that when the inducing beam was switched off the phase conjugation behaviour had a higher reflectivity (as shown in Figs. 4. 10 & 11). That proves that the inducing beam (either extraordinarily polarised or ordinarily polarised) plays a role that is helpful for establishing self-pumped phase conjugation but it is detrimental to obtaining the highest efficiencies if left on.

4.5 Multiple Beams Induced Phase-Conjugate Mirrors

In the previous sections we have theoretical and experimentally demonstrated that the performance of a conventional SPPCM can be significantly improved by introducing an inducing beam. Here we extend the research to encompass multiple input beams incident on a photorefractive $BaTiO_3$ crystal. The following experiments show the phase-conjugate performance and the behaviour of the beams in the crystal during phase conjugation when the technique of *induced phase conjugation* is used.

4.5.1 Four-beam induced PCM

We carried out an induced phase conjugation experiment similar to that described in Section 4.4 for a single input beam but this time we used 4 differently angled input beams (Fig. 4.6).

When the input beams , I_j (j=1,4), entered the crystal their behaviour depended to some extent on their angle of incidence (Fig. 4.6(A)). Beams nearly normal to the surface travelled almost in a straight line through the crystal with the usual fanning of the beam towards the +C direction. Beams entering the crystal at more inclined angles bent more while continuing to fan out, until for the steepest angles the bent beams became incident on the adjacent *-c* face of the crystal where they reflected internally. The inducing beam I_{ind} (= 4.4 mW) extracted from the laser was extraordinarily polarised and made to travel a different path to be incident on the +C face (5.16 mm x 5.00 mm) of the crystal. This "inducing beam" was angled (Fig. 4.6(B)) so that the beam after entering the crystal would reflect from the adjacent crystal face giving total internal reflection (as described in the previous section). The inducing beam was focused to a point well outside the crystal so it diverged into the crystal and this angular spread is particularly apparent after total internal reflection. This spread of angles is thought to enable at least some gratings to be formed at correct angles for setting up the necessary phase conjugating loops. The inducing beam travelled a much longer path length than the beams to be phase conjugated and so was effectively incoherent. The position of the inducing beam was selected to place the point of reflection on the adjacent face above the fan of beams entering the crystal. We found that the angle and position were not critical to obtain induced phase conjugation but we adjusted both to obtain the highest efficiency and found that an inducing beam placed 1 mm from the crystal corner at an angle of 60 degrees (i.e., $\theta=30°$ as shown in Fig. 4.6(B)) to the normal gave the optimum reflection efficiency of 20% for our case of four beams.

We noticed that the phase-conjugate reflectivity of the inner two beams of the fan was larger than for two outer beams and that I_4 gave the lowest phase conjugate reflectivity indicating that efficiency may depend on angle of incidence. As soon as the inducing beam began to illuminate the crystal, phase conjugate beams appeared in each of the incident fan beams but travelling in the reverse directions. These grew until they reached a stable saturation value. We observed slight oscillations in the power of these beams with time. The growth of the phase-conjugate beams is shown in Fig. 4.12 and took about 10s.

Fig. 4.12 *The plot of the phase-conjugate reflectivities against the inducing time t_{ind}. These phase-conjugate powers were coupled out by beamsplitter BS_j (j=1,5), respectively, as shown in Fig. 4.5. The total power phase conjugated (i.e. the sum of the 4 phase-conjugate beam power) is shown a solid curve.*

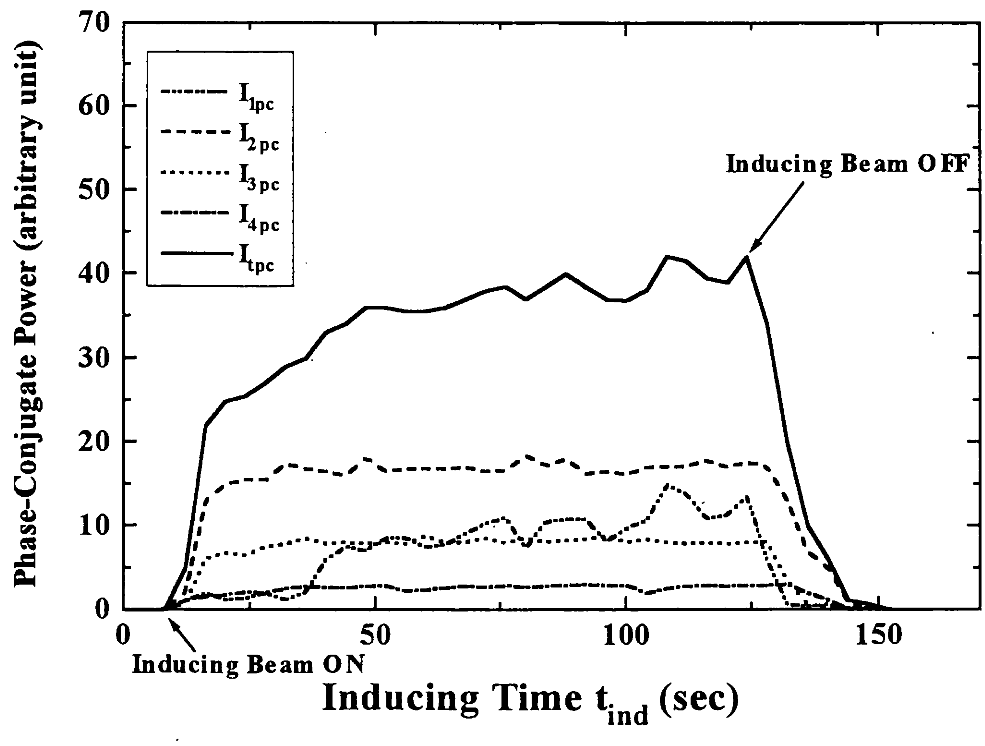

At the same time within the crystal we observed the spontaneous development and strengthening of two loops of light. One loop connected the outer two beams and one the inner two beams by reflections at a perpendicular pair of faces (Figs 4.13(b)). Each loop appeared to be similar to that reported [Smo87 & Eas87] in mutually-pumped phase conjugation of two incoherent beams (mutually incoherent beam coupler; MIPC). Perhaps MIPC is occurring in which there is little cross-talk between inner and outer loops but this was not confirmed. This demonstrates four beam induced phase conjugation. When the inducing beam was switched off the phase-conjugate signals vanished quickly unlike the case for single beam induced phase conjugation reported by Yau et al [Yau92].

Fig. 4.13 *The photos show the beam paths of the multiple beams (four beams) in a photorefractive $BaTiO_3$ crystal, (a) before the inducing beam is applied, and (b) after inducing beam is applied.*

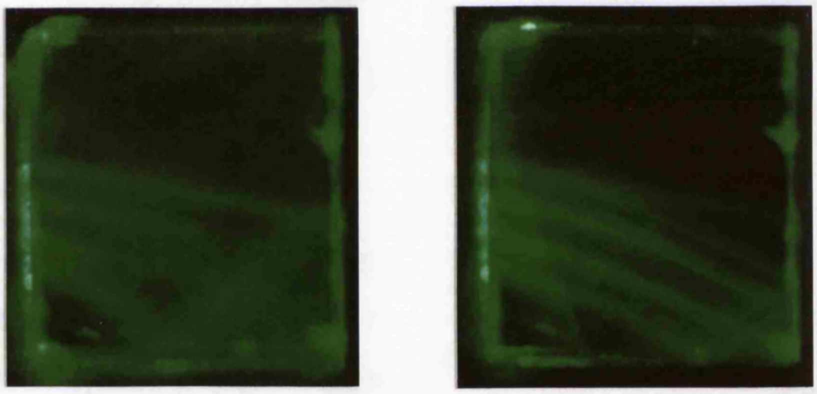

(a) **(b)**

In next experiment we examine the positional alignment required for the inducing beam for MIPCM. In Fig. 4.14 the measurements show the total phase-conjugate reflectivity on the lateral position of the inducing beam. Phase-conjugate signals could be observed over a wide range over a range of about 1.5 mm in lateral positioning. The maximum total phase-conjugate reflectivity in the four-beam induced phase-conjugate mirror was measured to be 30% for z_0=1 mm at θ=30°.

Fig. 4.14 *The positional dependence of inducing beam of the growth of 4-beam total phase conjugation power with time after introduction of inducing beam.*

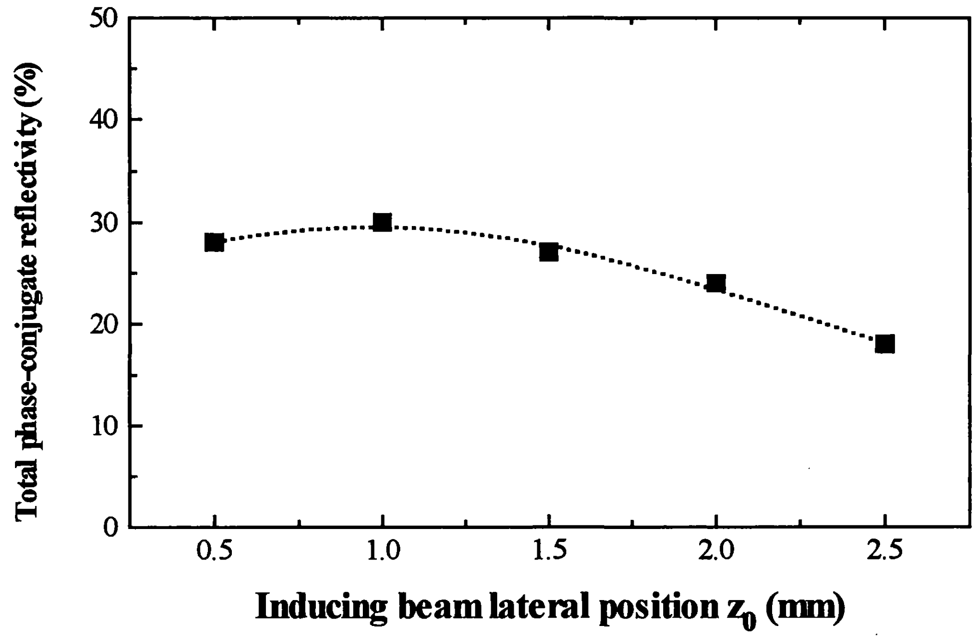

In a further experiment (shown as Fig. 4.15) we replaced only the inducing beam described at 514.5 nm with one from a He-Ne laser at 632.8 nm with a power of about 4 mW. We observed phase conjugation of each of the 4 green fan beams although the strength of the phase-conjugate beams was about one third of that achieved using an inducing beam of a similar 514.5 nm green wavelength. This is the first observation of this type of behaviour and we refer to this as "non-degenerate multi-beam induced phase conjugation (NMIPC)".

Fig. 4.15 *Experimental setup for non-degenerate multi-beam induced phase conjugation (NMIPC).*

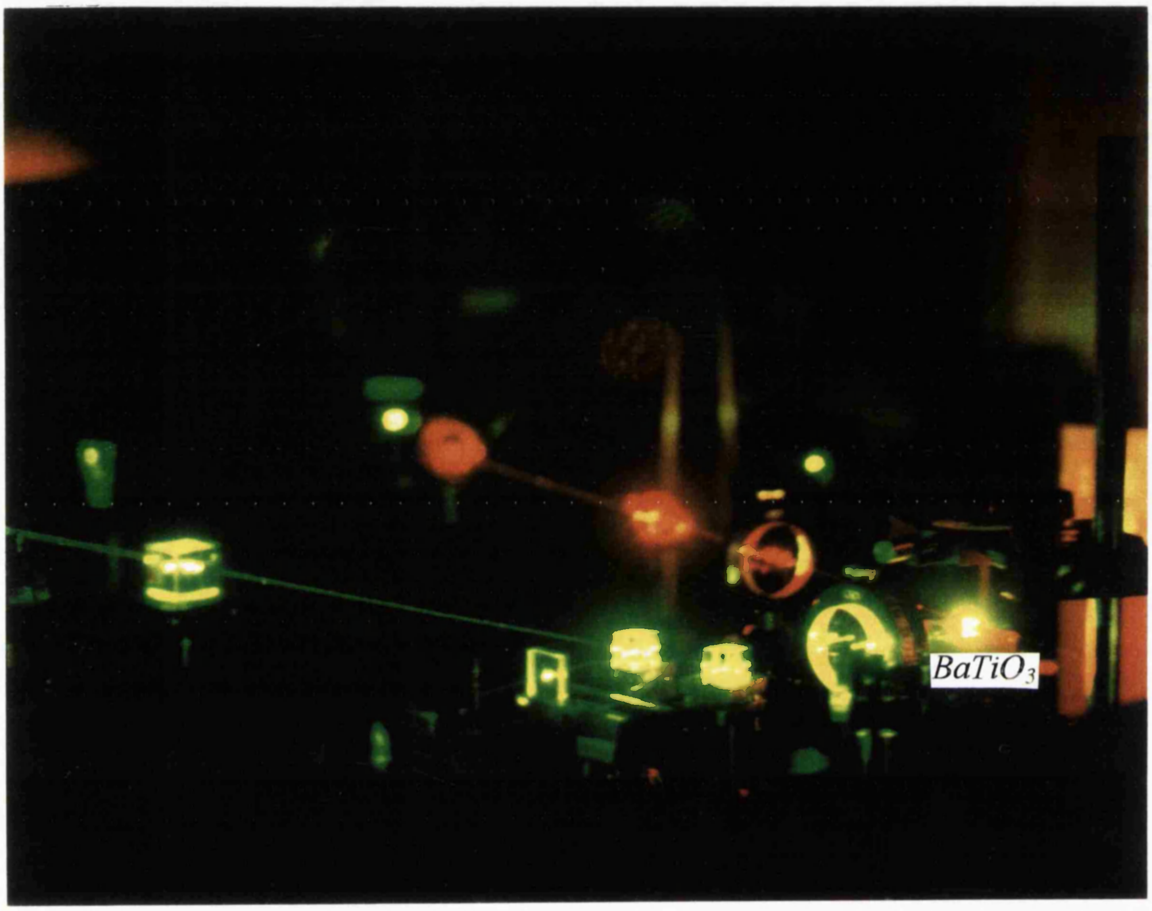

4.5.2 Triple and dual beam induced PCM

After the experiment using 4 input beams described in last section we blocked one of the inner beams, I_2, in the input fan of 4 beams to give three beams as shown in Fig. 4.16. We observed that the strength of the total phase-conjugate signal dropped and within the crystal. We noticed that the previous loops changed and that new loops were set up in which the outer two beams formed 2 loops, which are as usual as MIPC whilst the single remaining inner beam spontaneously set up a loop on its own which appeared similar to that occurring in self-pumped phase conjugation (see Fig. 4.17 (B)). Perhaps both mutually-pumped and self-pumped phase conjugation were occurring independently but this was not confirmed. This behaviour occurred whenever we had three beams incident on the crystal no matter which beams.

Fig. 4.16 *Schematic of triple beams induced phase conjugation (a) before the inducing beam, I_{ind}, was applied and (b) after the inducing beam was applied.*

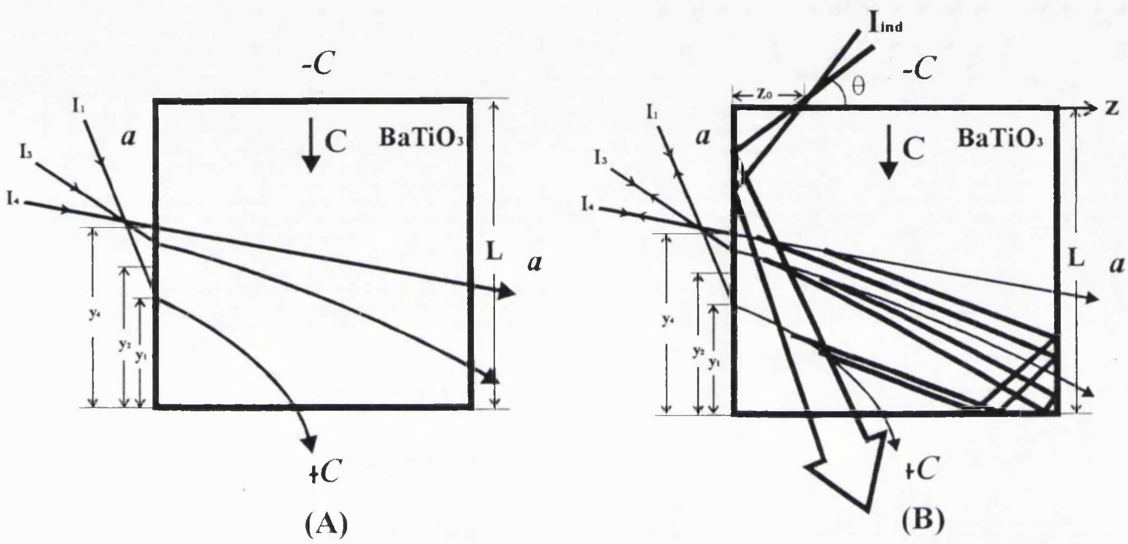

Fig. 4.17 *The photos show the beam paths of triple beams in a photorefractive $BaTiO_3$ crystal, (a) before the inducing beam is applied, and (b) after the inducing beam is applied.*

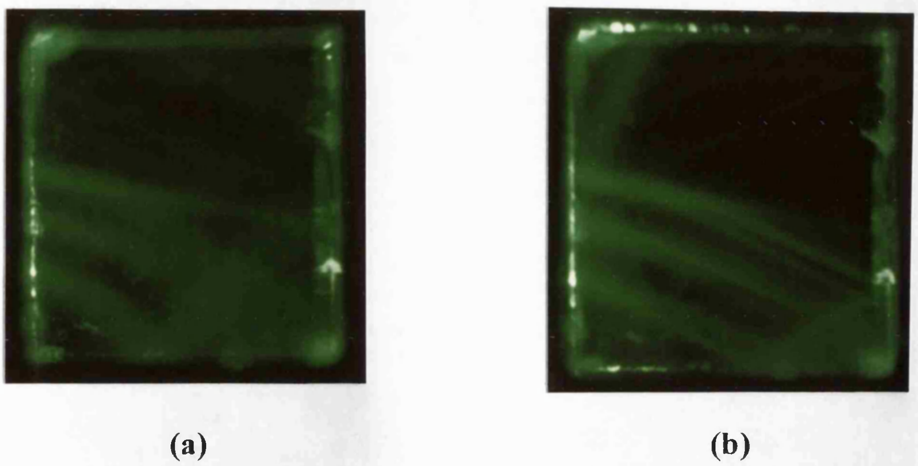

During phase conjugation, we found that the triple-beam induced PCM configuration formed in the $BaTiO_3$ consisted of two types of PCM, i.e. one is being a SPPCM and the other one a MIBC. The triple-beam induced phase conjugation depends on the lateral position of the inducing beam (as in the earlier cases). We think that the optical beam paths of the three input beam are scattered by the fanning grating created by the inducing beam with itself after internal reflection. Fig. 4.18 shows the beam behaviour in the triple-beam induced PCM in three inducing cases, z_0= 0.5mm, 1mm, and 1.5 mm, where z_0 is the distance of inducing beam away from the upper left corner of the crystal. It is worth mentioning that while we are smoothly shifting the postion of the inducing beam the configurations (SPPCM + MIBC) remained within the $BaTiO_3$ crystal. However, the total phase-conjugate reflectivity was different in these three cases.

Fig. 4.18 *The photos show the beam paths of the three beams in a photorefractive $BaTiO_3$ crystal after an inducing beam has been applied. The maximum total phase-conjugate reflectivity was measured to be 35% for z_0=1 mm at θ=30^o (defined in Fig. 4.16).*

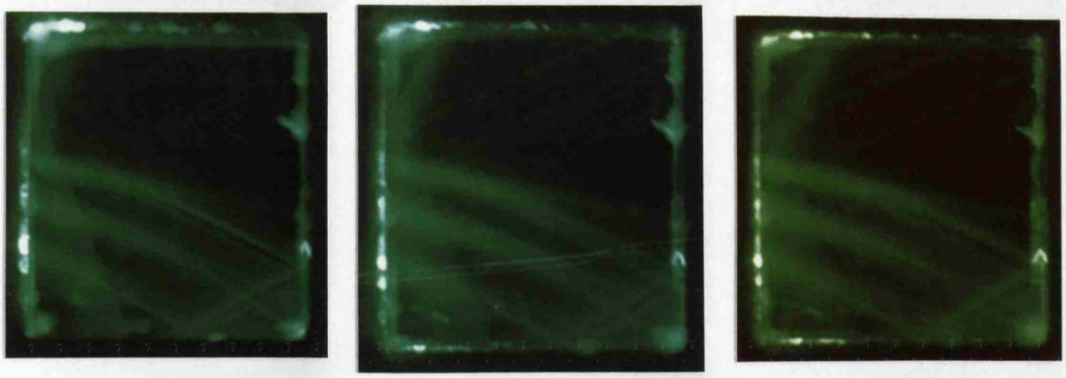

z_0=0.5 mm z_0=1.0 mm z_0=1.5 mm

(a) **(b)** **(c)**

This seems to fit in with our proposed mechanism in that we would expect that changing the position of the inducing beam would alter the vertical (Fig. 4.18) portion of the grating formed by internal reflection of the inducing beam from the adjoining face (*a*), and that this would change the overlaping volume with the incident beams (to be phase conjugated). Also, it can be seen from Fig. 4.18(A) that, for a wider angular range of fanning gratings formed by the inducing beam (which occurs for longer propagating paths of the inducing beam, i.e. larger z_0), the input beams could be diffracted more effectively into the crystal's corner giving higher phase-conjugate reflection values. The growth of the total phase-conjugate signal with time after switching on the inducing beam is shown in Fig. 4.19.

Fig. 4.19 *The growth of the total phase-conjugate power of three input beams with time after introduction of the inducing beam.*

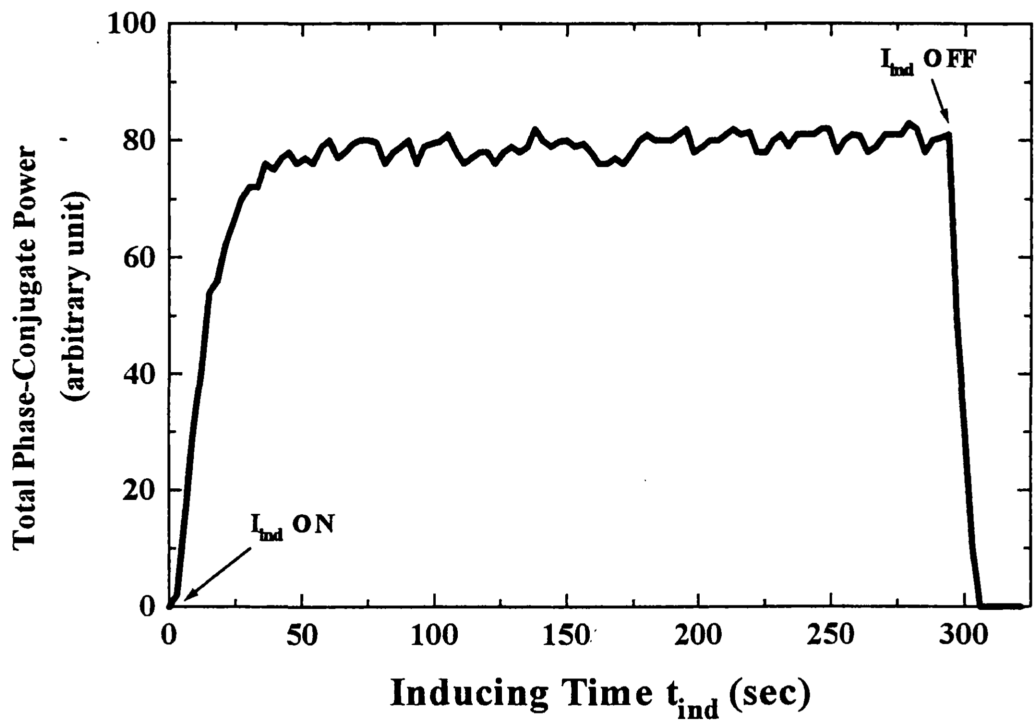

When only two of the incident beams were switched on (or any two of the same four beams were blocked) a loop formed between the two beams remaining showing induced mutually incoherent beam coupling [Smo87 & Eas87] phase conjugation as shown in Figs. 4.20. The dependence of the induced geometries on the lateral position of the inducing beam was obtained (Fig. 4.21). Note that the output of the IMIBC formed between 1 & 3 is weaker in the presence of beam 2. It appears that there is a competition for energy between the IMIBC loop between beams 1 & 2 and the induced self-pumped phase-conjugate (ISPPC) loop of beam 2.

Fig. 4.20 *Schematic of IMIBC (A) without applying an inducing beam, (B) after applying an inducing beam. Photographs showing the beam paths for two beams in a photorefractive $BaTiO_3$ crystal, (C) before the inducing beam is applied, and (D) after the inducing beam is applied.*

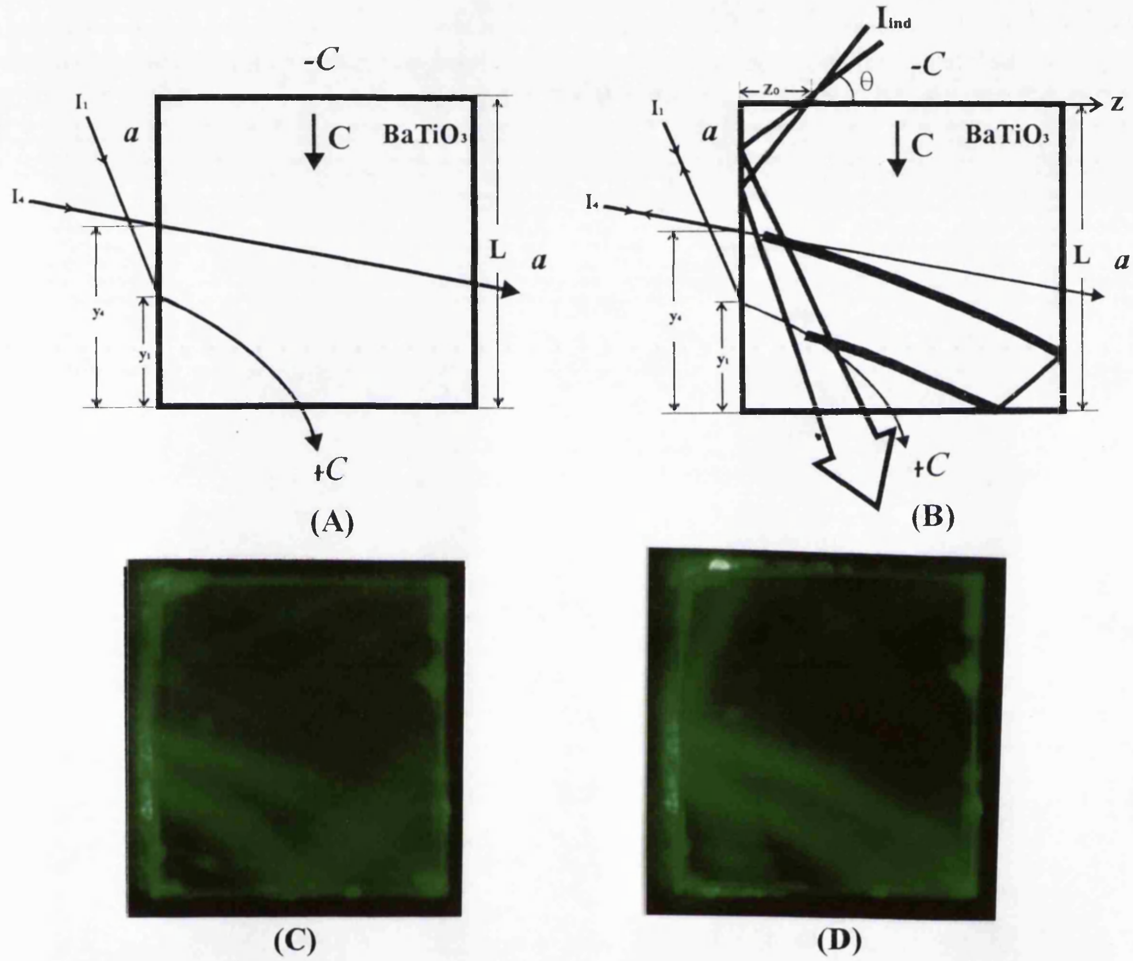

Fig. 4.21 *Photographs showing the beam paths for two beams in a photorefractive $BaTiO_3$ crystal after the inducing beam is applied for various positions of the inducing beam at θ=30° (a) z_0=0.5mm, (b) z_0=1 mm, and (c) z_0=1.5mm.*

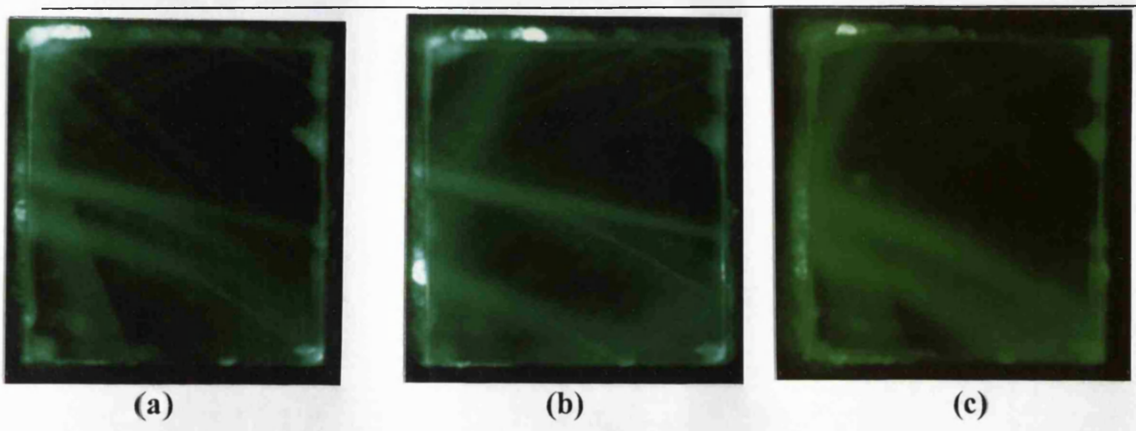

To understand this competition further we investigated by adding a third beam, I_1 (or I_2 or I_3 depending on the existing choice of the pair of beams), to the induced mutually incoherent beam coupler, as shown Fig. 4.21(a) (or Fig. 4.21(b) or (c)) setup between beams 2 & 3 just discussed. There are three phase-conjugate outputs but this time the mutually incoherent phase conjugation coupler between beams 1 and 2 is destroyed. Beam 2 now forms a ISPPCM that produces an output I_{2SP}. Beams 1 and 3 form a new IMIBC that generates the phase-conjugate output I_{1MP} and I_{3MP}, respectively. In the triple-beam interaction, the coupling between beams 1 and 2 is weaker than that between beams 1 and 3. Thus, the IMIBC formed between beams 1 and 2 is destroyed by the introduction of beam 3. Now beams 1 and 3, having a coupling stronger than that between beams 1 and 2, form a IMIBC and beam 2 returns to a ISPPCM. In our experiment with the inputs I_1=4.0 mW, I_2=5.0 mW, I_3=4.7 mW, I_{ind}= 4 mW, the phase-conjugate outputs I_{1MP}=1.9 mW, I_{2SP}= 2.8 mW, and I_{3MP}=1.6 mW are obtained, i.e. reflectivities of 47.5%, 56.0%, and 34.9%.

We now briefly discuss the principle of operation of the phase conjugation of three beams using the analysis of the SPPCM [Fei82] and MIBC [Smo87 & Eas87]. In reality, competition takes place between three IMIBCs and three ISPPCMs (shown as Fig. 4.21), the first IMIBC of beams 1& 2, the second of beams 2 & 3, and the third of beams 1 & 3, the ISPPCM of beam 1, the ISPPCM of beam 2 and the ISPPCM of beam3. The IMIBC process of beams 1 & 3 has a large coupling strength compared to the others of beams 1 & 2 and of beams 2 & 3. This mode competition favouring the IMIBC of beams 1 & 3 will continue while the ISPPCM of beam 2 is establishing. The ISPPC process prevents the IMIBC processes occurring of beams 1& 2 and of beams 2 & 3. But the ISPPC loop of beam 2 introduces a fluctuation (shown as a ripple in time if Fig. 4.19) into the interaction of the IMIBC for beams 1 & 3. The phase conjugation output for the IMIBC with beam 2 is lower than that without beam 2. The ISPPC output of beam 2 is also lower for the case of the triple-beam configuration than that of beam 2 alone. This is due to the fact that the gratings of the IMIBC of beams 1 & 3 introduces a fluctuation into the ISPPC loop and decreases its gain. So the IMIBC of beam 1 and 3 competes with the ISPPCM of beam 2, each drawing energy from the other.

4.6 *Discussion*

It should be pointed out that the performance of the "cat" SPPC not only basically relies on the self-organisation of the gratings due to interaction of beams having the largest coupling but also on the photorefractive response time of the crystal. The former determines the phase-conjugate efficiency and the latter determines the time required to initiate the phase conjugation. Certain arrangements exist which do not meet the conditions nexessary for self-pumped phase conjugation to self-start. This is particularly the case when large positional and angular ranges uniform phase-conjugate reflectivities are required which is often required for practical systems. We may initiate phase conjugation in there cases using a weak inducing beam.

The appearance of various self-pumped FWM geometries for phase-conjugation and mutual-conjugation (or double phase conjugation) of laser radiation have been shown in photorefractive media. The output characteristics of these geometries, such as their nonlinear reflectivity, are determined by the value of the gain-length product γl of the photorefractive crystal. According to theory described in Section 4.2, in all these geometries the value of the gain-length product exceeds some threshold value. In fact, the effect of the gain-length product saturates above a certain optimum value, since further increases result not in the improvement but in the degradation of the performance of the SPPCM or MPPCM, especially when multiple beams are incident on the crystal at the same time (shown as Fig 4.6).

The reason for the existence of an optimum value for the gain-length product is related to the fact that photorefractive crystals that are suitable for self-pumped FWM phase-conjugation and mutual-conjugations frequently characterised by a significant level of fanning. It is not unusual for a single laser beam, after passing through a crystal, to lose as much as 90% (and sometimes more) of its energy through fanning. When a self-pumped FWM geometry is operative in the crystal, the level of fanning may drop to small values, but this does not mean that fanning exerts no influence on the operation of this geometry. Indeed, the final state of the electromagnetic fields is the result of a balance between the phase-conjugate radiation and fanning; both are competing for the energy of the same pump beam. The level of fanning as compared with that for a single pump beam is diminished because of this competition. Similarly, the value of the FWM reflectivity is reduced compared with the value that would be attained in the absence of fanning. In the case of a SPPCM with a high non-linearity, fanning always wins, strongly suppressing FWM. This latter statement has simple underlying physics, which is connected with the different characters of the depletion of the pump radiation by fanning and by FWM. For high values of non-linearity, fanning significantly reduces the intensity of the pump radiation inside the crystal. In contrast, in the geometry of the MIPCM the intensities of the pump beams remain high, even when this geometry operates at high values of non-linearity, giving the maximum possible output.

4.7 Applications in Optical Resonant Systems

We now turn our attention to some devices and systems which can be realised using the multi-beam induced phase conjugation discussed in the previous section. Potential system applications will then be descibed in which such induced phase conjugation may be utilised for providing a feedback capability.

4.7.1 Phase-conjugate resonator via a beamspiltter between two ISPPCMs

A novel resonator configuration was designed (Fig 4.22) between two self-pumped phase conjugate mirrors and was tested using a 50% beamsplitter initially before later replacing this by first one and then multiple holographic gratings. The losses in the system were offset by continuous injection of a sustaining laser beam via the beamsplitter. Although faster response times could be achieved using the phase conjugate mirrors if high powers were used we tried to minimise the optical power to still achieve phase conjugation in about 10s. This was so that later when the unfixed holographic gratings in a photorefractive crystal were substituted for the beamsplitter they would not be erased too quickly. Clearly higher powers and faster response times can be achieved using fixed holograms. We used a 532 nm 400 mW ADLAS frequency doubled, diode pumped Nd:YAG laser for these experiments. This laser was sufficiently stable that no spatial filter was required nor electro-optic amplitude stabiliser which would have introduced extra loss.

Fig. 4.22 *Self-pumped Phase Conjugate Resonator incorporating a 50% beam splitter. (a) schematic and (b)experimental setup.*

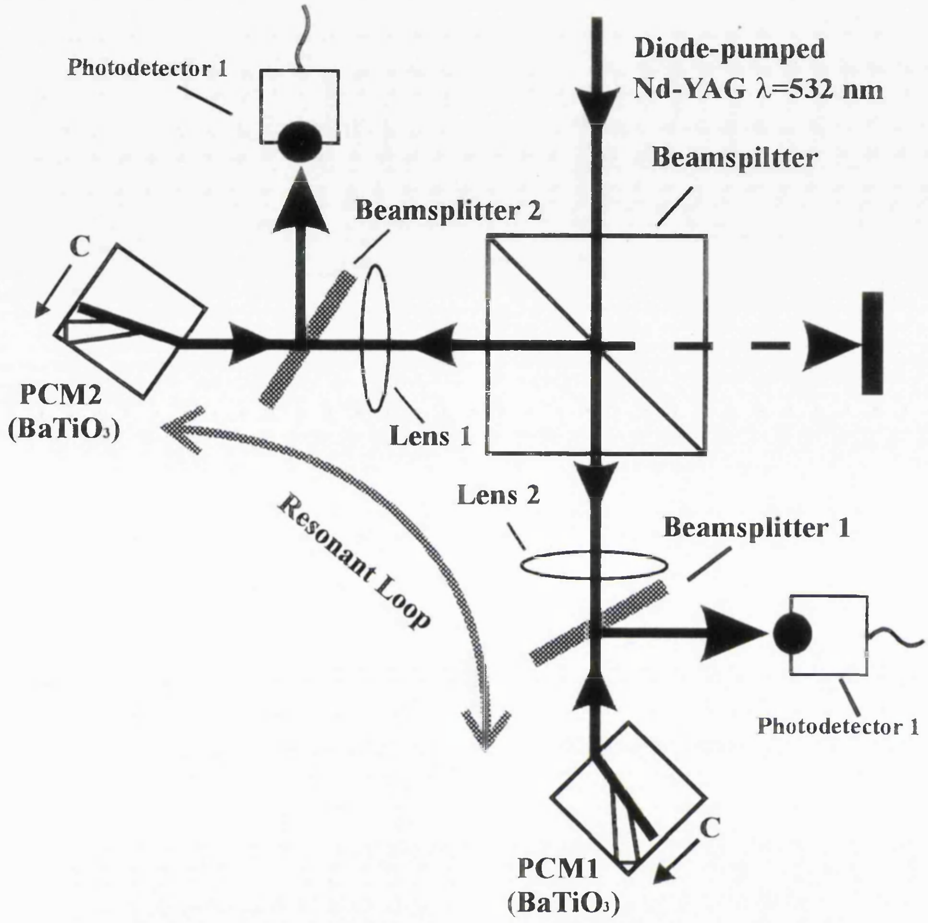

(a)

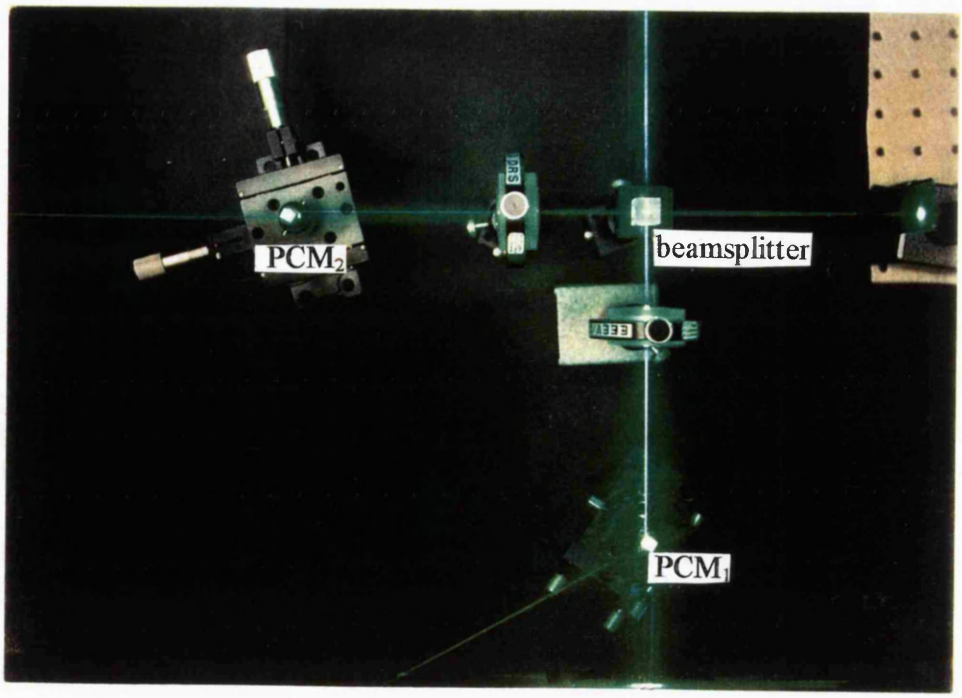

As the self-pumped phase conjugate reflectivities of our barium titanate crystals were 30% and 35% only 10.5% of the incoming signal remains after two reflections (neglecting the beamsplitter) and this continues to fall on subsequent reflections. However, the incoming signal itself continues to pump the system, provided it is cw, and so can maintain the resonance. There will always be more power entering the lower crystal in figure 4.22 as the incoming beam is directed there first. Ideally the laser should have a very long temporal coherence length so that incoming light arrives in phase with light resonating in the system at the beamsplitter. Nevertheless even if it does not arrive in phase the resonator should still operate but now the phase measured at the beamsplitter will change on each iteration. After n iterations the power oscillating in the system will grow to

$$P_0T[1-(r_1r_2)n]/(1-r_1r_2), \tag{4.5}$$

measured after the beamsplitter in the beam travelling towards the left, where P_0 is the initially incident power assumed to be completely coupled in, r_1 and r_2 are the reflectivities of each of the PCMs and the transmittance of the beamsplitter is T. After a larger number of iterations the power stabilises at

$$P_0T/(1-r_1r_2). \tag{4.6}$$

In order to raise the reflectivities of the PCMs and to increase their speed as well as allowing a relatively large angular range of 4.2° to be phase conjugated at the same time in a self-phase conjugate manner we used again the technique of "induced" phase conjugation [Yau92 and Qiu93a & b]. In this method another beam is allowed to diverge into the crystal from quite a different angle and position. The best results are achieved using an incoherently related beam. We also found that the inducing beam could be of another wavelength [Sel93] which we termed "non-degenerate multi-beam induced phase conjugation" (MIPC). This has the advantage that it can easily be filtered out to maintain a good signal to noise ratio. In this work we used an inducing beam from a He-Ne laser of 632.8 nm for one of the phase conjugate mirrors to increase the angular range over which phase conjugation could occur. Only one PCM was induced since the other one did not have incident beams over a wide range of angles and so did not require inducing. We set up the orientation of the PCMs so that no phase conjugation occurred until the inducing beam was turned on. This shows how the inducing beam can be used to lower the threshold powers at which the PCMs would begin phase conjugation which was particularly useful as we were using the lowest power to avoid erasure of the holograms in the lithium niobate crystal which replaced the central beamsplitter.

The experimental results are shown in figure 4.23 which shows how the phase-conjugate beams emerging from each of the PCMs increase quickly to a saturation level only after the inducing beam has been turned on. The different magnitudes of the final saturation values are due to the different powers incident on each PCM and on their different efficiencies (Fig. 4.24). In Fig. 4.23 the two traces show similar behaviour. Both curves have an oscillatory fluctuation. This is purely an artifact caused by the particular laser that we borrowed which had a photodiode at its exit pupil which was linked in an electronic control feedback loop to stabilise the light power emitted. The phase-conjugate mirrors sent back a phase conjugate signal to the laser which increased the light at the output detected by the photodetector. This caused the power of the laser to change under the control of the electronic feedback loop. Combined with timing delays within the optical and electronic feedback loops and resulting temperature fluctuations this gave rise to the power fluctuations observed. This problem could easily be overcome by the use of an optical isolator placed at the laser exit.

Fig. 4.23 *Plots of the power of the phase conjugate beams emerging from the first PCM (curve 1) and the second PCM (curve 2), as a function of time after the inducing beam is turned on.*

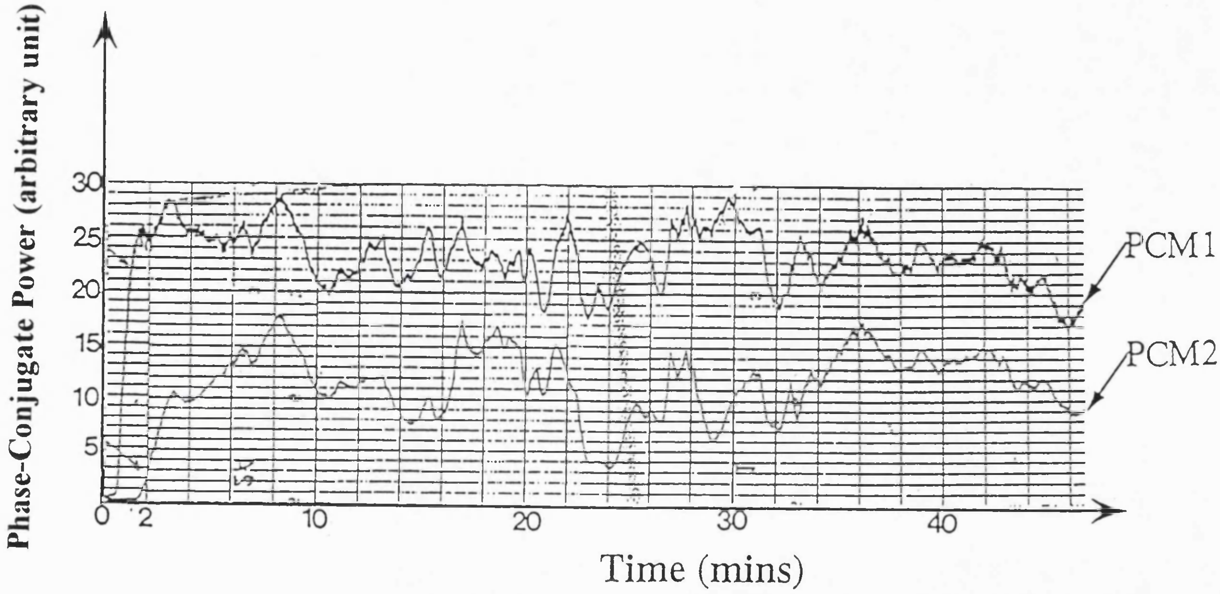

Fig. 4.24 *Plots of the power of the phase-conjugate beams emerging from the second PCM as a function of time after the inducing beam is turned on for four input cases with incident powers 6.2 mW, 4.2 mW, 3.6 mW, and 2.8 mW, respectively.*

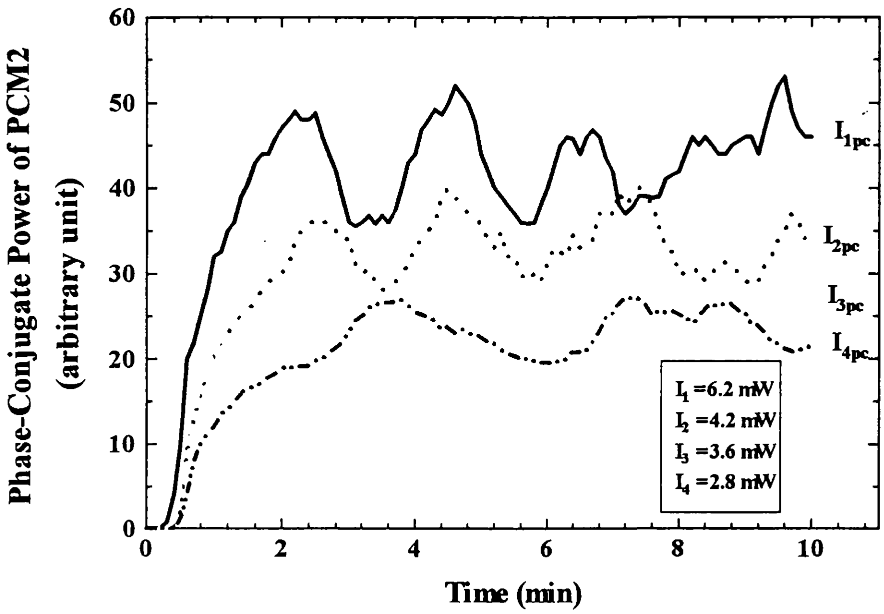

4.7.2 Phase-conjugate resonator via multiple holographic gratings between a MIPCM and a ISPPCM

In this section we setup a resonator via multiple holographic grating between a MIPCM and a ISPPCM and demonstrate experimental results . The beamsplitter was then replaced by a single holographic grating recorded in a photorefractive crystal (as shown in Fig 4.25). This grating initially had a diffraction efficiency of 32% ,which is the highest reported efficiency to our knowledge in this crystal, and was recorded using our new method described in the previous chapter. This is higher than that achieved using the argon laser. It was not fixed and so on subsequent iterations was gradually erased. The incident beam power was very carefully selected so as to be high enough to just stimulate self-pumped phase-conjugate behaviour in both of the barium titanate crystals in a short time (~a few seconds) and yet low enough not to erase the grating too quickly (~10mins).

This problem was made more difficult by the fact that the light falling on the right hand PCM was substantially reduced in intensity by the loss experienced in diffraction from the hologram. After n iterations the power oscillating in the system will grow to

$$P_0\eta[1-(r_1r_2)n]/(1-r_1r_2) \tag{4.7}$$

where P_0 is the initially incident power assumed to be completely coupled in, r_1 and r_2 are the reflectivities of each of the PCMs and η is the diffraction efficiency of the hologram. After a larger number of iterations the power stabilises at

$$P_0\eta/(1-r_1r_2). \tag{4.8}$$

Fig. 4.25 *Self-Pumped Phase Conjugate Resonator incorporating a single holographic grating recorded in a photorefractive crystal.*

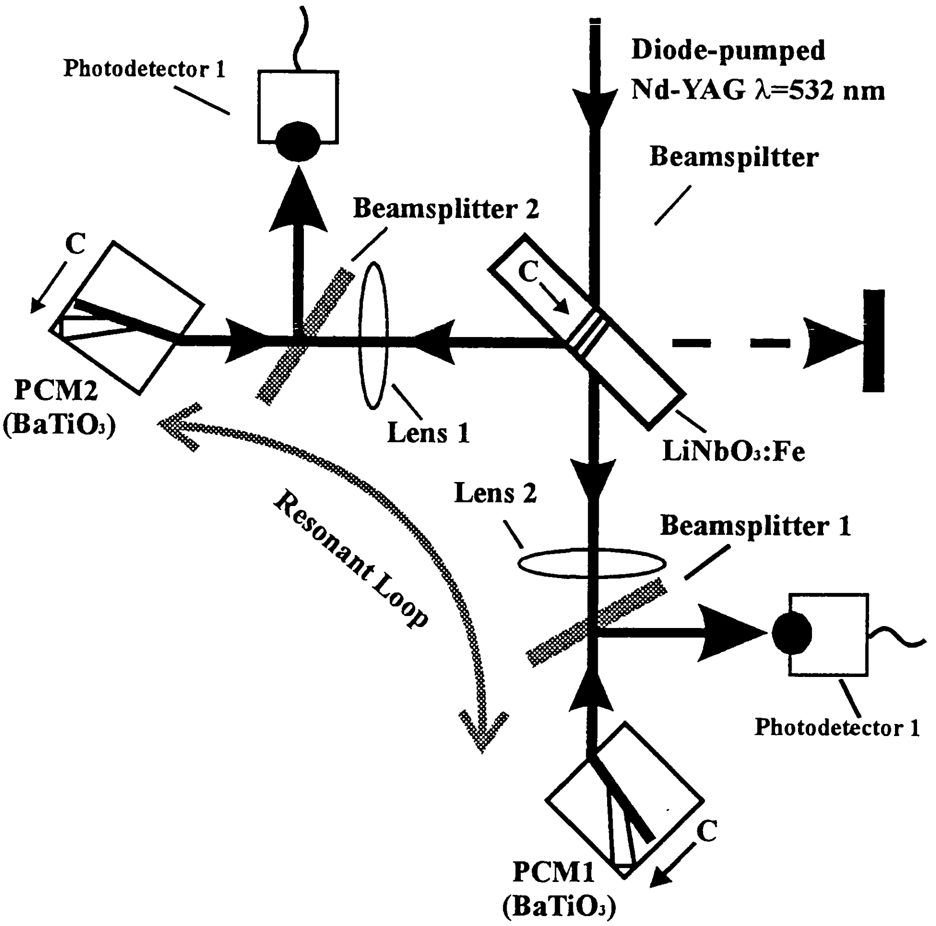

We verified that the power in the resonator did, indeed, grow by plotting the power measured at the power meter shown (photodetector 1 in Fig. 4.25). The power was observed to rise initially and then to fall due to the erasure of the holograms. The room temperature was recorded to be 24±0.1°C.

The experiment was repeated storing 4, 9, 13, 15, 17 and 21 gratings. The angularly multiplexed transmission gratings were formed in a small part of a 4cm x 4cm x 7mm 0.01 % iron doped lithium niobate crystal using our new recording technique described in section 4 of previous chapter to improve the diffraction efficiencies. High efficiency gratings were needed to ensure that the power incident on the second PCM was above its threshold and would give a response time under 10 minutes which was chosen to aid experimentation and to avoid complete erasure of the multiplexed gratings. The object and reference beams were initially at 90° and the reference beam was stepped several times either side of its original position in steps of 0.3° by means of a unity magnification 4f telescope arrangement as in ref [Tao93]. In the case of 15 beams this gave a maximum angular range of 4.2°. The room temperature was recorded to be 24±0.1°C. The object beam power had a magnitude of 5.4 mW and the same intensity beam was used for reading the gratings. Each angled reference beam had a magnitude of 4.2 mW during recording and each beam had a diameter of 2.5 mm. The experimental system shown in Fig 4.26 uses lenses with focal lengths of 125 mm, and 200 mm. We found the experiment much easier to align and set up when the polarising components were included. The beam entering the second PCM was found to be extraordinarily polarised after checking by a polariser.

Consider the case of 15 beams as an example. The power entering the first PCM (PCM2 in Fig. 4.26) immediately after recording on initial playback was 0.3 mW before the inducing beam was applied. After the inducing beam had been switched on and phase conjugation had begun and had stabilised the power was 20 mW giving a 11.4% reflectivity which is less than the 35% measured earlier using a single beam. The holographic gratings were gradually erased by the reading beam as we did not fix them (to allow us to use reuse the crystal easily). This can clearly be seen in Fig. 4.27 which shows the light power phase conjugated by the first PCM as measured after the 50% beamsplitter.

Fig. 4.26 *Multimode Self-Pumped Phase-Conjugate Resonator incorporating angularly multiplexed gratings. (a) schematic and (b) experimental setup. M:mirror; BS:beamsplitter; VBS:variable beamsplitter; HWP:half-wave plate; L:lens; FTL:Fourier transform lens; ES:electronic shutter; MCM:motor-controlled mirror; CR:x-t chart recorder; S:screen; PD:photodetecter; IB:inducing beam; OB:object beam; RB:reference beam.*

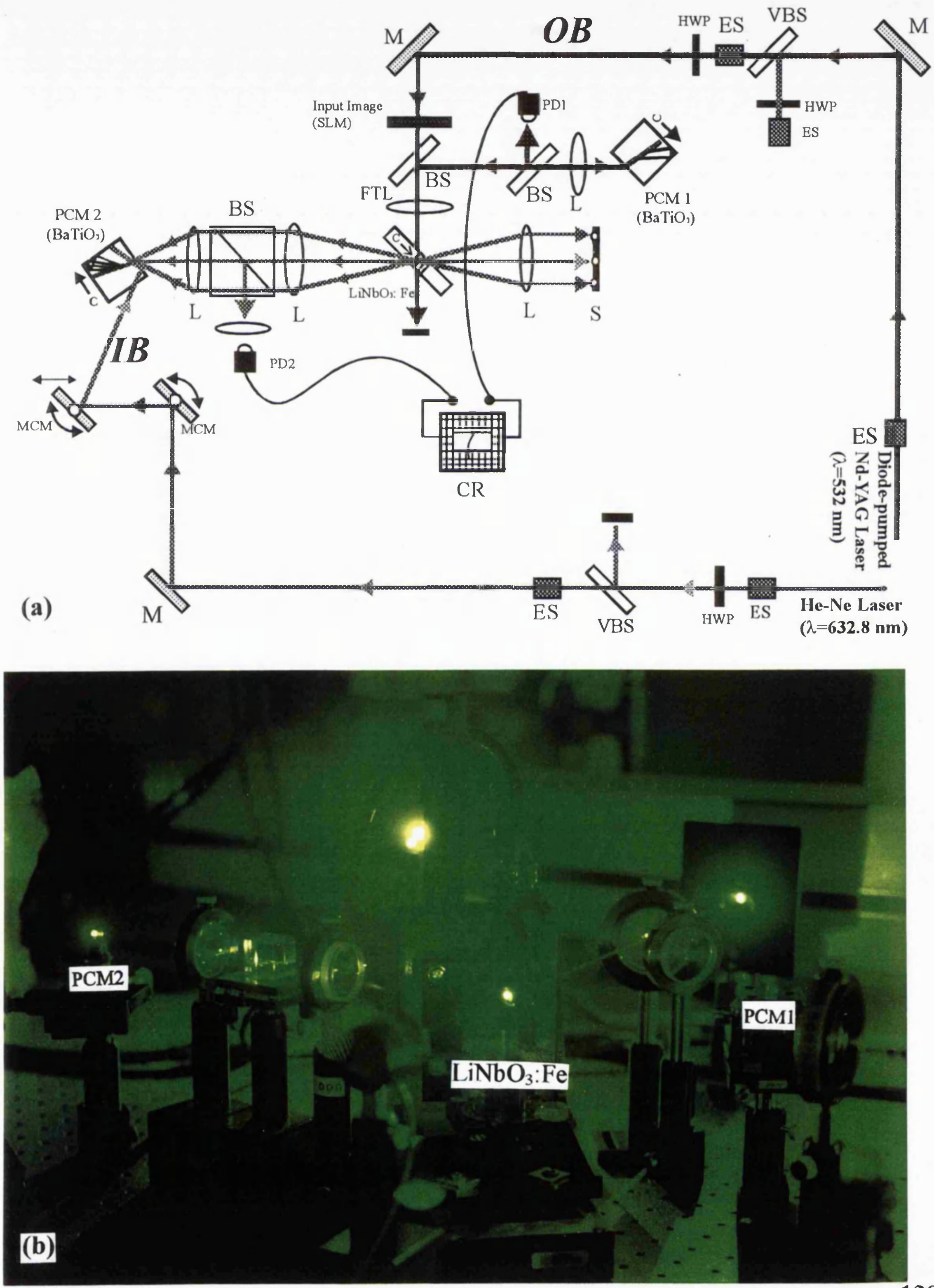

In Fig. 4.27, zero time corresponds to when all of the 15 green beams illuminated the crystal. After one minute a red (He-Ne) inducing beam was also made to illuminate the crystal with a power of 3 mW at and angle of θ=30° at a distance of 1 mm from the corner of the crystal following the method reported in earlier section (Section 4.5.1). The curve clearly shows that the phase conjugated power suddenly increases from zero to 20mW in 2.5 minutes. At this time the inducing beam was turned off and the subsequent exponential decay is due to the erasure of the holograms in the lithium niobate. After 25 minutes when the power had decayed to 4 mW it suddenly dropped to 0.3 mW. This indicates the thresholding effect of the PCM. We believe the power of 0.3 mW is simply due to light scattered from the PCM2 and is not a ture phase-conjugate output. Effectively the phase conjugation has stopped.

Fig. 4.27 *Total optical power phase conjugated by the first phase conjugate mirror rises abruptly when the inducing beam (IB) is turned on and then decays exponentially with time.*

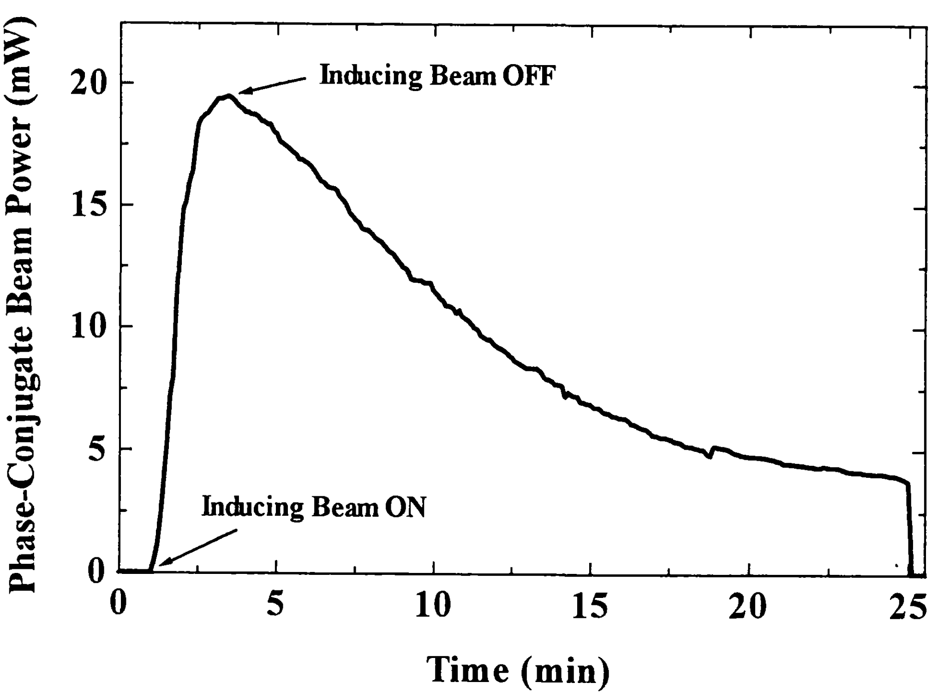

The first PCM (PCM2) clearly phase conjugated the angled beams since by looking to the right of the crystal in the observation plane labelled S in Fig. 4.26, a linear array of spots could be obtained due to beams transmitted and not diffracted by the holograms.

Fig. 4.28 shows the 14 and 17 spots obtained when 14 and 17 gratings had been multiplexed, repectively. The phase conjugate replay via the holograms gave the initial object beam and this was reflected towards the second PCM. After phase conjugation by this second PCM some of the signal was coupled out to a CCD camera while the rest continued to retrace the same path around the loop. By observing the beams incident on the CCD camera we checked that the signal vanished when the beams passing into and out of the first PCM were blocked. Likewise the signal vanished when the beams entering and exiting the second PCM were blocked. These tests confirmed that signals were passing around the loop via both PCMs and via the holographic gratings.

Fig. 4.29 *(a) forteen and (b) seventeen modes simultaneously supported in the phase-conjugate resonator as observed on screen S in Fig. 4.26.*

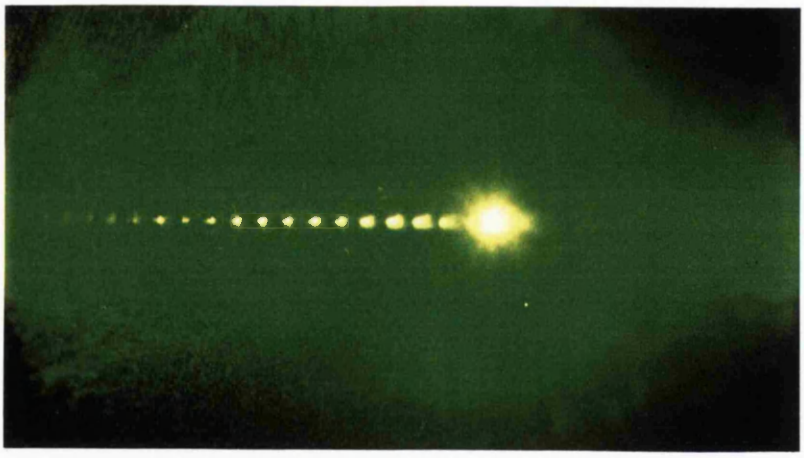

(a)

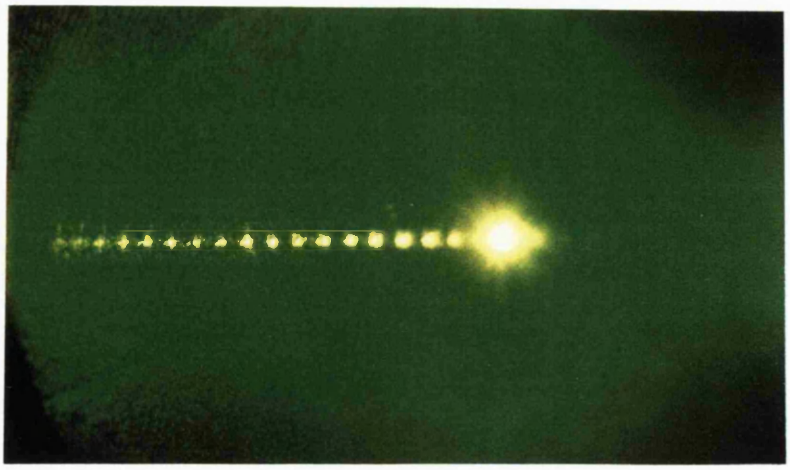

(b)

On screen S the eigenmodes of the system were spatially separate, however, on the CCD camera the eigenmodes were added taking account of spatial variations of phase and variations from mode to mode. We observed a single large spot which appeared to be composed of several smaller spots. The brightness of each of the smaller spots appeared to vary slowly as energy was transferred from one mode to another. In addition the number, shape and distribution of the spots appeared to change slowly (of the order of minutes). This appears to be similar to the, so called, "dreaming" state observed by other authors. The experiment was performed successfully several times for each number of multiplexed gratings from 4 to 21 and similar results were achieved using different spatially separate regions of the lithium niobate crystal.

The alignment and setting of optimum power levels was found to be difficult when a single hologram was used but became easier as more gratings were stored since the combined power diffracted from all of the gratings into the original beam was larger and so the power falling on the second PCM was increased. This occurred despite the fact that the efficiency of each individual grating was reduced as more gratings were recorded in the same volume. Once the resonance has been established by self-pumping in the PCMs the injected sustaining signal maintains a constant power level.

4.7.3 Discussions

Let us now, briefly, discuss the further experimentation required to realise an optical resonator associative memory similar to those suggested by Owechko in ref [Owe87]. Clearly detailed images must be stored in the iron doped lithium niobate crystal as opposed to the simple gratings reported in these experiments, otherwise the memories would not be distinct. It would be most convenient to use angular multiplexing in order to be compatible with these experiments and because large numbers of detailed images have been stored in this manner [Mok 93]. The new recording technique of section 3.4.2 in previous chapter can be used to enhance efficiency although it has yet to be confirmed that this can continue to work effectively for larger numbers of angularly multiplexed images above 24. For ease of experimentation it would be best to fix the images inside the crystal to avoid the holograms being erased too quickly. In this case higher reading powers could be used to enhance the signal to noise ratio and to reduce the response times of the PCMs.

In the reported experiments it appeared that all of the eigenmodes had similar intensities although this could not be confirmed as the gratings were constantly being erased. We would expect similar intensities because each replayed grating had been recorded using object beams incident in the same direction. This has the effect that if only one grating is replayed by a beam in the direction of the phase conjugate of its reference beam this will recreate an object beam which after phase conjugation will replay all of the angularly multiplexed gratings. This results in serious mode coupling tending to redistribute energy from one mode into all of the others to give modes of equal strength. The modes could be decoupled by angling the object beam between recordings as well as the reference beam. However, the present geometry has advantages if this system is to be used as an associative memory. Figure 4.26 shows how an SLM can be used to record angularly multiplexed Fourier Transform holograms of a set of memory templates images for the image database. If a similar SLM or transparency of an image to be recognised is placed in a similar position in the experiment of Fig 4.26, in the input beam, then the unknown image can be injected into the resonator. Each of the angled replayed reference beams diffracted from the angularly multiplexed holograms with have an intensity dependent on the similarity of the input pattern and the pattern stored using that particular angled reference beam. If we simply allow these beams to phase conjugate and resonate they will replay the stored patterns which will add together to recreate the original input pattern and we will be no better off than we were at the start. In order to stimulate the net to converge to only one pattern the system requires a non-linearity or thresholding process. This could be done, for example, by placing a saturable absorber in the path of the angled reference beams within the resonator as used by Duelli et al [Due93]. High intensity beams would continue to resonate and weaker beams would be attenuated on subsequent iterations resulting in injection locking. In practice, the stored patterns will not, generally, be orthogonal and so will have finite cross-correlations which will result in some coupling between eigenmodes of the system. This will result in a background noise level. Provided this is sufficiently less that the signal it can be removed by binary thresholding of the output pattern, assuming the patterns stored were not gray-level images. In order to fully exploit the resonator geometry the round trip loss will need to be reduced to allow a larger number of iterations before vanishing.

4.8 Conclusions

In conclusion, we demonstrated the simultaneous phase conjugation of up to 24 beams oriented at various angles without crosstalk. This direction of research was prompted by my earlier work on induced self-pumped phase conjugation (ISPPC) and on how this effect exhibits higher phase-conjugate efficiencies and faster response times [Yau92]. In the new Multiple Beam Induced Phase Conjugation (MIPC) four beams were initially phase conjugated in a barium titanate crystal only when an inducing beam was also incident. We also discovered that an inducing beam of a completely different wavelength could also stimulate the onset of phase conjugate beahviour (non-degenerate MIPC).

We constructed and demonstrated an optical resonator between two self-pumped phase conjugate mirrors via a photorefractive crystal in which 24 gratings had been recorded. 24 eigen modes were shown to be present with similar intensities. The system configuration was also novel as the resonance was maintained by an injected sustaining beam. One of the phase-conjugate mirrors was induced by a beam of another colour to increase the angular range over which phase conjugation could be performed.

Several applications for these phenomena can be envisioned. Although we have not phrased our findings in digital terminology following the work of Qiu et al [Qiu93], we have demonstrated logical AND operations with multiple inputs on one channel. Alternatively we have used a single incoherent inducing beam to switch the phase conjugation of up to four other beams on and off in a type of relay. However, perhaps the most promising area of application will be found in pattern recognition systems such as the HOFNET [Sel90 & 91, and Mao92] or in resonator optical neural nets. These were first proposed by Owechko et al [Owe89 & 93] where the authors proposed and analysed an optical system with phase-conjugate mirror at each end. This caused the light to travel back and forth between the mirrors through the optical system. The eigenmodes of the system were the patterns stored in the system. The systems operation depended on the ability of a phase-conjugate mirror to phase conjugate several beams travelling at different angles in a fan in parallel. The introduction of a lens converts the fan of beams into a one to two dimensional array of spots of light effectively forming an image which could be phase conjugated. By the use of MIPC the fan can be phase conjugated without the need for a lens making a more compact system.

Chapter Five

SELF-PUMPED PHASE-CONJUGATE MIRRORS WITH NOVEL CONFIGURATIONS

Our purpose in this chapter is to use 0°-cut undoped $BaTiO_3$ crystals to experimentally demonstrate SPPCMs with three new configurations. We hope to provide an insight into the mechanism of self-pumped phase conjugation. This chapter is organised as follows. We start on introductory section and illustrate the motivation of this chapter in Section 5.1. After a schematic description of our new geometry for SPPCMs in Section 5.2, we describe in Section 5.3 the experimental arrangement in detail. Section 5.4 shows our measurements of the temporal and spatial beam dynamics including the fanning effect inside the crystals during the self-pumped phase conjugation process. Experimental results show that the fanning profiles of our new confiugration were different from those of the conventional configuration for SPPCM. The experimental performance for our SPPCMs is special in that we observe a large angular AND lateral positional acceptance, with high resolution which makes these particularly useful in practice. The similarities and distinguishable differences between these configurations and the popular "Cat" configuration are highlighted in Section 5.5. In Section 5.5, we propose one possible mechanism, based on a four-interaction-region (FIR) model, to account for our discoveries and show that the transition between these regions is responsible for the optical path, beam spatial behaviour, and changes inside the $BaTiO_3$ crystal. This provides a good understanding of our new SPPCMs. Section 5.6 summaries the findings of this chapter.

5.1 Introduction and Motivation

Since Feinberg [Fei82] first demonstrated self-pumped phase conjugation using four-wave mixing (FWM) and totally internal reflection (TIR) in a photorefractive $BaTiO_3$ crystal, this effect has been demonstrated in many photorefractive materials, including ferroelectric oxides (SBN [Sal86], NBN [Odu87], BSKNN [Rod87], $KNbO_3$ [Ryt89, Med90, Zha90, Aoy93, D'Ya91, Med94, and Din95]), sillenites (BTO [Ste89]), and photorefractive semiconductors (GaAs [Chu91] & InP [Din93]). More recently, $BaTiO_3$ nominally undoped [Ros92] or accidentally doped with impurities [Ros93, & 95] has been used to implement a phase-conjugate mirror for a near infra-red laser source between 720 nm and 1004 nm. The self-pumped phase-conjugate efficiency, time response, and image fidelity have been improved in doped crystals, such as Ce, Co, Cu, and Rh doped $BaTiO_3$ crystals [Lia94a & b, Zhu94, Yan94 & 95], Fe doped KTN [Lia 93 & 94b], Cr doped SBN [Tom94], Cu doped KNSBN [Xu91, Yue92, & Zha94], Fe doped KLTN [Wei94], and Fe, Mn, Co Doped $KNbO_3$ [Din95], and Rh: doped $BaTiO_3$ [Kac94] and also for special crystal cuts and orientations, such as 45°-cut $BaTiO_3$ [For89], 45°-cut *n*-type $BaTiO_3$:Co [Gar93] and 18°-cut Ce-doped KNSBN [Bia93]. Several further configurations for self-pumped phase conjugate generation, such as the stimulated photorefractive backward scattering configuration [Cha85, Val92, & Yan94], the stimulated photorefractive backward scattering four-wave mixing configuration [Lia93a, b, & 94], and self-pumped and four-wave mixing (SPFWM) using single-pusle laser [Tro95] have been suggested according to their experimental observations. All earlier configurations are reviewed in chapter 2. However, in practice, it is difficult to control the growth conditions for doping and it may be time consuming to select a precise crystal orientation for cutting. Currently, 0°-cut undoped $BaTiO_3$ is still the leading candidate for self-pumped phase-conjugate mirrors (SPPCMs) for applications in many areas (described in chapter 2) and keeps attracting researcher's attention since it not only has been demonstrated as an important non-linear optical material for photorefractive phase conjugation but can be easily grown and is cheaper than doped and specially cut crystals. The development of practical applications depends on a further improvement in the SPPCM's performance, which in turn depends on a deeper understanding of the mechanisms by which it is formed.

5.2 Geometric Configurations for Our New SPPCM (the -C^3)

In the last decade 4 configurations have been reported for SPPCMs using cw laser. The various configurations can be classified according to the number of internal reflections and the direction of the incident beam relative to the C-axis (defined here as pointing along the spontaneous polarization direction) which is the direction into which any beam or beams entering the crystal in any orientation would tend to bend. No internal reflections appear to occur in the "Stimulated Backward Scattering" [Cha85, Val92, & Yan94] configuration (the beam is incident at an acute angle to the +C direction of both $BaTiO_3$ and $BaTiO_3$:Ce crystals) or in the "Stimulated Backward Scattering FWM" [Lia93a, b, & 94] configuration (the beam is incident at an acute angle to the +C direction of both KTN:Fe and $BaTiO_3$:Co crystals), in both of these the phase-conjugate beam is generated by backward scattering in the volume of the crystal; Two internal reflections occur in the popular "Cat" configuration (the beam is incident at an acute angle to the +C direction of $BaTiO_3$ crystal or to the -C direction of an SBN crystal); Six internal reflections appeared to occur in a configuration mentioned briefly by Chang et al. [Cha85] (the incident beam traveled at an acute angle to the -C direction of a $BaTiO_3$ crystal).

The geometries for the nonlinear interaction responsible for the "Cat" and for our self-pumped phase conjugation processing are shown in Fig. 5.1. We experimentally set up a "Cat" and then our new configuration in the same crystal and the experimental results are shown in Fig. 5.2. In the "Cat" SPPCM [Fei82] configuration shown in schematic form in Fig. 5.1(a) and experimentally in a barium titanate crystal in Fig. 5.2(a), the beam enters a crystal face, *a*, which lies parallel to the C-axis and, thereupon, begins to diverge or fan out, bending as it does so, into the +C direction. After about 10 seconds (with an incident beam power of 25 mW illuminating an area of ~0.2 mm^2 on the crystal face and with an incident angle, θ, of 45°) a single loop of light (or closed beam path) is observed to form involving two internal reflections from two orthogonal adjacent faces and at this time the phase-conjugate reflected image is observed. In our configuration the beam is incident (Figs. 5.1(b), 5.2(c)) at an angle onto the crystal face normal to the C-axis at its most positive end (+*c* face) and travels at an acute angle, ϕ, to the -C direction. We observed that the incident beam begins almost immediately to fan-out towards one of the opposite corners (Fig. 5.2(b)). The angular range of beams within the fan appear to be larger than that in the "Cat". After 15 seconds (with an incident power of 25 mW illuminating an area of ~0.2 mm^2 on the crystal face at an incident angle, ϕ, of 45°) one or more loops of light are observed to form depending upon the incident angle and lateral position of the incident beam on the first crystal face and at this time the phase-conjugate reflection is observed to occur. Since the beam enters close to the -C direction and curves towards one corner we refer to it as the "-C Curve Configuration (or -C^3)" SPPCM.

Fig. 5.1 *Schematics of a two-interaction region and a four-interaction region model in $BaTiO_3$ crystals for (a) the "Cat" and (b) the "-C^3" self-pumped phase-conjugate mirror (SPPCM).*

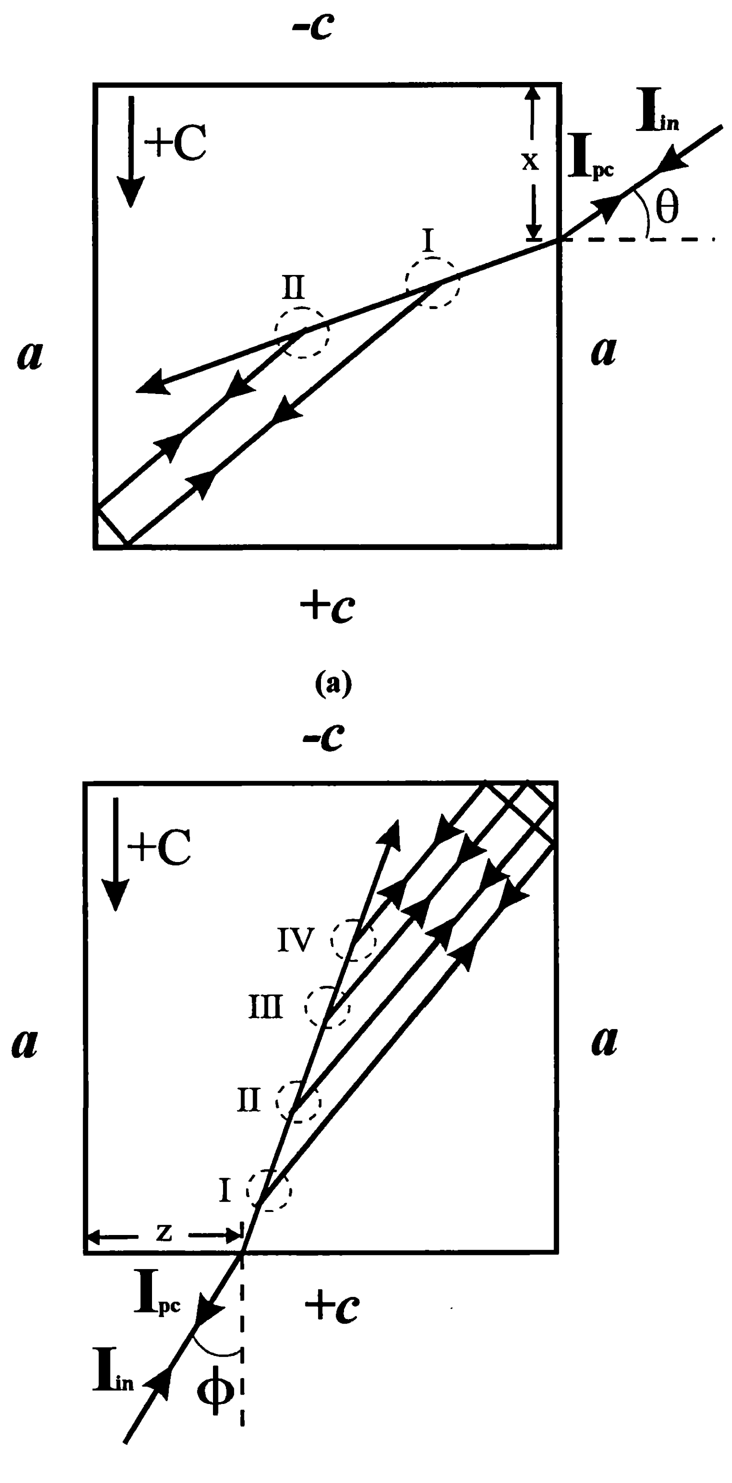

Fig. 5.2 *The optical path inside the 0^o-cut undoped $BaTiO_3$ crystal for (a) the "Cat" during phase conjugation, (b) the "-C^3" SPPCM before phase conjugation, and (c) the "-C^3" SPPCM during phase conjugation showing the presence of 2 loops of light.*

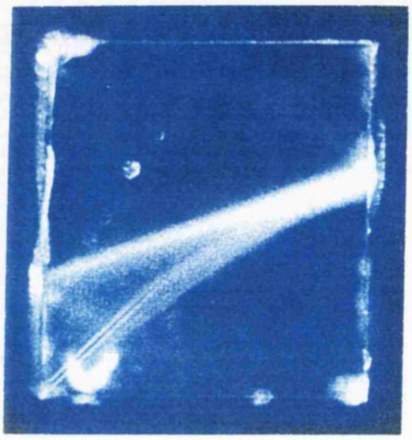

(a)

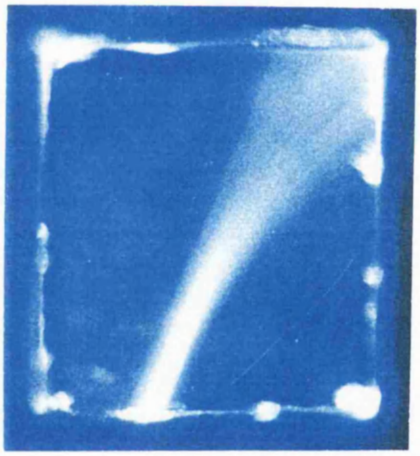

(b)

(c)

Obviously in SBN we could expect a similar result but with the beam entering close to +C direction as the c-axis is defined in an opposite sense to the direction into which beams tend to bend in the crystal than is the case for $BaTiO_3$. In Fig. 5.1(b) we show a schematic of what appears to be taking place within the crystal using a model with four-interaction regions (will be discussed in detail in Section 5.5). It should be noted that we repeated the "Cat" and the new "-C^3" SPPCMs successfully in another nominally 0°-cut undoped crystal of $BaTiO_3$ grown by another group in another country. This shows that our configuration is of general usefulness and not just a peculiarity of imputities in one crystal.

5.3 Experimental Arrangement for -C^3 SPPCMs

The experimental arrangement used to measure the self-pumped phase-conjugate reflectivties, response times, and fidelity for our configurations is shown in Fig. 5.3. The light source is an argon ion laser with multi-longitudinal modes operating at 488 nm in the blue without intracavity étalon giving a coherence length of ~3 cm. The laser output polarisation was controlled using a $\lambda/2$ waveplate as a polarization rotator to provide the flexibility of either ordinary or extraordinary states. We used extraordinary polarised light for writing gratings for the phase-conjugation process while ordinary polarised light was used to erase these gratings to measure the time response. The beamsplitter was used to couple out the phase-conjugate output and to separate the input from the conjugated output light. The input beam and the phase-conjugate beam were monitored with matched photodetectors (a Newport laser picowatt digital power meter, model 835), which were connected to an *x-t* chart recorder. We use a Sony video camera and a Nikon FM camera (with micro-NIKKOR 55 mm lens), which were not shown in Figure 5.3, to record the optical path within the $BaTiO_3$ crystal in real-time.

In the self-pumped phase-conjugation process, an extraordinarily polarised light beam illuminated the entrance face (labeled +*c*) in an ellipse of area ~0.2 mm^2 and approximate diameter 0.5 mm. The variable beamsplitter was used to vary the input power in the range 25 mW to 150 mW. That is incident power densities of 150 mW/mm^2 - 750 mW/mm^2. The beam was focused by a lens with 125 mm focal length to a point about 20 mm outside of the crystal so that the beam diverged into the crystal. This increased the intensity inside the crystal and the angular spread of the incident beam to ensure an even larger angular spread of beams within the fan generated.

Fig. 5.3 *Experimental arrangement for measuring self-pumped phase-conjugate reflectivities and time responses in "Cat" SPPCMs and "-C^3" SPPCMs.*

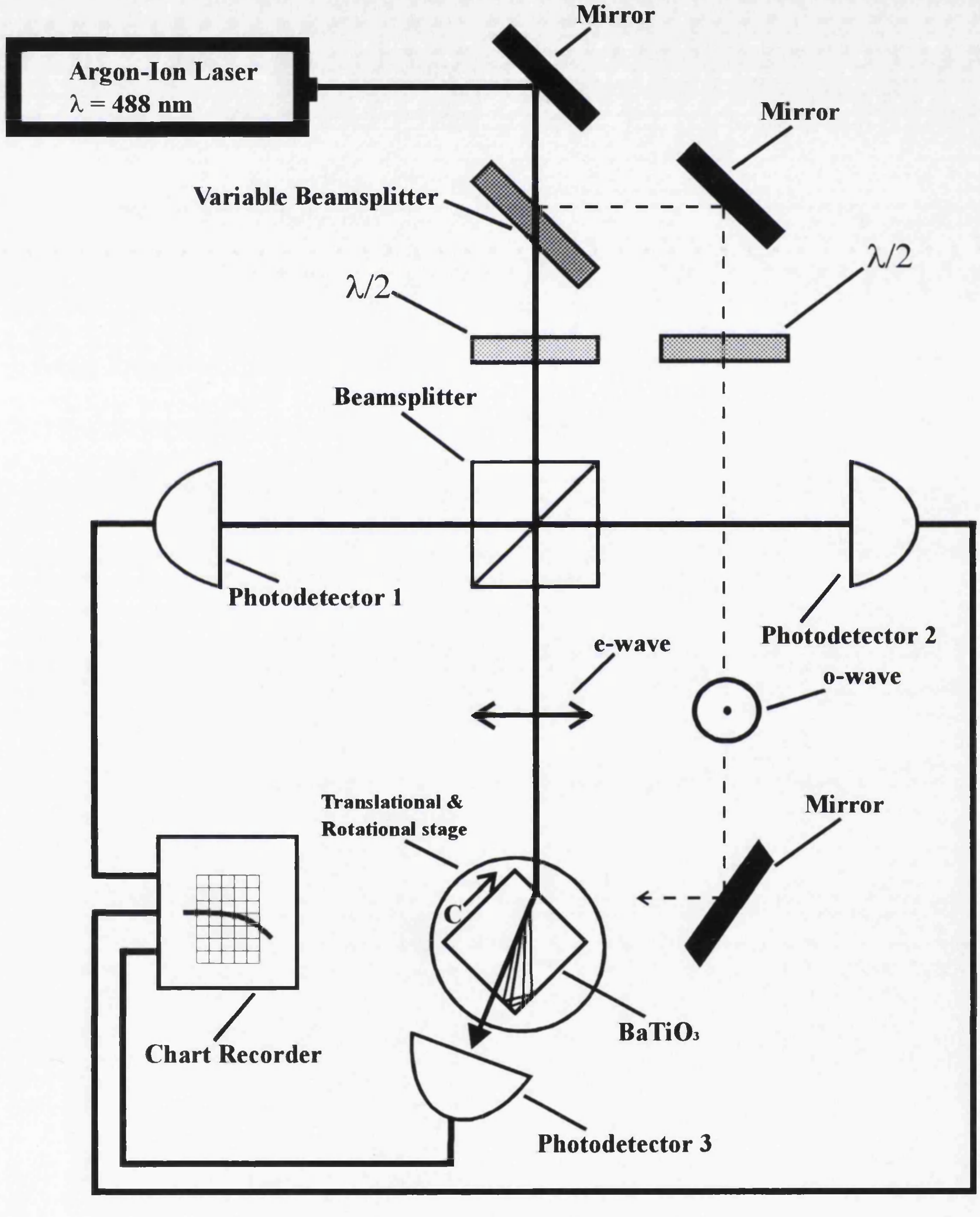

Our lateral alignment and angular tolerance experiments reported later were carried out by arbitrarily choosing an incident beam power of 40 mW. We used two crystals of 0°-cut undoped barium titanate with dimensions (a x b x c= 5.16 mm x 4.74 mm x 5.00 mm (grown in the China and supplied by the Photox Optical Systems Ltd in the UK) and 5.00 mm x 5.00 mm x 5.00 mm (grown and supplied to us by Sanders Associate Corp. in the USA.)) having six polished faces. For accurate lateral alignment and angular tolerance measurement, our two crystals were mounted on computer-controlled translation and rotation stages, respectively.

5.4 Experimental Results and Discussion

In this section we present our main experimental results and characterisation of our new SPPCMs and discuss them.

5.4.1 Spatial beam behaviour inside the crystals

We first investigated the spatial beam behaviour qualitatively inside the $BaTiO_3$ crystals by shining an extraordinary polarised light beam onto each face of the crystal to obtain the larger coupling strength, respectively. The experiments were performed at ~20 sec intervals and the observation were monitored by taking photographs from the top overview of the crystal. The incident beam entering the crystal on any face will fan (due to the anisotropic amplification) and tends to bend toward the +C direction along the c-axis (the direction of the spontaneous ferroelectric polarisation) as shown in Fig. 5.4.

In Fig. 5.4 there are four SPPCMs, two were formed by the "Cat" configuration as shown in Fig. 5.4(c) & (h) in which the incident beam seems to make a single sudden change in direction. The other two SPPCMs were formed by the new "-C^3" configuration as shown in Fig. 5.4(e) & (f) in which the light smoothly bends, arcs or curves continuously along the path towards the +C direction along the c-axis.

We also examined the spatial behaviour of the incident beam during phase-conjugate formation in detail by monitoring the beam behaviour outside the crystal. The spatial behaviour of fanning (the main factor for initiating self-pumped phase conjugation) inside the crystal was detected in the far-field pattern (the photos were taken from a screen which was 15 cm away from the *a* face in the "Cat" and +*c* face in the "-C[3]" for a $BaTiO_3$ crystal).

Fig. 5.4 *The middle part of this figure is a schematic showing how beams were incident at various angles and on various faces. Around this is are figures showing the experimental results at these positions. The experiments were carried out using an incident beam with a power of 25 mW with 0.5 mm diameter at incident angle 45°.*

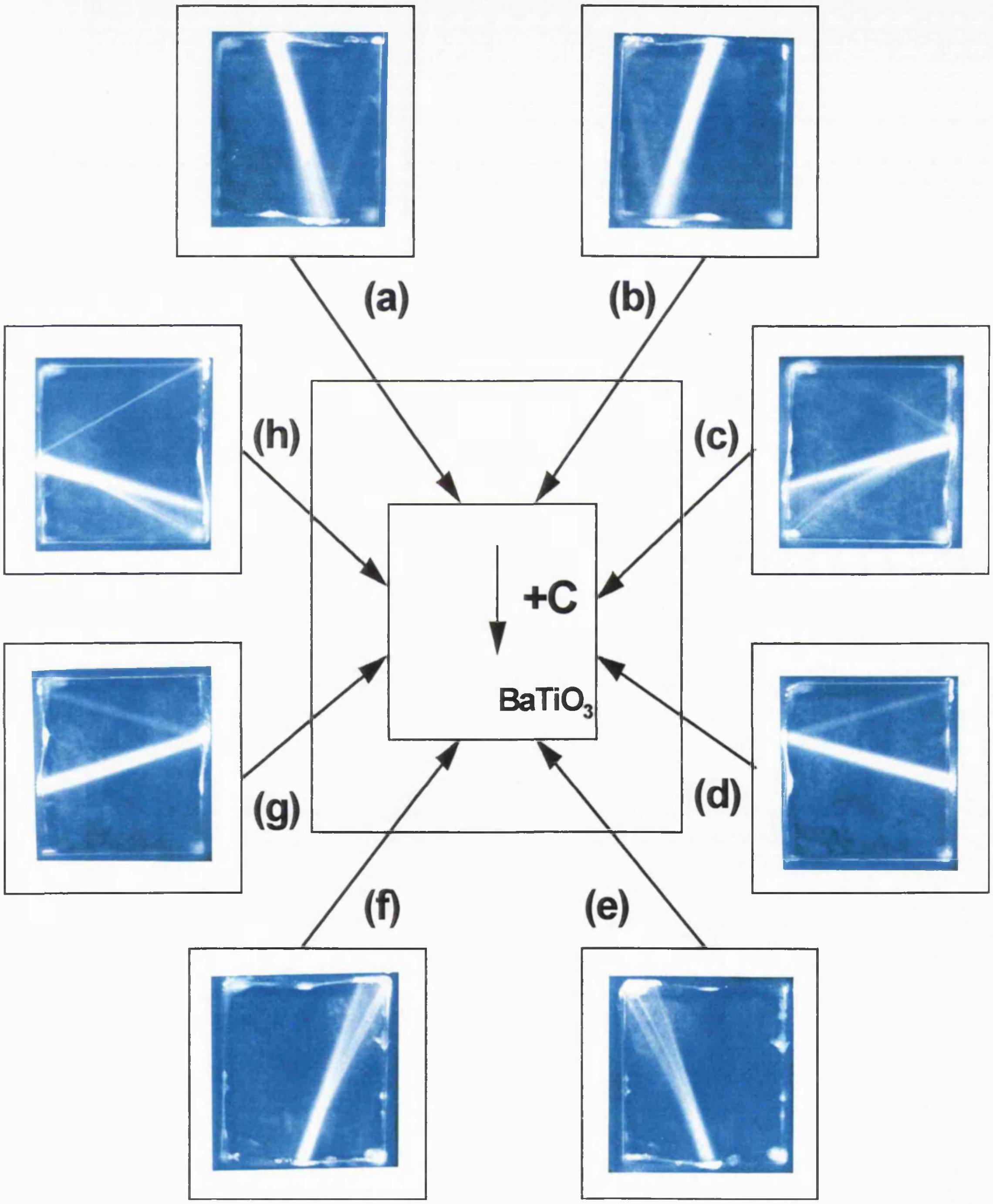

Fig. 5.5 *Photographs of the far-field intensity distribution of fanning for an incident beam (λ=514.5 nm) propagating through $BaTiO_3$ in the "Cat" SPPCM. The crystal c-axis points from left to right. The incident angle, θ, which is defined in Fig. 5.1(a) is (a) zero. and (b) 45 degrees, respectively. The incident beam is blocked by the dark spot in the middle to show up the less intnese detail.*

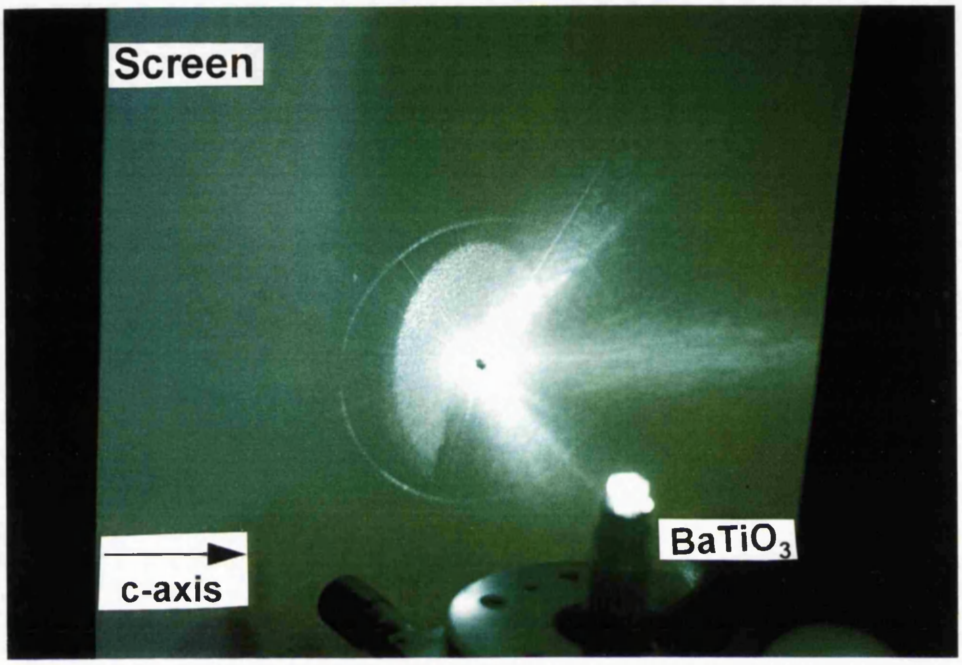

(a)

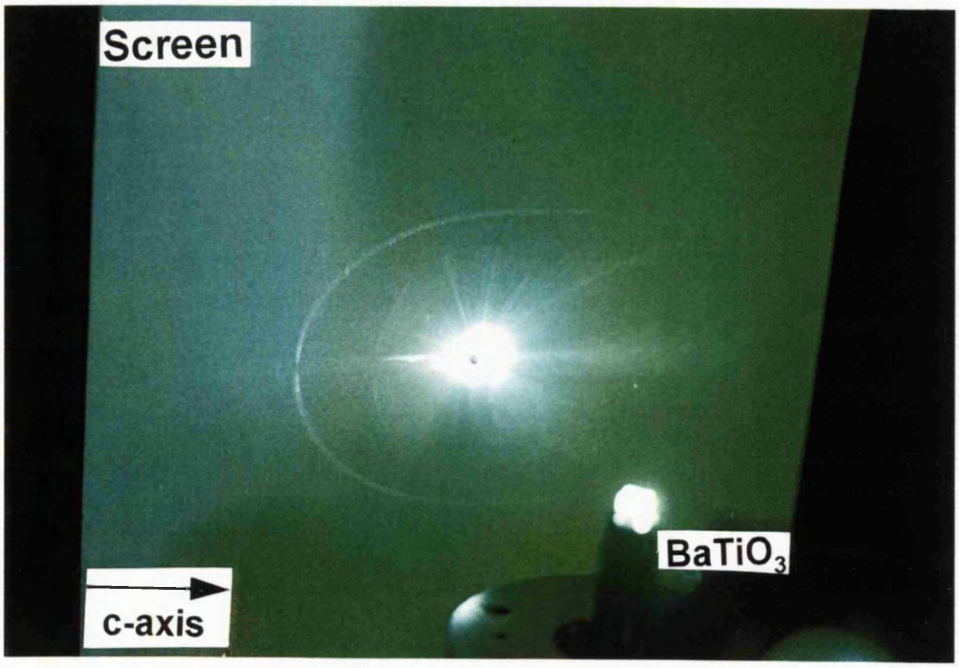

(b)

Fig. 5.6 *Photographs of the far-field intensity distributions of fanned beams for an incident beam (λ=514.5 nm) propagating through $BaTiO_3$ in the new "-C^3" SPPCM. The crystal c-axis point out from the screen. The incident angle, ϕ, which is defined in Fig. 5.1(b) is (a) zero. and (b) 45 degrees, respectively. The incident beam is blocked by a dark spot in the middle to show up the less intnese detail.*

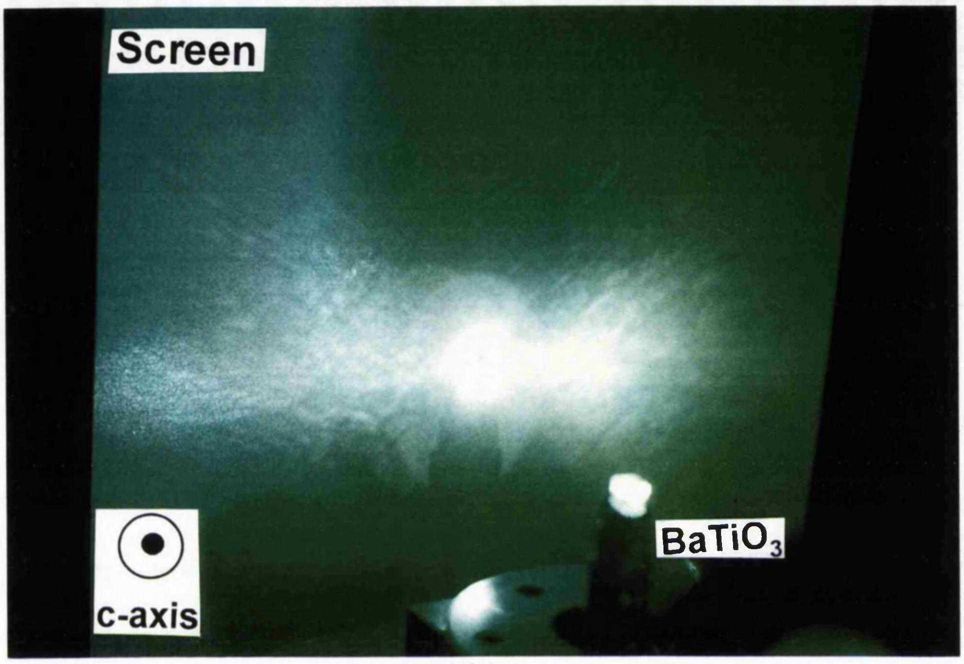

(a)

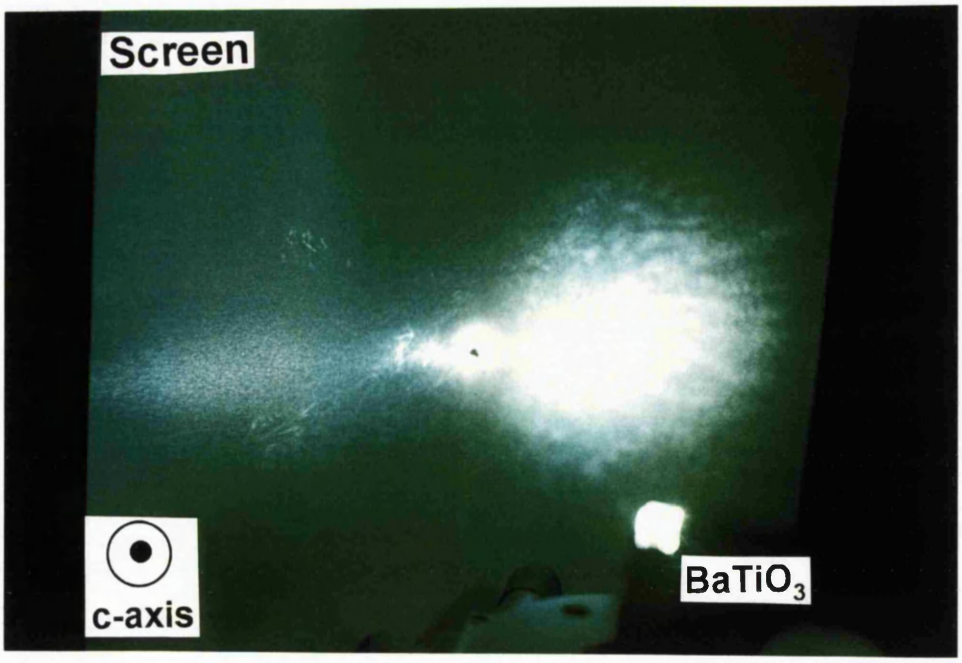

(b)

When the laser is turned on, fanning with three petals [Mon95] is observed in the "Cat" configuration as shown in Fig. 5.5. This reaches its peak intensity in less than 50 ms. However, we observed two symmetrically distributed petals in the "-C^3" configuration (Fig. 5.6) which take ~100 ms to reach their peak intensity. That is to say, the time required to set up the phase conjugation process is shorter in the "Cat" configuration than that in the "-C^3"configuration.

In addition, one anisotropic diffraction ring is always found in the "Cat" configuration, in which the incident beam is diffracted due to phase matching [Yeh85]. This is not observed, however, in the "-C^3" configuration. In other words, some of the incident energy is diffracted away during phase conjugation in the "Cat" configuration. That is part of the reason why the phase conjugation efficiency is higher for the "-C^3" SPPCM than that for the "Cat" SPPCM.

5.4.2 Temporal beam behaviour during phase conjugation

In the following experiments, we demonstrate the time evolution of the phase conjugation process in "-C^3" and "Cat" SPPCMs. Using a power of 25 mW we measured the dynamic increase in power with time in the phase-conjugate beam, I_{pc}, and the consequent decrease in power of the incident beam, I_{in}, after transmission through the crystal until a steady state response was achieved (Fig. 5.7).

The phase-conjugate signal was found to begin to develop 15 seconds after the incident beam began to illuminate the crystal. This phase-conjugate beam then grew over the next 10 s, as the loops were observed forming in the crystal, to reach a more stable value. The transmitted beam appeared to decrease very quickly (during the first 3 s) while the beam was developing into a fan within the crystal. The intensity remained constant for about a further 15 s before again decreasing, as the loops formed within the crystal, to reach a lower, more stable level. All experiments were performed at a room temperature of 26.0±0.2 °C.

Fig. 5.7 *Time evolution of the phase conjugate reflectivity in the "-C^3" SPPCM (solid line) and the decay of the transmitted beam power (dashed line) after the incident beam is turned on.*

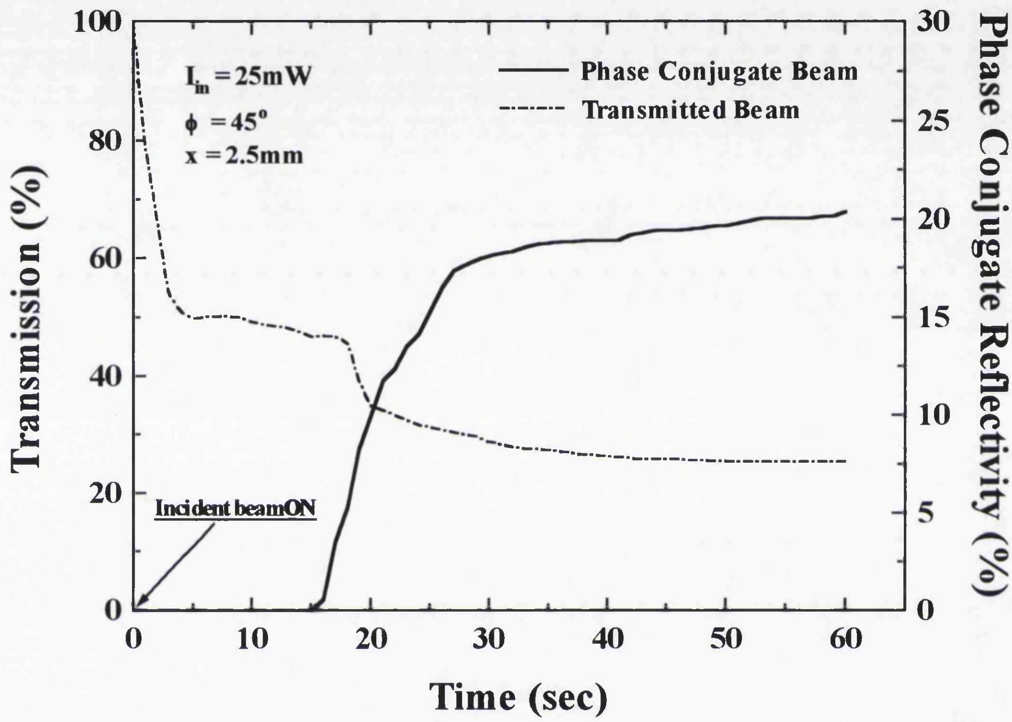

Fig. 5.8 shows the comparison of temporal behaviour in the "Cat" and "-C^3" configuration for self-pumped phase-conjugation. In Fig. 5.8. the time required to begin phase conjugation in the "Cat" configuration is shorter than that in "-C^3" configuration. However, after initiating the phase conjugation process the "-C^3" configuration grows more rapidly to reach a higher value of phase conjugate power.

5.4.3 Response time

The time required for the onset of the phase-conjugate beam in our new -C^3 SPPCM was also measured as a function of the intensity of the incident beam as shown in Fig. 5.9. Before each measurement the crystal was flooded with ordinary polarised light first for about 5 mins to optical erase any residual gratings remaining from earlier measurements at a given intensity. The intensity range of the incident beam for response onset time measurements was from 10 to 100 W/cm^2.

Fig. 5.8 *Time evolution of the phase conjugate reflectivity in the "-C^3" SPPCM (solid line) and in the "Cat" SPPCM (dashed line) after the incident beam is switched on.*

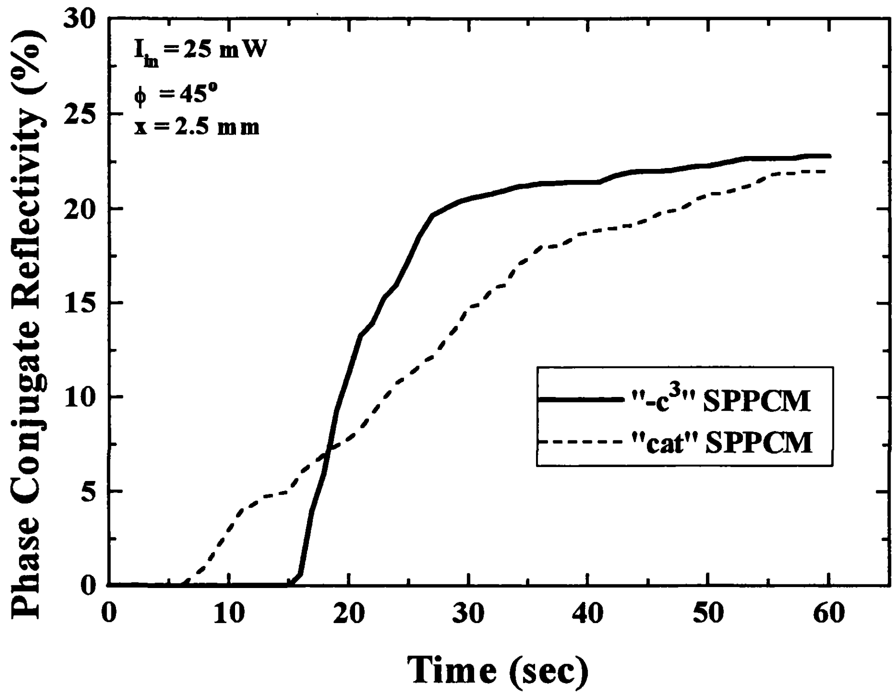

We measured the time required from turning on the illuminating beam to the time when the phase-conjugate beam reached 1-e^{-1} of its final stable equilibrium value. The same apparatus shown in Fig. 5.3 used to obtain the phase-conjugate reflectivity measurements was used to obtain the phase-conjugation response time, τ. The measurements were taken at an angle of ϕ=45°, using the 488 nm blue line with multi-longitudinal modes in the argon ion laser. As can be seen from the result shown in figure 5.9, the response time appears to follow a behaviour close to $\tau = AI_{in}^{-B}$ (the analytical expression representing the best fit to the data), where A is 2.46 and B= -1.09.

Fig. 5.9 *Time response of -C^3 SPPCM with respect to incident intensity.*

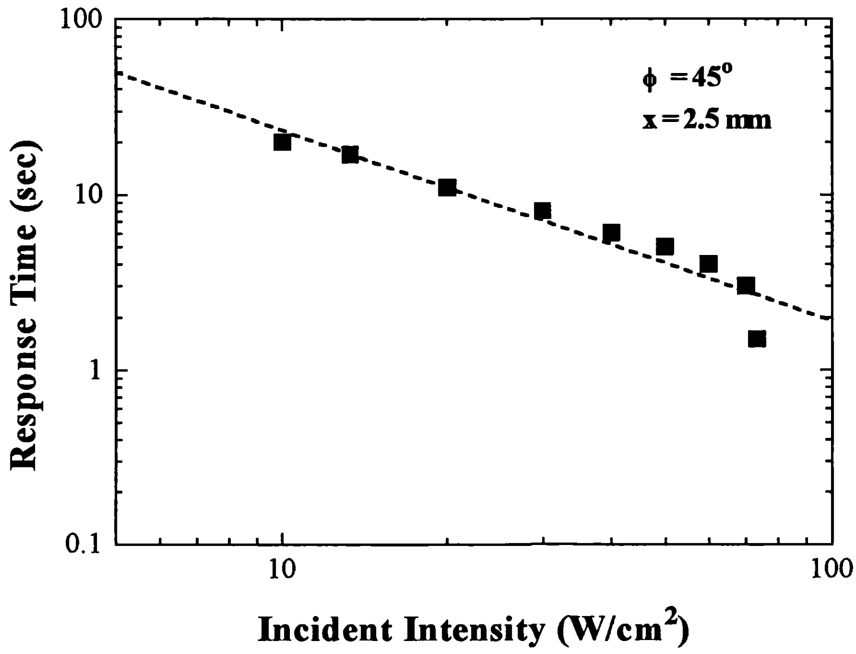

5.4.4 Lateral positional and angular dependence of the reflectivity

In this subsection, measurements are presented of the dependence of the phase-conjugate reflectivity on lateral position and angle of the incident beam on the crystal face. Figures 5.10 and 5.11 show the dependence of the phase-conjugate reflectivity on the lateral position and angular orientation of the incident beam.

Phase-conjugate signals could be observed over a wide range of angles of the incident beam of at least 40 degrees and over a range of about 4 mm in lateral positioning. The maximum phase-conjugate reflectivity in the "-C Curve Configuration" was observed to be about 30% for z=2 mm and ϕ=62.5°. Similar results were obtained using two crystals: one grown in the USA and the other in China. The angular and lateral positional dependence of phase conjugation were examined in the crystal grown in the USA for the case in which the incident beam varied in lateral position, z, at four different incident angles, ϕ, respectively. The phase conjugator with a wide field of view without any auxiliary inducing beam is more attractive for use in practical devices and applications.

Fig. 5.10 *Plot of the phase-conjugate reflectivity against lateral beam position of the incident beam on the crystal entrance face, z (mm) (defined in Fig. 5.1).*

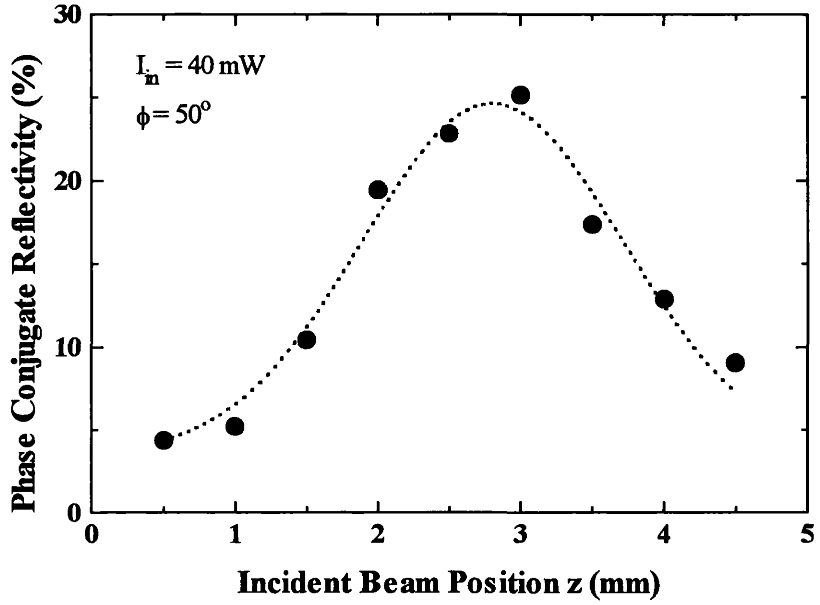

Fig. 5.11 *Plot of the phase conjugate reflectivity against the angle, ϕ (deg), of the incident beam (defined in Fig. 6.1) on the entrance face.*

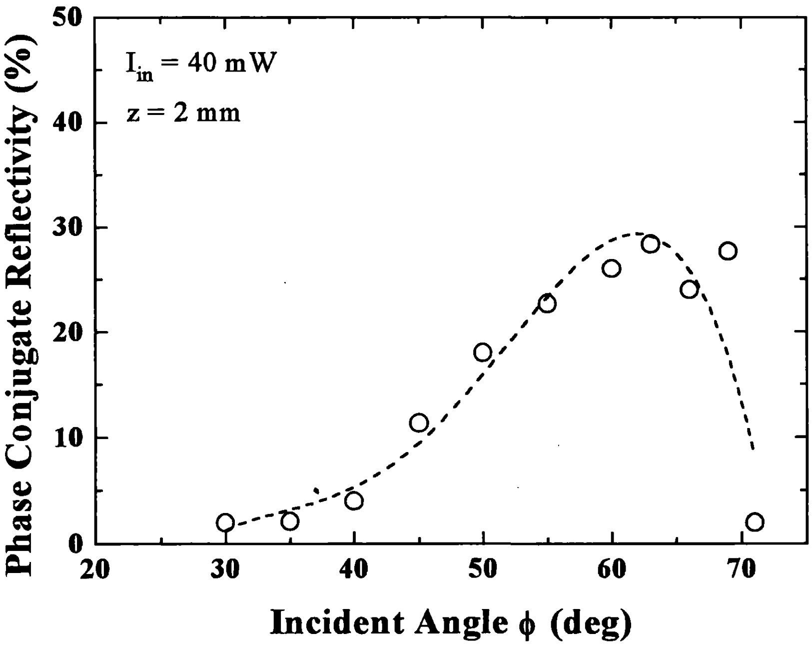

Fig 5.12 shows results as a function of lateral position using the crystal grown in USA. Phase-conjugate signals could be observed once more over a large range of about 4 mm in lateral positioning.

Fig. 5.12 *Plot of the phase-conjugate reflectivity against lateral beam position of the incident beam on the crystal entrance face, z (mm) at four different incident angles , respectively.*

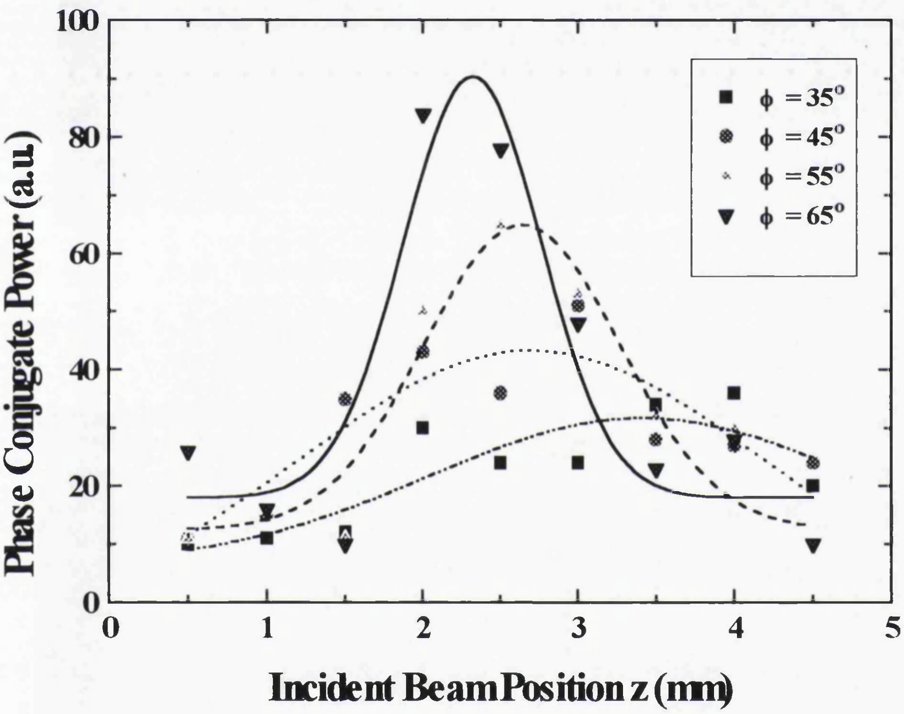

5.4.5 Optical paths within the crystal

The optical paths inside the crystal during the phase conjugation process were carefully studied in this section. When the crystal was acting as a self-pumped phase-conjugate mirror, we observed that the incident beam entering the crystal fanned into a corner where several beams appeared to be retroreflected back toward the incident beam. Figure 5.13 is a photograph showing the top view of a $BaTiO_3$ crystal while the crystal phase conjugates in several configurations with initial beam propagation at small angles to the c-axis in the -C direction. The c axis of the crystal is directed from top to bottom in the figure and the incident Gaussian beam is extraordinarily polarised and propagates from the bottom to top entering the crystal with a positive angle ϕ.

Fig. 5.13 *Photographs of the optical path within the $BaTiO_3$ crystal when the lateral position of the incident beam was altered.*

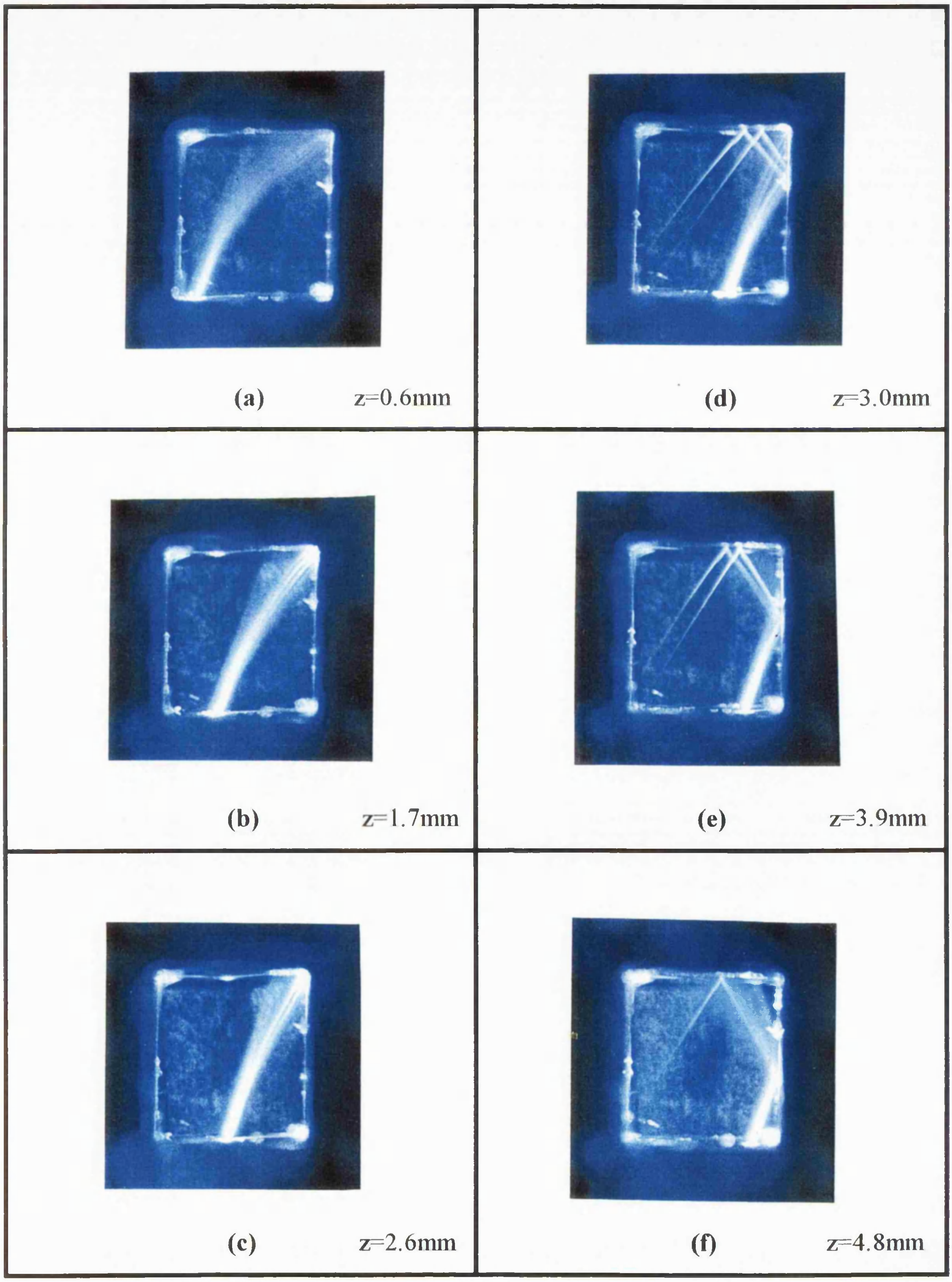

We have observed that by slightly altering the lateral position at which the beam illuminates the first crystal (+*c*) face we can induce on of serval internal beam paths:

i) the pattern observable are the largest range of angle and position two loops of light (as shown in Fig. 5.13(b)) (when z=1.7 mm, ϕ=51°),

ii) one loop of light such as the central loop in Fig. 5.13(c) (when z=2.6 mm, ϕ=51°),

iii) another two different loops of light (when z=3mm, ϕ=51°) can be formed including one "-C^3" configuration and another six internal reflection configuration [Chang85] as shown in Fig. 5.13(d).

Fig. 5.14(a) schematically shows the SPPCM with the "J" and "-C^3" loops coexisting and in Fig. 5.14(b) with only the "J" loop configuration.

Fig. 5.14 *Schematic of SPPCM with (a) both "-C^3" and "J" configurations, and (b) "J" only in $BaTiO_3$ crystal.*

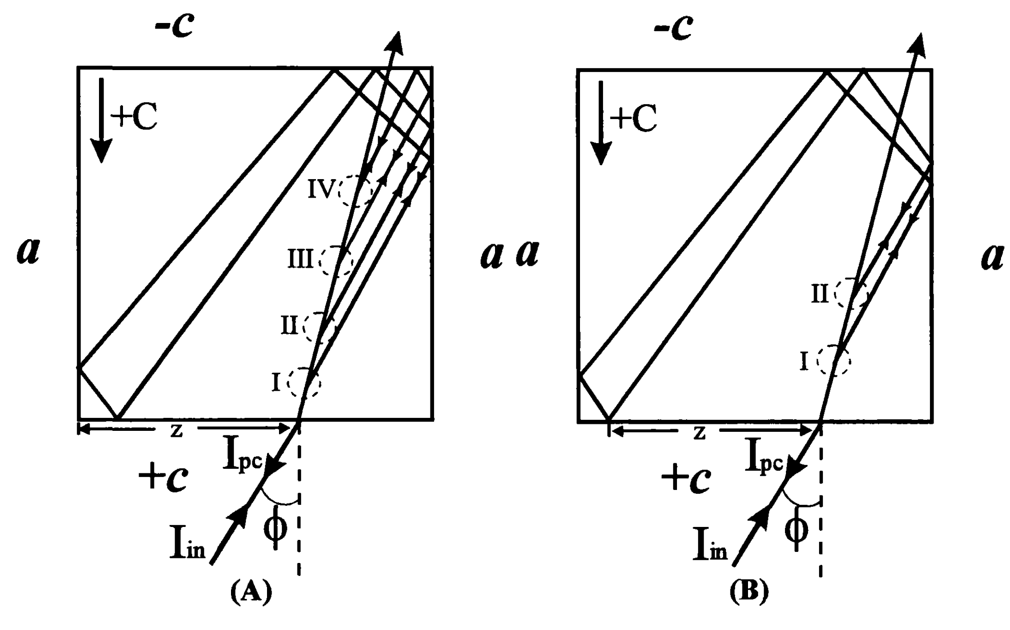

With larger changes of angle of incidence and power (when z=1.7 mm, ϕ=51°, and I_{in}=60 mW) the crystal demonstrated stronger fanning effects and almost all of the incident beam energy was transferred to the fanning beams so that we can induce BOTH one loop of the new "-C Curve Configuration" AND one loop of a new four internal reflection configuration as shown in Fig. 5.15. This appears to be the first time to our knowledge that two quite different phase conjugation loops, each of which can exist independently, have been reported to occur at the same time in certain critical conditions. For the sake of clarity we will refer to the 6 internal reflection configuration as the "J Configuration" as the beam path appears to form a J shape within the crystal (Fig. 5.13(d)) and the 4 internal reflection configuration as the "Tick Configuration" (Fig. 5.15(c)) since it looks like the tick symbol. We observed that over a range of angles and positions the J and -C^3 phase-conjugate loops coexist (for a range from z=2.9 mm and 3.3 mm with ϕ=51°).

Fig. 5.15 *The optical path inside the $BaTiO_3$ crystal when a more intense incident beam (I=60 mW) was directed into the crystal at a larger angle ϕ=70°. (a) schematic representation of the SPPCM with "Tick" and "-C^3" single loop, and (b) the experimental result before phase conjugation and (c) the experimental result during phase conjugation showing the presence of the "Tick" and "-C^3" single loop shapes of light.*

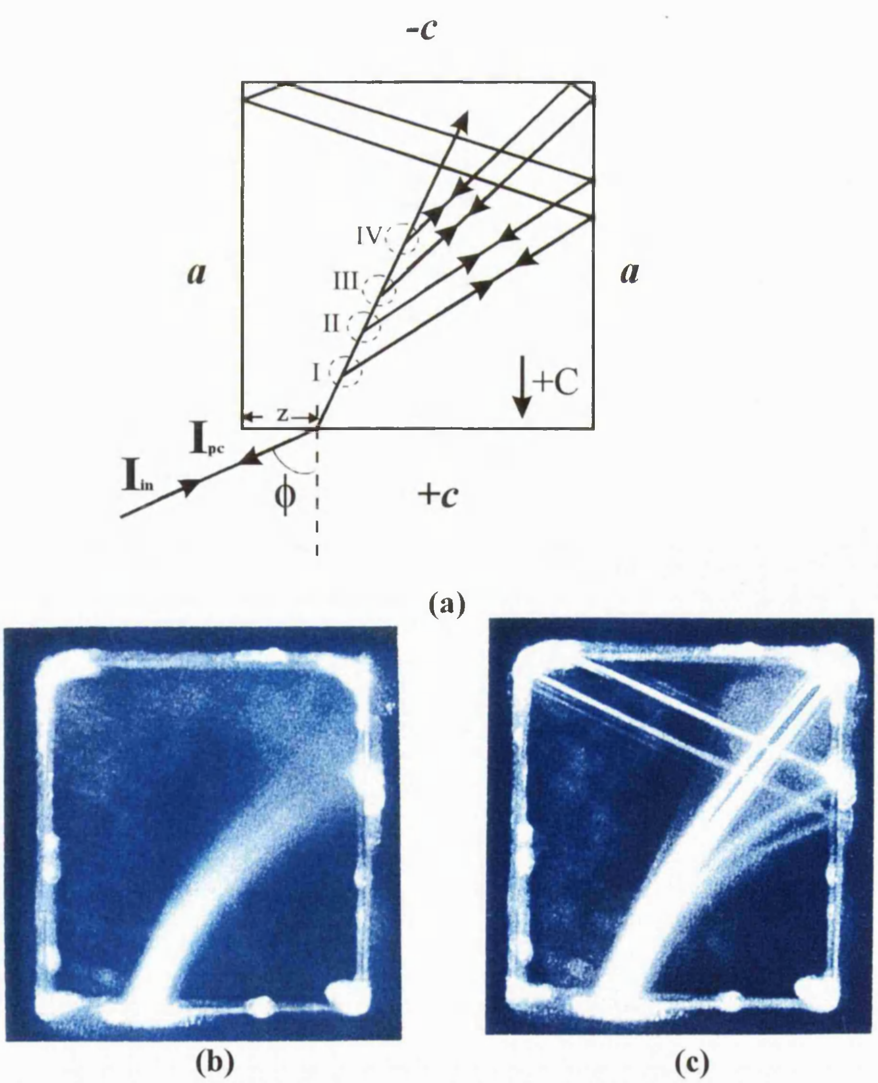

5.4.6 Resolution and fidelity of the phase-conjugate image from the -C^3 SPPCM

The resolution of a phase-conjugate image is dependent on the effective spatial frequency range that the optical configuration can reconstruct. The phase-conjugate image of a USAF resolution chart was photographed (or captured by a high resolution CCD camera) after the beam had been transmitted through the chart and had passed twice (Fig. 5.16) through a phase aberrator after reflection from the phase-conjugate mirror. For the "-C^3" configuration one can see from Fig. 5.11 that the reflectivity is sufficient for imaging purposes over a wide range of angle ϕ.

Fig. 5.16 *Experimental arrangement for measuring the resolution of phase-conjugate images.*

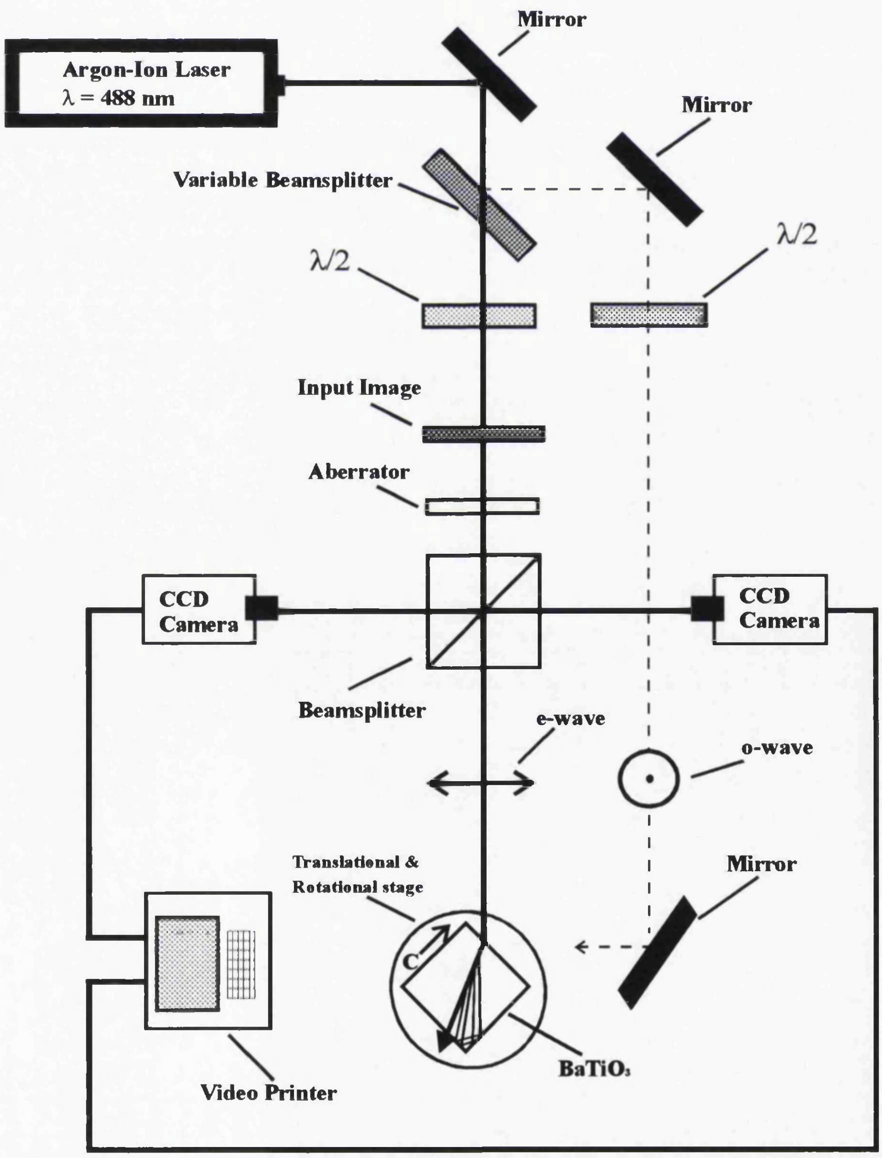

We used a plastic screen (which also caused some scattering) as a phase distorter. This was placed between the object and the crystal to distort the input image. The phase distorted image and phase-conjugate image were subsequently monitored with the CCD camera. The phase-conjugate image of the resolution target was recorded with the following conditions: with the phase aberrator in position and after reversing its path through the aberrator. The phase-conjugate images are compared in Fig. 5.17.

Fig. 5.17 *Phase distorted resolution target input to $BaTiO_3$ crystal, (b) phase- conjugate reconstructed image using "-C^3" SPPCM, and (c) phase-conjugate reconstructed image by means of "Cat" SPPCM.*

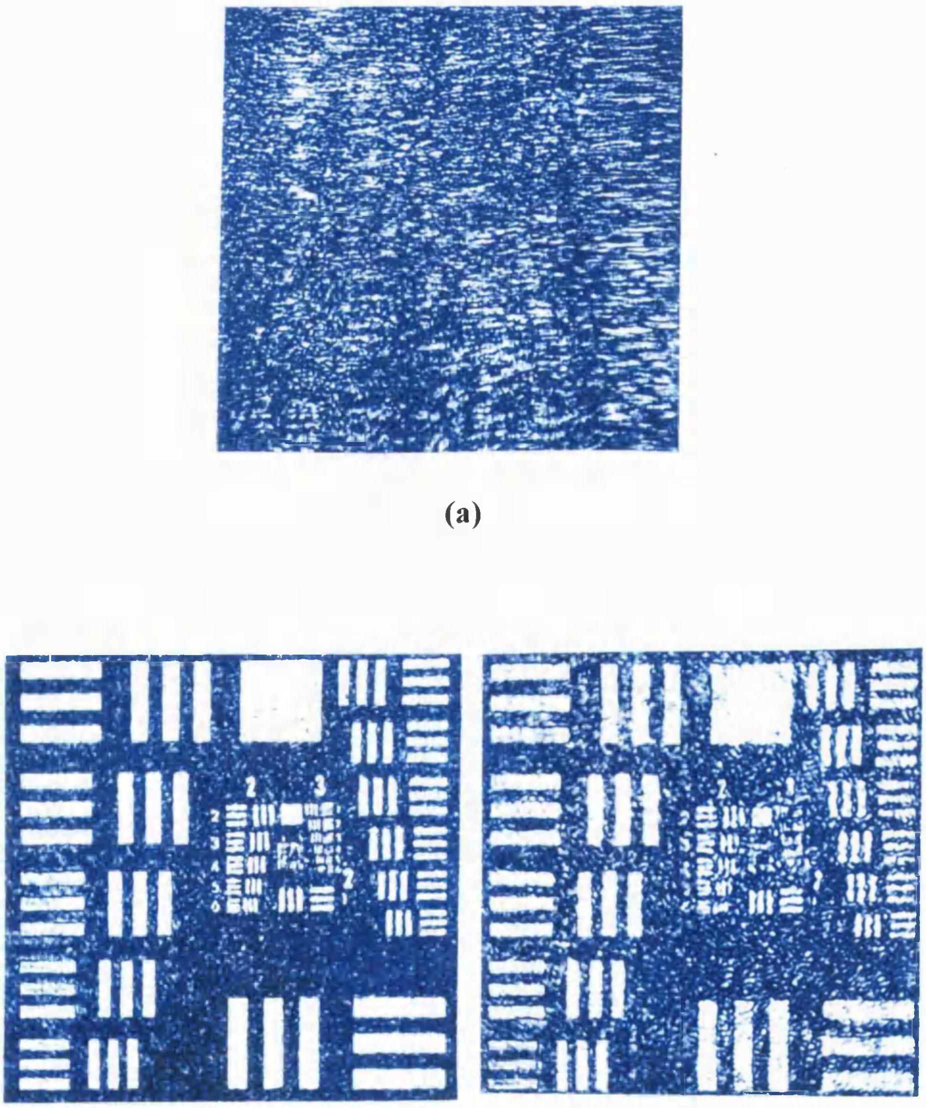

(a)

(b) (c)

Figure 5.17(a) shows the seriously distorted image appearing after the phase distorting screen just before the beam entered the crystal. Figure 5.17(b) shows the very clear phase-conjugate image of the resolution target using our "-C^3" phase-conjugate geometry after a second pass through the phase distorting screen. For comparison we show in Fig. 5.17(c) a similar reconstructed image resulting from the "Cat" phase-conjugate geometry formed in the same crystal using the same phase distorter. Our -C^3 geometry gives a better resolution of 12.7 lp/mm (39μm) while the Cat gives 7.13 lp/mm (70μm). It suggests that the higher resolution (corresponding to a wider angular range in the image spectrum of plane waves) domanstrated in the "-C^3" SPPCM compared to that of the 'Cat" SPPCM is due to the large range of acceptance angles.

5.5 Discussions

Based on our series of experimental results presented in previous sections (Section 5.3 to 5.4), we can briefly conclude that the optical path formed inside a $BaTiO_3$ crystal is not only related to the geometry between the incident beam and the crystal, but also depends on the lateral position and angle and intensity of the incident beam. The optimum results were obtained for our "-C^3" configuration in which a phase-conjugate efficiency of 30% was obtained and phase conjugation was maintained (but at lower efficiencies) over a range of 4mm in lateral translations of the beam and over a range of 40 degrees in the incident angle of the beam. Several existing mechanisms have been previously proposed such as the two-interaction-region mechanism [Fei82 & Mac83] and stimulated photorefractive backward scattering mechanism [Cha85 & Val92], and these can be used to explain some of our configurations (as shown in Fig. 5.13(c) & (e) and Fig. 5.14(c)) independently. Nevertheless, it would appear that for some of our new configurations especially in the -C^3, J, and Tick configurations the conventional two-interaction-region model would have difficulty in explaining these phenomena. That is to say, a more advanced model may be required. In the next section, we propose a tentative mechanism, the four-interaction-region model, to attempt to provide some explanation of these self-pumped phase-conjugate configurations.

5.6 Physical Mechanism

We first consider the optimisation of the coupling gain for SPPCMs with our new configurations. This is the main factor for determining the direction of the fanning beam inside the crystal and the optical path [Mac83]. Physically, the imperfections in the photorefractive crystal scatter the incident beam. Interference of each beam with its coherently scattered light creates a multitude of randomly oriented refractive index gratings by the photorefractive effect,. The amplitude of a light-induced refractive-index grating depends strongly on the angle between the grating wave vector and the crystal c axis. Therefore, as long as the beam crossing angle from the grating is small enough that κ_g (as shown in Fig. 5.18) is well separated in direction from the grating wave vectors formed by the other pairs of beams, it is possible to orient the crystal so that κ_g is the only effective grating. In our configurations the incident beam was arranged to travel at an acute angle to the c axis in the -C direction and the continuous fanning effects make a larger angle between the fanning beam and the negative c-axis (as shown 5.13). The larger the incident angle, the larger the angle between the fanning beam and the negative c-axis to create an effective grating for beam coupling.

In $BaTiO_3$, the physical mechanism by which four-wave mixing takes place is the photorefractive effect as described in Chapter 2. In this effect, trapped charges in the crystal are excited by light absorption and migrate from the high intensity regions to the low intensity regions. As a result, a dynamic non-uniform charge density is created which generates a static electric field in the crystal. This electric field brings about a refractive index change by means of the electro-optic effect. The resulting index pattern then causes phase grating effects which result in four-wave mixing. The amount of refractive index change and, hence, the strength of the four-wave coupling depends on the material parameters, such as the density of mobile charges, the Pockels coefficients of the crystal, and the angle of each of the optical beams in the crystal relative to the c axis, the crystal's optical axis. In order to obtain the highest phase-conjugate reflectivity, the value of coupling strength must be nearly maximised for a chosen piece of $BaTiO_3$ crystal. Let the pump beam and the diffracted beam in the crystal make angles, α and β, with respect to the c axis of the crystal, as shown in Figs. 5.18(a) & (b).

Fig. 5.18 *Geometries for two-wave mixing between the incident beam and the fanned light in interaction region I in (a) the "Cat" Configuration, and (b) the "-C³" configuration, respectively. α is the interior angle between the incident beam and +C, the crystal's optic axis, and β is the interior angle between the enhanced fanned beam and +C at interaction region I, respectively; φ is the angle between the grating vector, κ_g, and +C.*

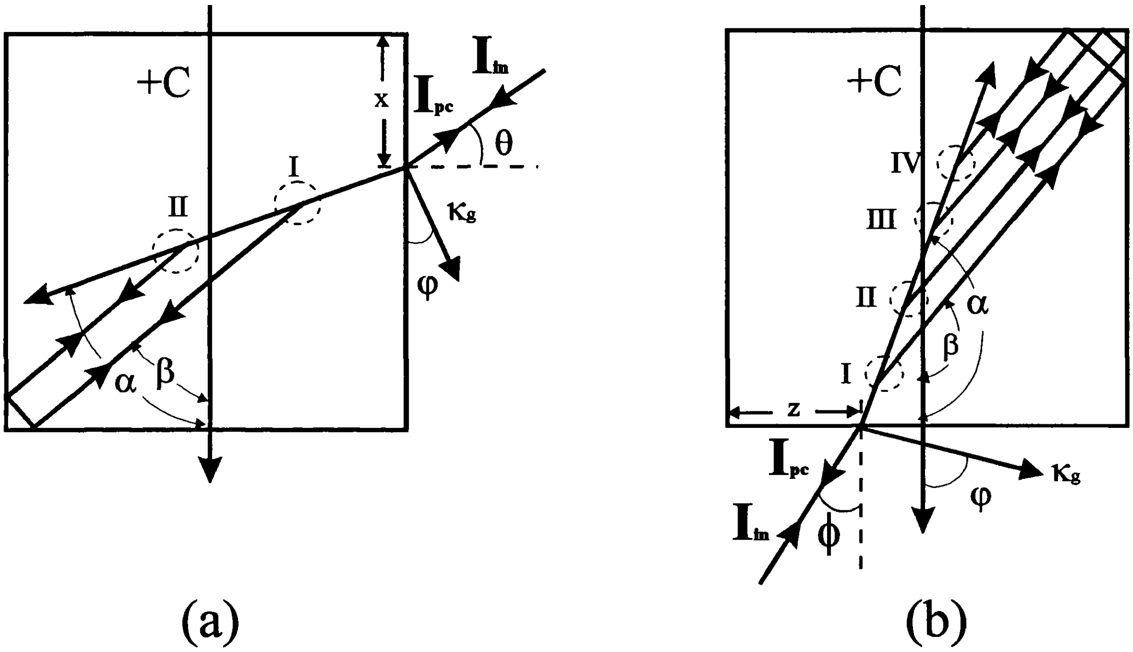

Assuming that the recorded refractive index grating is phase shift by π/2 relative to the intensity distribution (diffusion dominated), the steady-state coupling strength per unit length, γ, is given by [Fei80 & Mac83]

$$\gamma = \frac{\omega}{2nc}\frac{r_{\text{eff}}E_{\text{sce}}}{\cos\left(\frac{\alpha-\beta}{2}\right)}, \tag{6.1}$$

where ω is the optical angular frequency, c is the speed of light, and n is the refractive index chosen according to the beam polarisation. In the absence of any applied or intrinsic electric fields, the formula for the total space-charge electric field, E_{sce}, induced by the interference pattern is given by

$$E_{\text{sce}} = \frac{k_B T}{q}\frac{\kappa_g \cos(\alpha-\beta)}{1+(\kappa_g/\kappa_0)^2}, \tag{6.2}$$

where $k_B T$ is the thermal energy, $\kappa_g = 2/\Lambda_g$, $\Lambda_g = \lambda/2n_e\sin(\alpha-\beta)$, is the magnitude of the grating vector, q is the charge on each of the mobile charge carriers, and, k_0, is the material constant depending on the number density, N, of the charge carriers:

$$k_0 = \left(\frac{Nq^2}{\varepsilon\varepsilon_0 k_B T}\right)^{1/2} \tag{6.3}$$

where ε_0 is the permitivity of free space, ε is the effective dielectric constant of the material.

For extraordinary rays, the effective Pockels coefficient, r_{eff}, is

$$r_{eff} = \left[n_o^4 r_{13}\cos\alpha\cos\beta + 2n_e^2 n_o^2 r_{42}\cos\left(\tfrac{\alpha+\beta}{2}\right) + n_e^4 r_{33}\sin\alpha\sin\beta\right]\sin\left(\tfrac{\alpha+\beta}{2}\right) \tag{6.4}$$

where n_o and n_e are the ordinary and extraordinary refractive indices, respectively, at frequency and, r_{ij}, are Pockels coefficients (elements of the electro-optic tensor). In $BaTiO_3$ the largest electro-optic coefficient is r_{42}. To observe the largest effects it is necessary to use extraordinary polarisation and to orient the crystal so that the grating wave vector is not parallel to any of the crystal axes.

Since the refraction index of $BaTiO_3$ is about 2.4, which is higher than that of air , the input beam are strongly refracted at the entrance face. This confines the angular range of grating vector, κ_g, to $0° < \varphi < 23°$ for "Cat" SPPCM (Fig. 6.18(a)) or $67° < \varphi < 90°$ for "-C^3" SPPCM (Fig. 6.18(b)). Note that, from our calculation, the coupling strength γl for a photorefractive crystal of barium titanate is independent of the optical intensity of any of the pump beams. However, the amount of fanning (that initiates phase conjugation) is strongly dependent on the pump beam intensity and continuing bending occurs. The fan scattering form of the "-C^3" SPPCM is different from the "Cat" SPPCM a scattered light spreads into a large angle. It is worth mentioned that the above two SPPCMs [Fei82, Mac83, Gün85] depend on beam fanning inside the photorefractive crystal for their initiation, the magnitude of which relies on the number of scattering centres (or imperfections) encountered by the input beam and the interaction length of the two beam coupling occuring between the input beam and the scattered light. However, if we want to optimise the reflectivity and response time of SPPCMs, the angle, position, and intensity of the incident beam must satisfy some critical conditions. The use of a spherical lens to focus the signal beam tightly decreases the fanning response time by increasing the intensity (power density) but reduces the magnitude of the beam fanning by decreasing both the number of scattering centres accessed and the two-beam coupling interaction length. Use of a cylindrical lens to produce a line focus parallel to the extraordinary polarization direction increases both the number of scattering centres accessed in the high-gain direction and the interaction length and results in an order-of-magnitude decrease in the self-pumped phase-conjugate response time [Sal91].

Now we turn to consider the interaction regions which may exist in SPPCMs. The idea of interaction regions was first proposed and discussed in a one interaction model by Cronin-Golomb et al [Cro82]. Thereafter, Feinberg et al. [Fei82] proposed two interaction regions coupled by a simple reflection to account for four-wave mixing. In Feinberg's analysis the pump beams in the two interaction-region phase conjugator have more degrees of freedom than those in the one interaction-region phase conjugator to adjust their mode pattern to provide the maximum overlap with the incident, especially image-bearing beam. In addition, the phase-conjugate reflectivity is largest when the self-generated pump beams are phase conjugates of each other. Here, we propose a new mechanism for our self-pumped phase conjugation process which is based on a four interaction-region model. For a self-pumped phase conjugate mirror, the incident beam initially propagates at acute angle to the -C axis, that uses four-wave mixing in four coupled interaction regions. With four interaction regions, the device is free to choose the optimum mode pattern for the pump beams to maximise the phase-conjugate reflectivity. Large sized images, even with high resolution can be phase conjugated, and so the four-interaction scheme has, in general, more gain. In our configuration we think there are transitions between interaction regions giving the "-C^3", "J", and "Tick" configurations.

In our experimental configurations (Fig. 5.2(c), 5.13(b), and 15(c)) the incident beam initially propagates at an acute angle to the -C direction of the barium titanate crystal. This causes a fan to develop which has constituent beams over a wide range of angles. This gives rise to a large range of gratings, formed as the beams in the fan interact with each other, having a wide range of angles and periodicities. Therefore, there is a high chance of mutual scattering occurring from these fanning gratings via the process of simultaneous degenerate four-wave mixing (DFWM). Unlike the two-interaction-region model exploited in the "Cat" configuration, here four interaction regions give rise to the 2 loops of the "-C^3" configuration (Fig. 5.1(b)), both the "-C^3" and "J" coexisting loops configuration (Fig. 5.14(a)) and both the "-C^3" and "Tick" coexisting loops configuration (Fig. 5.15(a)). In "-C^3" with two stable loops it appears that the outer loop forms between regions **I** and **IV** while the inner between regions **II** and **III**.

When the incident beam enters close to the edge of the crystal (larger z) several of the beams in the fan can be internally reflected from adjacent crystal faces to give rise to the J loop with six internal reflections. To obtain phase conjugation we again make recourse to the four- interaction-region model (Fig. 5.14(a)). Two stable loops, "-C^3" and "J" (Fig. 5.14(a)), can form and coexist as the loops form between regions **I** and **II** for the "J" and between **III** and **IV** regions for the "-C^3" configuration. When the intense light enters into crystal at larger angles two stable loops, "-C^3" and "Tick" (Fig. 5.15(a)), can form and coexist as the loops form between regions **I** and **II** for the "Tick" and between **III** and **IV** regions for the "-C^3" configuration. It appears that the presence of two loops may improve the efficiency, angular range, lateral range and temporal stability as only the most efficient loops are self sustaining and may erase other gratings preventing other loops being formed although this remains to be fully confirmed.

5.7 Conclusions

In summary, we have proposed and demonstrated novel configurations for self-pumped phase conjugation that have either only one internal loop, or beam path, which curves into one corner or two loops of similar form or two loops of quite different form depending on the exact geometry when the incident beam enters a 0°-cut undoped barium titanate crystal at an acute angle to the -C axis. We have described experimental observations of these optical features, "-C^3" ,"J", and "Tick" geometries, associated with interaction region transitions.

Phase conjugation is demonstrated over a wide range (40 degrees) of incident angles and over a range of 4mm in lateral position with efficiencies up to 30%. This can provide a large effective numerical aperture giving high-resolution imaging which is important for transmission of detailed images within or between slowly vibrating systems or those suffering from dynamic random spatial phase variations. In free space optical communications, for example, the lateral position and incident angle of the arriving beam may vary with time due to convection currents in the intervening air. We also characterised the dynamic response, compared our configuration with that of the "Cat" and measured the time required for the initiation of the phase-conjugate beam to reach $1-e^{-1}$ of its equilibrium value for the "-C^3" SPPCM.

Finally, we have suggested tentative mechanisms, *four-interaction-region transitions*, to explain the spatial features of the optical path observed in the $BaTiO_3$ crystals. In other words, under certain critical condition several distinguishable spatial features of the beam path or loop were observed within the $BaTiO_3$ crystal corresponding to interaction-region transitions. In our mechanism we have suggested that both the $2k$ grating (a grating formed inside the crystal by the interaction between the incident beam and the backscattered beam) and DFWM in the interaction regions or both the stimulated photorefractive backward scattering and DFWM in interaction regions play their role during the generation of self-pumped phase conjugation.

Chapter Six

MUTUALLY PUMPED PHASE-CONJUGATE MIRRORS WITH NOVEL CONFIGURATIONS

6.1 Introduction and Motivation

The concept of a mutually pumped phase-conjugate mirror (MPPCM) was originlly developed for phase-locking two mutually incoherent, even independent, laser sources of the same or different wavelength [Ste86]. Several configurations [Wei87, Sha90, Wan89, Ewb88, Smo87, and Ewb90] of MPPCMs with their applications were reported in recent years. The major applications of these MPPCMs are for optical processing [Cau87, Wei87a and 87b, and And93], for coupling two incoherent laser beams [Seg87, Shi93, and Wri93], in photorefractive spatial mode converters [Chi95], and in optical neural networks [Dun87, 90, and 91] for pattern recognition. Most recently, theoretical modelling has been carried out by several research groups for the purpose of unifying the concepts and optimising the phase-conjugate efficiency, response time, and fidelity in existing configurations for mutually pumped phase-conjugation [Fis89, Bog92, Orl94, Eng94, and Kor95]. Recently, a 2-D model proposed by Zozulya et. al. [Zoz94 & 95] use a numerical approach for to investigate light propagation and formation of complex structures of light in photorefractive crystals.

Performance optimisation of the MPPCM is required for practical applications. MPPCMs depend for their operation on self-pumped four-wave mixing (SPFWM) [Fei82]. To obtain a high-performance MPPCM, the following aspects should be considered: firstly, in the chosen geometry of MPPCM, there should be a large diffraction efficiency for SPFWM, which requires a large coupling constant and an extensive two-dimensional interaction region. Secondly, in the chosen geometry of MPPCM, the light losses should be small. The light losses include the absorption and scattering loss inside the crystal, and the specular reflection loss on the extrance and exit surfaces of the crystal. Thirdly, a high efficiency will contribute to the stable operation of a MPPCM with large lateral positional and angular acceptance.

In this chapter we describe our experimental research on the formation of high-performance MPPCMs with several novel configurations in $BaTiO_3$ crystals. We start by reviewing in Section 6.2 existing configurations for MPPCM discovered in the last decade and then go on to describe in detail our novel configurations. In Section 6.3 we experimentally demonstrate our new "Arch" configuration, and show that it is in good agreement with the later numerical simulations carried out by Zozulya et al.[Zoz94 & 95]. Certain phenomena in mutually pumped phase conjugation are also demonstrated in this section, such as the appearance of anisotropic diffraction and fanning. Three further new configurations for MPPCM having three internal reflections are described in Section 6.4. In Section 6.4 we first described the second configuration, the "Fish-Head", for MPPCM. Its phase-conjugate behaviour is established relatively quickly (~1 sec) to give a reasonable reflectivity (28%) without observable crosstalk between the two incident beams. In addition, the output response is stable in time and exists over a range of angular and lateral positions of the two incident beams which makes it particularly interesting for practical applications such as for the phase locking of lasers and for optical free space communications. We also experimentally demonstrate our third and forth configurations, "Fish", and "Manta Ray", for MPPCMs. In Section 6.5 we give our physical interpretation for the "Fish-Head", "Fish", and "Manta Ray" MPPCMs and theoretical consider the MPPCM which was formed by two coherent incident beams. The degree of coherence of the two incident pump beams govern the gratings formed in the MPPCM so in this we also consider the mutual coherence of the two incident pump beams in the MPPCM especially with regard to practical applications in laser phase locking and high efficiency holographic storage (discussed in Chapter 3). We experimentally demonstrate the performance of MPPCMs with our novel configurations of two mutually coherent incident beams. In Section 6.6 a new double MPPCMs in a $BaTiO_3$ crystal is described in demonstrating a thresholding ability which can be useful for non-linear logical devices or as a threshold in neural networks. Conclusions will given in Section 6.7.

6.2 Configuration Interpretation for MPPCMs

The MPPCMs consists of a photorefractive crystal where two mutually incoherent beams indirectly interact and emerge as phase conjugates of each other (i.e., the beams exchange lateral spatial amplitudes and invert their own lateral spatial phase profiles). When the two incident beams are incidnet, the input beams fan and at the same time scatter from each other's fanning gratings. This process proceeds most efficiently if the beams diffract with automatic Bragg-matching everywhere throughout the entire volume from a set of shared gratings, which is possible only if the beams are phase conjugates of each other throughout the entire volume, that permits the exchange of spatial information without crosstalk. Beam coupling using the class of MPPCMs can be regarded as an effective holographic link between two mutually incoherent laser sources.

Six geometries for MPPCM have already been discovered in photorefractive materials [Wei87, Sha90, Wan89, Ewb88, Smo87, and Ewb90] to effectively couple two mutually incoherent laser sources. The various configurations reported to date can be categorised by the number of internal reflections that the beams experience: no reflections in the double phase conjugate (DPC) [Wei87], bridge [Sha90], and modified-bridge [Wan89] configurations; one reflection in the bird-wing [Ewb88] configuration; two in the mutually incoherent beam coupling (MIBC) [Smo87] configuration; and three in the frog-legs [Ewb90] configuration. Several selection mechanisms have been proposed, including one-common grating model for the "DPC" configuration [Yeh88] and two-common grating model for "MIBC", "bird-wing", "frog-legs", "bridge", and "modified bridge" configurations [He88] (as shown in Fig. 6.1), in which common gratings are enhanced and non-overlapping gratings are suppressed governing the establishment of the MPPCM. Eventually, if the gain Γ (average coupling coefficient, γ, multiplied by the interaction length l) is large enough, the SPFWM interaction stabilises in a MPPCM allowing a self-reinforcing self-aligning interconnect to form between the two laser sources.

In this section, we first briefly recall the geometry of earlier configurations in order to highlight the distinctive features of our novel arrangements. In the DPC cofiguration both beams are incident on opposite surfaces labeled $+c$ and $-c$ in figure 6.1(a) and once inside the crystal one beam travels at an acute (non-zero) angle to the +C direction and the other at an acute (non-zero) angle to the -C direction. In the MIBC configuration both beams enter the crystal at the same surface labeled a in figure 6.1(b). In the "bird-wings", "bridge", and "frog-legs" configurations the beams are incident on opposite surfaces (labeled a in figure 6.2) and once inside the crystal travel at an acute (non-zero) angle to the C axis in the +C direction, in the case of the "bird-wing" (as shown in Fig. 6.1(c)), or at an acute (non-zero) angle to the -C direction, in the case of the " bridge" (Fig. 6.1(d)) and "frog-legs" (Fig. 6.1(f)) configurations. In the modified bridge (as shown in Fig. 6.1(e)) configuration both beams are incident on adjacent surfaces +*c* and either of the surfaces labeled *a* and once within the crystal one beam travels at a non-zero acute angle to the +C direction and the other at a non-zero acute angle to the -C direction.

Fig. 6.1 *Schematics of existing geometries for MPPCMs (a) double phase conjugation (DPC) (Sternklar86), (b) mutually incoherent beam coupling (MIPC) (Smount87), (c) the bird-wings phase-conjugate mirror [Ewbank88], (d) the bridge phase-conjugate mirror [Sharp90], (e) the modified-bridge phase-conjugate mirror [Wang89], and (f) the Frog-legs phase-conjugate mirror (Ewbank90).*

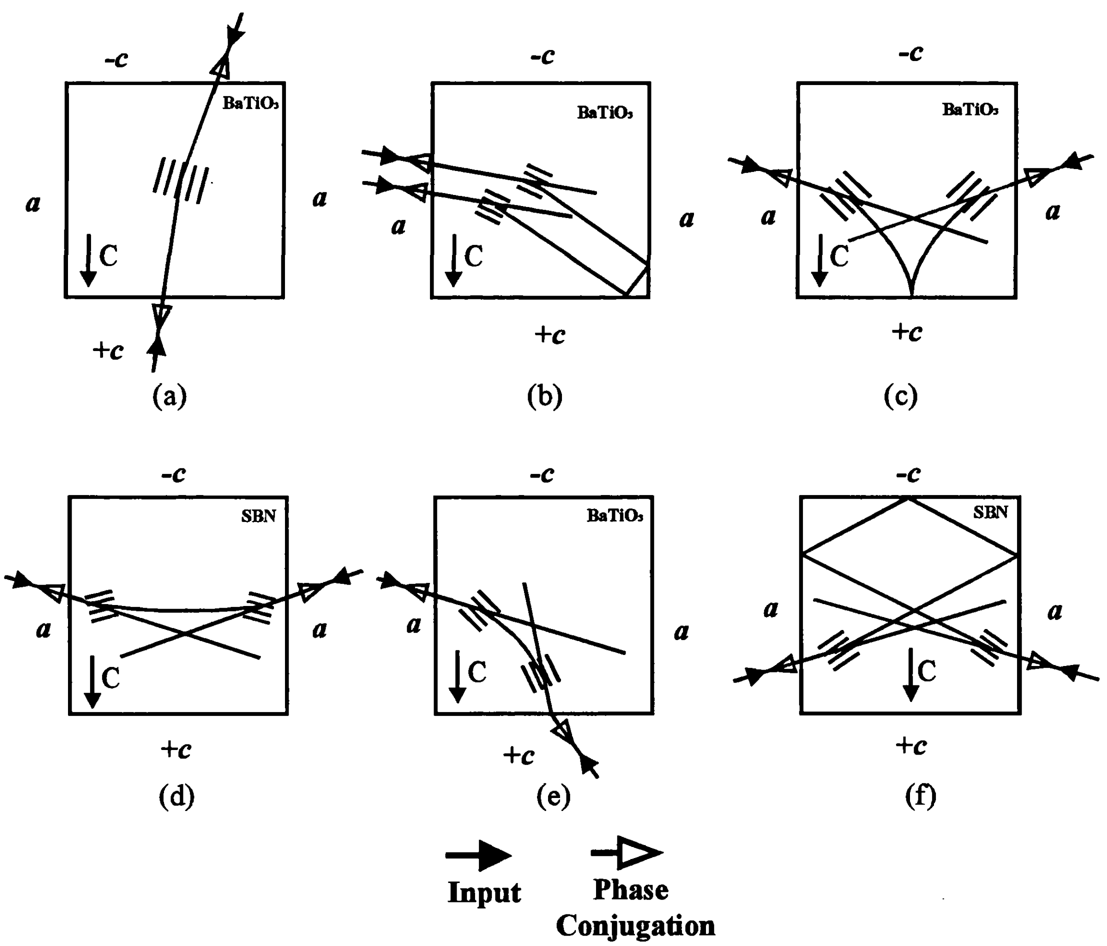

In our four configurations, the initial propagation state of the incident beams (i.e. input beams to be phase-conjugated) in that configuration is distinct from the earlier configurations (as shown in Fig. 6.1). The incident beams, I_{1p} and I_{2p}, both initially travel at an non-zero acute angle to the crystal's c-axis in the -C direction within the $BaTiO_3$ crystal.

(a) In the first configuration of MPPCM two input beams are incident on opposite crystal faces (labeled *a*) (defined in Fig. 6.2(a)) with acute angles of θ_1 and θ_2 to the normals of the *a* faces at distances, y_1 and y_2, from the crystal corners. Afterwhatwards these beams travel at an acute angle to the c-axis in the -C direction. Once the phase-conjugation process has been established (Fig. 6.2(e)) the illuminated beam path inside the crystal resembles the structure of an arch, so following the existing naming convention [Sha90], after different forms of architecture, we refer to this as the "Arch" configuration.

(b) In the second configuration, two input beams with an external intersection angle, ϕ, both enter into the crystal at the $+c$ face. Once inside the crystal both beams travel at an acute angle to the crystal's c-axis in the -C direction. In figure 6.2(b) the beams with incident angles, θ_1 and θ_2, to the normal to the $+c$ face are distant, z_1 and z_2, from the crystal corner. Once the phase-conjugation behaviour has been established either one or two stable loops of light (as shown in Fig. 6.2(f)) can be seen inside the $BaTiO_3$ crystal in this configuration. The illuminated beam path inside the crystal resembles the outline of the head of a small fish so following the existing naming convention, after different parts of different species of animal, we refer to this as the "fish-head" configuration.

(c) In the third configuration, two input beams with internal intersection angle, ψ, both enter the crystal at the $+c$ face (Fig. 6.2(c)). Inside the crystal both beams travel at an acute angle to the -C direction. In figure 6.2(c) the beams with incident angles, θ_1 and θ_2, to the normal of the $+c$ surface are distant, z_1 and z_2, from the crystal corners. When the phase-conjugation operation has been established at least two stable loops of light (as shown in Fig. 6.2(g)) can be seen inside the $BaTiO_3$ crystal in this configuration. The optical path inside the crystal resembles the contour of fish so we refer to this as the "fish" configuration.

(d) In the fourth configuration, two input beams cross together at the entrance face with an angle, ϕ, and then enter into the crystal from the $-c$ face. Once inside the crystal both beams travel at an acute angle to the crystal's c-axis in the -C direction. In figure 7.2(d) the beams with incident angles, θ_1 and θ_2, to the normal of the $+c$ surface are distant, z_1 and z_2, from the left corner of the crystal. Once the phase-conjugation process has been established at least one stable loop of light (as shown in Fig. 6.2(h)) can be observed within the $BaTiO_3$ crystal in this configuration. The illuminated beam path traveling inside the crystal resembles the structure of a spearhead or Manta-Ray so we refer to this as the "Ray" configuration for short.

Fig. 6.2 *Schematics and experimental photographs of our four new MPPCM grometries (a), (e) "Arch" phase-conjugate mirror, (b), (f) "Fish-Head" phase- conjugate mirror, (c), (g) "Fish" phase-conjugate mirror, and (d), (h) "Ray" phase-conjugate mirror, respectively.*

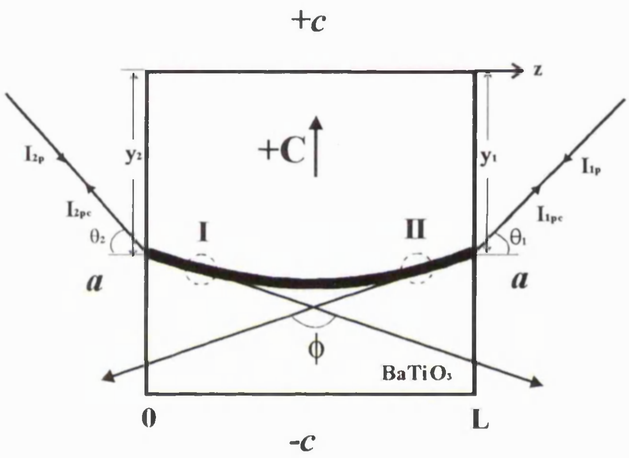

(a)

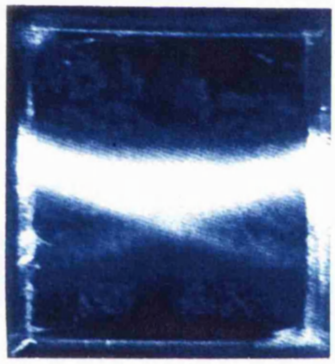

(e)

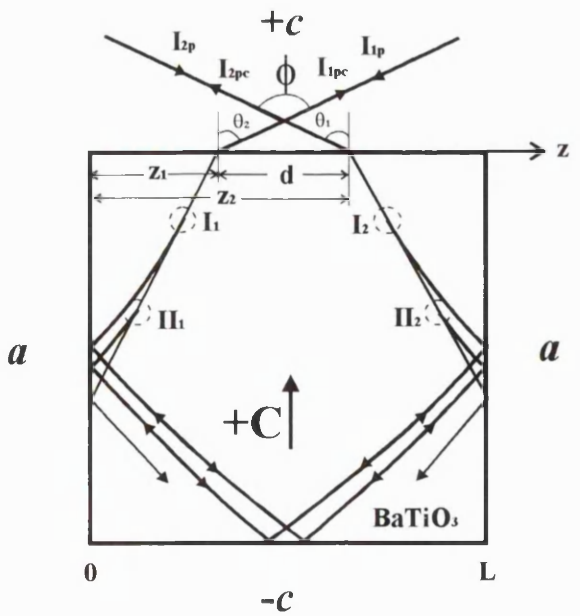

(b)

(f)

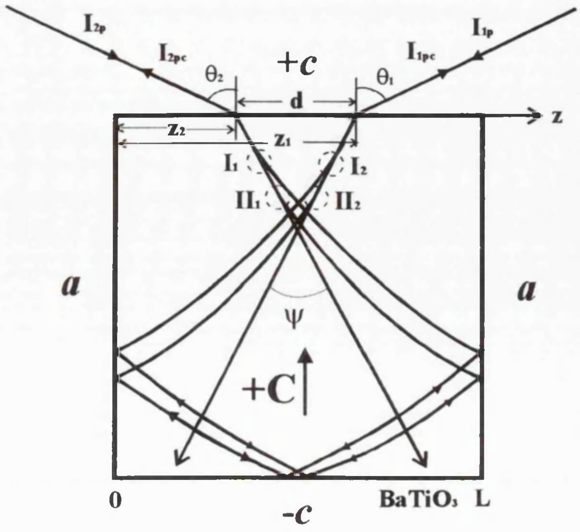

(c)

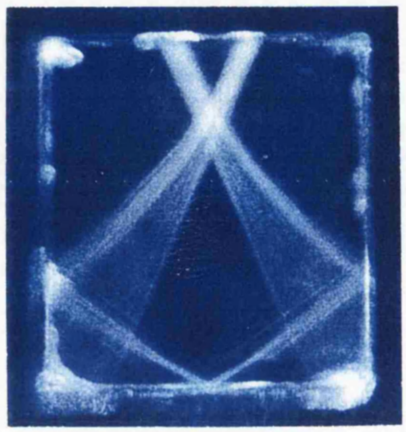

(g)

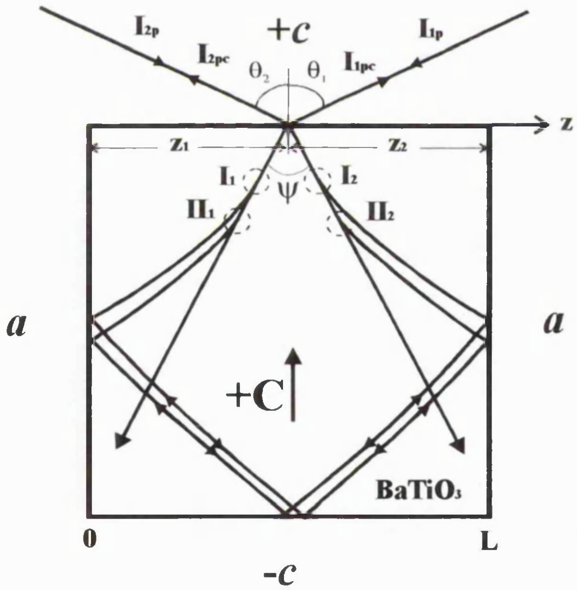

(d)

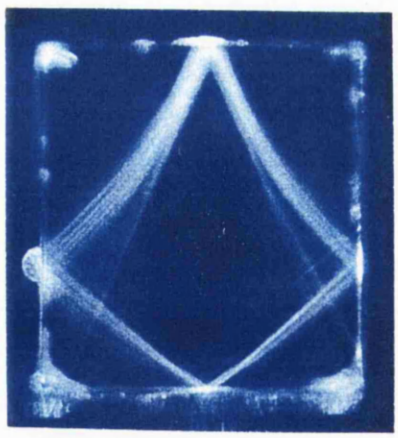

(h)

Notice that in these configurations when the input beams are traveling at an acute angle to the -C direction they tend to bend towards the +C direction. As a result they create a wide range of gratings in the fans and a large interacting area so reinforcing self-pumped four-wave mixing in each interacting area providing effective coupling between two laser sources.

It must be mentioned that for comparative consideration, we arrange the geometry as shown in Fig. 6.3 to distingish our configuration (Fig. 6.3(a)) fabricated in the $BaTiO_3$ crystal from the bridge configuration [Sha90] formed in an SBN crystal (Fig. 6.4(b)). In Fig. 6.3, the crystal's c-axis of both crystal point from top to bottom.

Fig. 6.3 *The geometry of (a) the Arch MPPCM in $BaTiO_3$ [Chang95] and (b) the Bridge MPPCM in SBN [Sharp90], where η ($=I_{1pc}/I_{1p}=I_{2pc}/I_{2p}$) is the phase conjugation efficiency.*

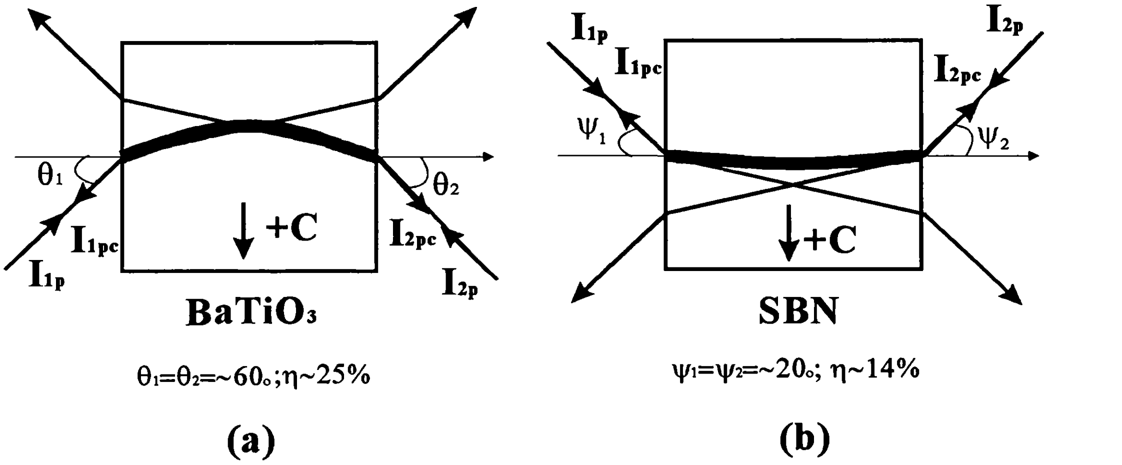

Before embarking on a detailed discussion of the experimental method for obtaining mutually pumped phase conjugation, it may be useful to describe the general properties of such MPPCM. The phase-conjugate behaviours of the Arch, Fish-head, Fish and Ray MPPCMs are related by the following common characteristics, in other words, these MPPCMs must meet conditions as follows:

The following tests were carried out to ensure that our 4 geometries are indeed mutually pumped phase-conjugate mirrors.

(a) no phase-conjugate reflection of each incident beam could be generated by itself only, in these configurations;

(b) phase-conjugate beam I_{2pc} resulted from beam I_{2p} and beam I_{1pc} from beam I_{1p}. When one of the two incident beams was blocked e.g. when I_{1p} was blocked off the beam I_{2pc} disappeared suddenly and I_{1pc} decayed gradually due to the holograms formed between the two beams being erased by I_{2p} gradually; and vice verse if I_{2p} was blocked;

(c) the phase-conjugate reflection fidelity of beam I_{1p} (beam I_{2p}), beam I_{1pc} (beam I_{2p}) was described by using the usual phase-conjugate imaging technique;

(d) there was no image cross-talk in phase-conjugate imaging when both the incident beams contained image information.

6.3 *Experimental Details of the Arch-MPPCMs*

In this section we describe the experimental configuration and procedure necessary to observe our first new MPPCM geometry (shown in Fig. 6.2(a)). All of our experiments have been performed using 0°-cut undoped $BaTiO_3$ photorefractive crystals. It is possible that related results could be achieved in other cuts. The Arch MPPCM has no internal reflections. This geometry provides a broad interacting area for the phase conjugation of two mutually incoherent laser beams coupling inside a photorefractive crystal (avoiding Fresnel losses).

The experimental arrangement for the Arch MPPCM is shown in Fig. 6.4. In our experiments, we used an Ar^+ laser operating with multi-longitudinal modes at 488 nm and in single logitudinal mode at 514.5 nm, respectively. Our crystals were a six-surface polished single domain crystal of $BaTiO_3$ with dimensions (a x b x c= 5.16mm x 4.74mm x 5.00mm (grown in the China and supplied by the Photonix System in the UK) and a 5.00mm x 5.00mm x 5.00mm crystal (grown and supplied by the Sanders Associate Corp. in the USA)).

One or other of our two crystals were mounted on computer or manually (precisely adjustable using a vernier scale) controlled translational and rotational stages allowing controlled rotation ($\pm$ 0.001deg) and lateral displacement ($\pm$ 1μm) so that the effect of the incident beam input position (y) and angle (θ) (as shown in Fig. 6.2(a)) could be determined. The laser output was divided by a variable beamsplitter, VBS, into two pump beams with different or similar intensities. These beams, were reflected and transmitted by BS_1 and BS_2, resulting in beams of several milliwatts in each and were incident upon two opposite faces (labeled *a*) of the $BaTiO_3$ crystal to form an "arch" configuration. The beamsplitters BS_1 and BS_2 were used to monitor the simultaneous phase-conjugate outputs, I_{1pc} and I_{2pc},. The electric shutters, ES_1 and ES_2, switched the two incident beams on and off. The two incident angles, θ_1 and θ_2, were set to be the same as each other (measured outside the crystal), and both incident beams were extraordinarily polarised to ensure maximum coupling strength. It was necessary to use lenses, L_1 and L_2, with focal length f = 125mm to diverge the two incident beams before they shone on the crystal to provide sufficiently large beam diameters to achieve significant beam fanning and subsequent beam overlap inside the crystal. To observe the scattering in the "Arch" phase conjugation process one screen was placed behind the crystal for capturing the far-field pattern after the scattered light had been transmitted through the crystal.

Fig. 6.4 *Experimental arrangement for demonstrating and investigating novel mutually pumped phase-conjugate mirrors.*

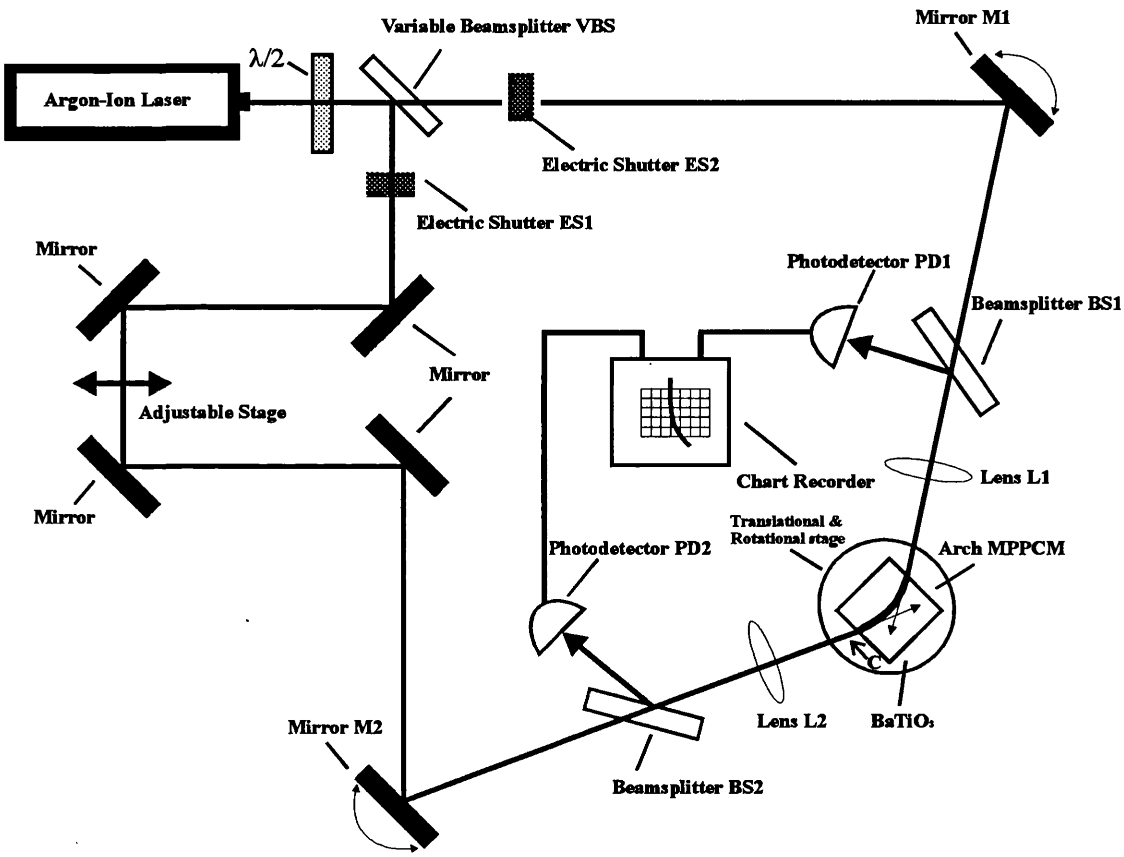

The degree of coherence between the two pump beams in our configurations was controlled so that competing photorefractive gratings, such as reflection grating formed by the two pumped beams, did not form. This mutual incoherence was achieved by previously demonstrated MPPCM's [Sei87, Eas87, Smo87, Ewb88, Sal91] either by simply removing the étalon from the Ar^+ laser and by making the optical path lengths between the laser and the photorefractive crystal, for the two incident beams, differ by more than the Ar^+ laser coherence length (~3cm) or by using two different wavelength lasers. In our experiment we used two arrangements for achieving incoherent pump beams:

(I) the path length between the two beams, I_{1p} and I_{2p}, was arranged to be ≅ 45cm (several times the coherence length of the laser without the étalon) at 488 nm, or

(ii) ≅ 6m (twice the coherence length of the laser with the étalon) at 514 nm.

6.3.1 Experimental results of the Arch- MPPCM

(i) In the first set of experiments, the Arch-MPPCM formation process was studied. In Fig. 6.5(a) only one beam was incident on the crystal, and it propagated directly inside the crystal, as shown, but with strong beam fanning because the incident beam diverged inside the crystal. Fig. 6.5(b) is a photomicrograph taken when two incident beams had been shining together on the crystal for 0.5 second. It can be seen that the two straight incident beams had begun to branch out and bend toward the +C direction, and the arch structure had begun to form. When the two beams had been on for 1 second, more energy could be seen to have been transferred to the arch from the two incident beams to give the final steady state arch, as shown in Fig. 6.6.

Comparing our experimental results with those of the simulation carried out by numerical modeling [Zoz94 & 95] as shown in Figs. 6.5(d)-(f) we can see that there is good experimental agreement.

(ii) in the second set of experiments, the formation of the MPPCM was studied using two mutually incoherent pump beams (λ=514.5nm) derived from a single Ar+ laser operating with a single-longitudinal mode. In Figs. 6.6(a) and (b) two 25 mW beams with area of ~ 0.8mm^2 were incident on opposite faces (labelled *a*) of the crystal at angles of 60° and propagated initially straight inside the crystal, as shown, but with strong beam fanning because the incident beam diverged inside the crystal. Fig. 6.6(c) & (d) are photomicrographs taken when two incident beams had been shining together on the crystal for 0.5 and 1.5 seconds, respectively, in symmetrical conditions, i.e., with $I_{1p}=I_{2p}$=25 mW; $\theta_1=\theta_2$ = 60°.

Fig. 6.5 *A set of photographs illustrating the formation of the Arch MPPCM, taken from above the $BaTiO_3$ crystal with (a) one input beam incident on the crystal for t=0.5 sec, and (b) & (c) two beams simultaneously incident with $\theta_1=\theta_2=60^o$ for, t=0.5 and 1 sec, respectively. The laser was operated with multi-longitudinal modes at $\lambda=488$ nm. (d)-(f) show simulation results from Zozluya et al. [Zozluya94] for comparison.*

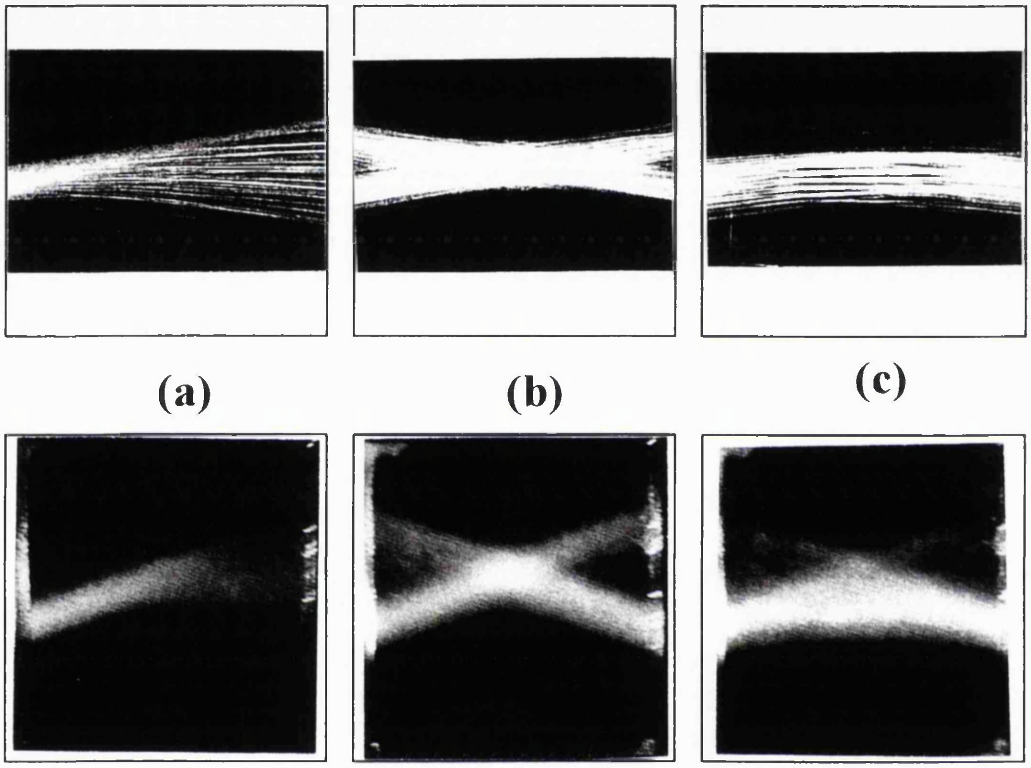

(a) **(b)** **(c)**

(d) **(e)** **(f)**

It can be seen that the two diverging incident beams had begun to branch out and bend toward the +C axis after 0.5 sec, and the arch had begun to form. When the two beams had been together turned on for 1.5 seconds, more energy was transferred to the arch from the two incident beams and the final steady state arch was achieved with 25% phase-conjugate reflectivity, as shown in Fig. 6.6(d).

Fig. 6.6 *A temporal sequence of photographs illustrating the formation of the Arch MPPCM, taken from above the* $BaTiO_3$ *crystal (a) and (b) after two beams had been individually incident on the crystal for t=0.5 sec, (c) and (d) after two beams had been simultaneously incident for t=0.5, t=1.5 seconds, respectively.*

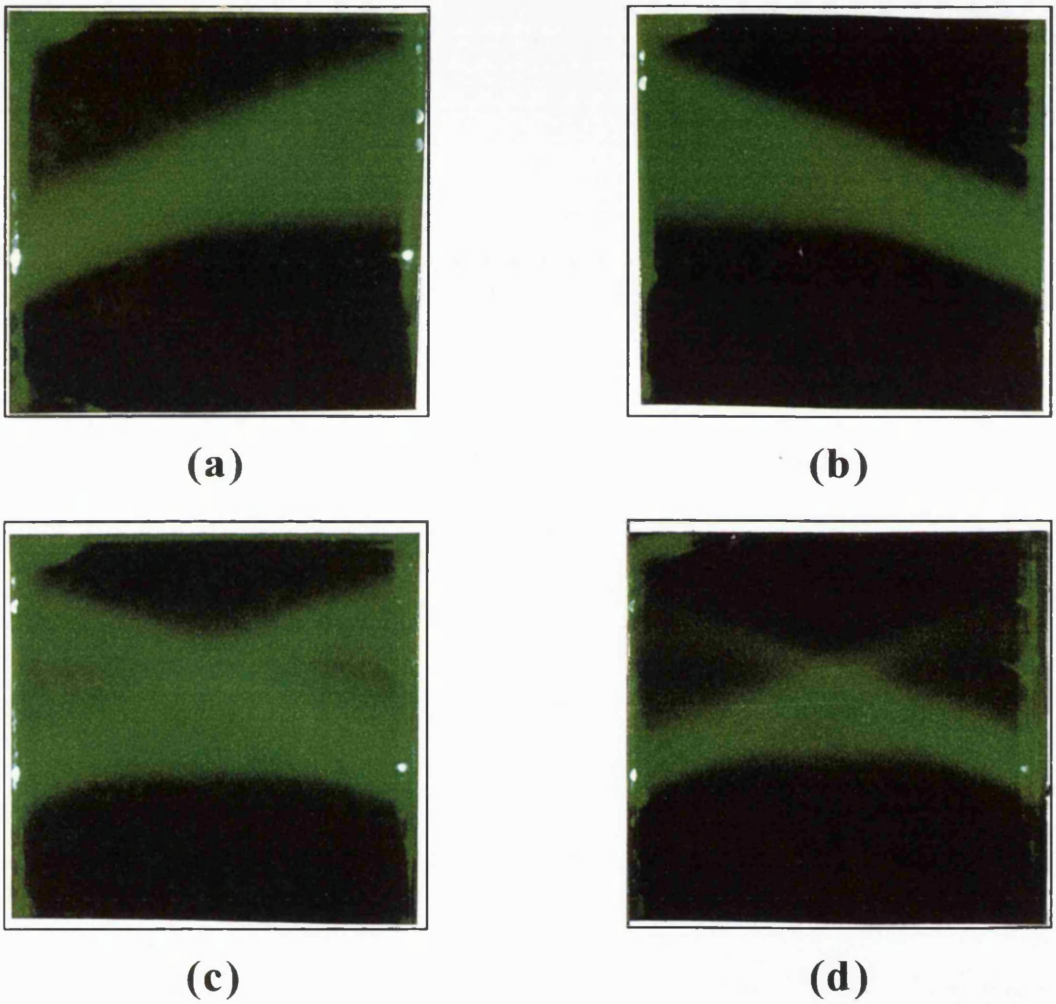

6.3.2 Lateral dependence

As for the existing MPPCMs, the performance of our Arch MPPCM, especially the positional and angular acceptances, is not only important for coupling two incoherent laser sources, but also for practical system in such as laser phase locking applications.

We examine the positional acceptance of our Arch MPPCM by measuring the phase-conjugate reflectivity of I_{2p} for three different input lateral positions on the *a* faces of the pair of two beams. The crystal is shifted along the ±C direction between the positions but the beams remain in symetrical i.e., $y_1=y_2$ and $\theta_1=\theta_2=60^o$ (defined in Fig. 6.2(a)). In Fig 6.7, the mutual phase-conjugation behaviour was estabilished with slighty different phase conjugation efficiency with two 25 mW input beams after 1.5 seconds as shown in figures 6.7(a)-(c).

Fig. 6.7 *A set of photographs illustrating the beam paths in the Arch MPPCM, taken from above the BaTiO3 crystal with the two beams simultaneously incident on the crystal for 1.5 s at lateral position (a) $y_1=y_2=1.84$ mm, and (b) $y_1=y_2=2.58$ mm, and (c) $y_1=y_2=4.30$ mm. The phase conjugation efficiency measured in three cases were 23%, 25% and 22%, respectively.*

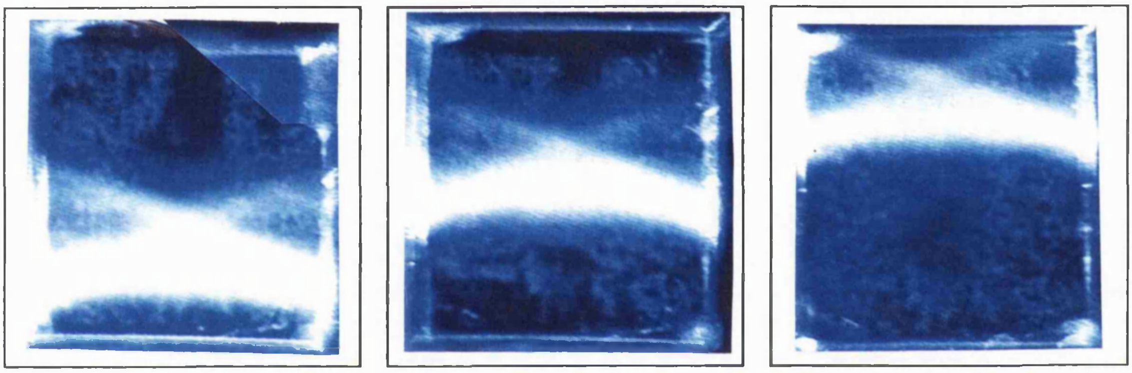

$\eta=23\%$ $\eta=25\%$ $\eta=22\%$

(a) **(b)** **(c)**

6.3.3 Angular dependence

In the following experiment we measured the range of angles over which the Arch MPPCM could be demonstrated. We measured the phase-conjugate reflectivity in three different input cases in which the input positions of two beams were altered by rotating the crystal in clockwise and couterclockwise directions as shown in Fig. 6.8.

In figure 6.8(a) two input beams are incident symmetrically on the $BaTiO_3$ crystal at $y_1=y_2$ and $\theta_1=\theta_2=60^o$ (without any rotation of the crystal) before phase conjugation and in Fig. 6.8(d) optical paths were estabilished after 1.5 seconds giving a phase- conjugate reflectivity of 23% of the input beam I_{2p}. Figs. 6.8(b) & (e) show the phase-conjugate behaviour before and after phase conjugation (with 20% reflectivity), respectively when the crystal was rotated in a clockwise ditection by 10 degrees. This rotation affected not only the incident angles of the two input beams but also the lateral positions on the entrance faces which were changed asymmetrically. Fig. 6.8(c) & (f) show the phase-conjugate behaviour before and after phase conjugation, respectively (with 17% reflectivity), of a crystal rotated in a counterclockwise direction by 10 degrees. From these experiments, it can be seen that the MPPCM with the "arch" configuration not only exhibits very wide angular and positional tolerance but has fairly acceptable phase-conjugate efficiencies.

Fig. 6.8 *A set of photographs illustrating the beam paths in the crystal in the Arch MPPCM, taken from above the $BaTiO_3$ crystal after the two beams had been simultaneously incident on the crystal for t=0.5 s (a) without rotating the crystal ($y_1=y_2=1.84$ mm and $\theta_1=\theta_2=60^o$), and (b) after rotating the crystal in a clockwise direction by 10^o ($y_1=2.32$ mm and $y_2=2.68$ mm), and (c) after rotating the crystal in a counterclockwise direction by 10^o ($y_1=68$ mm and $y_2=2.32$ mm). (d), (e), and (f) show the steady state arch in the orientation of (a), (b), and (c), respectively after t=1.5s.*

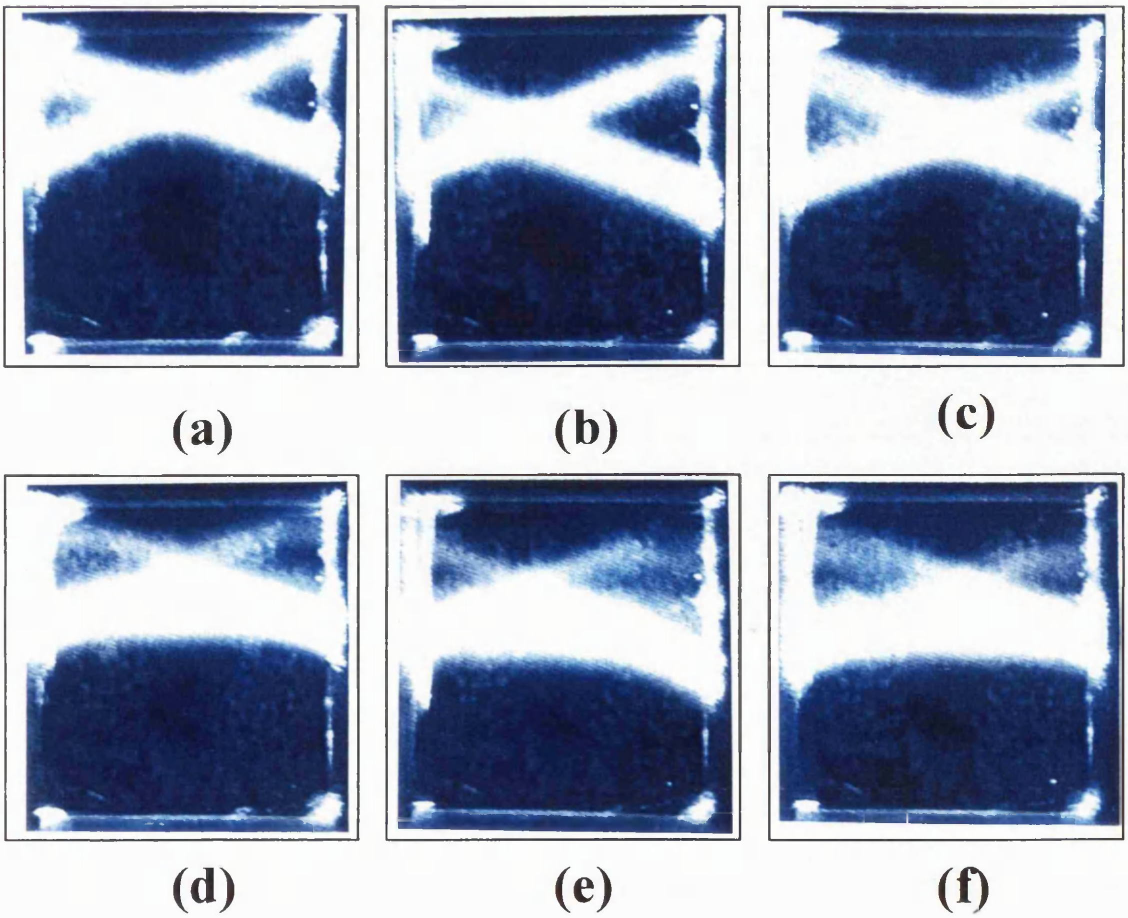

6.3.4 Arch compared to Bird-Wing MPPCM

When a $BaTiO_3$ crystal was used in this work to test the "bird-wing" geometry [Ewb88] and the "bridge" geometries [Sha90] (see Figs. 6.1(c) & (d)), the phase conjugation produced by the bird-wing geometry, was much easier to obtain than the bridge geometry.

To compare the performance of our Arch and the well-known Bird-wing MPPCM [Ewb88], we arranged geometries as shown in Fig. 6.9. The crystal's c-axis in both MPPCMs was directed from top to bottom on the figure. Similar incident conditions were used, $I_{1p}=I_{2p}=25mW$, $y_1=y_2=2.58mm$, except that the angles of the two input beams entering the crystal was different between the "arch" and "bird-wing" configurations.

Fig. 6.9 *Two sets of photographs illustrating the build-up process of the Arch and Bird-wing MPPCMs, respectively. (a)-(b) two input beams individually incident on the crystal with $\theta_1=\theta_2=60^o$ in the "arch" configuration and (d)-(e) two beams individually incident on the crystal with $\theta_1=\theta_2=\pi/2+60^o$ in the "bird-wing" configuration after t=0.5 sec. (c) and (f) show the optical path of the input beams after phase conjugation at t=1.5 sec in the "arch" and the "bird-wing" configurations, with reflectivities 25% and 30%, respectively.*

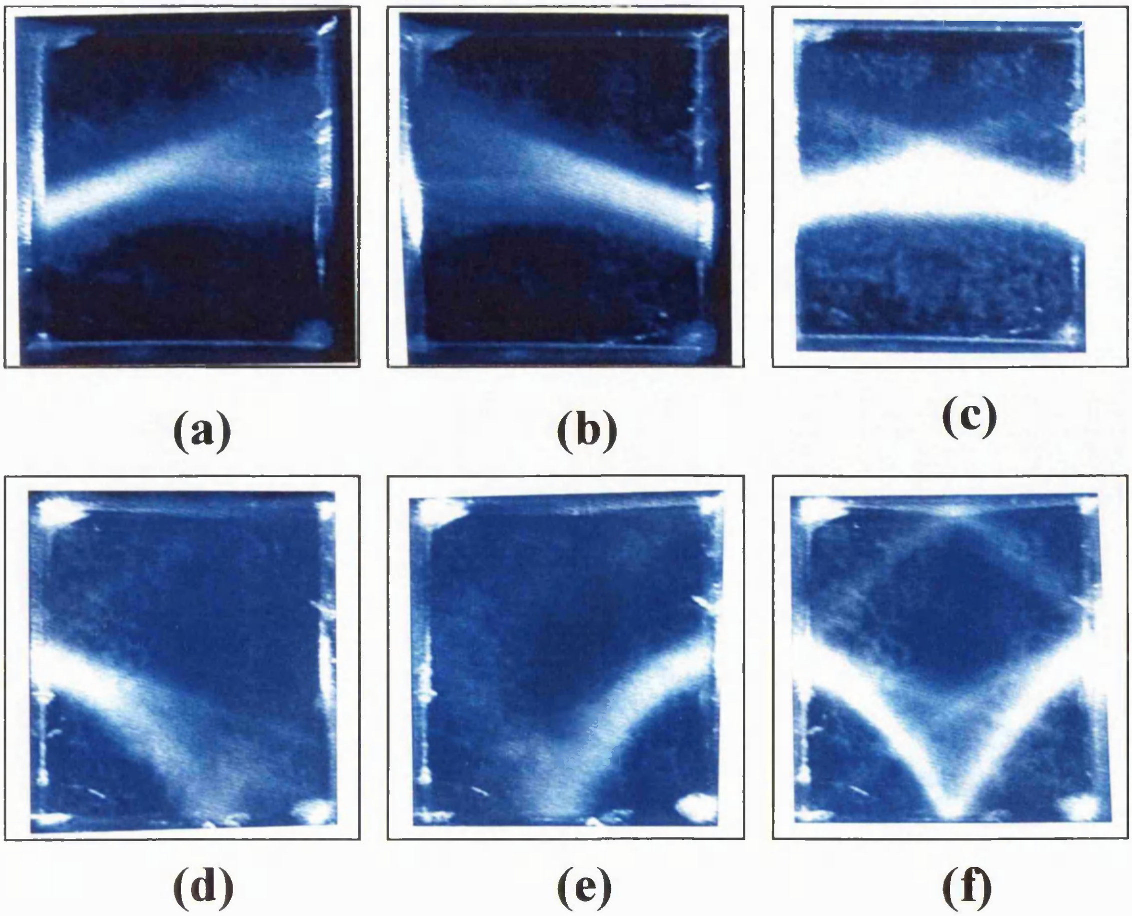

Once the phase conjugation has reached steady state we measured the phase-conjugate reflectivity of both configurations. It must be mentioned that although the phase-conjugate reflectivity of the Bird-wing MPPCM is higher than that of the Arch MPPCM the grating competition occuring in the Bird-wing MPPCM caused temporal instablity [Eas90].

6.3.5 Arch efficiency dependence on beam ratio

The relative phase-conjugate power as a function of input beam intensity ratio is shown in Fig. 6.10. The data does not take into account either Fresnel and absorption losses. It can be seen that the phase conjugate energy was transfered during the phase conjugation process in the Arch MPPCM.

Fig. 6.10 *Graph of the Arch MPPCM phase conjugation output powers as a function of the input beam ratio.*

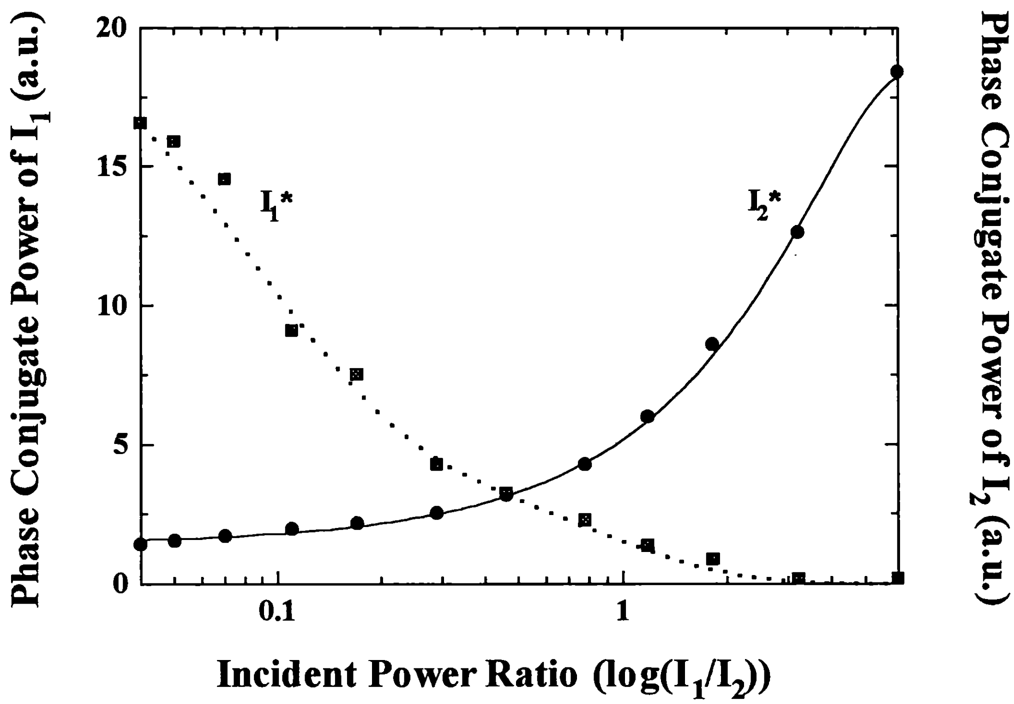

6.4 Discussion of the meaning of the experimental results obtained for the Arch MPPCM

Now, we suggest a mechanism that may be the possible reason for the Arch MPPCM to form. Theoretically, the most desirable geometry for double phase conjugation depends on the relative strength of the two-beam coupling coefficient [Fei82b] which, in turn, depends on the relative strength of the crystal electro-optic coefficient and the dopant concentration. For example, $BaTiO_3$ has a large r_{43}, resulting in the gain Γ or γ-dependence for extraordinary light waves. The curve indicates that γ is largest when the coupling light rays which write the index gratings are almost 45° to the crystal's +c-axis. This accounts for the much lower reflectivity of the Bridge MPPCM (Fig. 6.1(c)) [Sha90] and the ease of establishing the "bird-wing" configuration in $BaTiO_3$. However, when the crystal was rotated by 45° [Wan90] as shown in Fig. 6.1(e), the "modified bridge" configuration was much easier to establish and phase-conjugate signals were competing with the "bird-wing" arrangement. Despite the merits of the "modified bridge" MPPCM, one could rotate the $BaTiO_3$ crystal by 180° relative to Fig. 6.1, as shown in Fig. 6.4(a). The new configuration (named arch mutually pumped phase-conjugate mirror or Arch MPPCM which was much easier to establish than the "bird-wing" and "modified bridge" configurations and its phase-conjugate signals were competitive with those of the "bird-wing" and "modified bridge" arrangements. The higher reflectivity in this case (Arch MPCM) is due to the coupling beams being nearer the optimum angle for $BaTiO_3$. But it should be mentioned that there are also unavoidable scattering and anisotropic diffraction losses in the Arch-MPPCM.

Let us propose a possible mechnism to understand how the arch works. Two mutually incoherent incident beams enter the crystal from the two oppoiste, *a*, faces at angles, θ_1, & θ_2, (shown in Fig. 6.11), and generate strong photorefractive beam fanning towards to the +C direction. The fanned light resulting from one beam can Bragg diffract from the gratings formed by the beams in the other fan and can result in phase conjugation.

To understand the process of forming the Arch MPPCM consider the diagram shown in Fig. 6.11, which schematically shows the Arch MPPCM operating in a steady state. The two input beams have the same wavelength but are mutually incoherent. Therefore, each incident beam interferes with its own scattered light from some scattering centres inside the crystal and writes a set of fan gratings. A set of identical gratings, occurring in both fans, is reinforced by two-wave mixing (two-beam coupling). As a result, the fans couple and bend into each other, resembling an arch; hence, "arch" phase-conjugate mirror. The strong volume gratings shared by both beams are written throughout the crystal, but for convenience they are shown in Fig. 6.11 for regions ① and ② only. The insert in Fig. 6.11 shows the grating detail at location ①. The grating at ① is a transmission grating, written by input beam, I_{1p}, and fanned beam, I_{1fan}, and read by fanned beam I_{2fan}. From the theory of FWM (described in Chapter 2), the readout beam replays the phase conjugation of the incident beam I_{1p} i.e., I_{1pc}. Notice that the energy from beam I_{2p} is transferred to the phase-conjugate beam by reading the transmission grating with I_{2fan}. A similar picture applies for location ②, so in all two conjugate beams are produced at the same time i.e. I_{1pc} and I_{2pc} with magnitudes depending on I_{2p} and I_{1p}, respectively. In reality, regions ① & ② are a continuum of points and corresponding gratings throughout the crystal, which gradually bend the light between ① & ② and form the arch.

Fig. 6.11 *Schematic diagram of showing the physics and grating in the geometry of the Arch MPPCM. The inset shows the gratings at ①.*

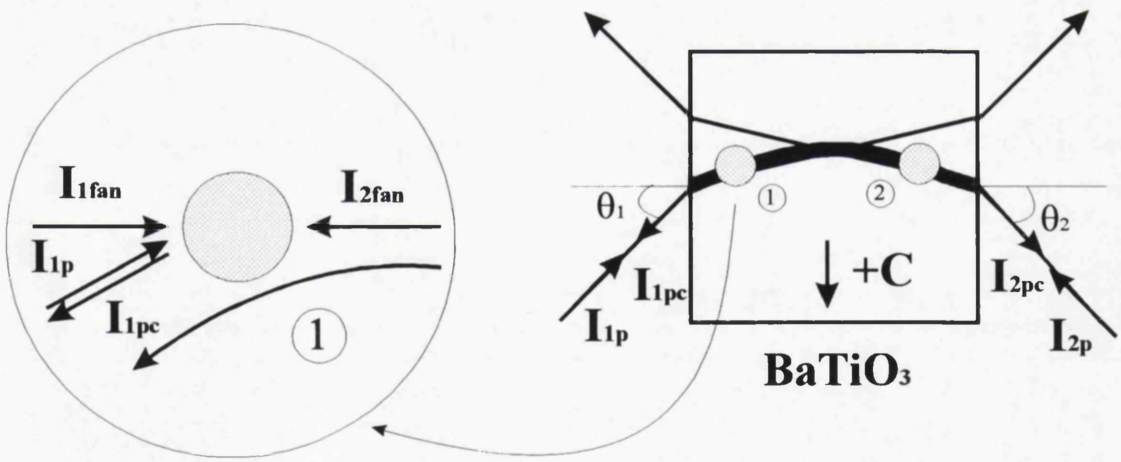

To summarise, in this section the Arch MPPCM is being proposed, a new geometry generating phase-conjugate waves from the interaction of mutually incoherent laser beams in shared photorefractive fan gratings. Our method is similar to that of other phase conjugators, differing only in the number of internal reflections off the crystal faces before phase conjugation (zero for the Bridge MPPCM, one for Bird-wing MPPCM, two for mutually incoherent beam coupling, and three for the Frog-legs MPPCM). These internal reflections, partly, dictate the orientation (and, hence, the efficiency) of the photorefractive fan gratings. The "arch" configuration results in a higher coupling efficiency of two mutually incoherent laser beams interacting inside a photorefractive crystal without internal reflections (avoiding Fresnel losses), but also provides phase locking of one laser to the other in this new configuration.

MPPCMs has been known for more than 10 years for coupling mutually incoherent laser sources, however, photorefractive scattering and conical diffraction as shown in Fig. 6.12 commonly occur in MPPCMs with exsiting configurations including the "arch" configuration in a photorefractive crystal.

Fig. 6.12 *Photographs showing experimental observation of scattering and anisotropic diffraction losses during the phase conjugation process of the Arch MPPCM after phase conjugation with two simultaneously incident beams. Where the arrow pointing is the anisotropic diffraction ring..*

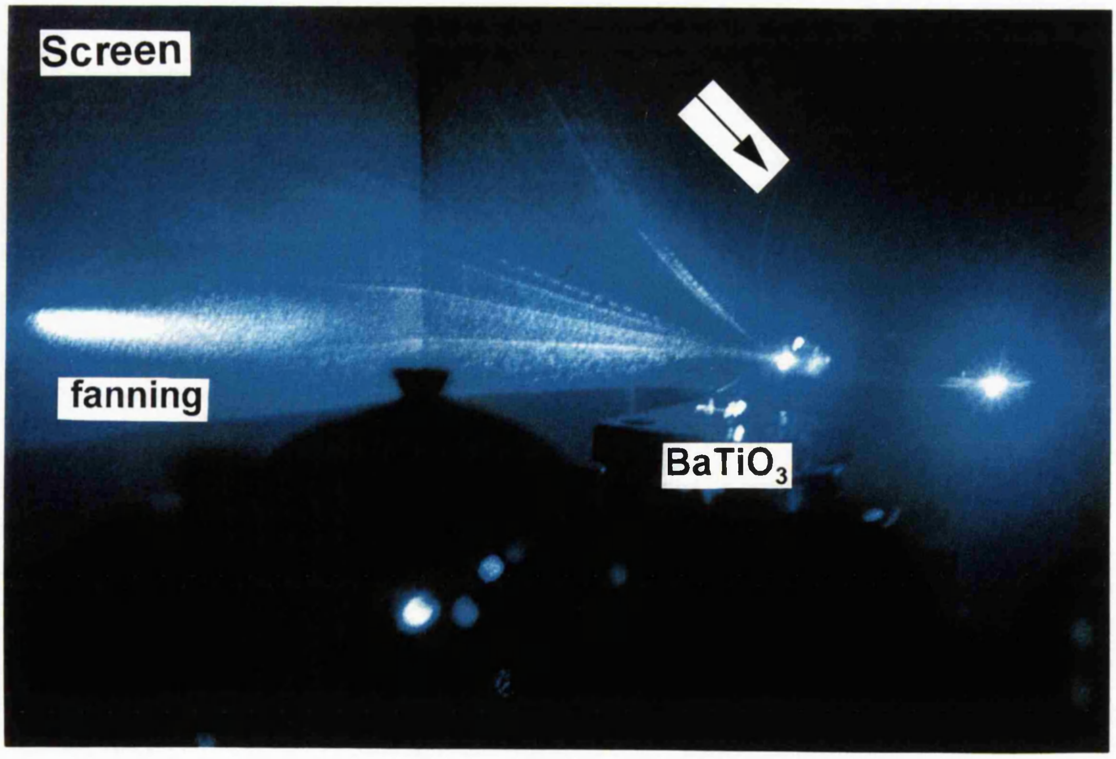

This scattering and anisotropic diffraction sometimes cause insufficiently stable output or low phase conjugation efficiencies. In the following sections we propose further novel configurations to optimise the peformance of MPPCMs.

6.5 "Fish-Head", "Fish", and "Manta Ray" MPPCM Configurations

In this section we propose three novel related configurations for mutually-pumped phase-conjugate mirror having two pump beams incident at the same face (labeled $+c$ (Fig. 6.2) with acute angle to the c-axis and travelling inside the crystal at an acute angle to the -C direction initially to avoid the losses caused from scattering and anisotropic diffraction. In these interacting beams can construct three distinguishable configurations in a $BaTiO_3$ crystal by choosing the geometry for the mutual phase conjugation process. In the following subsections we experimentally investigate and characterise these new configurations and discuss our results in detail and propose possible mechanisms to understand the observed behaviour.

6.5.1 Experimental arrangement and apparatus for Fish-Head, Fish, and Manta-Ray MPPCMs

Our experimental arrangement for examining the "fish-head", "fish", and "Manta Ray" MPPCMs configurations is shown in Fig. 6.13. It is similar to the arrangement we used to investigate the arch except that the incident face of the $BaTiO_3$ crystal onto which two incident beams are shone is the $+c$ face. Each pump beam was generated from an argon ion laser with multi-longitudinal modes operation at 488nm and 514.5nm without an intracavity étalon. The path length difference between the incident beams, I_{1p} and I_{2p}, was arranged to be greater (typically 15-45cm) than the coherence length (~3cm) of the laser, operating in this manner. This ensured that the beams were mutually incoherent so that competing gratings could not be written between counterpropagating light which would impede the formation of a loop of light. The interacting beams were extraordinarily polarised to provide the most effective utilisation of the linear electro-optic effect and to maximise the coupling strength inside the $BaTiO_3$ crystal and were focused, by lenses of 125 mm focal length, to foci located about 20 mm outside of the crystal so that each beam diverged into the crystal. This gave us large beam diameters to promote fanning and overlap of the beams within the crystal.

Fig. 6.13 *Experimental arrangement for fish-head, fish, and manta ray mutually pumped phase-conjugate mirrors.*

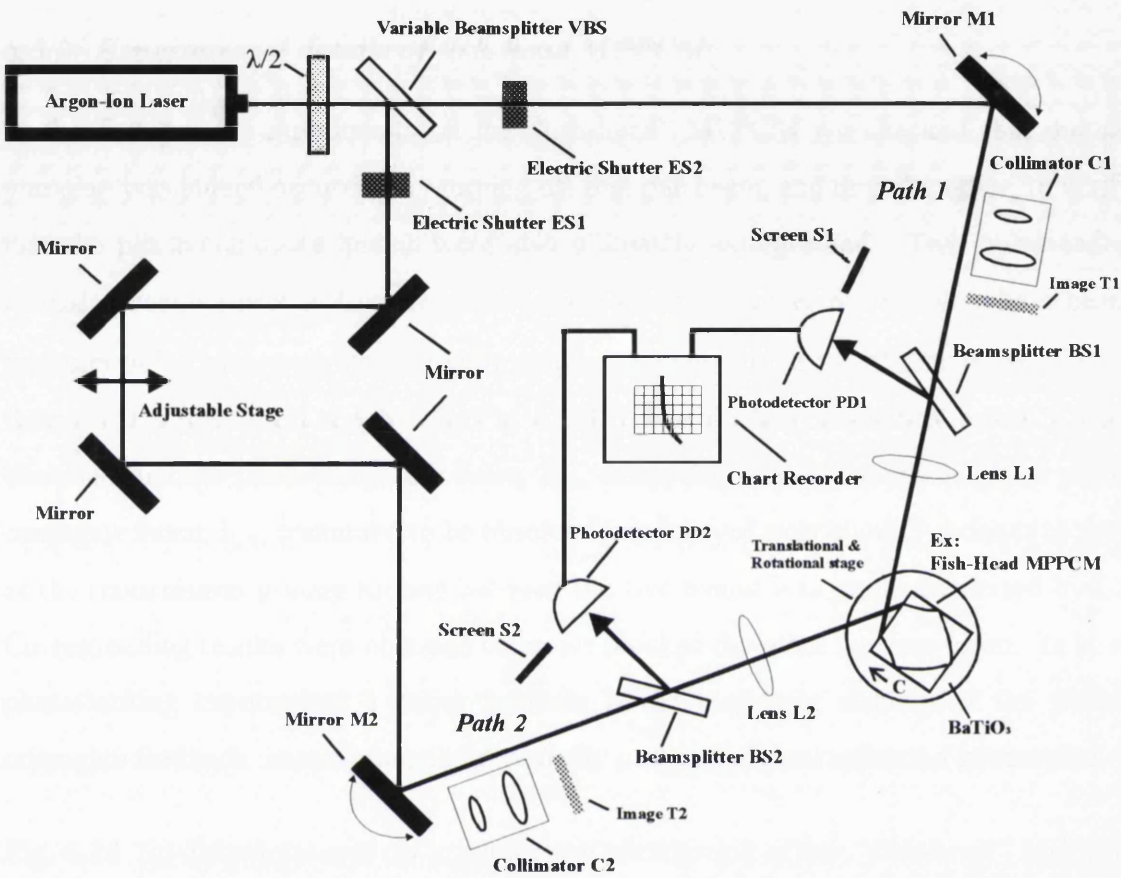

We repeated our experiments several times with similar results using two separate $BaTiO_3$ crystals from different suppliers: the Shanghai Institute of Ceramics at the Chinese Academy of Science and Sanders Associates in USA. The crystals were single domain and had dimensions 5.16mm x 5.00mm x 4.74mm and 5mm x 5mm x 5mm, respectively and each face was polished. The phase conjugate beams, I_{1pc} and I_{2pc}, were coupled out from the incident beam paths using beamsplitters, BS_1 & BS_2, and their powers were monitored by photodetectors, PD_1 & PD_2, (which were connected to an *x-t* chart recorder) as a function of time. Electric shutters, ES_1 & ES_2, were used to switch pump beams, I_{1p} & I_{2p}, on and off, respectively. The incident powers of both incident beams were adjusted using a variable beamsplitter. When the input images to be phase conjugated, T_1 and T_2, were inserted into paths 1 & 2, the photodetectors, PD_1 and PD_2, were replaced by two screens S_1 and S_2, or cameras (or CCDs) to capture the output images, respectively. Two collimators, C_1 and C_2, consisting of a spatial filter and collimation lenses, were introduced into the setup to input two images.

6.5.2 Experimental details of fish-head MPPCM

In the first several experiments on the "fish-head" MPPCM we checked that mutual pumping was indeed occurring by turning off first one beam, and then the other, to verify that the phase-conjugate beams were also ultimately extinguished. Two unexpanded Gaussian beams (directly from the laser), each having a power of 56 mW with a beam diameter of 0.3 mm, were incident in a symmetrical geometry: $z_1=z_2=1$ mm, $\theta_1=\theta_2=55^O$ to the normal of the crystal as defined in Fig. 6.14(a). We blocked the incident beam, I_{1p}, and observed that the phase-conjugate beam, I_{2pc}, disappeared immediately; the other phase conjugate beam, I_{1pc}, continued to be observed but decayed over about 5 seconds to zero as the transmission grating formed between the two beams was gradually erased by I_{2p}. Corresponding results were obtained when we blocked the other incident beam. In laser phase-locking experiments a major problem is the long-term stability of the phase-conjugate feedback in self-pumped or mutually pumped internal reflection geometries.

Fig. 6.14 *(a) Schematic and (b) experimental photograph of our "fish-head" MPPCM geometry.*

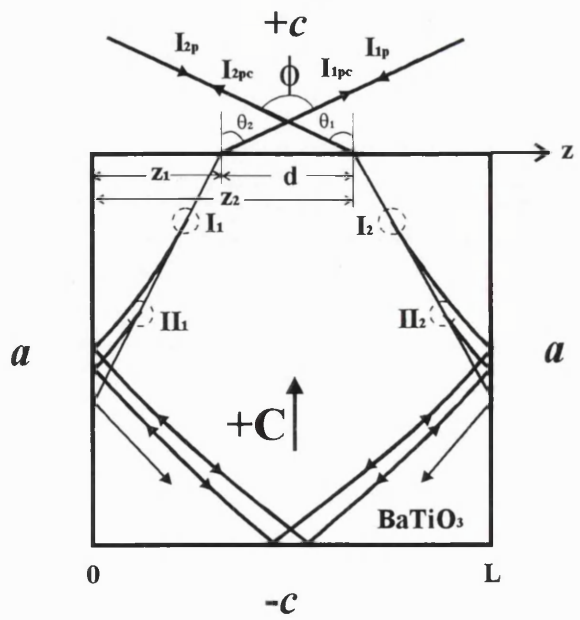

(a)

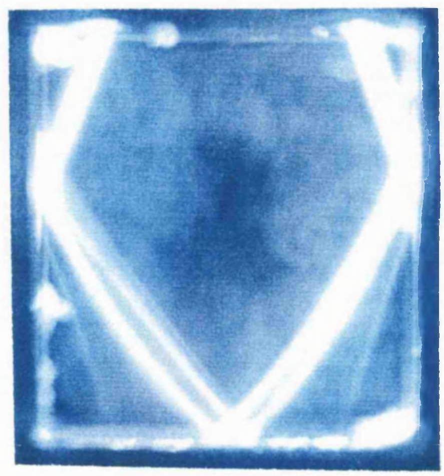

(b)

6.5.2.1 Time response of the fish-head MPPCM

Figure 6.15 shows how the phase conjugate reflectivity develops with time. The reflectivity rose in about 1s (after turning on the incident beams) to reach a final magnitude which was 30%, stable in time to ±5% standard deviation over 15mins.

Fig. 6.15 *Plot of the phase-conjugate reflectivity versus time for the "fish-head" configuration in MPPCM.*

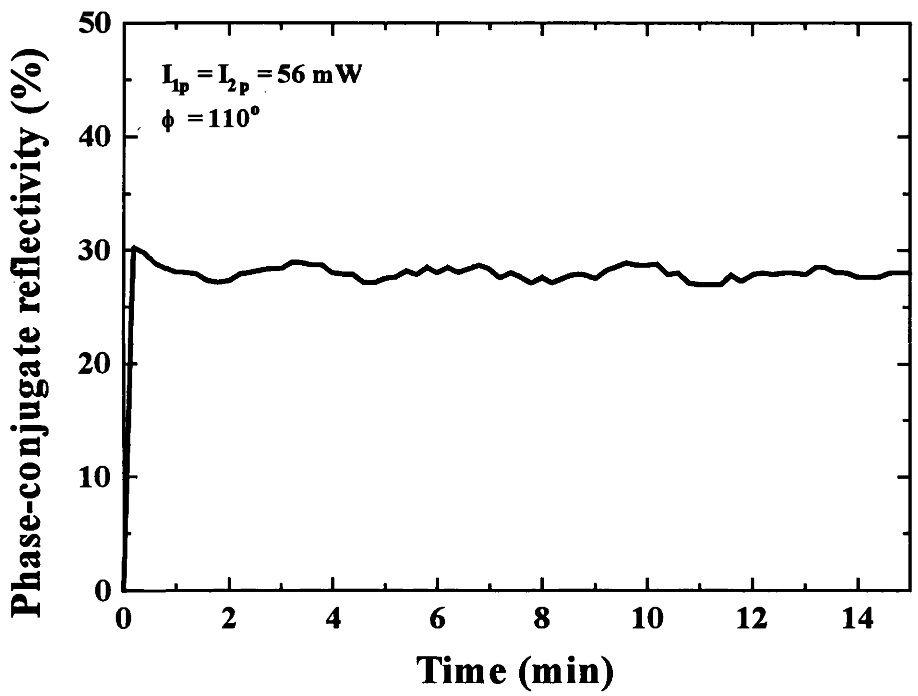

The time required for the onset of the phase-conjugate behaviour in the "fish-head" configuration was measured as a function of lateral distance between the two input beams as shown in Fig. 6.16. Before taking the final time response measurements, the crystal was flooded with 25 mW collimated and ordinary polarised He-Ne light (λ=632.8nm) from cryatal *a* face for about 10 mins to optically erase all residual gratings formed in previous time measurements. The lateral distances between the two input beams was in the range from 2 to 4 mm. We measured the time, τ, required for the phase-conjugate beam to grow to 1-e^{-1} of its final equilibrium value. The same apparatus as that shown in Fig. 6.13 which had been used to measure the phase-conjugate reflectivity was used to obtain the phase-conjugate formation times. The measurements were taken at an external interbeam angle of ϕ=110°, with two input beams operating with multiple logitudinal modes in the blue (λ=488nm) line of the argon laser under symmetrical incident conditions, i.e., z_1=L-z_2; $\theta_1=\theta_2$, and $I_{1p}=I_{2p}$. As can be seen from the results shown in Fig. 6.16, the fastest response time of ~1 sec appeared to occur when d=3mm. We observed that the more symmetrically disposed loop was more intense. The fastest response times were observed when two loops were present.

Fig. 6.16 *Plot of the response time, τ, against the lateral distance, d, between the two input beams.*

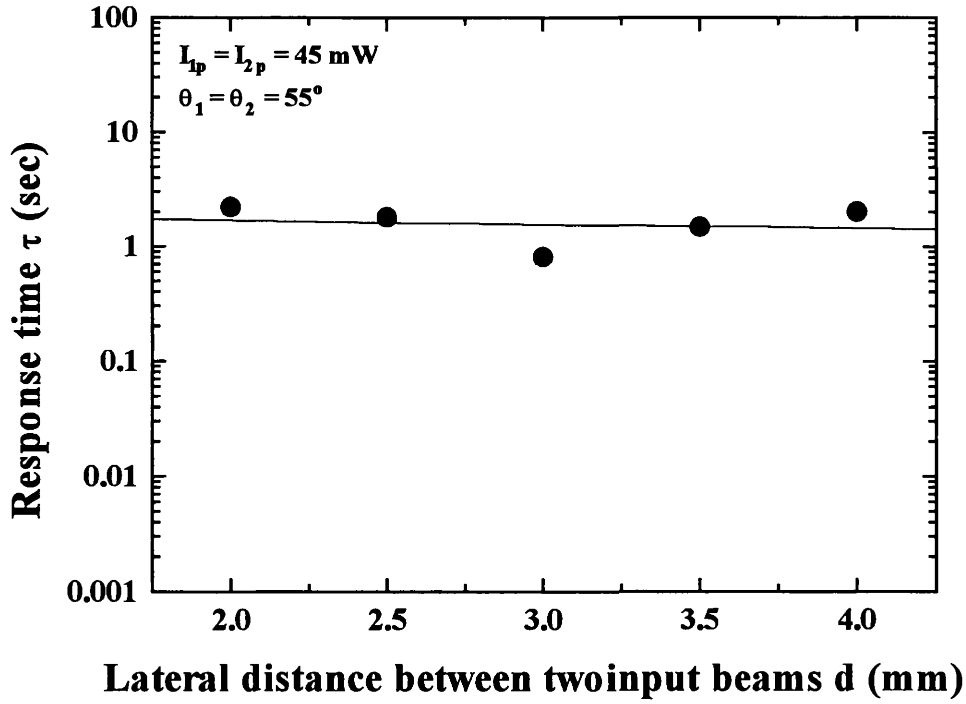

6.5.2.2 Lateral positional tolerance of the fish-head MPPCM

In order to investigate the tolerance of the phase conjugate reflectivity to lateral translations of the positions of each of the input beams we arranged them symmetrically, i.e., z_1=L-z_2, where L is the length of the crystal in the z direction. The power of each beam was 45mW and

(i) we varied the separation, d (=z_2-z_1), while keeping, ϕ, constant at 110° and

(ii) we varied ϕ with θ_1=θ_2 while keeping d constant at d=3.5mm (Fig. 6.14).

Fig 6.17 shows a plot of phase-conjugate reflectivity as a function of the lateral distance between the two beams, d. We observe that the phase-conjugate reflectivity exists at least over the range d=1.8 to 4.0mm attaining a peak value of 28% at d=3.5mm and varying by 40% across this range. At the edges of this range we observed a single loop of light (from d=1.8 to 2.5mm) while near the peak phase-conjugate reflectivities we observed two loops of light (from d=3.0 to 4.0mm). Figure 6.2(f) shows the two loops for d=3.5mm, ϕ=110° and we note that the more symmetrically disposed loop is more intense.

Fig. 6.17 *Plot of the phase-conjugate reflectivity in the Fish-Head MPPCM against the lateral distance, d, between the two incident beams in a symmetric arrangement (Fig. 6.14(a)).*

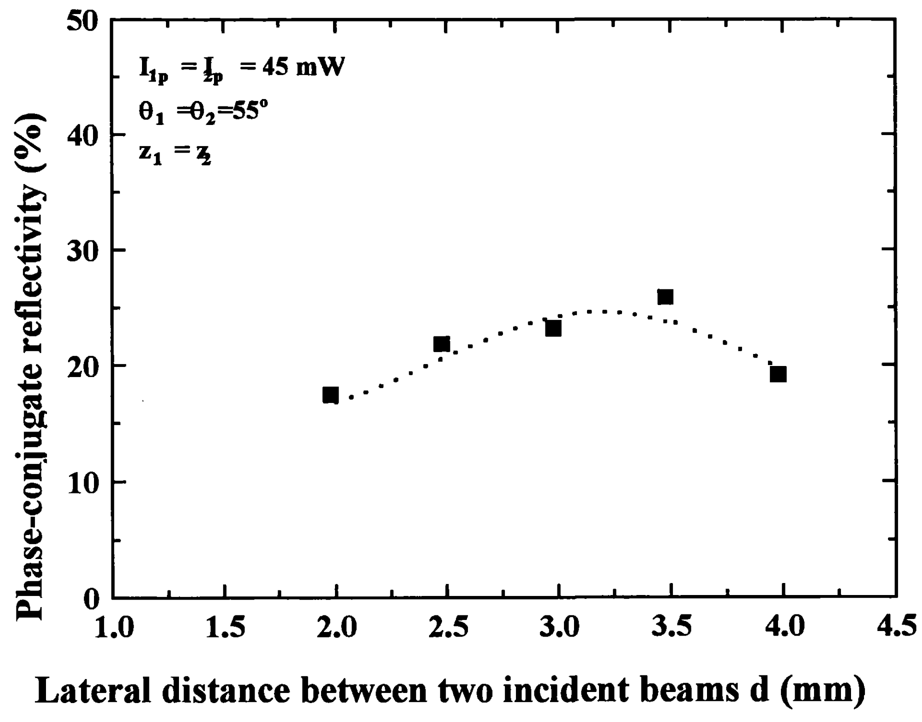

Fig. 6.18 shows the optical paths inside the $BaTiO_3$ crystal in the Fish-Head MPPCM for four different lateral separations of incident beams d=0.8, 1.6, 2.5, and 4.0 mm at ϕ=110°, repectively. Fig. 6.18 shows that the shape of of fish-head was changed giving 2 loops with a different reflection point on face *-c* in both (a) & (b) and 2 loops each reflecting at one point on face -c in both (c) and (d). This can be explained by the interaction-region transition mechanism (discussed in the next section) which gives stable loops with reasonable phase conjugation efficiency (shown in Fig. 6.15).

Fig. 6.18 *A series of photographs illustrating the optical path in the Fish-Head MPPCM in steady state, taken from above the BaTiO3 crystal at (a) d=4.0mm, (b) d=2.5mm, (c) d=1.6mm, and (d) d=0.8mm, respectively, where d is defined in Fig. 6.2(b).*

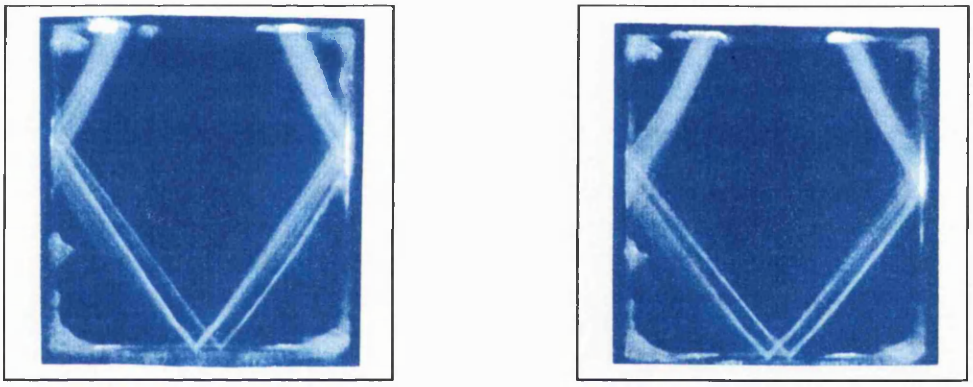

(a) **(b)**

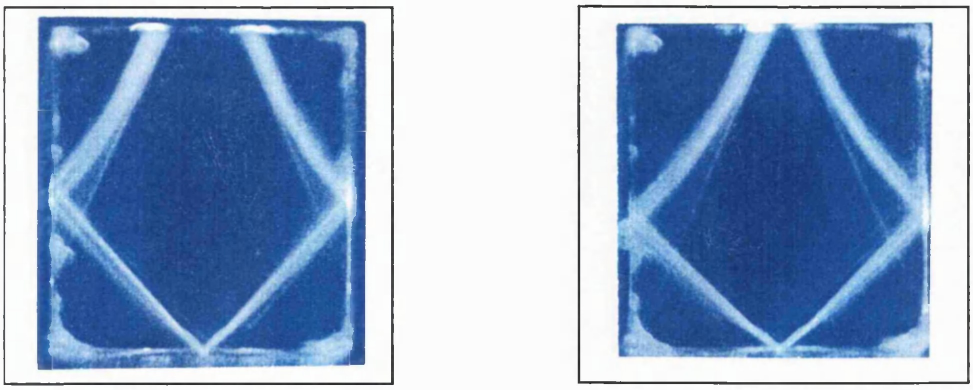

(c) **(d)**

A further set of experiments was performed to investigate the tolerance of the Fish-head MPPCM to lateral positional changes of just one of the incident beams. To assess the tolerance of the Fish-Head MPPCM to unequal shifts in the lateral positions of each input beam the input beams were rearranged asymmetrcally, i.e. $z_1 \neq L$-z_2. The incident position of input beam I_{2p}, at z_2, was held constant while varing the position of input beam, I_{1p} along the z direction from z_1=0.5mm to 4mm while z_2 was kept at 4.5 mm (Fig.6.14).

Fig. 6.19 shows a plot of the phase-conjugate reflectivity as a function of the lateral position of input beam, I_{1p}, at z_1. It can be seen that phase conjugation occured over the full range from z_1=0.5 to 3.8 mm and the highest phase-conjugate reflectivity of 25% was obtained when z_1= 1mm. The optical paths were changed as shown in Fig. 6.20 while phase conjugation was occurring between the two input beams in the fish-head configuration to simulate misaligment during operation; for example, due to slow vibration.

Fig. 6.19 *Plot of the phase-conjugate reflectivity against the lateral position of only one input beam, I_{2p} while the position of the other beam, I_{1p} was kept constant.*

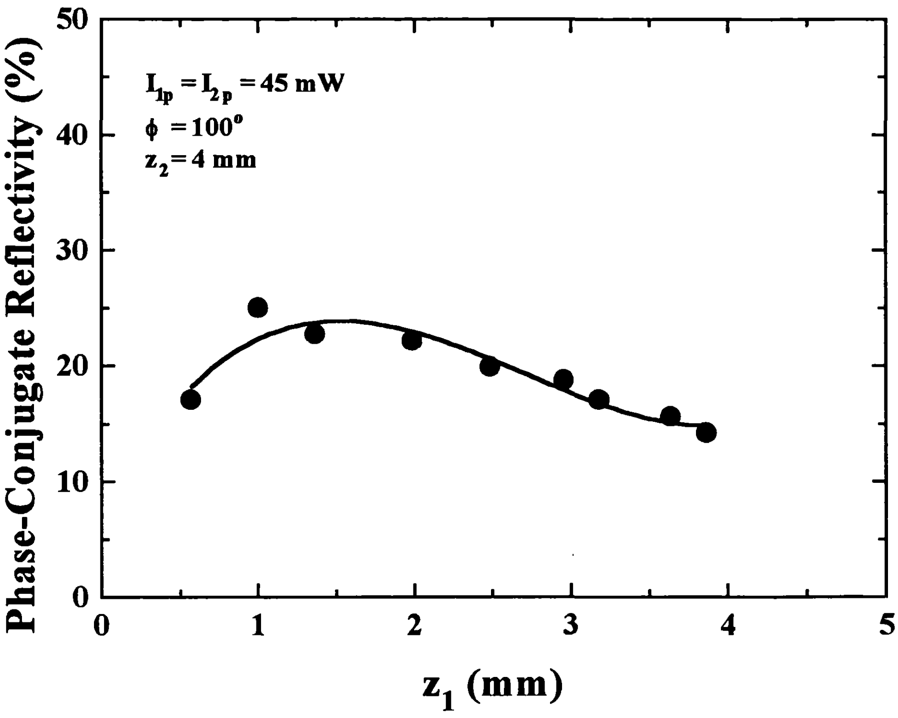

Fig. 6.20 *A series of photographs corresponding to Fig. 6.19 illustrating the optical path of the Fish-Head MPPCM in steady state, taken from above the BaTiO3 crystal, where d is definded in Fig. 6.2(b).*

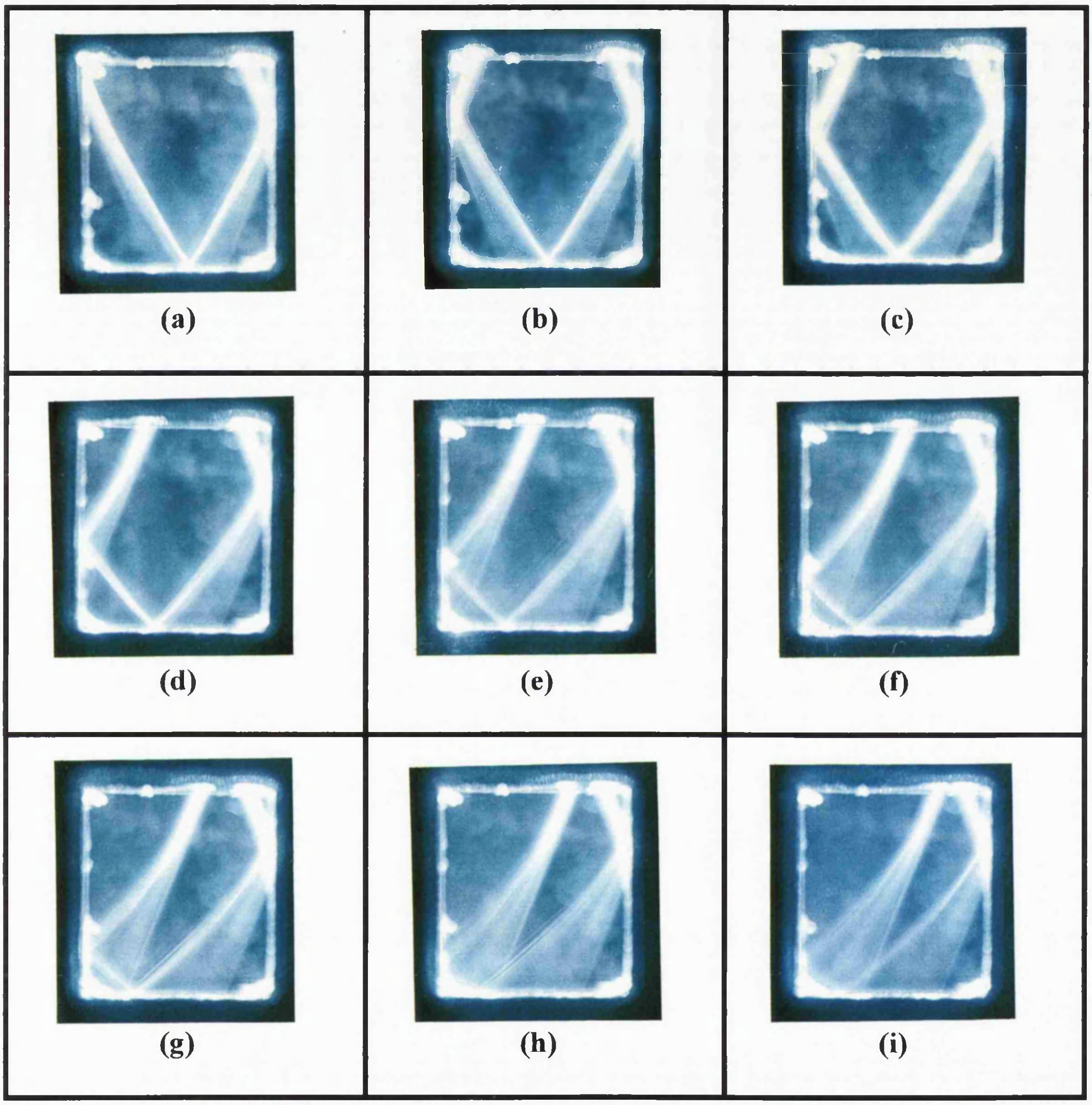

6.5.2.3 Angular tolerance of fish-head MPPCM

In order to investigate the tolerance of the phase-conjugate reflectivity to angles we varied the angle, ϕ, symmetrically while keeping $\theta_1=\theta_2$; $z_1=L-z_2$ and, d was held constant at d=3.5mm (defined in Fig. 6.14). Figure 6.21 shows how the phase-conjugate reflectivity varies as a function of the external angle between the two incident beams, ϕ. The phase-conjugate behaviour was found to exist over an angular range of $\phi=70^\circ$ to 110° reaching a maximum value of 28% at ϕ=100° and varying by 55% of 28% reflectivity across this range. The fanning of the input beams in the $BaTiO_3$ crystal not only depends on the power of the input beam but also on the angle between the incident beam and the crystal c axis and the initial divergence. The power of each input was kept constant and the incident angle of each beam was changed, it was found that the larger incident angle to the normal of +*c* surface, the greater the angular range of beamlets within the fan generated. So that as observed in figure 6.18 the optical paths were changed becoming significantly curved.

Fig. 6.21 *Plot of the phase conjugate reflectivity against the external angle ϕ between the two incident beams in a symmetric geometry.*

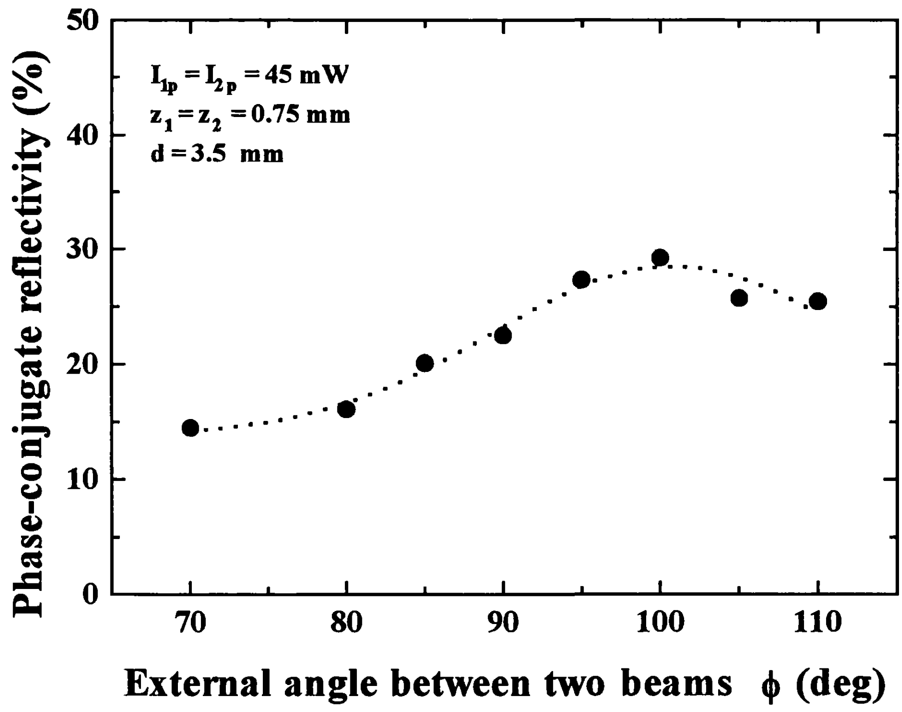

6.5.2.4 Influence of incident beam diameter of fish-head MPPCM

We experimentally investigate how the incident beam diameter influenced the phase conjugation efficiency in the Fish-Head MPPCM in the use of the diverging incident beam. The schematic of the experimental arrangement is shown in figure 6.22 where the inset picture shows the relationship between the foci of lenses and the incident position of the incident beams, I_1 & I_2.

Fig. 6.22 *Schematic showing the variation of the distance between the focus of the input lens and the entrance location of the input beam on the crystal.*

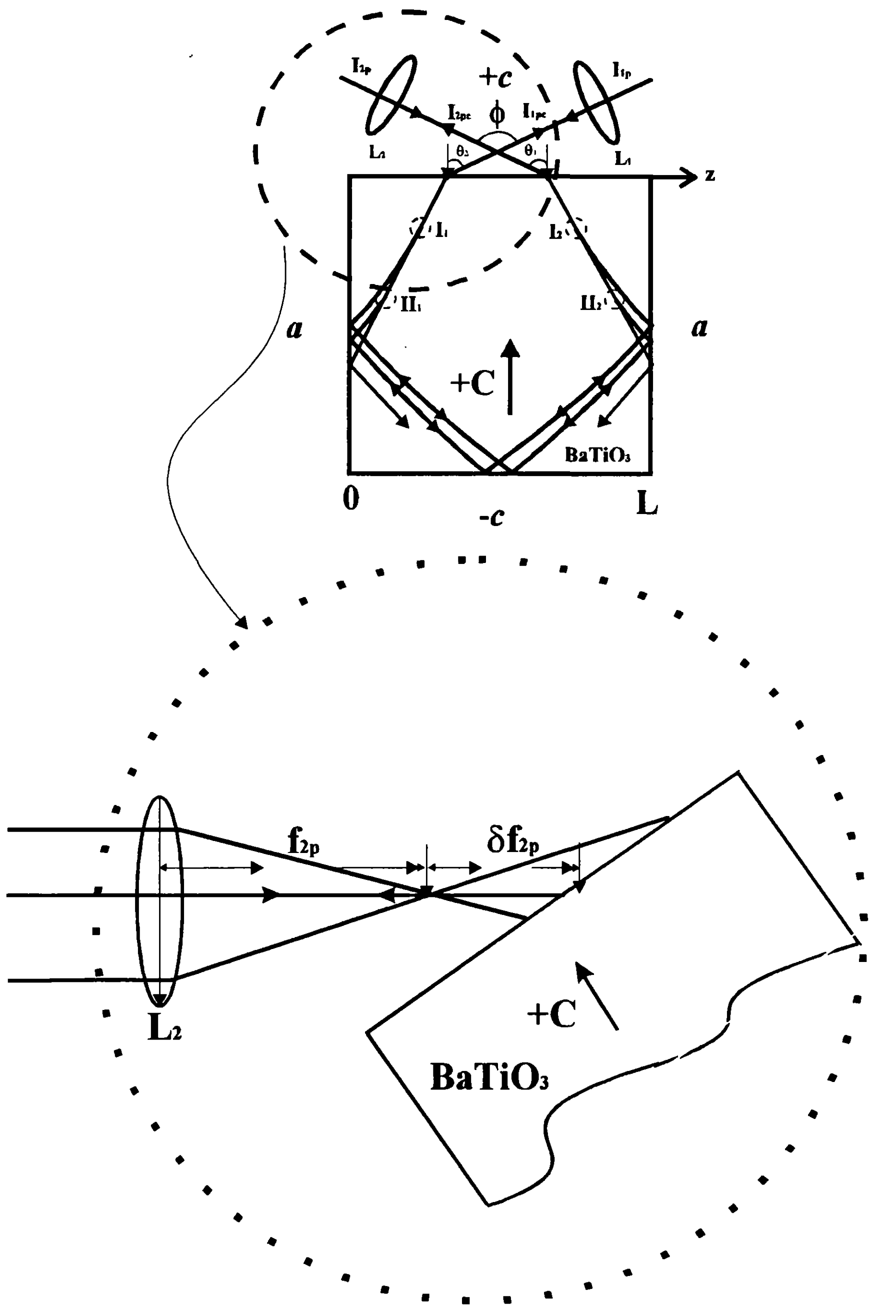

The two input beams were focused, by lenses L_1 & L_2 of 125 mm focal length, to foci located between 15 to 60 mm outside of the crystal depending on the position of each of the two focusing lenses. This gave us large beam diameters between 0.26mm to 0.89mm. We anticipated that this would increase to promote fanning and overlap of the beams within the crystal leading to greater coupling.

We measured the phase-conjugate reflectivities as a function of the distances between the foci and the entrance face, +*c*, by changing the position of the two input lenses, L_1 & L_2, together forwards and backwards along the incident direction whilst keeping the lateral distance between them constant, at d=3mm. We observed that the phase conjugate behaviour exists, at least, over a range of δf ($=\delta f_{1p}=\delta f_{2p}$) as shown (Fig. 6.22) from 15mm to 60mm with a maximum value of ~ 32% at $\delta f=\delta f_{1p}=\delta f_{2p}=45$ mm as shown in Fig. 6.23. Outside this range, when the input beams were either focused closed to or far away from the incident face, the phase-conjugate power dropped significantly since there was either not enough overlap for beam coupling within the crystal for a narrow beam with a small diameter or parts of the input light divering cone light l leaks around the crystal edges for wide beam with large diameter (Fig. 6.24) and so does not enter the crystal.

Fig. 6.23 *Plot of the phase-conjugate reflectivity against the distance, $\delta f=\delta f_{1p}=\delta f_{2p}$ (defined in figure 7.22), between the foci of input lenses and the crystal.*

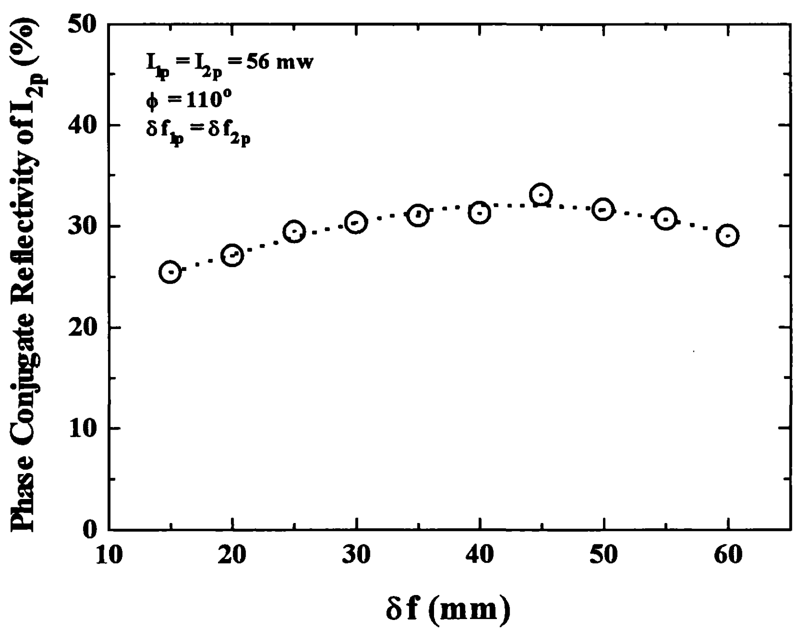

Fig. 6.24 *A series of photographs corresponding to Fig. 6.23 illustrating the optical path of the Fish-Head MPPCM in steady state, taken from above the $BaTiO_3$ crystal, where δf_{1p} and δf_{2p} are definded in Fig. 6.23.*

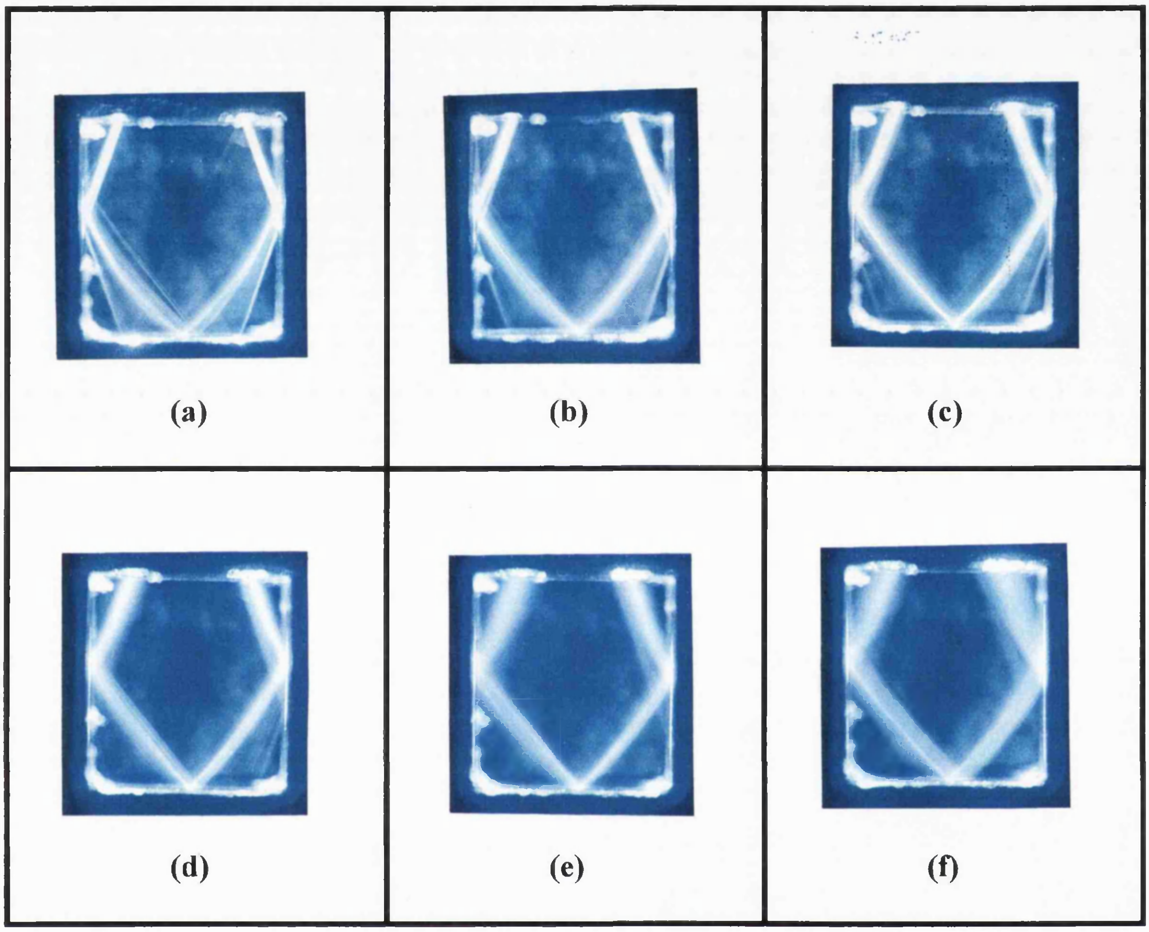

(a) (b) (c)

(d) (e) (f)

6.5.2.5 Fish-head MPPCM efficiency dependence on beam ratio

The phase-conjugate power as a function of input beam power ratio is also given. One attenuator (not shown in Fig. 6.13) consisted of a half-wave plate and one polariser was insert into path 1 (or 2) to vary the incident power without changing the polarisation of light. The variation of phase-conjugate reflectivity of each beam in the Fish-Head MPPCM as a function of two input beam power ratio is shown in Fig. 6.25. The data is not corrected and so includes both Fresnel and absorption losses. It can be seen that engery is transfered from one beam to the other during the phase conjugation process and the phase- conjugate reflectivity can reach ~50% "fish-head" MPPCM.

Fig. 6.25 *Graph of the experimental "fish-head" MPPCM phase conjugate output powers as a function of the input beam power ratio.*

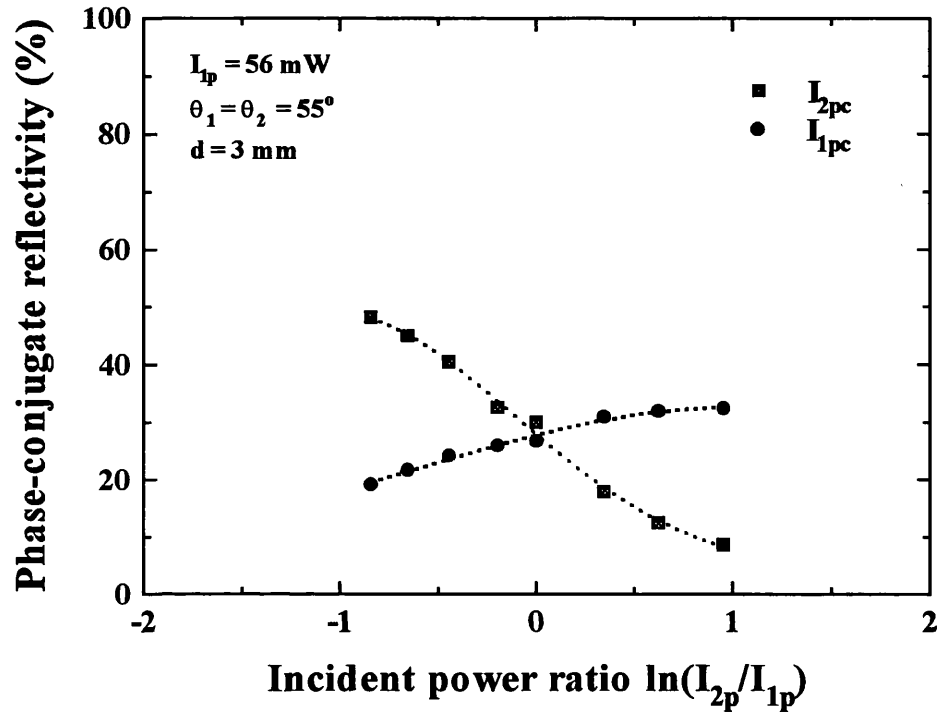

6.5.2.6 Fidelity and Resolution of fish-head MPPCM

We checked the fidelity of the mutual phase conjugation process in the Fish-Head MPPCM by placing two resolution targets (US Airforce resolution chart), one in each of the input path after spatially filtering, expanding and collimating the beams. One target was rotated by 90° with respect to the other to investigate crosstalk. The phase-conjugate images, displayed on screens S_1 and S_2 (shown in Fig. 6.13), are reproduced in Fig. 6.26 and it is clear that there is no crosstalk and that a resolution of 4.00 line pairs/mm (125 μm) has been obtained for each of the beams

Fig. 6.26 *Photographs of the phase-conjugate images from the "fish-head" MPPCM: for (a) pump beam I_{1p}, and (b) pump beam I_{2p}.*

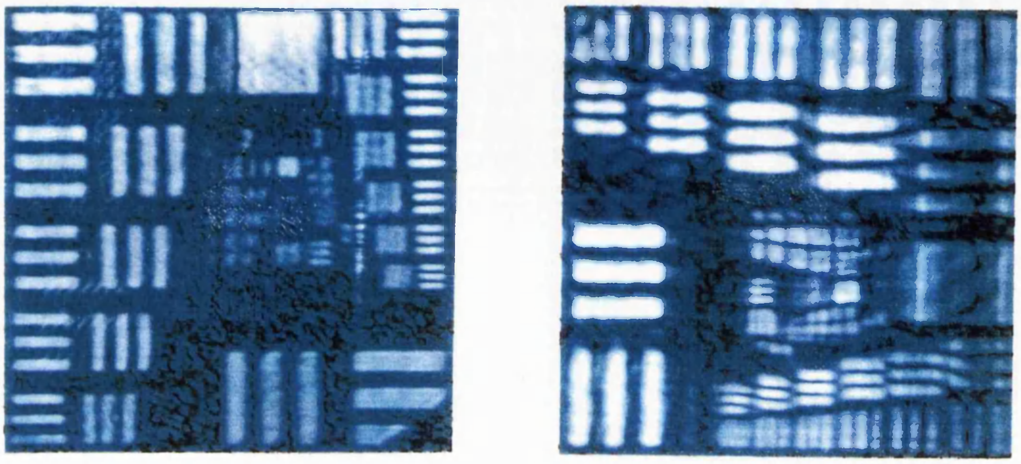

(a) **(b)**

6.5.3 Experimental Details and Results of Fish MPPCM

In previous this subsection we have demonstrated our second new configuration, the fish-head, MPPCM. In a series of in-depth studies we have shown that by optimally the choosing of geometry the performance can be improved considerably. This motivated us to make further changes to the geometry to further attempt to improve the performance. In this section we describe the experimental details of our third configuration, the fish, MPPCM formed in $BaTiO_3$ crystal.

Two mutually incoherent input beams each with a power of 25 mW derided from an Ar+ laser source with ~ 5 cm coherence length and operating with multilongitudinal modes at 514.5 nm without intracavity étalon, were incident on the crystal (Fig. 6.27). The beams were set to interact inside the crystal with an intersection of angle, ψ, before any internal reflections. Each beam will read one of the fan gratings formed by the other beam and so will be diffracted towards the inner face, *a*, of the crystal to generate a MPPCM with three internal reflections. In this phase conjugation process at least two stable loops were found within the MPPCM. The loops form paths which looks like the outline of a fish so that we refere to it as the "Fish" MPPCM for ease of reference.

Fig. 6.27 *(a) Schematics and (b) experimental photograph of "Fish" MPPCM*

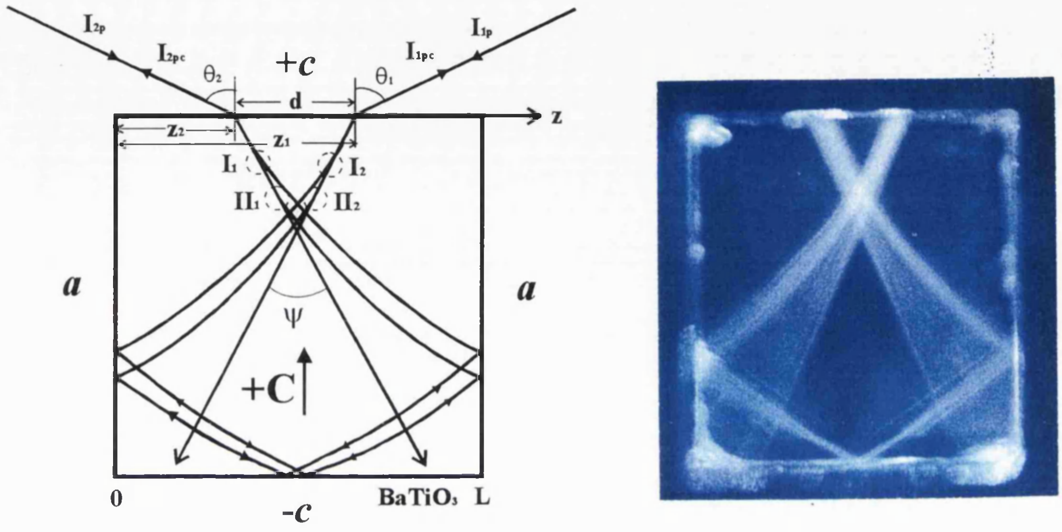

(a) (b)

We varied the incident position by shifting the crystal along the -c direction or z direction. Fig. 6.29 shows the investigation of the effect lateral position on the performance of the Fish MPPCM and on the internal loop light paths. In Figs. 6.28 (a)-(c) the phase-conjugate reflectivities obtained from the Fish MPPCM over a very wide range of d from 0.9mm to 2.5mm are 23.5%, 22.8%, and 17.0%, respectively. Figs (d)-(f) show the other three asymmetrial cases by translating the crystal along the z axis. In can be seen that when the two input beams are incident asymmetrically the shape formed in the MPPCM is modified significantly with a much reduced ~ 15% phase-conjugate reflectivity in both Figs 28(d) & (f). We note that not all of the light in the crystal is Bragg diffracted and internal reflected from crystal's faces to contribute to effective coupling resulting in a lower phase conjugation efficiency for these laterally shifted configurations. From these results we find that the Fish MPPCM prevails over a wide range of lateral shifts of the incident beams relative to the crystal.

Fig. 6.28 *A set of photographs illustrating the internal light path loops in the Fish MPPCM, taken from above the BaTiO3 crystal with two simultaneously incident beams at $\theta_1=\theta_2=57^o$ for (a) d=0.9mm , (b) d=1.3mm , and (c) d=2.5mm. (d)-(f) show three cases when the crystal was shifted along z direction at d=0.9mm, respectively.*

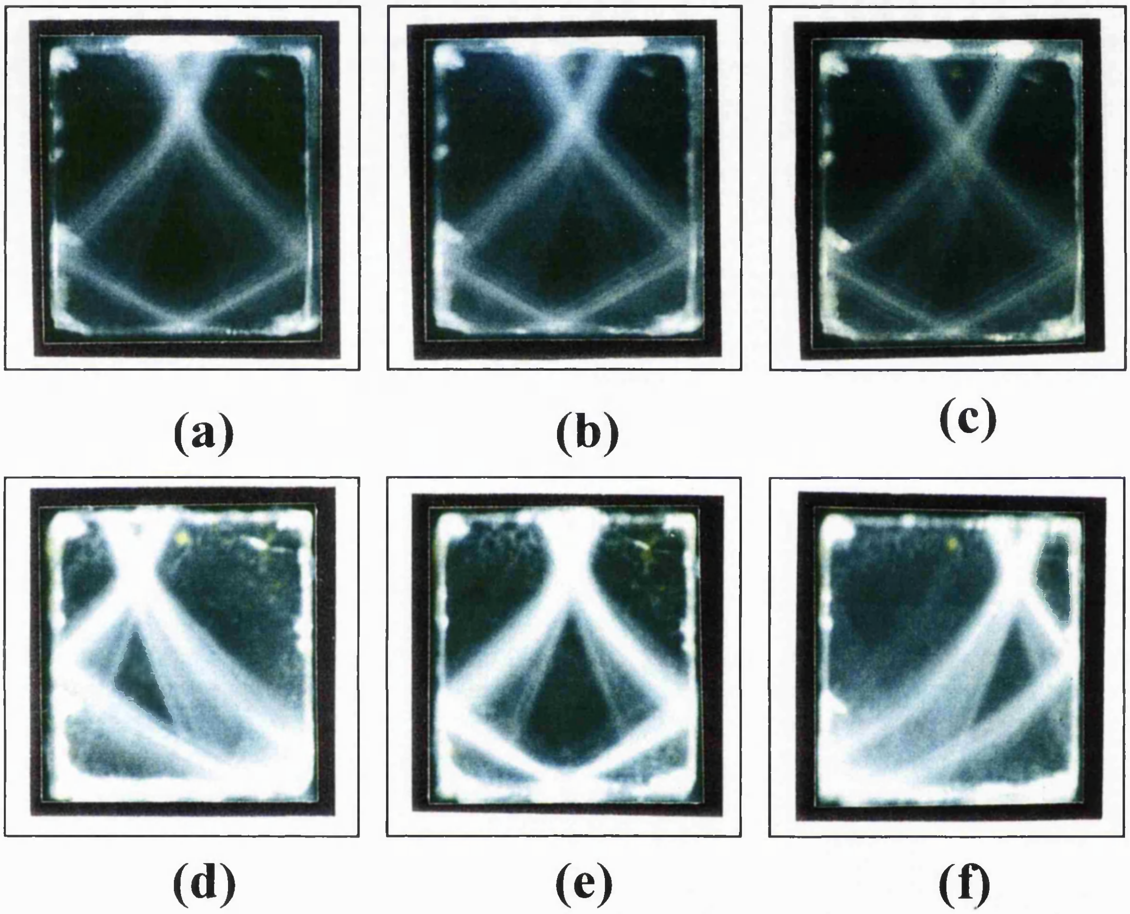

6.5.4 Experimental details and results of Ray MPPCM

In this subsection, we propose our fourth configuration, the ray MPPCM. Figs. 6.29 (a) and (b) show a photograph and the schematic of the internal beams inside the crystal , respectively. In Fig 6.29(a) it can be seen that incident beams I_{1p} and I_{2p} have formed a closed loop inside the crystal. Fig 6.30 shows a graph of the phase-conjugate reflectivity of input beam I_{2p} as a function of the lateral positon of the intersection point, z. Both beams are incident at the same point on the crystal $+c$ face at equal angles to the normal. Similarly both phase conjugate beams are incident at the same point intendly on the crystal $+c$ face at equal angles to the normal.

Fig. 6.29 *(a) Schematics and (b) experimental photograph of "Ray" MPPCM.*

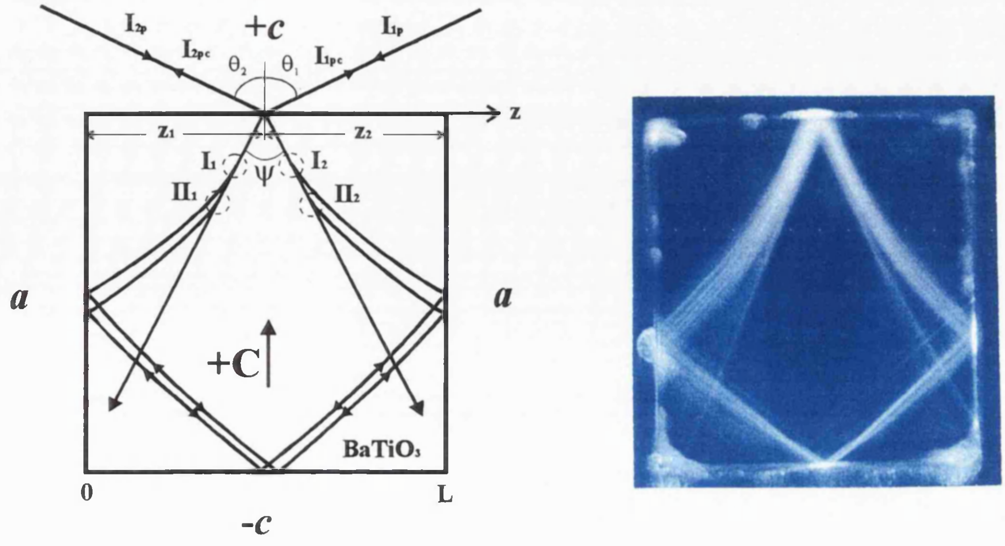

(a) (b)

Fig. 6.30 *Plot of the phase-conjugate reflectivity against the lateral position of the interaction loaction on crystal's +c face.*

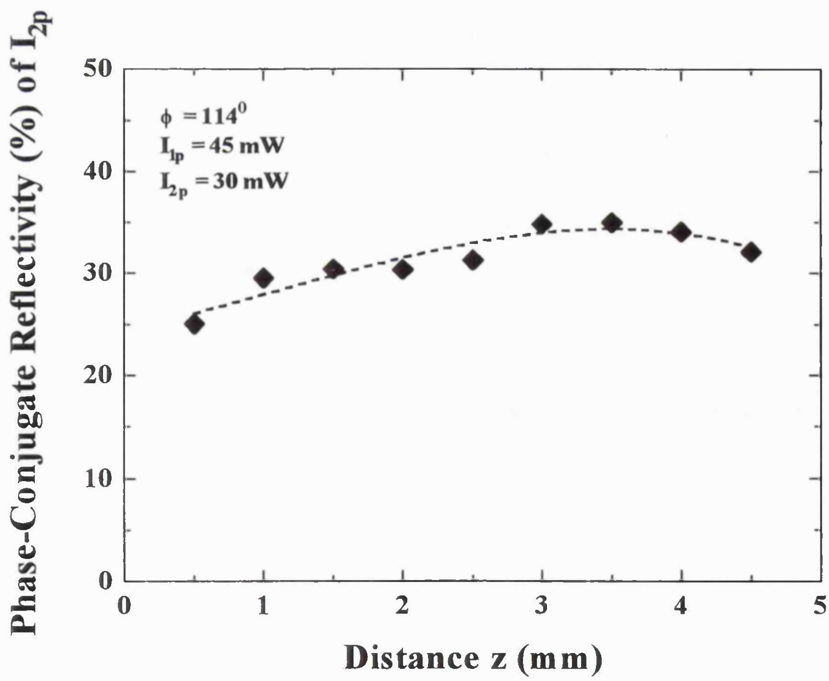

The measurement was carried out by sending two mutually incoherent input beams (=514.5 nm), I_{1p} and I_{2p}, each with a beam diameter of 0.48 mm having a power of 45 mW and 30 mW, respectively. The two input beams met on the +*c* face before interacting inside the crystal. We observed that the phase-conjugate response exists over an extremely wide range of lateral crystal translations from d=0.5 to 4.5 mm attaining a peak value of 35% at d=3.5mm and varying by 28% across this range.

In additons, the MPPCM "ray" configuration also has a wide range of angular acceptance. The experiment was performed out by rotating the crystal through an angle ω about the x-axis. The two mutually incoherent input beams each having a power of 28 mW with a beam diameter of 0.48mm were shone into the crystal simulaneously. We observed that the phase-conjugate reflectivity exists over an extremely wide range from ω=-15° to +15° (36° total) attaining a peak value of 37% at ω=0 (Fig.6.31) since the more symmetrically disposed loops were more intense as shown in Fig. 6.32. It can be seen that the MPPCM in the "ray" configuration very tolerant of lateral positioning and angular orientation. The phase-conjugate outputs for the Ray MPPCM is as great as 37% which is only a little over than the Fish or Fish-head MPPCMs. However, it plays an important role in stablising the phase-conjugate output.

Fig. 6.31 *The plot of phase-conjugate reflectivity against the rotation angle, ω, (defined is text) of a $BaTiO_3$ crystal in "ray" configuration*

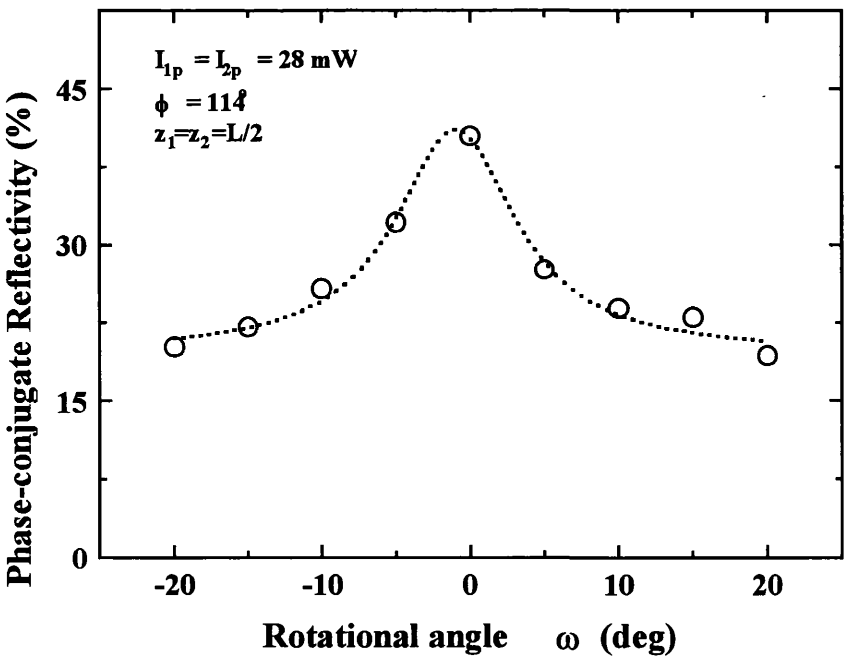

Fig. 6.31 *A set of photographs illustrating the steady state phase conjugation process of the Ring MPPCM while the two beams are simultaneously incident on the crystal at $\phi = 114^o$ (or $\theta_1=\theta_2=57^o$) without lateral crystal translation d=0. (a) show the schematic of ring configuration, (b)-(l) show the light paths inside crystal for rotations through different angles ω^o; -15^o, -12^o, -9^o, -6^o, -3^o, 0^o, 3^o, 6^o, 9^o, 12^o, and 15^o, respectively.*

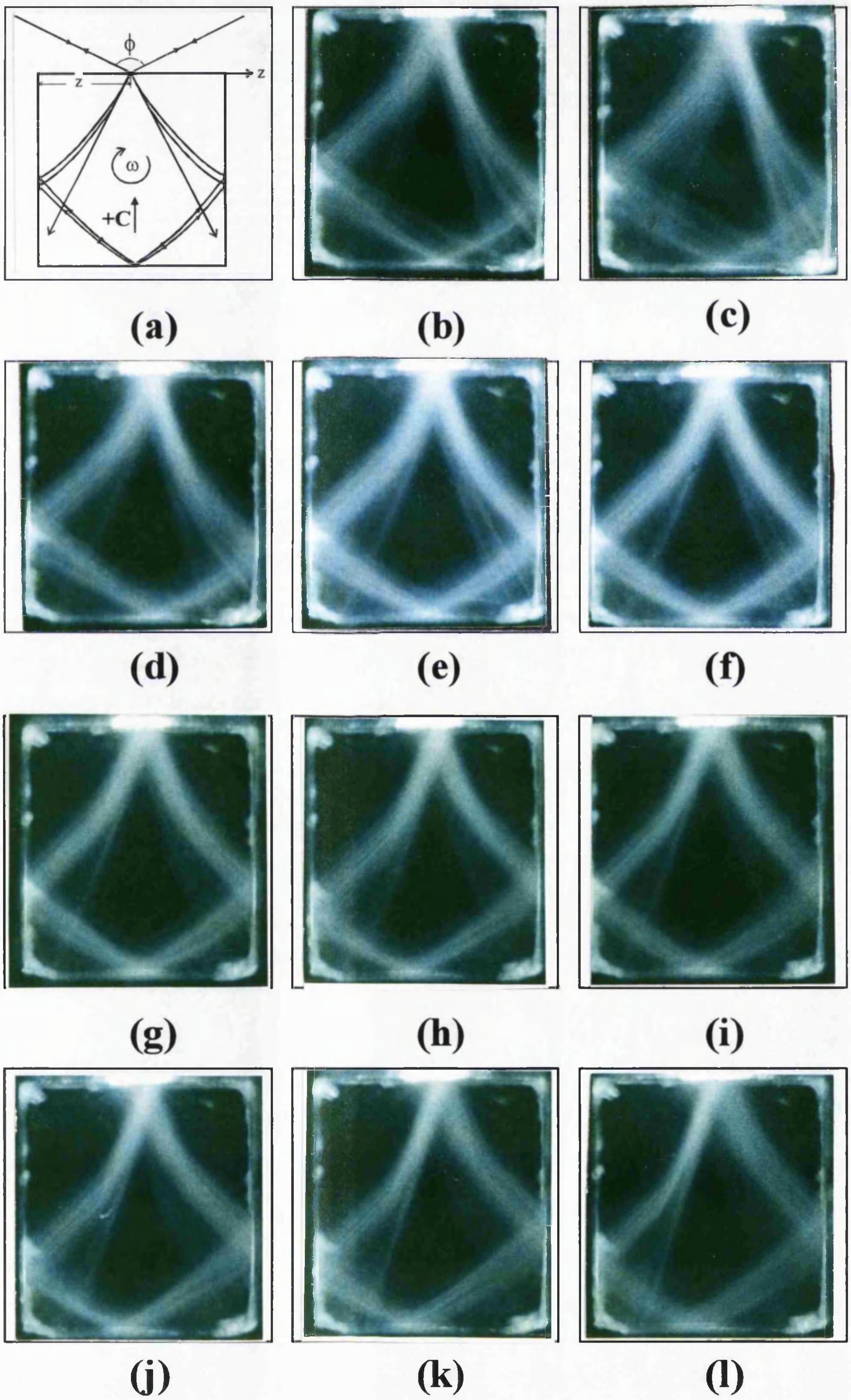

When the ray light channels within the crystal are not clearly apparant, the phase-conjugate outputs decrease notably, and image fidelity is reduced. We checked the fidelity of the mutual phase conjugation process in the Ring MPPCM by placing one resolution target in path 1 (input 1), and one in each of the inputs after spatially filtering, expanding and collimating the beams. One target was doll image transparency inserted into path 2 (input 2) to investigate crosstalk. Two input beams, I_{1p} & I_{2p}, carrying images were incident on the middle of the *+c* face, i.e., $z=z_1=z_2=2.5$mm at $\phi=114°$. The phase-conjugate images, displayed on screens S_1 and S_2 or captured by CCD cameras (shown in Fig. 6.13), are reproduced in Fig. 6.32 and it is clear that there is no crosstalk.

Fig. 6.32 *Photographs of the phase-conjugate images by the "ring" MPPCM: for (a) pump beam I_{1p}, and (b) pump beam I_{2p}.*

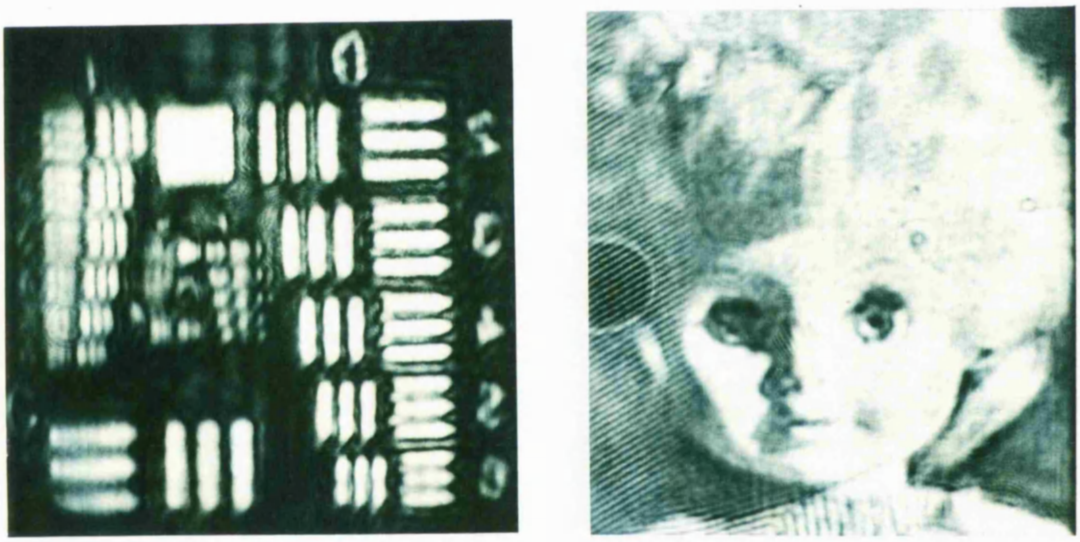

(a) (b)

In this section we have explained and demonstrated our discovery of a series of novel configurations for MPPCM and briefly reported their performance. In the next section we concentrate on the theoretical understanding underlying and unifying our discoveries.

6.6 Physical Understanding of Fish-Head, Fish, and Ray MPPCMs

The mutually pumped phase-conjugation process was explained in terms of several theories, such as the one-interactive-region four-wave-mixing self-oscillation theory [Cro84], the two coupled-region self-oscillation theory [He88], and the hologram sharing theory [Yeh89]. If a mutually pumped phase conjugate configuration has only one interaction region (such as in the double phase-conjugate mirror), the orientation and the spacing of its self-generated grating are fixed by the direction of the two incident beams. However, when a phase conjugator use a more than one interaction region, it gains a larger degree of freedom to choose both the orientation and the spacing of its self-generated gratings. In general, the phase conjugator will setup loops which maximise the two-beam-coupling gain coefficient and the beam-overlap length in each interaction region (increasing the net two-coupling gain) while minimising the optical-path distance between adjacent interaction regions (decreasing the absorptive loss). If necessary, the phase conjugator can also use total internal reflection at its crystal faces to connect adjacent interaction regions and thereby minimise reflection losses.

Actually, several types of grating can be established in MPPCMs depending on the geometry between the mixing waves and the orientation of crystal [Ste95] and the degree of mutual coherence between mixing waves in crystal [He95]. Any combination of interacting geometry and coherence and intensity of two input beams will affect the peformance of MPPCM. According to the widely accepted theory of the photorefractive effect, in each interaction region there are four contributions to the intensity-induced index gratings in the standard FWM geometry: a large-spaced transmission grating, a small-spaced reflection (2k) grating, and two additional contributions, usually overlooked, coming from the mixing of the pump beams and of the probe beam and its conjugate beam. When the pump beams are much stronger than the probe beam and the conjugate, the last contribution can safely be ignored. Then the pump beams are not depleted by the probe or the conjugate beam, and hence their evolution can be solved independently. But in certain cases such as our fish-head, fish, ray configurations in MPPCM there are more than one interaction region in the photorefractive medium so the last grating strength could be reinforced

In fact, the degree of coherence between the incident beams determines how many kinds of grating can be formed within the photorefractive crystal which possibly affect the performance of the MPPCMs. Here, we describe the general formation of all possible gratings, such as transmission, reflection, and *2k* gratings, in the photorefractive medium and discuss how to determine dominating or set the grating existing in the crystal by choosing the geometries of the pump beams with respect to the crystal. Model can be by refer the basic equation set proposed by Yeh et al. [Yeh95].

It is well known that the transmission gratings are responsible for the mutually pumped phase conjugation process in most of the configurations. For simplicity, we consider the case of one interaction region in the mutually pumped phase-conjugation process as shown in Fig. 6.33. We assume the diffusion-dominated photorefractive effect, i.e., with real coupling constants.

Fig. 6.33 *Schematic of geometry of MPPCM with -C direction propagation aspect in a $BaTiO_3$ crystal.*

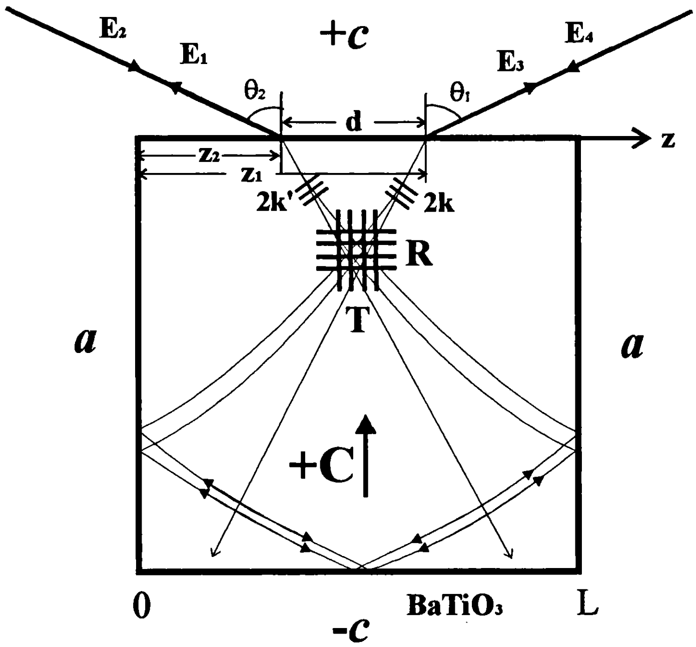

Referring to Fig. 6.33, we consider two plane waves of amplitude of E_1 and E_2 with a degree of mutual coherence of ν $(0 \le \nu \le 1)$ incident on a photorefractive crystal. When the pump beams are partially coherent, besides the transmission grating $g_T = E_1E_4^* + E_2^*E_3$, reflection grating $g_R = E_1E_3^* + E_2^*E_4$, $2k$ grating $g_{2k} = E_1E_2^*$, and

$g_{2k'} = E_3 E_4^*$ are all present in the photorefractive medium. The nonlinear coupled wave equations are written as:

$$\begin{aligned}
\frac{\partial E_1}{\partial z} &= \frac{1}{I_0}\left[\gamma_T g_T E_4 + \nu\left(\gamma_R g_R E_3 + \gamma_{2k} g_{2k} E_2\right)\right], \\
\frac{\partial E_2^*}{\partial z} &= \frac{1}{I_0}\left[\gamma_T g_T E_3^* + \nu\left(\gamma_R g_R E_4^* + \gamma_{2k} g_{2k} E_1^*\right)\right], \\
\frac{\partial E_3}{\partial z} &= \frac{1}{I_0}\left[-\gamma_T g_T E_2^* + \nu\left(\gamma_R g_R^* E_1 - \gamma_{2k'} g_{2k'} E_4\right)\right], \\
\frac{\partial E_4^*}{\partial z} &= \frac{1}{I_0}\left[-\gamma_T g_T E_1^* + \nu\left(\gamma_R g_R^* E_2^* - \gamma_{2k'} g_{2k'} E_3\right)\right],
\end{aligned} \tag{6.1}$$

and the boundary condition are

(i) "Arch" configuration

$$E_1(0) = E_3(L) = 0, \text{ and, } \frac{|E_4(L)|^2}{|E_2(0)|^2} = q, \tag{6.2}$$

and

(ii) "Fish-Heas", "Fish", and "Ring", configurations

$$E_1(z_1) = E_3(z_2) = 0, \text{ and, } \frac{|E_4(z_2)|^2}{|E_2(z_1)|^2} = q, \tag{6.3}$$

where $I_0 = \Sigma |E_j|^2 \, (j = 1,4)$ is the total intensity of all the beams, γ_T, γ_R, γ_{2k}, and $\gamma_{2k'}$, are the photorefractive coupling coefficients for transmission, reflection, and *2k*-reflection grating, respectively, q is the intensity ratio of the pump beams, L is the interaction length. It is clear that when two pump beams are mutually incoherent, i.e., ν=0, the coupled wave equations reduce to the convenient ones,

$$\begin{aligned}
\frac{\partial E_1}{\partial z} &= \frac{1}{I_0}\left[\gamma_T g_T E_4\right], \\
\frac{\partial E_2^*}{\partial z} &= \frac{1}{I_0}\left[\gamma_T g_T E_3^*\right], \\
\frac{\partial E_3}{\partial z} &= \frac{1}{I_0}\left[-\gamma_T g_T E_2^*\right], \\
\frac{\partial E_4^*}{\partial z} &= \frac{1}{I_0}\left[-\gamma_T g_T E_1^*\right],
\end{aligned} \tag{6.4}$$

where only the transmission grating is present [Cro84 & He88]. The gratings set up by a four-wave interaction have the property that their period is precisely that which maximises their ability to reflect electromagnetic energy, i.e., they automatically satisfy the Bragg condition for constructive addition to the fields reflected from successive elements of the grating. Moreover, the reflections from the long-period grating (transmission grating) are precisely in the directions defined by the two sets of counterpropagating waves, e.g., the reflection of the wave by the long-period grating yields a field traveling along the direction of the waves 3 and 1.

However, it is difficult to identify exactly from where the two loops emerge and where they rejoin the incident beams in the "fish-head", "fish", and "ray" MPPCMs. Nevertheless, following the earlier proposed mechanism of J. Feinberg et al. [Fei82], we can tentatively suggest that each incident beam intersects each loop in an interaction region. Figs. 6.2(b)-(d) schematically shows these four interaction regions, $\mathbf{I}_1$, $\mathbf{II}_1$, $\mathbf{I}_2$, and $\mathbf{II}_2$. In our experiments we observed that the two beams entered the crystal and instantly fanned out to form two overlapping fans. Little appeared to happen due to competition between numerous gratings which were being written, erased and enhanced resulting in the formation of either one or two loops of light. Ultimately, only those gratings giving rise to the phase conjugate reflections survived. The grating at region $\mathbf{I}_1$ is a transmission grating, written by an interaction between the input beam I_{1p} and the fanned beams arising from it. This grating is read by I_{2p} after scattering at $\mathbf{II}_2$ and after three internal reflections and this beam is diffracted by four wave mixing to form the beam I_{1pc} which is the phase conjugate of the incident beam I_{1p}.

Similarly a loop is formed by beam I_{2p} between interaction regions $\mathbf{I}_2$ and $\mathbf{II}_1$. It seems unlikely that loops will form between similar ($\mathbf{I}_1$ and $\mathbf{I}_2$; $\mathbf{II}_1$ and $\mathbf{II}_2$) interaction regions because this would require the loops to cross which is not observed. Cross-linking between regions allows each loop to share differently angled gratings at different locations leading to increased stability. A single loop can arise when the interaction regions move together and merge. A second possible mechanism requires a single but more complex interaction region on each incident beam giving rise to two differently angled beams from two angularly multiplexed gratings which are cross-linked.

In order to be useful for long-term laser phase locking, these configurations must be able to initiate coupling with mutually incoherent light and maintain coupling with mutually coherent input. The transmission properties of the MPPCM as a function of the degree of mutual coherence of the pump beams can be obtained by solving the nonlinear coupled wave equations, (6.1) & (6.4) with numerical methods, such as the conventional 4-th-order Runge-Kutta algorithm. And, by taking account of the depletion of the pumped beams since strong beam coupling occurs in photorefractive materials, and pump depletion is common in most of the photorefractive phase conjugation processes, especially in the MPPCM of our four novel configurations. But this is beyond the scope of this work. Here, we just demonstrate the results of an experimental study of the effects of laser coherence on the operation of the "fish-head", "fish", and "ray" MPPCMs. Fig. 6.33 shows the phase-conjugate reflectivity of MPPCMs formed by two mutually coherent light sources interacting inside the crystal.

Fig. 6.33 *The plot of phase-conjugate reflectivity of two mutually coherent laser light source interacting in a $BaTiO_3$ crystal occurring in three different cases. The "fish-head" configuration was formed in area I, the "ray" configuration was formed in area II, and the "fish" configuration was formed in area III, respectively.*

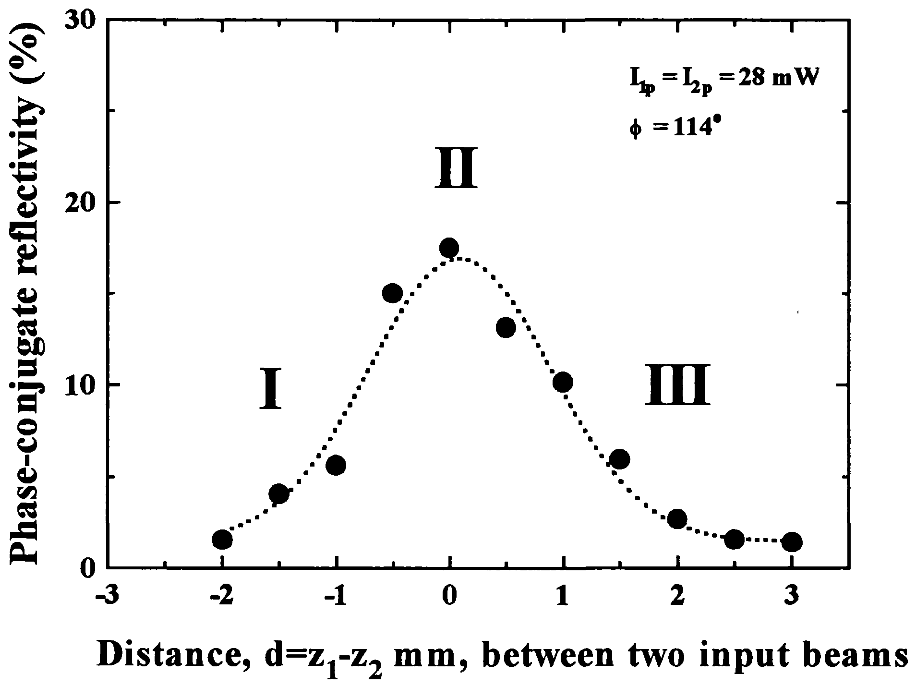

In Fig. 6.33, one can be seen that the highest phase- conjugate efficiency occurs in ray configuration as shown in area II. It can be explained that two input beams, I_{1p} and I_{2p}, will be diffracted by their shared grating T, formed by the two input beams, on the crystal $+c$ face becoming rays and beams along the ring-oscillation channels reinforce to produce four internal reflections at four faces. Naturally, parts of the phase-conjugate outputs join at the cross readout of the grating T. This plays an importment role in stablising the phase-conjugate outputs and channels.

It worth mention that in Ray MPPCM when beams are coherent then they can write a grating at the entrance point. Beams I_{1p} and I_{2p} pass through and diffracted their shared grating to produce four internal reflections at four faces. Naturally, parts of the phase-conjugate outputs meet at same point again writing a grating before leaving. This appears to generate a ring resonator.

6.7 Dual Mutually Pumped Phase-Conjugate Mirrors

In this section we extend our work to fabricate a MPPCM for a three incident beam interation. The configuration is a double fish-head configuration formed in a $BaTiO_3$ crystal and, for the first time to our knowledge, exhibits threshold behaviour and may be useful for optical gates, computing, and neural networks.

6.7.1 General Description

In this double fish-head configuration, the initial propagation state of the incident beams (or input beams which will be phase-conjugated) in each configuration is particularly distinct from the existing configurations (as shown in Fig. 6.1), in that the incident beams, I_{1p} , I_{2p}, and I_{3p} are initially travelling close to the crystal's c-axis in the -C direction within the $BaTiO_3$ at the crystal face (labeled $+c$) with acute angles of θ_1, θ_2, and θ_3 to normal of the $+c$ face at distances, z_1 , z_2, and z_3, from the crystal corners (defined in Fig. 6.34(a)). When the phase-conjugation behavior has been established two stable loops of light with fish-head shape (as shown in Fig. 6.31(b)) can be seen inside the $BaTiO_3$ crystal in this geometry.

Fig. 6.34 *Schematic of double fish- head MPPCM configuration inside a $BaTiO_3$ crystal.*

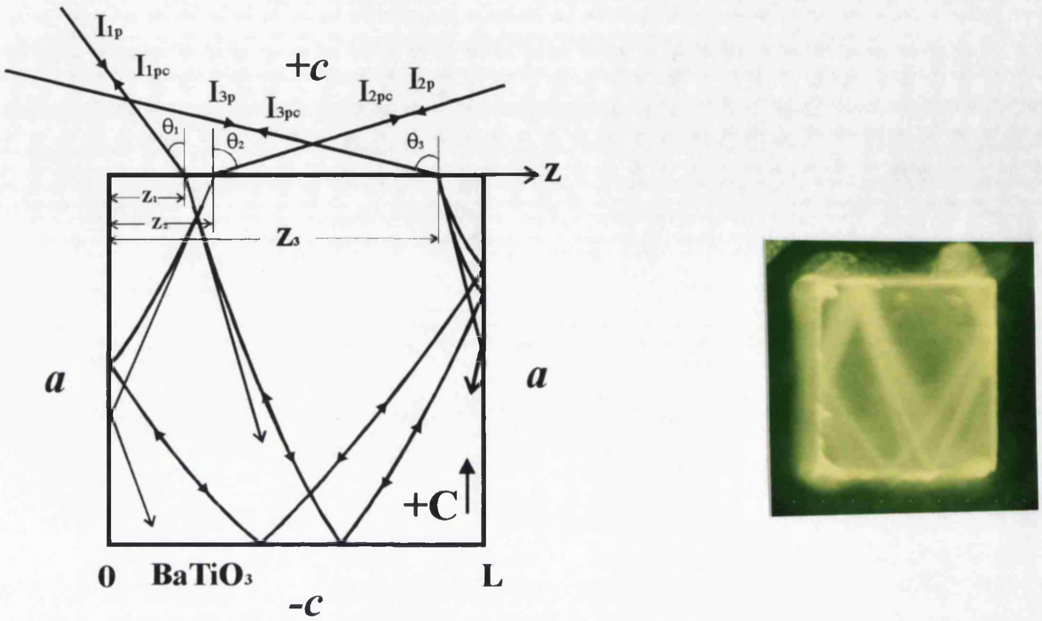

(a) **(b)**

6.7.2 Experimental Arrangement

The experimental arrangement for examining the double MPPCMs with two "fish-head"s, configuration in a $BaTiO_3$ is shown as in Fig. 6.35. the face of the crystal onto which three incident beams shone is the $+c$ face of a $BaTiO_3$ crystal. Each pump beam was generated from an argon ion laser (Coherent Inova 4) in multi-longitudinal mode operation at 514.5nm without an intracavity étalon. The path length difference between each pair of the incident beams was arranged to be greater (typically 15-70cm) than the coherence length (~5cm) of the laser, operating in this manner so the beams can be considered to be incoherent. The interacting beams were extraordinarily polarized and were focused, by Fourier transform lenses of 350 mm focal length, to foci located about 25 mm outside of the crystal so that each beam diverged into the crystal. This gave us initial angular spread to promote fanning and overlap of the beams within the $BaTiO_3$ crystal (5.16mm x 5.00mm x 4.74mm).

The phase-conjugate beams, I_{1pc}, I_{2pc}, and I_{3pc}, of three incident beams, I_{1p}, I_{2p}, and I_{3p}, were coupled out from the incident beam paths by using beamsplitters BS_1, BS_2, and

BS_3, and the powers were monitored by PD_1, PD_2, and PD_3 (which are connected to an *x-t* chart recorder) as a function of time. The incident power of each beam was adjusted using a set of nutural density filters. Two input images, T_1 and T_2, to be phase conjugated are inserted into the path 1 & 2. Two photodetectors, PD_1 and PD_2, are replaced by two screen S_1 and S_2, or cameras (or CCDs) to capture the output images, respectively. Two collimators C_1 and C_2, consisted of spatial filter and collimation lenses, one of each were introduced into the setup to input two images.

Fig. 6.35 *Experimental arrangement for the double MPPCM.*

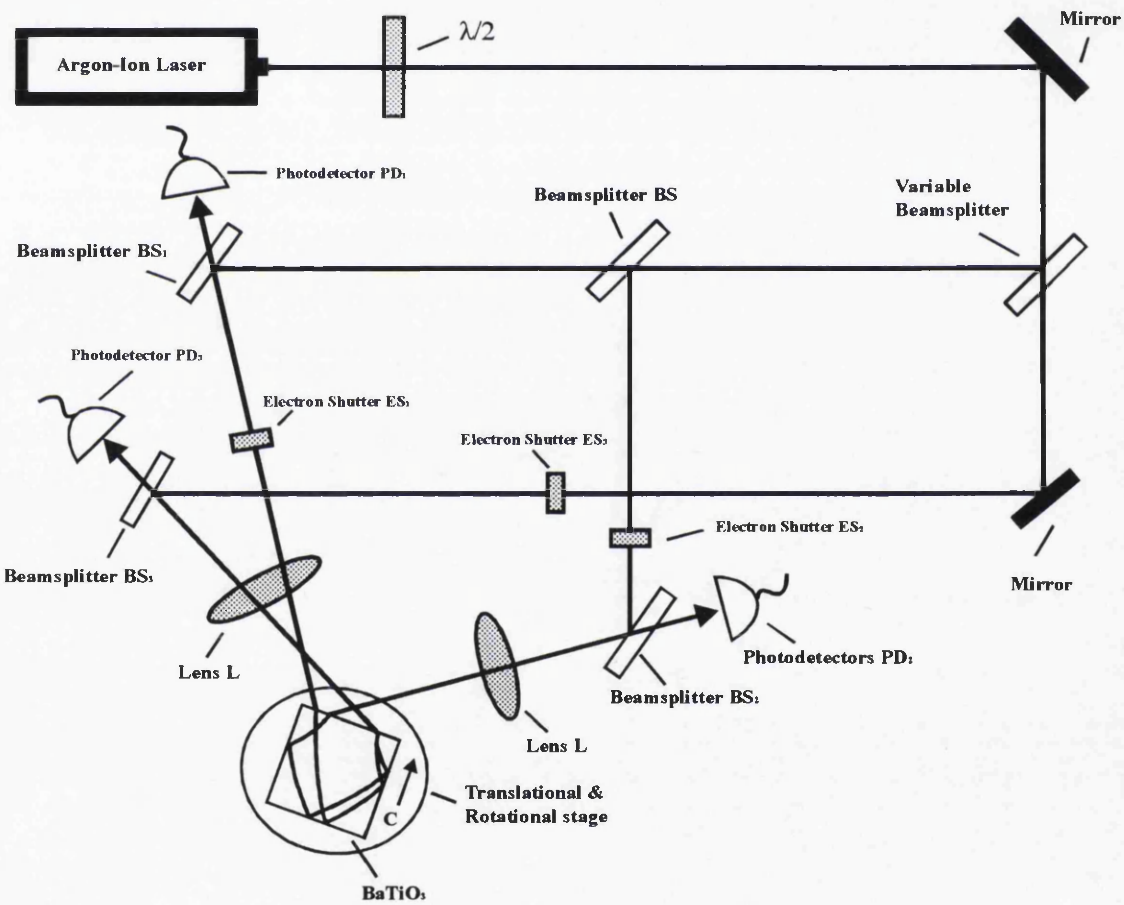

6.7.3 Experimental Results and Analysis

In this section we examine our new double mutually pumped phase-conjugate mirror (DMPPCM) experimentally, for the first time to our knowledge, in a barium titanate crystal which phase conjugates three incident beams in pairs operating as two MPPCMs in the same crystal at the same time but in different orientations.

Three unexpanded Gaussian beams (directly from the laser), each having a power of 35 mW with a beam diameter of 0.48 mm, is incident: z_1=0.8mm, $\theta_1=40^O$; z_2=1.4mm, $\theta_2=65^O$; z_3 =4.6mm, $\theta_3=75^O$, where θ_i (i=1,3) is the incident angle with respect to the normal of the crystal as defined in Fig. 6.34(a). We have measured the mutually pumped phase-conjugate reflectivties of each input beam are 25%, 23%, and 45%, respectively. It can be seen that the reflectivty of third beam, I_{3p}, is about twice higher than those of beams, I_{1p} and I_{2p}. The light channels within the crystal are clearly apparant when the phase-conjugate outputs of each input beam (to be phase conjugated) increase notably. Fig. 6.36 show the build-up process of the double MPPCMs in a $BaTiO_3$ crystal.

Fig. 6.36 *A set of photographs illustrating the internal light path loops in the DMPPCM (a) after three beam swiching on, (b) after beam, I_{3p}, turnning off (c) after beam, I_{1p}, turnning off, and (d) after beam, I_{2p}, turnning off on the steady state phase conjugation process of the DMPPCM.*

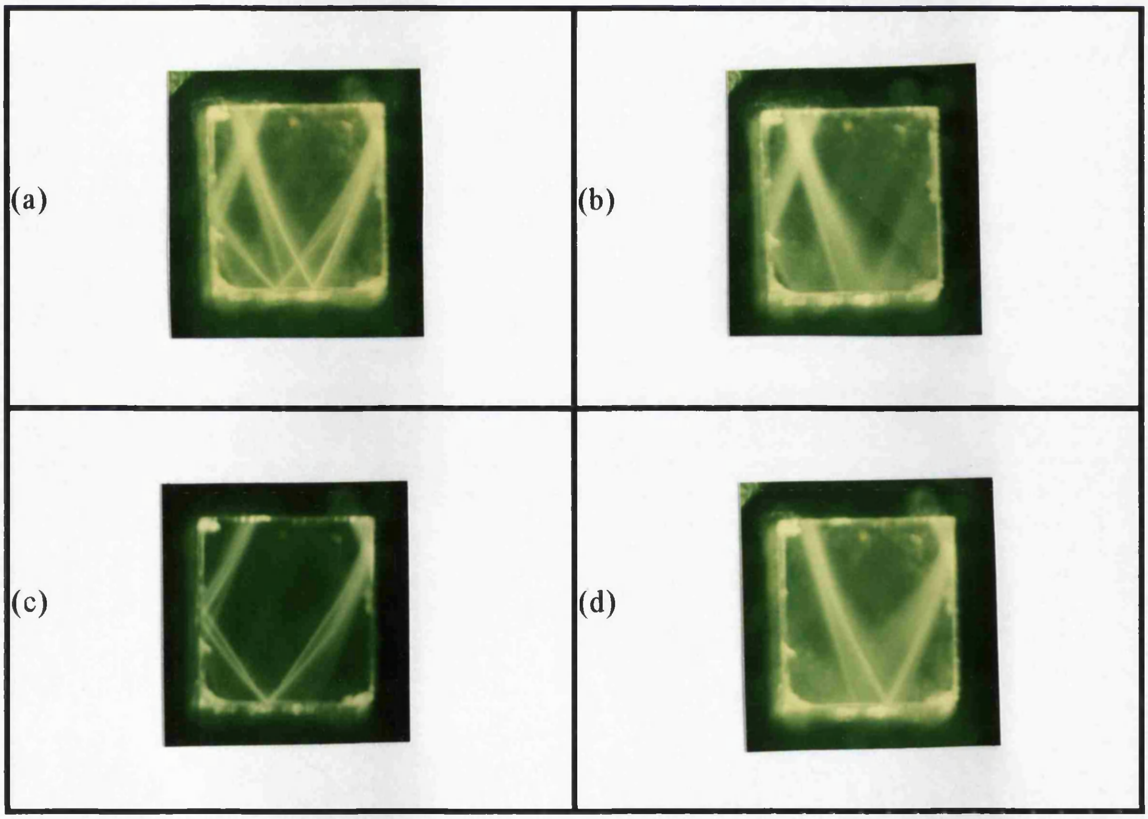

Then we check that mutual pumping were indeed occurring by turning off one beam, I_{3p}, to verify that the phase-conjugate beams of two I_{1p}, and I_{2p}, were ultimately extinguished. However, when blocked one of the incident beam, I_{1p} (I_{2p}), the other phase conjugate beam, I_{2pc} (I_{1p}), continued to be observe. In can be explained that the two mutually pumped pairs are coupled as they share one beam (I_{3p}) and they share some similar volumes of the crystal.

We checked the fidelity of the mutual phase conjugation process in the DMPPCM by placing one resolution target in path 1 (input 1), the other one target was doll image transparency inserted into path 2 (input 2) to investigate crosstalk. The third one input after spatially filtering, expanding and collimating. Two input beams, I_{1p} & I_{2p}, carrying images, USAF resouliton chart and doll image transparency, were incident on the $+c$ face at (i) z_1 =2.5mm and θ_2=114°, z_2=2.5mm and θ_2=114°. The phase-conjugate images, displayed on screens S_1 and S_2 or captured by CCD cameras (shown in Fig. 6.35), are reproduced in Fig. 6.37.

Fig. 6.37 *Photographs of the phase-conjugate images by the double MPPCM: for (a) pump beam I_{1p}, and (b) pump beam I_{2p}.*

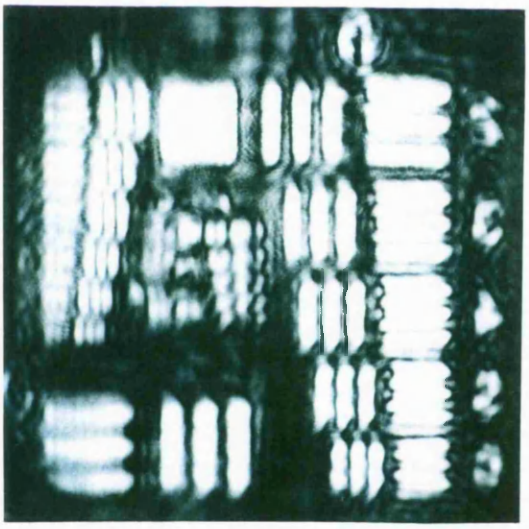

(a)

(b)

6.8 Conclusions

In this chapter we have discovered for mutually pumped phase conjugation of two incoherent beams which are all remarkably insensitive to angular and lateral postional changes in either of the two input beams or in the crystal itself. The four configurations are also notable in that they have high reflectivity efficiencies and fast response times and are also relatively insensitive to the incident beams power ratio. We first show that our experimental characterisations of the "Arch" beam path within the barium titanate crystal are in good agreement with later numerical simulations carried out by Zozulya et al.[Zoz94 & 95]. We have also discussd its underlying physical mechanism and show that it is superior to the popular "bird-wing" configuration as it had a better stability, efficiency and tolerance to angular and translational movements in either of beams and in the crystal itself but it takes slightly longer to set up. However, once set up it adapts quickly to new beam orientations.

The "Fish-Head", "Fish" and "Manta Ray" configurations are the three other of our four new configurations that we have discovered for mutually pumped phase conjugation of two incoherent beams which are all remarkably insensitive to angular and lateral postional changes in either of the two input beams or in the crystal itself. The four configurations are also notable in that they have high reflectivity efficiencies and fast response times and are also relatively insensitive to the incident beams power ratio. These three configurations are part of a family of mutually pumped phase conjugate mirrors all of which have similar internal beam paths within the crystal having three internal reflections. The phase conjugate behaviour of the Fish-Head is established relatively fast (~1sec) and has a high reflectivity efficiency (30%) and no crosstalk is observable between the two beams. The phase conjugate output is far more stable than the "bird-wing" and this stability is also a characteristic of this configuration. These characteristics make these configurations particularly interesting for practical applications such as for phase locking lasers and for optical free space communications.

We have also demonstrated the mutual phase conjugation of two coherently related beams using the same new configurations "Fish-Head", "Fish", and "Manta Ray" described above. The physical reasons for this unusual behaviour are identified. The degree of coherence of the two incident beams determines which gratings are formed in the crystal. We discuss the importance of this effect for practical applications such as laser phase locking and high efficiency holographic storage (discussed in Chapter 3).

We have discovered a new double mutually pumped phase-conjugate mirror (DMPPCM) in a barium titanate crystal which phase conjugates three incident beams in pairs operating as two MPPCMs in the same crystal at the same time but in different orientations. The two mutually pumped pairs are coupled as they share one beam and they share some similar volumes of the crystal.

Chapter Seven

CONCLUSIONS AND FUTURE WORK

CONCLUSIONS This chapter begins with a brief overview of the PhD thesis and then lists all of the new achievements which were a result of this research. The chapter ends with a list of the future work possible to develop this research further.

The research described in this PhD thesis is aimed at the design of an optical feedback system (resonator) with photorefractive phase-conjugate mirrors (PCMs) and a holographic memory which can be developed into an optical neural network (ONN) for use as an optical associative memory (OAM). In this thesis we have also reported in detail the achievements that were necessary before such a system could be developed. These new discoveries were in the field of optical phase conjugation (OPC) and in the basic physics and original holographic technology underlying them. The novel research in this thesis:

A. A compact optical photorefractive holographic correlator employing a 2-f correlation system has been proposed. This compact scheme is suitable for incorporation into an optical photorefractive resonator with the spatio-angular multiplexing (SAM) (Tao93) scheme for recording holograms to implement a high order feedback neural network (HOFNET) [Sel90 & 91] system (Chapter3). Based on the merits of the HOFNET the 2f systems physical length can be shortened to half as much as in the conventional 4f correlation system and losses can be avoided.

B. We have increased the diffraction efficiency of volume holograms stored in a photorefractive crystal by making use of two self-pumped phase conjugate mirrors (SPPCMs) as part of the recording technique. One of the SPPCMs was induced to widen the angular range over which phase conjugation of beams could take place which again has not been done before. We recorded 21 angularly multiplexed holograms. When a single grating was stored the highest efficiency of 32% was obtained using a diode pumped frequency doubled YAG. To our knowledge this is the highest efficiency reported to date for volume holograms in this material.

C. We discovered that the Bragg-shift depends on the total exposure during the recording and not just on the beam ratio (Chapter 3). The Bragg-shift effect was discovered several years earlier at UCL by Tao et al. [Tao93] when she found that higher efficiency replay of volume gratings formed in photorefractive crystals was possible by altering the replay angle very slightly from that used for recording in the case when the two recording beams had had different intensities. In some case we found that an increase in efficiency from 3.4% to 32.8% was possible by choosing the correct angle. These results suggest that to obtain the optimum readout performance from gratings written by two beams in $LiNbO_3$ crystal, readout beams must be angularly shifted with a desirable angle. In the other words, to implement the neural-like associative memory using holographically multiplexed stored memories (database) with uniformly high efficiencies written in photorefractive materials, the effects of this diffraction efficiency enhancement must be take into account.

D. We demonstrated the simultaneous phase conjugation of up to 21 beams oriented at various angles without crosstalk. This direction of research was prompted by my earlier work on induced self-pumped phase conjugation (ISPPC) and on how this effect exhibits higher phase-conjugate efficiencies and faster response times [Yau92]. In the new Multiple Beam Induced Phase Conjugation (MIPC) four beams were initially phase conjugated in a barium titanate crystal only when an inducing beam was also incident. We also discovered that an inducing beam of a completely different wavelength could also stimulate the onset of phase conjugate beahviour (Chapter 4) (non-degenerate MIPC). The introduction of the inducing beam changes the paths of the beams within the crystal. We found that multi-beam phase conjugation is not sensitive to the relative positions, angles or intensities of the interacting beams and the coherence requirement is very relaxed. We also showed that a single incoherent inducing beam could be used to switch the phase conjugation of up to four other beams on and off in a type of light controlled relay. In chapter 4 we conjugated 21 beams as part of an optical resonator.

E. We constructed and demonstrated an optical resonator between two self-pumped phase conjugate mirrors via a photorefractive crystal in which 21 gratings had been recorded. 21 eigen modes were shown to be present with similar intensities. The system configuration was also novel as the resonance was maintained by an injected sustaining beam. One of the phase-conjugate mirrors was induced by a beam of another colour to increase the angular range over which phase conjugation could be performed (Chapter 4).

F. We discovered 3 new distinct configurations, the "-C^3", "J" , and "Tick", for self-pumped phase conjugation in a 0^o-cut undoped barium titanate crystal (chapter 5). These are notable for their high efficiencies, fast set up times, their tolerance to a wide range of both angular and translational shifts in the input beams and finaly for their high resolution. We also found numerous variations of these configurations which also gave phase conjugation but which had similar beam paths within the crystal. We compared these with the popular and conventional "Cat" configuration for self-pumped phase conjugation and concluded that each of our new configurations is a lot more insensitive to lateral positional shifts of the incident beam and angular changes in the incident beam. The optimum results were obtained for our "-C^3" configuration in which a phase-conjugate efficiency of 30% was obtained and phase conjugation was maintained (but at lower efficiencies) over a range of 4mm in lateral translations of the beam and over a range of 40 degrees in the incident angle of the beam. Moreover the efficiency of the "-C^3" configuration is somewhat higher than that of the "cat". This tolerance to lateral positional and angular changes also means that the resolution of our configurations are improved, for example, the "-C^3" configuration was shown to have a higher resolution of 30 μm and fidelity than the "Cat" (70 μm).

G. We have have identified the physical mechanisms underlying our discoveries. All of our new configurations rely on the fact that the incident beams are propagating at an acute angle to the -C direction of the crystal and so experience increased fanning over a wide range of angles. We additionally enchance the range of the angled beams by using initially divergent incident beams in all cases including for the inducing beam. This range of angles in the fan has the effect of incresasing the interaction length in the crystal which raises the coupling strength and in addition gives a wide angular and spatial range of gratings in the crystal which in turn deflect beams to most parts of the crystal over a wide range of angles at each place; some beams, at least, meet the conditions for self-pumped phase conjugation. The increased coupling gives a fast response time and high efficiency, the wide fan gives a large angular and lateral positional acceptance and also a high resolution.

H. We have proposed a simple model with Four Interaction Regions (FIR) to further account for our discoveries in a little more detail and to give an intuitive insight into the operation of self phase conjugation. In this model transitions between the four interaction regions can account for the double loop optical paths observed in many of our self-pumped phase-conjugate mirrors. The similarities and distinguishable differences between our four interaction region model for these configurations and the existing two interaction region model of the popular "Cat" configuration are also highlighted (Chapter 5).

I. The "Arch" (chapter 6) is just one of four new configurations we have discovered for mutually pumped phase conjugation of two incoherent beams which are all remarkably insensitive to angular and lateral postional changes in either of the two input beams or in the crystal itself. The four configurations are also notable in that they have high reflectivity efficiencies and fast response times and are also relatively insensitive to the incident beams power ratio. We show that our experimental characterisations of the "Arch" beam path within the barium titanate crystal are in good agreement with later numerical simulations carried out by Zozulya et al.[Zoz94 & 95]. We discuss its underlying physical mechanism and show that it is superior to the popular "bird-wing" configuration as it has a better stability, efficiency and tolerance to angular and translational movements in either of beams and in the crystal itself but it takes slightly longer to set up. However, once set up it adapts quickly to new beam orientations.

J. The "Fish-Head", "Fish" and "Manta Ray" configurations (chapter 6) are the three other of our four new configurations that we have discovered for mutually pumped phase conjugation of two incoherent beams which are all remarkably insensitive to angular and lateral postional changes in either of the two input beams or in the crystal itself. The four configurations are also notable in that they have high reflectivity efficiencies and fast response times and are also relatively insensitive to the incident beams power ratio. These three configurations are part of a family of mutually pumped phase conjugate mirrors all of which have similar internal beam paths within the crystal having three internal reflections. The phase conjugate behaviour of the Fish-Head is established relatively fast (~1sec) and has a high reflectivity efficiency (30%) and no crosstalk is observable between the two beams. The phase conjugate output is far more stable than the "bird-wing" and this stability is also a characteristic of this configuration. These characteristics makes these configurations particularly interesting for practical applications such as for phase locking lasers and for optical free space communications (Chapter 6).

K. We have also demonstrated the mutual phase conjugation of two COHERENTLY related beams using the same new configurations "Fish-Head", "Fish", and "Manta Ray" described above. The physical reasons for this unusual behaviour are identified. The degree of coherence of the two incident beams determines which gratings are formed in the crystal. We discuss the importance of this effect for practical applications such as laser phase locking and high efficiency holographic storage (chapter 3).

L. We have discovered a new DOUBLE mutually pumped phase-conjugate mirror in a barium titanate crystal which phase conjugates three incident beams in pairs operating as two mutually pumped phase conjugate mirrors in the same crystal at the same time but in different orientations. The two mutually pumped pairs are coupled as they share one beam and they share some similar volumes of the crystal. This coupling leads to a thresholding ability which can be useful for making non-linear logical devices or as a threshold for optical neural networks (Chapter 6).

FUTURE WORK Some suggestions and ideas, inevitably proved to be outside the scope of thesis and now, in conclusion, we briefly propose solutions to the most important problems which should be investigated in deeper detail in the near future, and recommend some longer term research directions. It is hoped to use the experience gained from the photorefractive phase conjugate resonator and the optical storage technique (SAM) [Tao93] and possibly apply it to realising optical neural networks (HOFNET) [Sel 90 &

91, Mao92]. An attempt should be made to determine the optimum photorefractive resonator design and examine their applications in optical neural networks. Hopefully, the problem of how a high order feedback neural network can be most effectively applied in order to make the system more compact will be addressed with particular regard to the feedback system and memory.

Here the principal challenge has been to realise practical systems incorporating the SAM and the multi-mode self-pumped resonator into a compact HOFNET system. Although the preliminary experiments of the main part of the resonator (feedback system) have been achieved, the system is of little practical use. Therefore, the remainder of the future studies should carry on as follows:

A. The multi-mode self-pumped resonator implementation could be improved in a number of ways, for instance, in applications requiring two-dimensional optical feedback, future work may be focused on implementing 2-D induced phase conjugation for use as a feedback technique. Additionally, only a small number of memories were realised in the multi-mode self-pumped resonator. Thus, future work should also concentrate on the actual realisation of a large number of highly diffraction efficient holograms in a single crystal. Note that the SAM scheme could be used for this purpose, however, crosstalk behaviour is known to become more pronounced due to photorefractive scattering. Finally, although a proposal was made for a "compact" OAM its physical implementation was largely avoided in this thesis. Thus, in its present form the compact model is essentially a OAM. In applications requiring iteration, future work is needed to implement iteration which could be sustained by providing gain to overcome losses by the use of external pump in, for example, four-wave mixing (FWM) .

B. A beam coupler could be developed using the double mutually pumped phase conjugate mirror shown in the "Fish Head "configurations. This could be applied to phase lock several independent lasers. Future work may extend to implementing thresholding and incorporating it into a practical optical neural network system for realising optical feedback in an associative memories. This would make an interesting and potentially useful project in its own right. If successful the MPPCM would be quite versatile, being suitable as both a threshold and for feedback.

C. Recent developments in semiconductor lasers emitting in the near infrared with high power and efficiency lead to an increasing interest in optical phase conjugation in this wavelength range particularly for use in optical communication systems. Also space communications using optical frequencies has a growing importance in a world where the capacity of data transport has to be enlarged in order to increase the data flow and to make it more reliable. Only 0°-cut undoped $BaTiO_3$ crystals were actually used and implemented in our novel SPPCMs and MPPCMs in this thesis. The implementation of other useful doped crystals such as Rh:$BaTiO_3$ and a varity of light sources such as IR and ultra-short pulse lasers is left as an area for future development. This would conceivably facilitate the realisation of various practical PCMs that exhibit the advantageous attributes associated with the respective classes of self- and mutual-phase conjugation implemented. Lastly alternative theories and mechanisms for explaining such phase-conjugate devices in different configurations should be explored.

REFERENCES

[Abu87] Abu-Mostafa, Y. S. and Psaltis, D., Sci. Am. **256**(3), 66 (1987).

[Ada91] Adams, L. E. and Bondurant, R. S., Opt. Lett. **16**, 832 (1991).

[Amo71] Amodei, J. J. and Staebler, D. L., Appl. Phys. Lett. **18**, 540 (1971).

[Amo72] Amodei, J. J. and Staebler, D. L., RCV Rev. **33**, 71 (1972).

[And86] Anderson, D. Z., Opt. Lett. **11**, 56 (1986).

[And87a] Anderson, D. Z., Lininger, D. M., and Feinberg, J., Opt. Lett. **12**, 123 (1987).

[And87b] Anderson, D. Z. and Erie, M. M., Opt. Eng. **26**, 585 (1987).

[And93] Anderson, R. J., Sharp, E. J., Wood, G. L., Clark III, W. W., Vuong, Q., Salamo, G. J. and Neurgaonka,r R. R., Opt. Lett. **18**, 986 (1993).

[Aoy93] Aoyama, T., Mizuta, S., Kurimura, S., Uesu, Y., and Seo, I., Jpn. J. Appl. Phys. **32**, 4307 (1993).

[Ash66] Ashkin, A., Boyd, G. D., Dziedzic, J. M., Smith, R. G., Ballman, A. A., Levenstein, H. J., and Nassau, K., Appl. Phys. Lett. **9**, 72 (1966).

[Ath86] Athale, R. A., Szu, H. H., and Friedlander, C. B., Opt. Lett., **11**, 482 (1986).

[Bar87] Barhen, J., Toomarian, N, and Protopopescu, V., Appl. Opt. **26**, 5007 (1987).

[Bas92] Bashaw, M. C., Aharoni, A. and Hesselink, L., Opt.Lett., **17**, 1149 (1992).

[Bea90] Beale, R. and Jackson, T., "*Neural Computing: An Introduction*," Adam Hilger, Bristol (1990).

[Bel94] Belic, M. R., Leonardy, J., Timotijevic, D., and Kaiser, F., Opt. Commun. **111**, 99 (1994).

[Bia86] Bialkowski, S. E., Opt. Lett. **14**, 1020 (1986).

[Bia93] Bian, S., Zhang, J., Su, X., Xu, K., Sun, W., Jiang, Q., Chen, H., and Sun, D., Opt. Lett. 18, 769 (1993).

[Blo77] Bloom, D. M. and Bjorklund, D. C., Appl. Phys. Lett. **31**, 592 (1977).

[Blo79] Bloembergen, N., "*Laser Spectroscopy IV*", ed by H. Walther and K. W. Rothe, Springer Ser. Opt. Sci., **21** (Springer, Berlin, Heidelberg 1979) p. 340.

[Bog92] Bogodaev, N. V., Eliseev, V. V., Ivleva, L. I., Korshunov, A. S., Orlov, S. S., Polozkov, N. M. and Zozulya, A. A., J. Opt. Soc. Am. **B9**, 1493 (1992).

[Bog93] Bogodaev, N. V., Ivleva, L. I., Korshunov, A. S., Mamaev, A. V., Polozkov, N. N., and Zozulya, A. A., J Opt. Soc. Am. B **10**, 1054 (1993).

[Bos89] Bostel, A. J., Stace, C., Swinburn, G., and Hall, T J. in *Proc. Int. Symp. on Optics in Computing, SFO. Toulouse, Oct. 17-18*, 187 (1989).

[Bur94] Burr, G. W., Mok, F. H., and Psaltis, D., OSA Annual meeting/ **ILS-X**, paper MD4 (1994).

[Byl87] Bylsma, R. B., Bridenbaugh, P. M., Olson, D. H., and Glass, A. M., Appl. Phys. Lett. **51**, 889 (1987).

[Car86] Carrascosa, M. and Agullo-lopez, F, IEEE J. Quantum Electron. **QE-22**, 1369 (1986).

[Car90] Carrascosa, M. and Agullo-lopez, F, J Opt. Soc. Am. B. **12**, 2317 (1990).

[Cas89] Casasent, D. P. and Telfer, B, Appl. Opt. **28**, 272 (1989).

[Cau87] Caulfield, H. J., Shamir J. and He, Q., Appl. Opt. **26**, 2291 (1987).

[Cau89] Caulfield, H. J., Kinser, J., and Rogers, S. K., Proc. IEEE **77**, 173-1583 (1989).

[Cha85] Chang, T. Y. and Hellwarth, R. W., Opt. Lett. **10**, 408 (1985).

[Cha92a] Chang, C. C., Yau, H. F., Tong, Y. P., and Puh, N. W., Opt. Commun. **87**, 219 (1992).

[Cha92b] Chang, C. C., Tong, Y. P., and Yau, H. F., Jpn. J. Appl. Phys. **31**, L43 (1992).

[Che68] Chen, F. S., La Macchia, J. T., and Frazer, D. B., Appl. Phys. Lett. **13**, 223 (1968).

[Che92] Chen, Z., Kasamatsu, T. and Shiosaki, T., Jpn. J. Appl. Phys., **31**(9B), Part 1, 3178 (1992).

[Chi95] Chiou, A., Yeh, P., Yang, C. X., and Gu, C, Digest of the Topical Meeting on Photorefractive Materials, Effects and Devices (Espen Lodge at Estes Park, Colorado, 1995), paper **WPD1**.

[Cho91] Chomsky, D., Sternklar, S., Jackel, S., and Zigler, A, Opt. Commun. 84, 104 (1991).

[Chu91] Chua, P. L., Liu, D. T. H., and Cheng, L. J., Appl. Phys. Lett. **57**, 2880 (1991).

[Cho96] Cohen, M. S., Appl. Opt. **25**, 2288 (1986).

[Con84] Connors, L., Foote, P., Hall, T. J., Jaura, R., Laycock, L. C., McCall, M. W., and Petts, C. R., European conference on Optics, Optical Systems and Applications '84 (Amsterdam), SPIE, **492**, 361 (1984).

[Cro78] Cronin-Golomb, M., Fischer, B, Kwong, S. K., White, J. O., and Yarv, A., IEEE J. Quantum Electron.**QE-20**, 12 (1978).

[Cro82a] Cronin-Golomb, M., Fischer, B., Nilsen, J., White, J. O., and Yariv, A., Appl. Phys. Lett. **41**, 219 (1982).

[Cro82b] Cronin-Golomb, M., Fischer, B., White, J. O., and Yariv, A., Appl. Phys. Lett. **41**, 689 (1982).

[Cro83] Cronin-Golomb, M., Fisher, B., White, J. O., and Yarv, A., Appl. Phys. Lett. **42**, 919 (1983).

[Cro84] Cronin-Golomb, M., Fischer, B, White, J. O., and Yariv, A., IEEE J. Quantum Electron. **QE-20**, 12 (1984).

[Cro85a] Cronin-Golomb, M. and Yariv, A. J. Appl. Phys. **57**, 4906 (1985).

[Cro85b] Cronin-Golomb, M., Fischer, B., Kwong, S. K., White, J. O., and Yarv, A., Opt. Lett. **10**, 353 (1985).

[Cro86a] Cronin-Golomb, M. and Yariv, A. " In *SPIE Proc. Int. Optical Computing Conf.*, 301 (1986).

[Crob6b] Cronic-Golomb, M. and Yariv, A., Opt. Lett. **11**, 455 (1986).

[D'Au73] D'Auria, L., Huignard,, J. P. and Spitz, E. IEEE Trans. Magn. **MA-9**, 83 (1973).

[D'Ya91] D'Yakov, V. A., Korol'kov, S. A., Manaev, A. V., Shkunov, V. V., and Zozulya A. A., Opt. Lett. **16**, 1614 (1991).

[Den92] Denz, C., Pauliat, G., Roosen, G., and Tschudi, T., Appl. Opt. **26**, 5700 (1992).

[Der84] Derthick, M., Carnegie-Mellon Univ. Tech. Rep. **CMU-CS-84-120** (1984).

[Din93] Ding, Y., R pnack, R., and Eichler, H. J., in Proceddings of the International Conference on Lasers '93 (Society for Optical and Quantum Electronics, McLean, Va., 1993), pp. 446.

[Din95] Ding, Y., Zhang, Z. G., Eichler, H. J., Shen, D. Z., Ma, X. Y., and Chen, J. Y., Opt. Lett. **20**, 686 (1995).

[Duc84] Ducharme, S. and Feinberg, J., J. Appl. Phys. **56**, 839 (1984).

[Due93] Duelli, M., Cudney, R. S., Keller, C., and Günter, P., OSA Photorefractive Materials, Effects and Devices conference proceedings, PRM'93, Kiev, Ukraine, 466 (1993).

[Dun87] Dunning, G. J., Marom, E., Owechko, Y., and Soffer, B. H., Opt. Lett. **12**, 346 (1987).

[Dun90] Dunning, G. J., Owechko, Y., and Soffer, B. H., Int. Meet. Nonlinear Opt. Mater. Phenom Devices, Kauai, Hawaii, NLO '90, 291 (1990).

[Dun91] Dunning, G. J., Owechko, Y. and Soffer, B. H., Opt. Lett. **16**, 928 (1991).

[Eas87] Eason, R. W and Smount, A. M., Opt. Lett. **12**, 51 (1987).

[Eng94] Engin, D., Segev, M., Orlov, S., Yariv, A. and Valley, G. C., J. Opt. Soc. Am. **B11**, 1708 (1994).

[Ewb87] Ewbank, M. D., J. Appl. Phys. **62**, 374 (1987).

[Ewb88] Ewbank, M. D., Opt. Lett. **13**, 47 (1988).

[Ewb90] Ewbank, M.D., Vazquez, R. A., Neurgaonkar, R. R. and Feinberg , J., J. Opt. Soc. Am **B7**, 2306 (1990).

[Yu91] Yu, T. S., Wu, S., Mayers, A. W., and Rajan, S., Opt. Commun. **81**, 343 (1991).

[Fab88] Fabre, J. C., Jonathan, J. M. C., and Rossen, G., J Opt. Soc. Am. **B5**, 1730 (1988).

[Fai86] Fainman, Y., Klancnik, E., and Lee, S. H., Opt. Eng. **25**, 228 (1986).

[Far85] Farhat, N. H., Psaltis, D., Prada, A., and Paek, E., Appl. Opt. **24**, 1469 (1985).

[Fei80a] Feinberg, J. and Hellwarth, R. W., Opt. Lett. **5**, 519 (1980).

[Fei80b] Feinberg, J., Heiman, D., Tanguay, A. R., and Hellwarth, R., J.Appl. Phys. **51**, 1297 (1980).

[Fei81] Feinberg, J., Heiman, D., Tanguay, A. R., and Hellwarth, R., J. Appl. Phys. **52**, 537 (1981).

[Fei82a] Feinberg J., Opt. Lett., **7**, 486 (1982).

[Fei82b] Feinberg, J., J. Opt. Soc. Am. **72**, 46 (1982).

[Fei83] Feinberg J., Opt. Lett. **8**, 569 (1983).

[Fei85] Feinberg, J. and Bacher, G. D., Opt. Lett. **9**, 420 (1985).

[Fei86] Feinberg J. and Bacher G. D., Appl. Phys. **48**, 570 (1986).

[Fis81] Fischer, B, Cronin-Golomb, M., White,J. O., and Yarv, A., Opt. Lett. **6**, 519 (1981).

[Fis87a] Fischer, B, Weiss S. and Sternklar, S., Appl. Phys. Lett. **50**, 483 (1987).

[Fis87b] Fische,r B. and Sternklar, S., Appl. Phys. Lett. **51**, 74 (1987).

[Fis87c] Fischer, A. D., Lippincott, W. L., and Lee, J. N., Appl. Opt. **26**, 5039 (1987).

[Fis89] Fischer, B., Sternklar, S and Weiss, S., IEEE J. Quantum Electron. **25**, 550 (1989).

[For89] Ford, J. E., Fainman, Y., and Lee, S. H., Appl. Opt. **28**, 4808 (1989).

[Gab48] Gabor, D., Nature (London) **161**, 777 (1948).

[Gao94] Gao, X., Sasaki, A., and Zhang, Y., Opt. Commun. **106**, 258 (1994).

[Gar93] Garrett, M. H., Chang, J. Y., Jenssen, H. P., and Warde, C., Opt. Lett. **18**, 405 (1993).

[Ger67] Gerritsen, H. J., Appl. Phys. Lett. **10**, 237 (1967).

[Gon93] Gong J., Chen J., and Yue Z, Laser Tech., **17**, 205 (1993).

[Goo68] Goodman, J. W., *Introduction to FOURIER OPTICS*, McGRAW-HILL (1968).

[Gru93] Gruneisen, M. T., Chakmakjian, S. H., Seeberger, E. D., Lockett, D. D., and Clayton, C. M, Opt. Commun. **100**, 173 (1993).

[Gün] Günter, P., Voit, E., Zha, M. Z., Albers, H., Opt. Commun. **55**, 210 (1985).

[Gün] Günter, P. and Huignard, J-P. ed., *Photorefractive Materials and Their Applications I: Fundamental phenomena* (Springer-Verlag, Berlin, 1988).

[Gün] Günter, P. and Huignard, J-P. ed., *Photorefractive Materials and Their Applications II: Servey of applications* (Springer-Verlag, Berlin, 1989).

[Hal85] Hall, T. J., Jaura, R., Connors, M. L., and Foote, P. D., Prog. Quantum Electron **10**, 77 (1985).

[He88] He, Q. C., IEEE J. QE-**24**, 2507 (1988).

[he89] He, Q. C., Duthie, G., and Gregory, D. A., Opt. Lett. **14**, 757 (1989).

[He90] He, Q. C. and Duthie, G., Opt. Commun. **75**, 311 (1990).

[He95] He, Q. C. and Yeh, P., Appl. Phys. B**60**, 47 (1995).

[Hea84] Heaton, J. M, Mills, P. A., Paige, E. G. S. Solymer, L., and Wilson, T, Optica Acta **31**, 885 (1984).

[Hel77] Hellwarth, R. W., J. Opt. Soc. Am. **67**, 1 (1977).

[Hen89] Henderson, G. N., Walkup, J. F., and Bochove, E. J., Opt. Lett., **14**, 770 (1989).

[Hil89] Hillman, P. D. and Marciniak, M., J. Appl. Phys. **66**, 5731 (1989).

[Hin84] Hinton, G. F., Sejnowski, T. J., and Ackley, D. H., Carnegie-Mellon Univ. Tech. Rep. **CMU-CS-84-119** (1984).

[Hop82] Hopfield J. J., Proc. Natl. Acad. Sci. USA **79**, 2554 (1982).

[Hop86] Hopfield, J. J. and Tank, D. W., Science **233**, 625 (1986).

[Hor89] Horner, J. L. and Makekau, C. K., Appl. Opt. **28**, 5199 (1989).

[How86a] Howes, W. L., Appl Opt. **25**, 473 (1986).

[How86b] Howes, W. L., Appl Opt. **25**, 3167 (1986).

[Ivl92] Ivleva,L. I., Mamaev, A. V., Polozkov, N. M., Shkunov, V. V., Vlasenko, S. V., and Zozulya, A. A., Opt. Commun. **93**, 107 (1992).

[Jag91] Jagannath, H. and Venkateswarlu, Opt. Commun. 85, 443 (1991).

[Jen93] Jenkins B. K., 4th International Conference on Holographic Systems, Components and Applications, Neuchatel, IEE No **379**, 21 (1993).

[Jos90] Joseph, J., Pillai, P. K. C., and Singh, K., Opt. Commun. **80**, 84 (1990).

[Kac94a] Kaczmarek, M., L. Solymar, and Pun, P., Opt. Commun **108**, 176 (1994).

[Kac94b] Kaczmarek, M., Richer, I., and Solymar, L., J. Opt. Soc. Am **B11**, 136 (1994).

[Kac95a] Kaczmarek, M., R. W, Garrett M. H., and Rytz, D., **Photorefractive Materials, Effects, and Devices '95**, Aspen Lodge, Colorado, USA, June 11-14, **ME1**, 132 (1995).

[Kac95b] Kaczmarek, M., and Eason, R. W, Opt. Lett **20**, 1850 (1995).

[Kan90] Kang, H., Yang, C. X., Mu, G. G., and Wu, Z. K., Opt. Lett. **15**, 637 (1990).

[Kia88] Kiamer, M. A., Sifuentes, S., and Clayton, C. M., Appl. Opt. **27**, 1371 (1988).

[Kir91] Kirillov, D. and Feinberg, J., Opt. Lett. **16**, 1520 (1991).

[Kog65] Kogelnik, H., Bell. Syst. Tech. J. **44**, 2451 (1965).

[Kog69] Kogelnik, H., Bell. Syst. Tech. J. **48**, 2909 (1969).

[Koh93] Kohler, B, Bernet, S., Renn, A., and Wild, U. P., Opt. Lett. **18,** 2144 (1993).

[Kon92] Kong, H., Cronin-Golomb, M., and Fischer, B., Opt. Commun. **93**, 92-98 (1992).

[Koh84] Kohonen, T., Springer Series No. **8** (Springer Berlin, 1984).

[Kor95] Korneev, N. A. and Sochava, S. L., Opt. Commun. **115**, 539 (1995).

[Kra88] Kramer, M. A., Sifuentes, S., and Clayton, C. M., Appl. Opt. **27**, 1371 (1988).

[Kro87] Krolikowski W. and Belic M, Opt. Lett. **13**, 149 (1987).

[Kuk74] Kukhtarev, N., Markov, V. B., Odulov, S. G., Soskin, M. S., and Vinetskii ibid. **22**, 961 (1974).

[Kuk79a] Kukhtarev, N., Markov, V. B., Odulov, S. G., Ferroelectronics **22**, 949 (1979).

[Kuk79b] Kukhtarev, N., Markov, V. B., Odulov, S. G., Ferroelectronics **22**, 961 (1979).

[Lee89] Lee, L. S., Stoll, H. M., and Tackitt, M. C., Opt. Lett. **14**, 162 (1989).

[Lem93] Lembcke, J., Denz, C., Barnes, T. H., and Tschudi, In *Topical Meet., PRM'93 KIEV, UKRAINE, Aug. 11-15*, **SaC02**, 574-577 (1993).

[Lev74] Levenson, M. D. and Bloembergen, N., Phys Rev. B**10**, 447 (1974).

[Lev81] Levenson, M. D., Johnson, K. M., Hanchett, V. C., and Chiang, K., J. Opt. Soc. Am. **71**, 737 (1981).

[Lia93a] Lian, Y., Dou, S. X., Dao, H., Zhu, Y., Wu, X., Yang, C., and Ye, P., Opt., Lett. **19**, 610 (1993).

[Lia93b] Lian, Y., Gao, H., Ye, P., Guan, Q., and Wang, J., Appl. Phys. Lett **63**, 1745 (1993).

[Lia94a] Lian, Y., Dou, S. X., Dao, H., Zhu, Y., Wu, X., Yang, C., and Ye, P., Opt., Lett. **19**, 610 (1994).

[Lia94b] Lian, Y., Dou, S. X., Zhang, J., Gao, H., Zhu, Y., Wu, X., Yang, C., and Ye, P., Opt. Commun. 110, 192-196 (1994).

[Lia94c] Lian, Y., Gao, H., Dou, S. X., Wang, H., Ye, P., Guan, Q., and Wang, J., Appl. Phys. B**59**, 655 (1994).

[Lia94d] Lian, Y., Gao, H., Dou, S. X., Wang, H., Ye P., Guan, Q., and Wang, J., Appl. Phys. B**59**, 655 (1994).

[Mac83] MacDonald, K. R. and Feinberg, J., J. Opt. Soc. Am.**73**, 548 (1983).

[Mag94] Magnusson, R. and Gaylord, T. K., Appl. Opt. **13**, 1546 (1974).

[Mak65] Maker, P. D. and Terhune, R. W., Phys. Rev. A**137** (1965).

[Mam91] Mamaev A. V. and Shkunov V. V., Opt. Lett. 16, 1144 (1991).

[Man90] Maniloff, E. S. and Johnson, K. M., Opt. Eng. **29**, 225 (1990).

[Man90] Maniloff, E. S. and Johnson, K. M., Appl. Phys. **70**, 4702 (1990).

[Man93] Maniloff E. S., Graf F., Altner J. B., Bernet S., Renn A., and Wild U. P, SPIE Proc. **2026,** 592 (1993).

[Mao91] Mao, Z. Q., Selviah, D. R., Tao, S., and Midwinter, J. E., Third Int. Conf. Holographic Systems, IEE **342**, 132 London, U. K (1991).

[Mao92] Mao, Z. Q., PhD Thesis, University of London (1992).

[Mar79] Markov, A., Odulov, S., and Soskin, M., Opt. Laser Tech. **11**, 95 (1979).

[Mar81] Marrakchi, A., Huignard, J. P., and Günter, P., J. Appl. Phys. **24**, 131 (1981).

[Maz93] Mazur, A. P., Novikov, S. G., Odulov, S. G., Soskin, M. S., and Vasnetsov, M. V., J. Opt. Soc. Am B10, 1408 (1993).

[McM87] McMichael, L., Beckwith, P., and Yeh, P., Opt. Lett. **12**, 507 (1987).

[Mde90] Medrano, C., Ingold, M., and G nter, P., Opt. Commun. **77**, 411 (1990).

[Mde94] Medrano, C., Ingold, M., Berents, S., Bernasconi, P., and G nter, P, J. Opt. Soc. Am. B **11**, 1718 (1994).

[Mok91] Mok, F. H," Opt. Lett., **16**, 605 (1991).

[Mok92] Mok, F. H. and Stoll, H. M., *Proc. SPIE Optical Pattern Recognition III.* **1701**, 312 (1992).

[Mok93] Mok, F. H., Opt. Lett., **18**, 915 (1993).

[Mon90] Montemezzani, G. and Günter, P., J. Opt. Soc. Am. B. **7**, 2323 (1990).

[Mon95] Montemezzani, G., Zozulya, A. A., Zgonik, M., Czaia, L., Anderson, D. Z., and Günter, P., OSA Photorefractive materials, Effects, and Devices Conference Proc., Estes Park, Colorado, **MPB15** 192-195 (1995).

[Odu84] Odulov, S. G. and Sukhoverkhova, L. G., Kvantovaya Elektron **11**, 575 (1984).

[Odu87] Odulov, S. G. and Oleinik, O. I., Sov. J. Quantum Electron. **17**, 562 (1987).

[Ogu90] Ogusu, M., Tanaka, S.-I., and Kuroda, K., Jpn. J. Appl. Phys. **29**, 1265 (1990).

[Orl94] Orlov, S., Segev M., and Yariv, A., Opt. Lett. **19**, 578 (1994).

[Owe87a] Owechko, Y., Appl. Opt. **26**, 5104 (1987).

[Owe87b] Owechko, Y., Dunning, G. J., Marom, E., and Soffer, B. H., Appl. Opt., **26**, 1900 (1987).

[Owe89a] Owechko, Y.; Dunning G. J., Marom, E., and Soffer, B. H., Appl. Opt. **26**, 566 (1989).

[Owe89b] Owechko, Y., IEEE J. Quantum Electron. **25**, 619 (1989).

[Owe90] Owechko, Y., Proc. SPIE **1359**, 142 (1990).

[Owe91a] Owechko, Y. and Soffer, B. H., Proc. SPIE **1455**, 136 (1991).

[Owe91b] Owechko, Y. and Soffer, B. H., Opt. Lett. **16**, 675 (1991).

[Owe93a] Owechko, Y., OSA Optical Computing topical meeting technical digest (Palm Springs, California), 7, 92 (1993).

[Owe93b] Owechko, Y., Private Communication (1993)

[Owe93c] Owechko, Y. and B. H. Soffer, In *Topical Meet. PRM'93 KIEV, UKRAINE, Aug. 11-15*, **SaC01**, 570 (1993).

[Yeh89] Yeh, Appl. Opt. 28, 1961 (1989).

[Pel90] Peltier, M. and Micheron, F., J. Appl. Phys. **48**, 3683 (1990).

[Pep89] Pepper, D. M., Phy. Rev. Lett. **62**, 2945-2948 (1989).

[Pet90] Peterson, C., Redfield, S., Keeler, J. D., and Hartman, E., Opt. Eng. **29**, 359 (1990).

[Psa85] Psaltis, D. and Farhat, N., Opt. Lett. **10** 98 (1985).

[Psa87] Psaltis, D., Yu, Y., Gu, G., and Lee, H., In *Proc. Optical Computing Meet., Lake Tahoe, OSA CA, March 18-20*, 129 (1987).

[Psabba] Psaltis, D., Siders, A., and Yamamura, A. A., IEEE Control Syst. Mag, April, 17-21 (1988).

[Psa88b] Psaltis, D., Brady, D., and Wagner, K., Appl. Opt. **27**, 1752 (1988).

[Psa90] Psaltis, D., Brady, D., and, Gu, X. G., and Lin, S., Nature (London). **343** 352 (1990).

[Qia93] Qiao, Y., Orlov, S., and Psaltis, D., Opt. Lett. **18**, 1004 (1993).

[Qiu93a] Qiu, Y. S., Li, H., Lu, T. S., Zhuang, J., and Gao, X. C., Opt. Commun., **98**, 29 (1993).

[Qiu93b] Qiu, Y. S., Lu, T. S., Zhuang, J., and Gao, X. C., Opt. Lett., **18**, 143 (1993).

[Raj89] Rajbenbach, H., Dellboulbe, A., and Huignard, J. P., Opt. Lett. **14**, 1275 (1989).

[Rab91] Rabinovich, W. S., Feldman, B. J., and Gillbreath, G. C., Opt. Lett. **16**, 1147 (1991).

[Rak92] Rakuljic, G. A., Leyva, V., and Yariv, A., Opt. Lett. **17**, 1471 (1992).

[Rem86a] Remelhart, D. E. and McCelland, J. L. (eds), *Parallel Distributed Processing*, MIT, Cambridge, MA (1986).

[Rem86b] Remelhart, D. E., Hinton, G. E., and Williams, R. J., Nature (London), **343**, 325 (1986).

[Riug93] Riu, Y. S., Lu, T. S., Zhuang, J., and Gao, X. C., Opt. Lett. **18**, 143 (1993).

[Rod87] Rodriguez, J., Siahmakoun, A., Salamo, G., Miller, M. J., Klerk III, W. W., Wood, G. L., Sharp, J. L., and Neurgaonkar, R. R., Appl. Opt. **26**, 1732 (1987).

[Ros92] Ross, G. W. and Eason, R. W., Opt. Lett. **17**, 1104 (1992).

[Ros93] Ross, G. W., Hribek, P., Eason, R. W., Garrett, M. H., and Rytz, D., Opt. Commun. **101**, 60 (1993).

[Ryt89] Rytz, D. and Zhong, S. D., Appl. Phys. Lett. **54**, 2625 (1989).

[Sal91] Salamo, G. J., Monson, B. D., Clark III, W. W., Wood, G. L., Sharp, E. J.,
and Neurgaonkar, R. R., Appl. Opt. **30**, 1847 (1991).

[Seg87] Segev M., Weiss S and Fischer B, Appl. Phys. Lett. **50**, 1397 (1987).

[Seg91] Segev M. and Yariv A., Opt. Lett. **16**, 1938-1940 (1991).

[Seg93] Segev M., Engin D., Yariv A., and Valley G. C., Opt. Lett. **21**, 1828 (1993).

[Sel90] Selviah, D. R., Mao, Z. Q., and Midwinter, J. E., Elec. Lett. **26**, 1954 (1990).

[Sel91] Selviah, D. R., Mao, Z. Q., and Midwinter, IEE Proc. **349**, 59 (1991).

[Sel93] Selviah D. R. and Chang C. C., OSA Photorefractive Materials, Effects and Devices conference proceedings, PRM'93, Kiev, Ukraine, 6.1-6.4 (1993).

[Sel94] Selviah D. R., *"Optical Computing, Encyclopedia of Advanced Materials,"* Eds. Bloor, D.; Brook, R. J.; Flemings, M. C. and Mahajan, S., Pergamon Press, (Oxford) **3**, 1820 (1994).

[Sha89] Shamir, J., Caufield, H. J., and Johnson, R. B., Appl. Opt. **28**, 311 (1989).

[Sha90] Sharp, E. J., Clark III, W. W., Miller, M. J., Wood, G. L., Monson, B. D., Salamo, G. J., and Neurgaonkar, R. R., Appl. Opt. **29**, 743 (1990).

[Sha92a] Shaw, K. D., Opt. Commun. **90**, 133 (1992).

[Sha92b0] Shaw, K. D., Opt. Commun. **94**, 458 (1992).

[Shi93] Shimura,T., Tamura, M. and Kuroda, K., Opt Lett. **18**, 1645 (1993).

[Smo87] Smount, A. M. C. and Eason, R. W., Opt. Lett. **12**, 498 (1987).

[Soc90] Sochava, S. L., Rossomakhin, I. M., and Stepanov, S. I., Opt. Commun. 78, 72 (1990).

[Sof86a] Soffer, B. H., Marom, E., Owechko, Y., and Dunning, G., Liquid Crystals and Spatial Light Modulator Materials, SPIE **684**, 2 (1986).

[Sof86b] Soffer, B. H., Dunning, G. J., Owechko, Y., and Marom, E., Opt. Lett **11**, 118 (1986).

[Sof90] Soffer, B. H., Owechko, Y., and Dunning, G. D., Optics in Complex Systems, SPIE **1319**, 196 (1990).

[Spe86] Special issue on dynamic gratings and four-wave mixing, IEEE J. Quantum Electron. QE-**22** (1986).

[Sta72] Staebler, D. J. and Amodei, J. J., J. Appl. Phys. **43**, 1042 (1972).

[Ste71] Stepanov, B. L., Ivakin, E. V., and Rubanov, A. S., Sov. Phys. Dokl. Tech. Phys. **16**, 46 (1971).

[Ste89] Stepanov, S. I., Petrov, M. P., and Sochava, S. L., Ferroelectrics **92**, 199 (1989).

[Ste86] Sternklar, S., Weiss, S., Segev, M., and Fischer, B., Opt. Lett. **11**, 528 (1986).

[Ste95] Sternklar, S., Opt. Lett. **20**, 249 (1995).

[Tak93] Takahasi, H., Zaleta, D., Ma, J., Ford, J. E., Fainman, Y., and Lee, S. H., OSA Optical Computing topical meeting technical digest (Palm Springs, California), 7, 254 (1993).

[Yan91] Tanaka, Y., Chen, Z., Kasamatsu, T., and Shiosaki, T., Jpn. J. Appl. Phys., 30(9B), Part 1, 2359 (1991).

[Tao93a] Tao, S., Selviah, D. R., and Midwinter, J. E., Opt. Lett., **18**, 912 (1993).

[Tao93b] Tao, S., PhD Thesis, University of London (1993).

[Tao94] Tao S., Song Z. H., and Selviah D. R., Opt. Commun., **108** 144 (1994).

[Tao95] Tao S., Song Z. H., and Selviah D. R., Appl.Opt., **34** 6729 (1995).

[Tik91] Tikhonchuk, V. T., Zhanuzakov M. G., and Zozulya A. A., Opt. Lett. 16, 288 (1991).

[Tom94] Tomita, Y. and Suzuki, A., Appl. Phys. A **59**, 579 (1994).

[Tro95] Troth, R. C, Ramos-Garcia, R., and Damsen M. J., Opt. Commun. **116**, 435 (1995).

[Vai87] Vainos, N. A. and Eason, R. W., Opt. Commun. **62**, 311 (1987).

[Val83] Valley, G. C. and Klein, M. B, Opt. Eng. 22, 704 (1983).

[Val84] Valley, G. C., J. Opt. Soc. Am. **B1**, 868 (1984).

[Val92] Valley, G. C., J. Opt. Soc. Am. **B9**, 1440 (1992).

[Vas91] Vasquez, R. A., Vaches, F. R., Neurgaonkar, R. R., and Ewbank, M. D., J. Opt. Soc. Am. **B8**, 1932 (1991).

[Vie91] Vieux, V., Gravey, P., Wolffer, N., and Picoli, G., Appl. Phys. Lett 58, 2880 (1991).

[Vin79] Vinetskii, L., Kukhtarev, N. V., Odulov, S. G., and Soskin, M. S., Sov. Phys. Usp. **22**, 742 (1979).

[Wan87] Wagner, K. and Psaltis, D., Appl. Opt. **26**, 5061 (1987).

[Wan91] Wagner, K. and Slagle, T., OSA Optical Computing topical meeting technical digest (Salt Lake City), **6**, 280 (1991).

[Wan89] Wang, D., Zhang, Z., Zhu, Y., Zhang, S. and Ye, P., Opt. Commun. **73**, 495 (1989).

[Wei87a] Weiss, S., Sternklar, S. and Fischer, B., Opt. Eng. **26**, 423 (1987).

[Wei87b] Weiss, S., Sternklar, S., and Fisher, B. Opt. Lett. **12**, 144-146 (1987).

[Whi82] White, J. O., Cronin-Golomb, M., Fisher, B., and Yariv, A., Appl. Phys. Lett. **40**, 450 (1982).

[Whi88] White, H. J., Aldridge, N. B., and Lindsay, I., Opt. Eng., **27**, 30-37 (1988).

[Wil88] Widrow, B., Winter, R. G., and Baxter, R. A., IEEE Trans. Acoust. Speech. Sig. Process., **36**, 1109-1118 (1988).

[Wil93] Wild, U. P., Bernet, S., Altner, S., Maniloff, E. S., and Renn, A., Optical Computing Topical Meeting Technical Digest, Palm Springs, California, **7**, 60 (1993).

[Wol89] Wolffer, N., Gravey, P., Moisan, J. Y., Laulan, C., and Launay, J. C., Opt. Commun. **73**, 351 (1989).

[Wol92] Wolffer, N., Gravey, P., Picoli, G., and Vieux, V., Opt. Commun. **89**, 17 (1992).

[Wol94] Wolffer, N. and Gravey, P., Opt. Commun. **107**, 115 (1994).

[Wri94] Wright, M. W. and McInerney, J. G., Opt. C ommun. **110**, 689 (1994).

[Wu93a] Wu, C. and Zhao, Y., Opt. Lett. **18**, 98 (1993).

[Wu93b] Wu, X., Hu X., Shao, Z., Chen, H., and Shong, Y., Opt. Commun. **101**, 381 (1993).

[Xu90] Xu, H., Yuan, Y., Yu, Y., Xu, K., and Xu, Y., Appl. Opt. **29**, 3375 (1990).

[Xu91] Xu, J., Wu, Y., Liu, S., Zhang, G., Sun, D., Song, Y., and Chen, H, Opt. Lett. **16**, 1255 (1991).

[Yab74] Yablonowitch, E., Bloembergen, N., and Wynne, J. J., Phys. Rev. **B10**, 447 (1974).

[Yan94] Yang, C., Zhu, Y., Hui, M., Niu, X., Liu, H., and Wu, X., Opt. Commun. **109**, 318 (1994).

[Yan96] Yang, C., Zhang, Y., Yeh, P., Zhu, Y., and Wu, X., Opt. Commun. **113**, 416 (1995).

[Yar76] Yariv, A., Appl. Phys. Lett. **28**, 88 (1976).

[Yar77] Yariv, A. and Pepper, D. M., Opt. Lett **1**, 166 (1977).

[Yar78] Yariv, A, IEEE J. Quantum Electron. **QE-14**, 650 (1978).

[Yar86a] Yariv, A. and Kwong, S. K, Opt. Lett. **11**, 186 (1986).

[Yar86b] Yariv, A., Kwong, S. K, and Kyuma, K, Appl. Phys. Lett. **48**, 1114 (1986).

[Yar91] Yariv, A., in Optical Electronics, 4th edition, Saunders College Publishing, Holt, Rinehart and Winston, Inc., 654 (1991).

[Yau92] Yau, H. F., Tong, Y. P., Chang, C. C., and Wang, N. C., Opt. Commun., **89**, 457 (1992).

[Yeh84] Yeh, P., Appl. Opt. 23, 2974 (1984).

[Yue92] Yue, X., Shao, Z., Lu, X., Song, Y., and Chen, H., Opt. Commun. **89**, 59 (1992).

[Zel72] Zel'dovich, Ya. B., Popovivhev, V. I., Ragul'skiy, V. V., and Faizullov, F. S., Sov. Phys. JETP **15**, 109 (1972).

[Zha90] Zhang, H. Y., He, X. H., Chan, E., and Liu, Y., Appl. Phys. Lett **57**, 1298 (1990).

[Zha93] Zhan Y., Lu M., Liu W., and Mu G., Chinese Journal of Lasers, **20**, 593 (1993).

[Zho86] Zhong, S. D., Mater. Res. Bull. **21**, 1375 (1986).

[Zhu94] Zhu, Y., Yang, C., Hui, M., Niu, X., Zhang, J., Zhou, T., and Wu, X., Appl. Phys. Lett. **64**, 2341 (1994).

[Zoz91] Zozulya ,A A., Opt. Lett. **16**, 545 (1991).

[Zoz93] Zozulya, A. A., IEEE J. Quantum Electron. **QE-29**, 538 (1993).

[Zoz94] Zozulya, A A., Saffman, M., and Anderson, D. Z., Phys. Rev. Lett. **73**, 818 (1994).

[Zoz95] Zozulya, A A., Saffman, M., and Anderson, D. Z., J. Opt. Soc. Am **B12**, 255 (1995).

PUBLICATIONS AND PATENT

Ariving from research directly carried out for the PhD

1. David R. Selviah and **Chi Ching Chang**, "*Multi-beam Induced Phase Conjugation (MIPC) in a Barium Titanate Crystals*," **OSA Topical Meeting on Photorefractive Materials, Effects, and Devices '93**, Kiev, Ukraine, Aug. 11-15, PD6.1-PD6.4 (1993).
2. **Chi Ching Chang** and David R. Selviah, " *High efficiency photorefractive storage for multimode phase-conjugate resonators,* " **International Conf. on Optical Computing '94**, Edinburgh, UK, PD12.27-PD12.28 (1994).
3. **Chi Ching Chang** and David R. Selviah, " *High efficiency photorefractive storage for multimode phase conjugate resonators,* " IOP (UK), Optical Computing **139**, 439-442 (1994).
4. **Chi Ching Chang** and David R. Selviah, " *Mutually Pumped Phase-Conjugate Mirror: Fish-Head Configuration,*" Opt. Lett. **20**, 677-679 (1995).
5. **Chi Ching Chang** and David R. Selviah, "*Self-Pumped Phase-Conjugate Mirror "-C Curve Configuration" in Photorefractive $BaTiO_3$ Crystals,*" **Photorefractive Materials, Effects, and Devices '95**, Aspen Lodge, Colorado, USA, June 11-14, **TPC3**, 280-283 (1995).
6. **Chi Ching Chang** and David R. Selviah, "*Mutually Pumped Phase-Conjugate Mirror "Fish-Head" Configuration in Photorefractive Barium Titanate Crystals,*" **Photorefractive Materials, Effects, and Devices '95**, Aspen Lodge, Colorado, USA, June 11-14, **TPC4**, 284-287 (1995).
7. **Chi Ching Chang** and David R. Selviah, "*Arch Double Phase Conjugation in Photorefractive $BaTiO_3$ Crystal,*" **The Pacific Rim Conference on Lasers and Electro-Optics**, Chiba, Japan, July11-14, **FM4**, 207-208 (1995).

8. **Chi Ching Chang** and David R. Selviah, " *Phase Conjugation Apparatus and Method of Phase Conjugating Light*," Patent **UK9506180.0,** 27 March 1995 (Pending).
9. David R. Selviah and **Chi Ching Chang**, " *Self-pumped phase-conjugate resonators and mirror for use in optical associative memories,*" Optics & Lasers in Eng. **23**, 145-166 (1995).
10. **Chi Ching Chang** and David R. Selviah, " *-C Curve Configuration (-C^3) Photorefractive Self-Pumped Phase Conjugator*," to be published in Opt. Commun. forthcoming issue (1995).

Page No.	**Para. No.**	**Line No.**	**Original Statement in Thesis**	**Corrigenda**
11		14	*BaTiO3* and $LiNbO_3$......	$BaTiO_3$ and $LiNbO_3$......
14		6	However, *practial*......	However, *pratical*......
15		12	Gbits/*cm2* [Koh93......	Gbits/cm^2 [Koh93......
15		16	*3o*C peresistence times......	3^oC peresistence times......
15		22	1 *cm3* to 3 *cm3*......	1 cm^3 to 3 cm^3......
15		23	12.3 *MBit*/cm^3 through 35.2 *Mbit*/cm^3 to 0.23 *gbit*/cm^3......	12.3 *MBits*/cm^3 through 35.2 *Mbits*/cm^3 to 0.23 *Gbits*/cm^3......

Page No.	Para. No.	Line No.	Original Statement in Thesis	Corrigenda
2	1	1	most helpful *advise*......	most helpful *advice*......
4		12	*Phtorefractive* phase-conjugate..	*Photorefractive* phase-conjugate..
9		12	*mutl*-beam induced phase-......	*multi*-beam induced phase-......
10		2	*TIR*: two-interaction regions......	*TIRs*: two-interaction regions......
10		3	*twe*-wave mixing....:	*two*-wave mixing......

Page No.	Para. No.	Line No.	Original Statement in Thesis	Corrigenda
38	1	6	And, the boundary *condition*......	And, the boundary *conditions*......
38	1	6	$A_2(0)=A_4(0)$......	$A_2(0)=A(0)$......
40	2	8	the *phptorefractive* media......	the *photorefractive* media......
41	Fig. 2.10	4	reflection from *acorner* of......	reflection from *a corner* of......
42	2	8	loops back *k* into the......	loops back into the......
42	3	2	In order *for comparing* with......	In order *to compare* with......
42	4	2	*Abeam* entering the crystal......	*A beam* entering the crystal......
42	4	5	The edge *act* as a two-......	The edge *acts* as a two-......
44	1	3	Phase-conjugate *reflectevities*......	Phase-conjugate *reflectivities*......
45	2	1	It is worth *mentioned* that......	It is worth *mentioning* that......
46	Fig. 2.13	3	inducing *be* is turned on......	inducing *beam* is turned on......
47	1	10	In last three years,......	In *the* last three years,......
47	1	11	*reaserch* we have obtained......	*research* we have obtained......
47	1	11	such as *muti*-beam induced....	such as *multi*-beam induced....
47	1	12	phase-conjugate *nirror* and.....	phase-conjugate m*irror* and.....
48	3	5	*othe* beam......	*other* beam......
49	1	12	internal *reflecitons* that the......	internal *reflections* that the......
49	2	2	*foreach* of the *MPPCs*......	*for each* of the *MPPCMs*......
49	2	2	*bendfits* to be derived from......	*benefits* to be derived from......
49	2	3	*magnitude of* the magnitude of.....	the magnitude of.....
49	2	4	the *phase-conjugat* signal......	the *phase-conjugate* signal......
50	Fig. 2.15	in Fig. (a)	the c-axis direction *from top to bottom.*	the c-axis direction *from left to right.*
51	2	8	(i) there *has* a slightly......	(i) there *is* a slightly......
52	2	3	*It was found that.* Theoretically..	Theoretically..
52	4	2	show that *theycan* act as......	show that *they can* act as......
52	4	2	give the most *promise*......	give the most *promising*......
53	1	5	and discussed here......	and *are* discussed here......
53	2	5	and addresses *to* a $LiNbO_3$......	and addresses a $LiNbO_3$......
53	Fig. 2.17	in Fig.	*Substrater*	*Substrate*
54	3	2	lasers *to* be locked......	lasers be locked......
55	Fig. Capt.	5	*o* the master laser *[Feinberg86]*..	*of* the master laser *[Fei86]*..
58	1	1	After Fourier *transform*......	After Fourier *transformation*......
58	1	4	and stands for convolution......	and * stands for convolution......
58	3	5	such in numerical algrorithms.....	such *as* in numerical algrorithms.....
58	4	10	*resonators*. Because the......	*resonates*. Because the......
59	Fig. Capt.	2	(a) *Recrding* the hologram......	(a) *Recording* the hologram......
59	Fig. Capt.	3	Optical gain is provided TWM....	Optical gain is provided *by* TWM....
59	1	3	show later that *can* even......	show later that *an* even......
59	2	5	an argon laser *has* available......	an argon laser *is* available......
59	3	1 & 2	*The self-pumped phase-conjugate mirror configurations that need no txternal mirrors and which are both self-starting in photorefractive $BaTiO_3$ crystals.*	*The self-pumped phase-conjugate configurations need no external mirrors and which are self-starting in photorefractive $BaTiO_3$ crystals.*
59	3	5 & 6	*This gives the most promising of applicable in practice systems.*	*This gives the most promising of application in practice systems.*
60	1	6	*Barium Titanate* for phase......	*barium titanate* for phase......
60	1	2	*Rhodium* doped *Barium Titanate.*	*rhodium* doped *barium Titanate*
60	1	3	semiconductor *laser*......	semiconductor *lasers*......

Page No.	Para. No.	Line No.	Original Statement in Thesis	Corrigenda
18	1	12	which mainly *occurrs* in......	which mainly *occurs* in......
19	1	10	*summary* in Section 2.8......	*summarise* in Section 2.8......
19	2		2.1 Optical *phase* Conjugation (OPC)	2.1 Optical *Phase* Conjugation (OPC) *[Eas93]*
20	1	12	such as *most*, gases, liquids......	such as, gases, liquids......
20	2	11	*gyros copes[*Yeh85 & 86......	*gyroscopes [*Yeh85 & 86......
20	2	12	concerned *and* mainly with......	concerned mainly with......
21	2	2	conjugation is *an* nonlinear......	conjugation is *a* nonlinear......
22	1	6	in following subsection......	in *the* following subsection......
22		2.1.2	phase-conjugate light *wave*......	phase-conjugate light *waves*......
23	1	6	*One* the other hand, if......	*On* the other hand, if......
23	Fig. 2.3	2	its *phas*-conjugate......	its *phase*-conjugate......
25	1	1	space-charge electric *filed*......	space-charge electric *field*......
25	2	2	a *sinsoidal* interference......	a *sinusoidal* interference......
25	2	2	produced by *interfer* of two......	produced by *interference* of two......
26	Fig. 2.5	in figure	*Prob*	*Probe*
27	2	3	can be treated *similarity*......	can be treated *similarly*......
27	4	last line	the form $\Delta n(r) = n_1 \sin qx$	the form $\Delta n(r) = n_1 \sin qx$, *where n_1 is an index mudulation amplitude.*
28	Fig. 2.6.	1	a pair of *interfering*......	a pair of *interfering beams*......
28	Fig. 2.6	4	medium via *Pockel's* effect......	medium via *Pockels* effect......
28	1	2	energy between *tow*......	energy between *two*......
28	1	5	*A asymmetric* two-......	*Asymmetric* two-......
28	1	8	of the *example*, and optical......	of the *sample*, and optical......
29	1	7	The *electrical* charracteristics......	The *physical* charracteristics......
29	Table2.1		*Transition*	*Mobility*
29	Table2.1		*43mm, 4mm*	*43m, 4m*
30	Table2.1		*43mm*	*43m*
31	4	6	both beams *ate polarized*......	both beams *are polarised*......
32	eq. 2.11		$I=I_1+I_2=$......	$I_0=I_1+I_2=$......
33	1	5	its sign *depend* on the......	its sign *dependent* on the......
33	1	6	The parameter, n_1, *depending*.....	The parameter, n_1, *depends*.....
33	eq. 2.12		*A1*	A_1
33	2	7	the *incident* intensity absorption *per unit length*, and......	the intensity absorption *coefficient*, and......
33	3	1	are [*Feinberg80*]......	are [*Fei80*]......
34	2	3	at input face (z=0)......	at *the* input face (z=0)......
34	2	4	$I_2(z)\approx I_2(0)e^{\gamma z}$ indicating that......	$I_2(z)\approx I_2(0)e^{\gamma z}$ *(for no absorption $\alpha=0$)* indicating that......
34	2	7	there is *no* phase shift $\varphi\neq 0$......	there is phase shift $\varphi\neq 0$......
34	2	13	when a DC *filed* is applied......	when a DC *field* is applied......
36	2	3	four refractive index caused....	four refractive index *gratings* caused...
36	2	5	(a) a *transmission* grating......	(a) a *reflection* grating......
36	2	6	(b) a *reflection* grating......	(b) a *transmission* grating......
36	2	9	Consider the *transmission* case,....	Consider the *reflection* case,....
36	2	11	$\boldsymbol{k}_3=\boldsymbol{k}_2-\boldsymbol{K}_g=\boldsymbol{k}_2-\boldsymbol{k}_4+\boldsymbol{k}_1=\mathbf{k}_4$......	$\boldsymbol{k}_3=\boldsymbol{k}_2-\boldsymbol{K}_g=\boldsymbol{k}_2-\boldsymbol{k}_4+\boldsymbol{k}_1=-\mathbf{k}_4$......
36	3	2	we use the *kogelnik*......	we use the *Kogelnik*......
37	2	1	the *stead*-state solution,......	the *steady*-state solution,......
37	2	5	*reatining* the main features......	*retaining* the main features......
37	Fig. 2.9	in figure	$E_3(0)$, $E_4(0)$	$E_4(0)$,$E_3(0)$
38	Eq. 2.19		I_0^2	I_0

Page No.	Para. No.	Line No.	Original Statement in Thesis	Corrigenda
94	1	1	a lot of gratings *is* formed......	a lot of gratings *are* formed......
94	2	12	precise *arrangements*, the......	precise *arrangement*, the......
95	1	15	already been shown *[Nai87]*......	already been shown *[Vai87]*......
96	1	1	*the possible explanation for our results. Applications such as self-pumped phase-*	delete this sentence
97	Fig. 4.2	2	where the c-axis of the crystal *is*...	where the c-axis of the crystal ...
97	Fig. 4.2	3	*pointed* from the top to bottom.....	*points* from the top to bottom.....
98	1	3	fanning will *disappear*......	fanning will *be depressed*......
98	2	12	where γ_{21} and γ_{43} *and* are the...	where γ_{21} and γ_{43} are the...
100	2	1	According to *above the* analysis,..	According to the *above* analysis,..
101	1	1	(or MIBC), the FWM *take* place,.	(or MIBC), the FWM *takes* place,......
101	3	1	*establishmentof* SPPCM or......	*establishment of* SPPCM or......
101	4	4	intra-cavity étalon was tuned *the*..	intra-cavity étalon was tuned *to*...
101	4	7	the Newport *8x12 feet* optical......	the Newport optical......
103	2	6	*incident* (Fig. 4.6(a)). Beams......	*incidence* (Fig. 4.6(a)). Beams......
103	2	9	the bent beam *become* incident....	the bent beam *became* incident.....
104	2	3	range of fanning *grating* were......	range of fanning *gratings* were......
104	2	9	in detail in following sections.......	in detail in *the* following sections.......
105	2	2	may *return meet* the incident......	may *meet* the incident......
106	1	7	it will have good chance to meet...	it will have *a* good chance to meet....
106	3	3	to form provided the *grating*......	to form provided the *gratings*......
106	3	8	the phase conjugation occur......	the phase conjugation *to* occur......
106	3	13	the ISPPCM *giving* a much......	the ISPPCM *gives* a much......
106	4	1	*intensity-* and *polarisation-*......	*intensity* and *polarisation*......
107	Fig. 4.9	3	the input beams is kept *in*......	the input beams is kept *to*......
108	1	5	the higher intensity *speed* up......	the higher intensity *speeds* up......
108	1	9	phase conjugation can speeded....	phase conjugation can *be* speeded......
108	Fig. 4.10	1	the inducing time t_{ind} *in*......	the inducing time t_{ind} *for*......
110	1	5	It *suggest* that we were able to......	It *suggests* that we were able to......
110	3	1	at the end of previous section......	at the end of *the* previous section......
110	4	3	which much slower that for......	which *is* much slower *than* that for.....
111	Fig. 4.11	in figure	I_{ind} OFF	I_{in} OFF
111	2	3	Reason is once onset the......	*The* Reason is *that* once onset the......
111	2	7	two polarisation states *existing* in	two polarisation states in......
112	2	1	*theoretical* and experimentally....	*theoretically* and experimentally.....
114	1	5	beam coupler; *MIPC*)......	beam coupler; *MIBC*)......
114	1	6	Perhaps *MIPC* is occurring in......	Perhaps *MIBC* is occurring in......
114	2	1	In next experiment we examine....	In *the* next experiment we examine....
116	1	3	signal dropped *and* within the......	signal dropped within the......
116	1	5	as usual as *MIPC* whilst the......	as usual as *MIBC* whilst the......
121	1	1	we *investigated by adding* a......	we *added* a......
122	1	6	conditions *nexessary* for self-......	conditions *necessary* for self-......
122	1	7	angular ranges uniform phase-.....	angular ranges *with* uniform phase-....
122	1	9	conjugation in *there* cases.....	conjugation in *these* cases.....
125	1	Eq. 4.5	$P_0T\left[1-(r_1r_2)n\right]/(1-r_1r_2)$	$P_0\left[1-\left(r_1r_2T^2\right)^n\right]/\left(1-r_1r_2T^2\right)$
125	1	Eq. 4.6	$P_0T/(1-r_1r_2)$	$P_0/\left(1-r_1r_2T^2\right)$
127	1	1	holographic *grating* between......	holographic *gratings* between......
128	1	Eq. 4.7	$P_0\eta\left[1-(r_1r_2)n\right]/(1-r_1r_2)$	$P_0\left[1-\left(r_1r_2\eta^2\right)^n\right]/\left(1-r_1r_2\eta^2\right)$

Page No.	Para. No.	Line No.	Original Statement in Thesis	Corrigenda
61	1	5	*networks (ONNs)* is proposed,....	*network (ONN)* is proposed,....
61	1	10	*networks* (HOFNET) [Sel91]......	*network* (HOFNET) [Sel91]......
61	2	5	and two *photoreractive* phase-....	and two *photorefractive* phase-....
61	2	10	theoretically *analyses* our......	theoretically *analyse* our......
62	1	3	in Section *3.6*.......	in Section *3.5*.......
62	2	2	during last decade; other......	during *the* last decade; other......
62	2	14	in four [*Tao93*].......	in four [*Tao93b*].......
62	2	19	proposed resonator system......	proposed *a* resonator system......
65	4	1	resonator neural *networks*......	resonator neural *network*......
66	1	2	did not *demonstrated* it) and......	did not *demonstrate* it) and......
67	1	4	to be memorised *are* recorded......	to be memorised *is* recorded......
67	1	13	[Tao93] *arrange* all the......	[Tao93] *arranged* all the......
67	1	14	transform lens, *use* distinct......	transform lens, *used* distinct......
68	2	1	the back focal *lens*......	the back focal *plane*......
68	3	2	*an* reference plane wave......	*a* reference plane wave......
70	1	7	can be treated *similarity*......	can be treated *similarly*......
70	2	1	all the *object* memorised,......	all the *objects* memorised,......
70	2	2	is *address* by g_m (x,y) in the......	is *addressed* by g_m (x,y) in the......
72	1	5	resonant loop between *the*......	resonant loop between ......
74	1	16	componenta such viedo......	componenta such *as* ~~viedo~~...video
74	2	1	neural network (*HOFNET*)......	neural network (*HORNET*)......
74	2	7	describe in following chapter......	describe in *the* following chapter......
74	2	9	HOFNET *in* short) and is......	HOFNET *for* short) and is......
75	3	1	as shown Fig. 3.6(b),......	as shown *in* Fig. 3.6(b),......
76	1	2	instead of f as in Eq. *3.6*......	instead of f as in Eq. *3.5*......
76	1	6	factor is proportional to......	factor is *inversely* proportional to......
76	2	1	correlator as shown Fig. 3.7(a).....	correlator as *in* shown Fig. 3.7(a).....
76	2	6	this product and *images*......	this product and *Fourier transforms*...
78	1	4	(*Lc*=1 when lens Lc......	(*Pc*=1 when lens Lc......
78	3	8	the *convolution* of the functions...	the *correlation* of the functions...
80	2	4	storage *system*, such as......	storage *systems*, such as......
82	1	6	is unable to eliminated.......	is unable to *be* eliminated.......
83	2	5	holograms, is unable to......	holograms, is unable to *be*......
83	2	10	*optical* implement associative......	*optically* implement associative......
83	3	1	the diffraction *efficienies*......	the diffraction *efficiencies*......
83	3	2	we propose *on* novel......	we propose *a* novel......
83	3		*In this section in order for increasing the diffraction efficiencies of holograms stored in volume photorefractive medium we propose one novel photorefractive holographic storage in the use of 2 self-pumped phase-conjugate mirrors (SPPCMs) and demonstrate experimental results.*	*In this section we propose one novel photorefractive holographic storage in the use of 2 self-pumped phase-conjugate mirrors (SPPCMs) in order for increasing the diffraction efficiencies of holograms stored in volume photorefractive medium and demonstrate experimental results.*
86	1	3	direction *with the same phase*......	direction......
89	2	title	3.4.3 *Bragg-off* diffraction in *a*	3.4.3 *Braggoff* diffraction in......
90	2	4	level, which *eliminated* erasing...	level, which *reduced* erasing...
90	Table 3.1	in Table	$q=I_R/I_o$=33mW/33mW=*10*......	$q=I_R/I_o$=33mW/33mW=*1*......
90	Table 3.1	in Table	$q=I_R/I_o$=33mW/33mW=*1*......	$q=I_R/I_o$=33mW/33mW=*10*......

Page No.	Para. No.	Line No.	Original Statement in Thesis	Corrigenda
137	1	15	using single-*pusle* laser......	using single-*pulse* laser......
137	2	2	for SPPCMs using cw *laser*......	for SPPCMs using cw *lasers*......
141	1	8	*imputities* in one......	*impurities* in one......
141	2	2	*reflectivties*, response times,......	*reflectivities*, response times,......
141	3	4	densities of *150* mW/mm^2......	densities of *125* mW/mm^2......
143	3	4	*larger* coupling strength,......	*largest* coupling strength,......
143	3	5	intervals and the *observation*......	intervals and the *observations*......
143	3	6	*overview* of the crystal......	of the crystal......
144	Fig. Capt.	2	Around this *is* are figures......	Around this are figures......
145	Fig. Capt.	5	the less *intnese* detail......	the less *intense* detail......
146	Fig. Capt.	6	*intnese* detail......	*intense* detail......
148	2	5	to *optical* erase any residual......	to *optically* erase any residual......
149	2	8	where A is 2.46 and B=*-1.09*......	where A is 2.46 and B=*1.09*......
154	1	2	we can induce *on* of serval......	we can induce *one* of serval......
154	1	3	the pattern observable *are*......	the pattern observable *is*......
156	Fig. 5.16	in figure		*the aberrator should sit behind the beamsplitter*
157	Fig. Capt.	1	Phase distorted resolution......	*(a)* Phase distorted resolution......
158	1	9	*domanstrated* in the "-C^3"......	*demonstrated* in the "-C^3"......
159	1	6	the photorefractive effect,........	the photorefractive effect........
160	1	1	phase *shift* by $\pi/2$ relative to......	phase *shifted* by $\pi/2$ relative to......
160	Eq. 6.2		E_{sec}=......	E_{sce}=......
161	1	1	$\kappa_g=2/\Lambda_g$,......	$\kappa_g=2\pi/\Lambda_g$,......
161	1	3	N, of the *charge carriers*:......	N, of the *charges available for light-induced charge migration*:......
161	1	7	effective Pockels coefficient......	effective Pockels coefficient *[Fei82]*..
161	3	2	the input *beam* are......	the input *beams* are......

Page No.	Para. No.	Line No.	Original Statement in Thesis	Corrigenda
128	1	Eq. 4.8	$P_0\eta/(1-r_1r_2)$	$P_0/(1-r_1r_2\eta^2)$
128	Fig. 4.25	in figure	photodetector *1* (upper left)	photodetector *2* (upper left)
129	3	7	allow us to *use* reuse the crystal....	allow us to reuse the crystal....
131	1	3	*at and* angle of θ=30° at a......	*and at* angle of θ=30° at a......
131	1	4	the method reported in earlier......	the method reported in *an* earlier......
131	1	10	and is not a *ture* phase-conjugate	and is not a *true* phase-conjugate...
135	1	8	phase conjugate *beahviour*......	phase conjugate *behaviour*......
135	2	3	24 *eigen modes* were shown to.....	24 *eigenmodes* were shown to......
135	3	2&3	We have demonstrated logical AND operations with multiple input on one channel.	delete this sentence
135	3	9	optical systam with phase-......	optical system with *a* phase-......
135	3	11	The *systems* operation depended..	The *system's* operation depended..

Page No.	Para. No.	Line No.	Original Statement in Thesis	Corrigenda
211	1	6	This plays an *importment* role......	This plays an *important* role......
211	2	1	It worth *mention* that in......	It *is* worth *mentioning* that in......
211	2	2	and diffracted their shared.....	and *were* diffracted *by* their shared.....
211	4	6	and θ_3 to normal of......	and θ_3 to *the* normal of......
212	1	8	considered to be......	considered to be *mutually*......
213	1	3	a set of *nutural* density filters......	a set of *neutral* density filters......
213	1	5	*screen* S_1 and S_2, or cameras......	*screens* S_1 and S_2, or cameras......
213	in Fig.		*Electron*	*Electronic*
214	2	2	0.48 mm, *is* inciden:t......	0.48 mm, *are* incident......
214	2	6	is about *twice* higher than......	is about *two times* higher than......
214	Fig. Capt.		*turnning*	*turning*
214	Fig. Capt.	3	off *on* the steady state phase......	off *in* the steady state phase......
214	3	1	mutual pumping *were* indeed......	mutual pumping *was* indeed......
215	2	5	USAF *resouliton* chart and......	USAF *resolution* chart and......

Page No.	Para. No.	Line No.	Original Statement in Thesis	Corrigenda
165	1	14	a numerical approach *for* to......	a numerical approach to......
166	1	16	and *forth* configurations......	and *fourth* configurations......
166	1	18	MPPCMs and *theoretical*......	MPPCMs and *theoretically*......
167	1	1	incident beams are *incidnet*......	incident beams are *incident*......
167	3	2	In the DPC *cofiguration*......	In the DPC *configuration*......
168	Fig. Capt.		*(Sternklar86); (Smount87); (Ewbank88); (Sharp90); (Wang89); (Ewbank90)*	*(Ste86); (Smo87); (Ewb88); (Sha90); (Wan89); (Ewb90)*
169	1.	1	at *an* non-zero acute angle......	at *a* non-zero acute angle......
169	1	5	*Afterwhatwards* these......	*Afterwards* these......
170	Fig. Capt.	2	*grometries* (a), (e) "Arch"......	*geometries* (a), (e) "Arch"......
172	Fig. Capt.		*(Chang95); (Sharp90)*	*(Cha95); (Sha90)*
173	3	2	*modes* at 488 nm and......	*mode* at 488 nm and......
174	2	4	[*Sei87*, Eas87, Smo87......	[*Wei87b*, Eas87, Smo87......
176	Fig. Capt.	5	results from *Zozluya*......	results from *Zozulya*......
176	Fig. Capt.	6	et al. [*Zozluya94*] for......	et al. [*Zoz94*] for......
176	in Fig.		*(a), (b), (c)* *(d), (e), (f)*	*(d), (e), (f)* *(a), (b), (c)*
178	1	3	estabilished with *slighty*......	estabilished with *slightly*......
181	1	5	instablity [*Eas90*]......	instablity [*Hus90*]......
182	1	7	has a large r_{43},......	has a large r_{42},......
182	1	9	coupling *light rays* which......	coupling *fields* which......
182	2	4	towards *to* the +C direction.......	towards the +C direction.......
183	Fig. Capt.		diagram *of* showing the *physics and gratings* in the geometry......	diagram showing the *formation of the Arch and gratings* in the geometry.....
185	2	3	phase-conjugate *mirror*......	phase-conjugate *mirrors*......
185	2	6	*In these interacting beams can construct*......	*These interacting beams can construct*......
188	2	5	*cryatal* a face for about 10......	*crystal* a face for about 10......
194	1	7	were changed becoming......	were changed, becoming......
196	2	7	either focused c*losed*......	either focused c*lose*......
196	2	11	for wide beam with large......	for *a* wide beam with large......
197	1	4	*insert* into path 1 (or 2) to......	*inserted* into path 1 (or 2) to......
197	1	6	beam power *ratio* is shown......	beam power *ratios* is shown......
198	1	4	the input *path* after spatially......	the input *paths* after spatially......
199	1	2	In previous *this* subsection......	In previous subsection......
199	1	3	that *by optimally* the......	that *optimally by* the......
199	1	5	geometry to *further* attempt to......	geometry to attempt to......
199	2	1	25 mW *derided* from......	25 mW *derived* from......
199	2	2	~ *5* cm coherence length......	~ *3* cm coherence length......
199	2	4	with an *intersection* of *angle*......	with an *angle* of *intersection*......
200	1	2	we *refere* to it as the......	we *refer* to it as the......
200	2	10	reflected from crystal's faces......	reflected from *the* crystal's faces......
203	2	1	the MPPCM "ray" configuration..	the MPPCM *in the* "ray" configuration..
203	2	2	experiment was *performed out*.....	experiment was *performed*......
203	2	8	"ray" configuration very......	"ray" configuration *is* very......
205	1	5	one target was doll image......	one target was *a* doll image......
206	1	8	use *a* more than one interaction....	use more than one interaction......
207	1	3		
207	1	4	Model can be by......	Model can be *used* by......
208	1	11	(ii) "*Fish-Heas*", "Fish", and "*Ring*", configurations	(ii) "*Fish-Head*", "Fish", and "*Ray*", configurations
211	1	1	*one* can be seen that......	*it* can be seen that......

Page No.	**Para. No.**	**Line No.**	**Original Statement in Thesis**	**Corrigenda**
218	1	6	In some *case* we......	In some *cases* we......
218	1	13	must be *take* into......	must be *taken* into......
219	2	4	beams and *finaly* for......	beams and *finally* for......
219	3	6	effect of *incresasing* the......	effect of *increasing* the......
222	3	13	the use of external pump......	the use of *an* external pump......
222	4	5	in *an* associative memories.......	in associative memories.......
223	1	2	a threshold and for feedback.......	a threshold *device* and for feedback....
223	2	8	Rh:$BaTiO_3$ and a *varity*......	Rh:$BaTiO_3$ and a *variety*......